COPPER ELECTROWINNING FROM CYANIDE SOLUTIONS

by

Jianming Lu

B. Eng., Northeastern University, P. R. China, 1983
M. Eng., Shanghai University, P. R. China, 1990
M. A. Sc., University of British Columbia, 1996

A THESIS SUBMITTED IN PARTIAL FULFILLMENT OF

THE REQUIREMENTS FOR THE DEGREE OF

DOCTOR OF PHILOSOPHY

in

THE FACULTY OF GRADUATE STUDIES

Department of Metals and Materials Engineering

We accept this thesis as conforming

to the required standard

THE UNIVERSITY OF BRITISH COLUMBIA

October 1999

Department of _Metals and Materials Eng._

The University of British Columbia
Vancouver, Canada

Date _Dec. 27, 1999_

ABSTRACT

The objective of this research was to explore an efficient process to recover cyanide and copper from barren gold cyanide solution. The research work described here concerns an investigation into fundamental and practical aspects of two options for electrowinning copper from cyanide solution. These two options are: (a) the use of an alternative anode reaction to limit the electro-oxidation of cyanide in concentrated cyanide solutions and (b) the use of a graphite fibre cathode to electrowin copper from dilute cyanide solution.

(1) A critical literature survey was conducted to examine the stability constants of copper cyanide species. The distributions and the equilibrium redox potentials of copper cyanide species were calculated using the most reliable stability constants. They are dependent on the mole ratio of cyanide to copper, total cyanide concentration, pH and temperature. Potential measurements have confirmed the validity of the calculated results. The pH-potential diagram was drawn using the Gibbs free energy data derived by selecting the most reliable stability constants.

(2) Direct copper electrowinning from dilute cyanide solutions was conducted in a membrane cell. The accumulation of deposited copper on the graphite felt as the plating proceeds significantly improves the conductivity of the graphite felt, increases the specific surface area and benefits copper deposition. Copper can be deposited on the graphite felt from low concentration solutions (1-2 gL^{-1} Cu and CN:Cu mole ratio = 3-4) with 50-80 % current efficiency, the removal of around 40% Cu and an energy consumption of 1-2 kWh/kg Cu in the superficial current density range 30 - 100 Am^{-2} at 40 °C.

(3) Copper electrowinning from concentrated copper cyanide solution (70 g L^{-1} Cu) was conducted using four sacrificial species (sulphite, methanol, thiocyanate and ammonia) at 40 to 60 °C. Only sulphite can decrease the anodic current efficiency of cyanide oxidation from $\sim$ 100 to 10-20 % over the current density range of 250-500 Am^{-2}. With increasing CN:Cu mole ratio from 3 to 4.5, the anodic current efficiency of cyanide oxidation increased and the copper deposition current efficiency decreased. As regards the recovery of copper from barren gold cyanide solution, it has been shown that using sulphite oxidation as an alternative anode reaction, copper can be electrowon from a cyanide electrolyte containing

about 70 gL^{-1} Cu (CN:Cu = about 3) and 0.5 M Na$_2$SO$_3$ at a cathode current efficiency of about 95% with a energy consumption of about 0.8 kWh/kg Cu at 250 Am^{-2}.

(4) In alkaline solutions, sulphite is oxidized to sulphate on the graphite anode in a two-electron reaction. The reaction order with respect to sulphite ions is below 1 at low potentials(< 0.4 V vs. SCE) and 1 at high potentials. The reaction order for hydroxide ions is close to zero. Two Tafel slopes were observed, 0.060 - 0.64 V decade^{-1} at low potentials and 0.19-0.20 V decade^{-1} at high potentials in the temperature range 40 - 60 °C . Sulphite oxidation in alkaline solution appears to undergo an electron-radical mechanism.

(5) The anodic oxidation of copper cyanide has been studied using a graphite rotating disk with reference to cyanide concentration (0.05-4 M), CN:Cu mole ratio (3-12), temperature (25-60 °C) and hydroxide concentration (0.01-0.25 M). Copper had a significant catalytic effect on cyanide oxidation. In the low polarization region (< about 0.4 V vs. SCE), cuprous cyanide is oxidized to cupric cyanide complexes which further react to form cyanate. At a CN:Cu ratio of 3 and [OH$^-$] = 0.25 M, the Tafel slope was about 0.12 V decade^{-1}. Cu(CN)$_3^{2-}$ was discharged on the electrode surface. With increasing CN:Cu mole ratio and decreasing pH, the dominant discharged species shifted to Cu(CN)$_4^{3-}$. In the high polarization region (about 0.4 -0.6 V vs. SCE), cuprous cyanide complexes were oxidized to copper oxide and cyanate. When the concentration of cyanide was high and the pH low, cyanogen was formed, but no copper oxide.

(6) Sulphite oxidation is enhanced by the presence of copper cyanide. The effect of sulphite on limiting the oxidation of copper cyanide decreases with increasing mole ratio of cyanide to copper. This is related to the shift in the discharged species from Cu(CN)$_3^{2-}$ to Cu(CN)$_4^{3-}$ with increasing mole ratio of cyanide to copper. Sulphite is oxidized to sulphate. At [Cu] = around 1 M, CN:Cu = 3 -3.2, [OH$^-$] = 0.05-0.25 M, [SO$_3^{2-}$] = 0.4-0.6 M and the temperature = 50 - 60 °C, the anode current efficiency of sulphite oxidation reached 80-90% as the anodic current efficiency of cyanide fell to 20 to 10 %.

TABLE OF CONTENTS

LIST of TABLES

LIST OF FIGURES

Na_2SO_4

°C, 0.5 V vs. SCE, and 100 rpm

Nomenclature

Lists of symbols

a	specific area (m^{-1})
a_i	activity of species i
C	concentration ($mol\ dm^{-3}$)
C_b	bulk concentration ($mol\ dm^{-3}$)
C_s	surface concentration ($mole\ dm^{-3}$)
C. E.	current efficiency
D	diffusion coefficient ($m^2\ s^{-1}$)
d	diameter of graphite fibre
E	potential of the electrode (V)
e	porosity of matrix
e_0	initial porosity of matrix
E°	standard potential (V)
E_P	peak potential in linear potential sweep (V)
$E_{P/2}$	potential where $i = i_p/2$ in linear potential sweep (V)
E.C.	energy consumption ($kWhr\ kg^{-1}$)
EDTA	ethylenediaminetetra-acetic acid
en	ethylenediamine
F	Faraday constant = 96487 A s mol^{-1}
G^{ex}	excess Gibbs free energy
I	current (A) or ionic strength
I_l	current in the liquid phase (A)

I_s	current in the solid phase (A)
i	current density, (A m^{-2})
i_{Cu}	current density of copper deposition (A m^{-2})
i_d	diffusion current density (Am^{-2})
i_H	current density of hydrogen evolution (A m^{-2})
i_k	kinetically controlled current density (A m^{-2})
i_l	limiting current density (Am^{-2})
i_p	peak current density (A m^{-2})
k	heterogeneous rate constant (m s^{-1})
K_a	constant of HCN dissociation
K_{sp}	solubility product of CuCN
k_m	mass transfer coefficient (m^2 s^{-1})
K_1	equilibrium constant between SO_2(aq.) and HSO_3^-
K_2	equilibrium constant between HSO_3^- and SO_3^{2-}
$K_{2,3}$	equilibrium constant for $Cu(CN)_2^- + CN^- \rightarrow Cu(CN)_3^{2-}$
$K_{3,4}$	equilibrium constant for $Cu(CN)_3^{2-} + CN^- \rightarrow Cu(CN)_4^{3-}$
M	molarity (mol dm^{-3})
m_i	molality of species i, (mol kg^{-1})
n	number of electrons transferred or moles of solutes i, j or k
n_r	reaction order
n_w	kilograms of solvent
pH	negative logarithm to base 10 of the activity of hydrogen ion
R	gas constant (8.314 J K^{-1} mol^{-1})

Re	Reynolds number
S	siemens (Ω^{-1})
SCE	saturated calomel electrode
Sh	Sherwood number
SHE	standard hydrogen electrode
T	absolute temperature, (°K)
u	velocity of the liquid (m s^{-1})
$U^{\neq}$	activation energy at the potential = 0 (J mol^{-1})
$U_a^{\neq}(E)$	activation energy at potential (E) (J mol^{-1})
v	scan rate of potential sweep (V s^{-1})
Z_i	ionic charge

Lists of Greek Symbols

α	charge transfer coefficent
α_a	anodic charge transfer coefficient
α_1	Pitzer's parameters (= 2.0 for 1-1, 2-1, 1-2,3-1, 4-1 electrolyte)
α_2	Pitzer's parameters (= 0.0 for 1-1, 2-1, 1-2,3-1, 4-1 electrolyte)
β_0	Pitzer's parameter
β_1	Pitzer's parameter
β_2	Pitzer's parameter for 2-2 electrolyte or the association constant for $Cu(CN)_2^-$
γ_i	activity coefficient of species i
θ	Pitzer's interaction parameter for like charged ions
λ_{ij}	term for describing the short-range interionic effects as a function of ionic

strength to display the type of behaviour caused by the hard core effect

μ_i chemical potential of the solute (molality)

μ^0_I chemical potential in the solute (molality) standard state

μ_{ijk} term for triple ion interactions which ignores any ionic strength dependence

δ_d thickness of the diffusion layer (m)

η overpotential (V)

ν kinematic viscosity ($m^2\ s^{-1}$)

Ω ohm or number of moles of solvent in a kilogram (55.51 for water)

ω angular velocity (s^{-1})

κ effective conductivity of the liquid (solution) phase ($S\ m^{-1}$)

σ effective conductivity of the solid (graphite fibre) phase ($S\ m^{-1}$)

Φ potential difference bewteen the solid phase and the liquid (V)

Φ_l potential of the liquid phase (V)

Φ_s potential of the solid phase (V)

ϕ osmotic coefficient

ψ Pitzer's ternary parameter

ACKNOWLEDGEMENTS

1. INTRODUCTION

Cyanide leaching has been widely accepted as an excellent industrial method to recover gold and silver [1, 2]. However, the cyanidation of copper-gold ores containing the common oxide and secondary sulfide copper minerals e.g. chalcocite (Cu_2S), bornite (Cu_5FeS_4), malachite ($CuCO_3$, $Cu(OH)_2$), covellite (CuS) and cuprite (Cu_2O) results in cyanide degradation and copper solubilization as cuprous cyanide complexes. In conventional gold processing, the copper and complexed cyanide are not recovered after the gold is removed from solution. This leads to a significant economic penalty in excess cyanide consumption, loss of a valuable copper by-product and significant cost in cyanide destruction during effluent treatment.

Several ways have been proposed to solve the above problems. For example, (1) pretreating ores to remove copper etc. before cyanidation such as pressure oxidation leaching [3], roasting-leaching [4-6], and bioleaching [7, 8]; (2) the application of alternative lixiviants to recover gold such as thiourea [9], ammonium thiosufate [10], chloride [2], and bromide [2, 11]; (3) the addition of other reagents such as ammonia to decrease the consumption of cyanide [12]. However, the above methods have their own drawbacks or application limits and so in most cases cyanide is still used to leach gold ores containing copper.

Therefore the recovery of copper and associated complexed cyanide from leach solutions has been approached in a variety of ways such as acidification-volatilization-regeneration (AVR), ion exchange and electrolysis [13-25]. The basic AVR process consists of the following steps: (1) acidifying the barren solution to pH 2-3 with sulphuric acid to dissociate copper cyanide complexes to form HCN and precipitate copper as CuCN or a mixture of CuCN and CuSCN, if there is SCN^- in the solution; (2) volatilizing HCN from the solution by intense air sparging, and (3) recovering the HCN by absorption in an alkaline solution (NaOH or $Ca(OH)_2$) [13 - 18]. In order to recover cyanide from the precipitates, oxidants such as H_2O_2 and O_3 have been tested to convert CuCN and CuSCN to Cu^{2+} and HCN in the AVR process [15, 17]. NaHS was tested to precipitate copper as Cu_2S and recover all of the cyanide in the AVR process [18]. Several ion-exchange process has been proposed to improve the recovery of cyanide in a combination with the AVR process [15, 19, 20].

Electrowinning was used to recover copper as metal and cyanide [21-25]. During electrowinning, cyanide is oxidized to cyanate, decreasing the recovery of cyanide, and copper deposition current efficiency was low due to the low copper concentration. Several methods have been proposed to solve the above problems. To increase the copper deposition current efficiency, porous electrodes were used to deposit copper [22-25]. Orocon Inc.[22] reported that the thiocyanate in the solution could be oxidized to CN^- and SO_4^{2-} to decrease the consumption of cyanide. However, the anodic current efficiency of thiocyanate was not given. To prevent the cyanide oxidation at the anode, an ion-exchange membrane was used to separate the anode and the cathode [25]. Recently a process was proposed which combines ion exchange, AVR, membrane cell electrolysis and improves the efficiency for recovering copper and cyanide [26, 27].

However, generally these processes suffer from the following drawbacks: incomplete recovery of cyanide, incomplete recovery of copper, low-value copper products (e.g. CuCN, CuSCN and Cu_2S) and complicated flowsheets. In order to overcome the above drawbacks, a solvent extraction-electrowinning process has been developed to recover copper and cyanide from gold mining effluents [28]. In summary, copper cyanide is extracted using a guanidine-based extractant (XI7950) or a mixed strong base extractant with nonylphenol (XI78), stripped with strong alkaline electrolyte and finally electrolyzed in a membrane cell to produce copper metal and a bleed stream for AVR to recover cyanide. The chemistry of the process is shown below:

Copper extraction:

$$Na_2Cu(CN)_3 + 2\overline{R} + 2H_2O \rightarrow \overline{R_2H_2Cu(CN)_3} + 2NaOH \qquad (1\text{-}1)$$
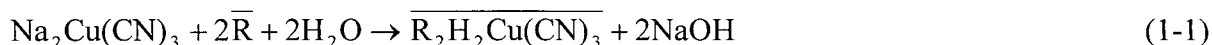
where R species refers to the guanidine solvent extractant.

Copper stripping:

$$\overline{R_2H_2Cu(CN)_3} + 2NaOH \rightarrow 2\overline{R} + Na_2Cu(CN)_3 + H_2O \qquad (1\text{-}2)$$
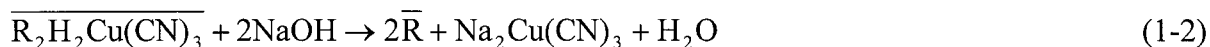
Copper electrowinning (in a membrane cell):

$$Na_2Cu(CN)_3 + NaOH \rightarrow Cu + 3NaCN + 1/4O_2 + 1/2H_2O \qquad (1\text{-}3)$$
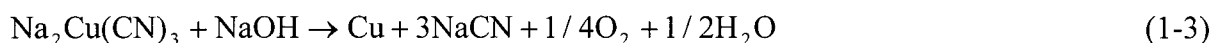
The use of a membrane (Nafion) cell in the copper electrowinning cell is necessary to prevent cyanide oxidation at the anode. However, the Nafion membrane is expensive and may be subject to mechanical damage by the growing metal deposit. In order to eliminate the use of a membrane cell, an alternative anode reaction is used to prevent the oxidation of

cyanide. This will result in a simpler cell design (no membrane) with reduced capital cost and low cell voltage (low energy consumption). Alternative anode reactions which have been suggested and tested are: (1) the oxidation of thiocyanate to cyanide and sulphate, (2) the oxidation of methanol to CO_2 and H_2O, (3) the oxidation of sulphite to sulphate and (4) the oxidation of ammonia to N_2 and H_2O. The inclusion of the above sacrificial species was tested in some proof-of-concept electrowinning experiments in our lab and was shown to be promising only for sulphite. With sulphite addition, the cell chemistry becomes:

$$Na_2Cu(CN)_3 + 1/2Na_2SO_3 + NaOH = Cu + 3NaCN + 1/2Na_2SO_4 + 1/2H_2O \qquad (1-4)$$
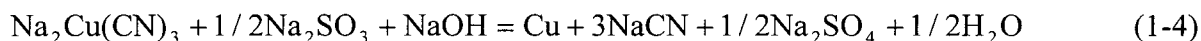
Therefore a process has been proposed by the Hydrometallurgy Group at UBC using the flowsheet shown in Figure 1-1 to recover copper and cyanide. In the first step (loading), barren cyanide solution (0.5 -2 g L^{-1} Cu, CN:Cu mole ratio = 3-4) is mixed with organic phase (extractant and solvent) and copper cyanide is extracted to the organic phase. In the second step (stripping), the organic phase loaded with copper cyanide is mixed with strong alkaline electrolyte (60 g L^{-1} Cu, CN:Cu = about 3, 4-10 g L^{-1} NaOH and 50-60 g L^{-1} Na_2SO_3) and copper cyanide is transferred to the electrolyte and the copper concentration of the electrolyte increases to about 70 g L^{-1}. In the third step (electrowinning), the electrolyte is returned to the electrowinning cell and copper is deposited on the cathode. In the fourth step (acidification), a bleed stream of electrolyte is taken out and mixed with H_2SO_4 and copper cyanide is dissociated to form HCN and CuCN at pH 2-3. CuCN was returned to the electrowinning cell and HCN is removed by sparging air and finally absorbed in alkaline solution (NaOH or $Ca(OH)_2$).

The direct electrowinning of copper from a barren cyanide leach solution may be preferred in some cases for the recovery of copper and recycle of cyanide. However, careful study of this process has not been reported. Therefore, the efficient deposition of copper from a barren cyanide solution is a promising alternative approach to the recovery of cyanide and copper. The process for the direct electrowinning process has been developed and consists of the following steps: (1) barren cyanide solution (1-2 g L^{-1} Cu and CN:Cu mole ratio = 3-4) enters the membrane cell and flows through the graphite felt cathode on which copper is deposited and the copper depleted cyanide solution returns to gold leaching and (2) copper is deposited on a metal sheet and then refined in a second electrorefining cell containing copper sulphate solution. The flowsheet is shown in Figure 1-2.

An initial economic assessment has been performed on direct electrowinning and on the SX-EW system(see Appendix 1). The assessment has been made using an assumed ore grade. The analysis indicates that a significant benefit may be available by applying one of these processes.

In order to improve the above processes, the two electrowinning processes should be studied as regards both the practical and fundamental aspects. Therefore the present research was undertaken with the following objectives:

(1) To study the aqueous chemistry of copper cyanide solutions in the temperature range 25 - 60 °C with reference to copper concentration, CN:Cu mole ratio and pH. The results could be generated by calculation using the equilibrium copper cyanide constants and then confirmed by potential measurement. It was expected that this study would lead to an improved understanding of the distribution of copper cyanide complexes under practical conditions and their role in the electrodeposition and the anodic oxidation of copper cyanide.

(2) To study the electrowinning of copper from concentrated cyanide solutions using an alternative anode reaction so as to limit the oxidation of cyanide. The study would be conducted with reference to CN:Cu mole ratio (3-4.5), temperature (40-60 °C) and the concentration of sacrificial species (for sulphite 50 -120 g L^{-1}). These parameters will significantly affect the cathode and anode processes. Copper concentration should be controlled at 60-70 g L^{-1} to get a reasonable copper deposition current efficiency and to simulate the copper content of the strong electrolyte in the electrowinning process.

(3) To study the electrowinning of copper on a graphite felt cathode with reference to copper concentration (1-2 g L^{-1}), mole ratio of cyanide to copper (3-4.5) and flow rate and current density (30-100 A m^{-2}) at an ambient temperature (25-40 °C) from viewpoint of industrial practice.

(4) To study the oxidation of sulphite on graphite with reference to temperature (25 -60 °C), Na$_2$SO$_3$ concentration (0.05-0.5 M) and hydroxide concentration (0.05-0.25 M) using rotating disk technique and linear potential sweep. The anodic behaviour of sulphite on the graphite (Tafel slope and rate constant) and the mass transfer (diffusion coefficient) can be obtained and compared to those of copper cyanide to decrease the anodic oxidation of cyanide.

(5) To study the oxidation of copper cyanide on graphite with reference to temperature (25-60 °C), mole ratio of cyanide to copper (3-12), cyanide concentration (0.05-4 M) and

hydroxide concentration (0.01-0.25 M) using the rotating disk technique. This research could lead to knowing how these parameters affect the anodic behaviour of copper cyanide.

(6) To study the anodic oxidation of copper cyanide and sulphite solutions with reference to their concentrations, CN:Cu mole ratio, temperature (25-60 °C), hydroxide concentration (0.05-0.25 M) and the current density using the rotating disk technique. The anodic behaviour of mixed sulphite and copper cyanide may not be the same as when they are present separately in the solution. Therefore it is necessary to know the anodic behaviour of the mixture.

The results of this study should help to increase the efficiency of recovering copper and cyanide from a barren gold solution and to decrease the cost.

This thesis consists of seven major chapters: Chapter 2 deals with a review of the literature, providing a summary of current ideas about the deposition of copper from cyanide solution, the anodic oxidation of copper cyanide and the anodic oxidation of sulphite, thiocyanate, methanol and ammonia. Chapter 3 considers the thermodyanics of copper cyanide. Chapters 4 - 8 present the experimental aspects, results and discussion of the direct copper electrowinning from a dilute cyanide solution, copper electrowinning using an alternative anodic reaction, the anodic oxidation of sulphite, anodic oxidation of copper cyanide and the anodic oxidation of mixed sulphite and copper cyanide solutions respectively. Chapter 9 summarizes the research work and Chapter 10 gives some suggestions for future studies.

Barren cyanide solution

H_2SO_4 ⟶ | Loading | ⟶Raffinate

Organic phase / Organic phase

NaOH⟶ | Stripping |

Electrolyte / Electrolyte

NaOH ⟶
Na_2SO_3 ⟶ | Electrowinning | ⟶ Cu
⟶ Barren solution

Bleed / CuCN

H_2SO_4 ⟶ | Acidification |

HCN

CaO ⟶ | Neutralization | ⟶ $Ca(CN)_2$
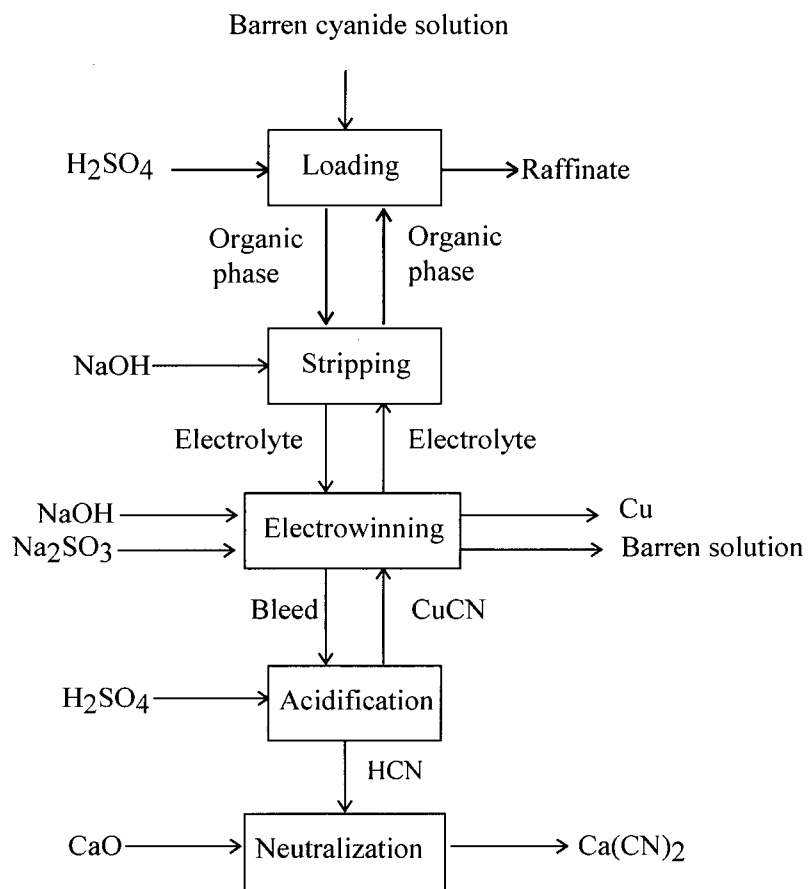
Figure 1-1 Flowsheet for solvent extraction - electrowinning process for the recovery of copper cyanide
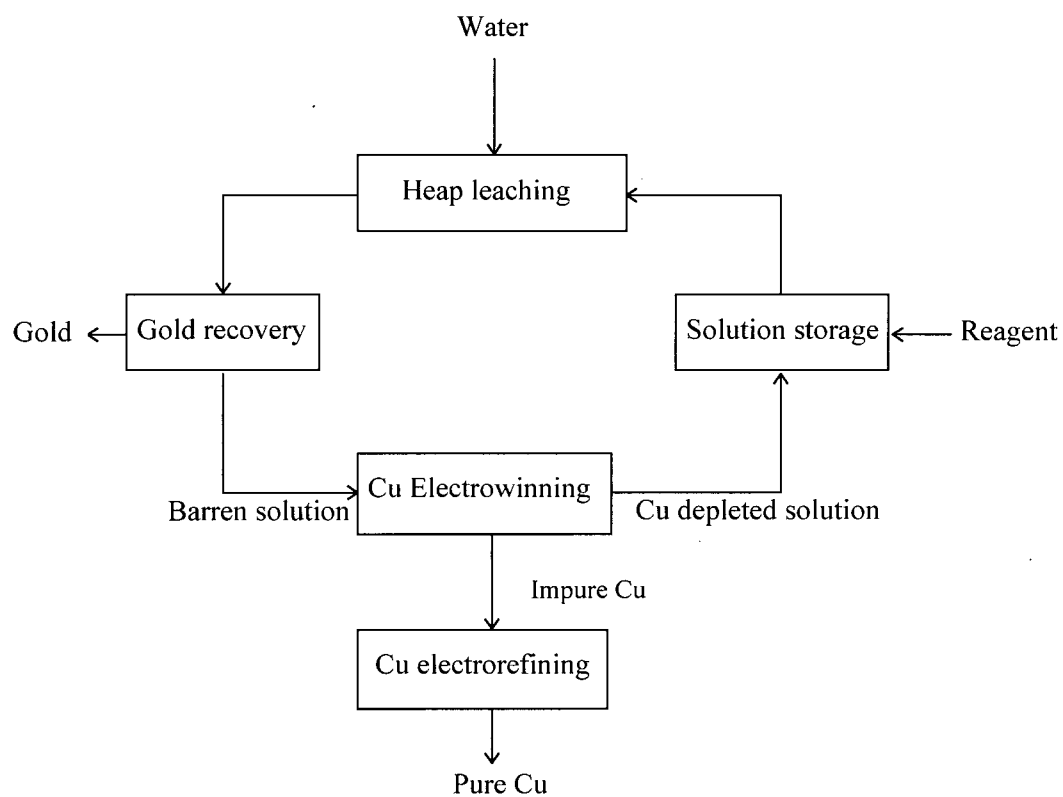
Figure 1-2 Flowsheet for direct electrowinning of copper from cyanide solutions

2. LITERATURE REVIEW

2.1 Aqueous Chemistry of the Copper-Cyanide System

Copper cyanide can be dissolved in the presence of excess cyanide to form cyanocuprate ions, $Cu(CN)_2^-$, $Cu(CN)_3^{2-}$ and $Cu(CN)_4^{3-}$ in aqueous solution. This dissolution has been studied by various methods [29-59]. These species undergo the following successive equilibrium steps in reaction with free cyanide and undissociated hydrocyanic acid.

$$CuCN = Cu^+ + CN^- \qquad\qquad K_{sp} \qquad\qquad (2\text{-}1)$$

$$CuCN + CN^- = Cu(CN)_2^- \qquad\qquad K_{1,2} \qquad\qquad (2\text{-}2)$$

$$Cu^+ + 2CN^- = Cu(CN)_2^- \qquad\qquad \beta_2 \qquad\qquad (2\text{-}3)$$

$$Cu(CN)_2^- + CN^- = Cu(CN)_3^{2-} \qquad\qquad K_{2,3} \qquad\qquad (2\text{-}4)$$

$$Cu(CN)_3^{2-} + CN^- = Cu(CN)_4^{3-} \qquad\qquad K_{3,4} \qquad\qquad (2\text{-}5)$$

$$HCN = H^+ + CN^- \qquad\qquad K_a \qquad\qquad (2\text{-}6)$$

Table 2-1 The association constants for copper cyanide complexes

Method	Temperature	Concentration	log β_2	log $K_{2,3}$	log $K_{3,4}$
Potentiometry [32]	25 °C	10^{-1} - 10^{-7} M CN⁻	23.72	-	-
Potentiometry [42]	20 °C	0.5 -5 M CN	21.7 ± 1.0	4.6 ± 0.30	2.3 ± 0.15
Potentiometry [46]	22 °C	0. 01 M Cu	21.7 ± 0.2	5.1 ± 0.2	1.1 ± 0.2
Potentiometry [47]	25 °C	0.15 M Cu	24 ± 0.23	4.8	2.25
Potentiometric titration [59]	25 °C	1 M NaCl	23.97 ±0.01	5.43 ± 0.04	2.38 ±
Infrared spectroscopy [33]	25 °C	0.1 - 0.2 M Cu	-	4.89	1.72
Ultraviolet spectroscopy [58]	25 °C	ionic strength: 0.01M	-	5.34	1.74
Ultraviolet spectroscopy [39]	25 °C	0.001 M Cu	-	4.1	-
Calorimetry	25 °C	1.0 M Cu	-	5.0	2.6
Calorimetry [38]	25 °C	ionic strength→ 0	-	5.3 ±0.01	1.5 ± 0.2

The solubility product (K_{sp}) of cuprous cyanide differs slightly between authors, a value of 10^{-20} at 25°C being generally accepted [44]. There is good agreement for the HCN dissociation constant (K_a) amongst the published data. The recommended value for K_a at 25 °C is $10^{-9.21}$ which was obtained by extrapolation to the ionic strength = 0 or by calculation using an extended form of the Debye-Hückel equation [44, 52]. The dissociation constant in aqueous solution containing different ionic media has also been reported [52, 54-57].

The equilibrium constants for copper cyanide complexes (Table 2-1) differ between authors due to the different methods of measurement and the processing of the data. Vladimirova and Kakovsky [32] obtained a value of $10^{23.72}$ for β_2 using potential measurements with pure copper and copper amalgam at pH 4.2. This was consistent with the value estimated from the equilibrium constant between CuCNS and $Cu(CN)_2^-$. This value was corrected to 10^{24} by some authors [33, 38, 39, 44] using the Debye-Hückel equation and a more reliable dissociation constant for HCN. Rothbaum [42] reported a value of $10^{21.7}$ for β_2 at 20 °C by measuring the copper potential in a solution of high copper cyanide concentration in the presence of air and simplifying the copper cyanide species for calculation without considering the activity coefficient, leading to some error. Hancock et al. [46] obtained a value of $10^{21.7}$ for β_2 using potential measurement in solutions containing 0.01 M Cu(I) and 0.025 - 0.1 M CN⁻ at pH 11 and 22 °C under an Ar atmosphere. However, β_2 could be underestimated because some of the potential data used for the calculation of β_2 were measured at a CN:Cu mole ratio > 4 and were well below the hydrogen equilibrium potential. The measured potentials were mixed potentials and higher than the corresponding equilibrium potentials. Bek and Zhukov [47] reported a value for 10^{24} for β_2 using potential measurements in solutions with 0.15 M Cu(I), CN:Cu = 4, and 0.1 M NaOH and an extended form of the Debye-Hückel equation. Kappenstein and Hugel [48] obtained a value of $10^{16.7}$ for β_2 using UV spectroscopy, changing the pH and assuming $Cu(CN)_2^-$ was the only copper complex in the solution. However, this value is much lower than the formation constant (1/Ksp) for CuCN and $Cu(CN)_2^-$ was not dominant under such conditions according to its β_2 value. Recently Hefter et al. [59] reported a value of $10^{23.97}$ for β_2 which was obtained by potentiometric titration using a Cu^+ solution produced by reduction of Cu^{2+} with an excess of copper and stabilized by chloride. So the most reliable value for β_2 appears to be 10^{24}.

The differences among the reported values of $K_{2,3}$, and $K_{3,4}$ are relatively small. The most reliable values of $K_{2,3}$ and $K_{3,4}$ are those reported by Izatt et al. [38]. They were obtained under well-defined conditions using pH measurements and calorimetry and the Debye-Hückel equation.

A ^{63}Cu and ^{65}Cu magnetic resonance study showed that $Cu(CN)_4^{3-}$ retains a tetrahedral symmetry and $Cu(CN)_3^{2-}$ has a distorted tetrahedral rather than a plane triangular configuration [43]. Cuprous ions form mixed complexes with the cyanide ligand and other

ligands such as thiourea, thiocyanate, iodide, ammonia and chloride, for example, $Cu(CN)_3SCN^{3-}$ and $Cu(CN)_4SCN^{4-}$ [43]. The complexed cyanide rapidly exchanges with aqueous free cyanide [29]. When the mole ratio of cyanide to copper is less than 3, the copper cyanide is readily oxidized by air, suggesting that $Cu(CN)_2^-$ is less stable [60].

Cupric ions react with CN^- and form cupric complexes, which are unstable and decompose rapidly [29, 58]. It was reported that when the mole ratio of CN:Cu is not high, cupric ions react with the cyanide in aqueous solution to give cupric cyanide as a yellowish-brown precipitate, which decomposes into cupric cyanide and cyanogen according to the following equations [61, 62]:

$$Cu^{2+} + 2CN^- \rightarrow Cu^{II}(CN)_2 \qquad (2\text{-}7)$$

$$2Cu^{II}(CN)_2 \rightarrow 2Cu^{I}CN + (CN)_2 \qquad (2\text{-}8)$$

The cyanogen thus formed is evolved as a gas from acidic solution, or it is decomposed in alkaline solution as follows:

$$(CN)_2 + 2OH^- \rightarrow CN^- + CNO^- + H_2O \qquad (2\text{-}9)$$

When the mole ratio of cyanide to copper is high, not copper(II) dicyanide but a purple intermediate is formed which rapidly decomposes into cyanogen and a copper species. Even at ordinary temperature a transient violet colour may be noted in neutral or slightly alkaline media [29, 63, 64]. The kinetics studies provided the first strong evidence for the formation of $Cu(CN)_4^{2-}$ in reactions between Cu^{2+} or its EDTA complex and CN^- [29, 58, 65, 66]. Longo and Bush [67] conducted the Cu^{2+} -CN^- reaction in methanol or dimethylformamide from -60 to -30 °C and concluded that the unstable purple species is a square planar complex $Cu(CN)_4^{2-}$. Monsted and Bjerrum [68] studied the reaction between Cu^{2+} and CN^- in aqueous methanol at - 70 °C and reported that the absorption maximum at 535 nm was nearly in the same position as that for $Cu(en)_2^{2+}$, suggesting a distorted tetrahedral structure. Neither the electron spin resonance nor the optical spectrum is influenced by the presence of excess of cyanide, showing that no pentacyano complex is formed.

There are two reports about the formation constant of cupric tetracyanide [69, 70]. Paterson and Bjerrum [69] estimated the formation constant of $Cu(CN)_4^{2-}$ as $10^{26.7}$ by potentiometric experiment in water-methanol solution (mole fraction of methanol = 0.45) at - 45 °C, with the ionic strength varying between 0.05 and 0.1 M (NaCN). Katagiri et al. [70,

71] oxidized $Cu(CN)_4^{3-}$ on a platinum electrode to generate $Cu(CN)_4^{2-}$ and measured the redox potential for the $Cu(CN)_4^{2-}/Cu(CN)_4^{3-}$ couple. They reported that the standard potential for the $Cu(CN)_4^{2-}/Cu(CN)_4^{3-}$ redox couple was 0.54 V vs. SHE and the overall formation constant for $Cu(CN)_4^{2-}$ was 10^{24}.

Baxendale and Westcott [58] studied the reaction between Cu^{2+} and CN^- in weakly acidic solution to keep the concentration of free cyanide ion low and decrease the reaction rate. They found that the reaction was second order in Cu^{2+} and 6th order in CN^- from the change in the concentration of the reaction product, $Cu(CN)_2^-$ using a UV spectrophotometer. They proposed the following mechanism:

$$Cu^{2+} + 3CN^- \Leftrightarrow Cu(CN)_3^- \qquad (2\text{-}10)$$

$$2Cu(CN)_3^- \rightarrow 2Cu(CN)_2^- + (CN)_2 \qquad (2\text{-}11)$$

Nord and Matthes [72] used the stopped-flow technique to study the reaction between Cu^{2+} and CN^- in aqueous solutions at 0 to 25 °C and found that the reaction was second order with respect to $Cu(CN)_4^{2-}$ and inversely proportional to the concentration of the free cyanide. On the basis of these results, they proposed the following reaction mechanism:

$$Cu(CN)_4^{2-} \Leftrightarrow Cu(CN)_3^- + CN^- \qquad (2\text{-}12)$$

$$Cu(CN)_4^{2-} + Cu(CN)_3^- \rightarrow Cu(CN)_3^{2-} + Cu(CN)_2^- + (CN)_2 \qquad (2\text{-}13)$$

Reaction 2-13 is considered to be the rate-controlling step. Katagiri et al. [70, 73] studied the kinetics and mechanism of the decomposition of $Cu(CN)_4^{2-}$ generated by the anodic oxidation of $Cu(CN)_4^{3-}$ and found that the rate of the decomposition was second order with respect to $Cu(CN)_4^{2-}$ and inversely proportional to the square of the concentration of the free cyanide concentration. The following decomposition mechanism was proposed:

$$2Cu(CN)_4^{2-} \Leftrightarrow Cu_2(CN)_6^{2-} + 2CN^- \qquad (2\text{-}14)$$

$$Cu_2(CN)_6^{2-} \rightarrow 2Cu(CN)_2^- + (CN)_2 \qquad (2\text{-}15)$$

Reaction 2-15 is proposed as the rate-determining step.

The rapid decomposition of cupric cyanide results in the oxidation of cyanide which has led to the use of cupric ions as a catalyst to destroy cyanide in waste water [74 - 76].

2.2 The Electrodeposition of Copper from Copper-Cyanide Solution

2.2.1 Practice of Copper Deposition from Cyanide Solution

The electrodeposition of copper from cyanide solution has been widely reported [21-29, 31, 77-128]. However, there are very few reports on copper electrowinning from copper cyanide solution and most reports deal with copper plating. An early copper electrowinning operation was carried out at the San Sebastian Mine in 1904 [79]. Clevenger [84, 85] reported that copper was recovered in Nevada and Mexico, but cyanide consumption was high (30% of cyanide was destroyed) and the current efficiency for copper deposition was low. Lower [21] reported that the direct electrowinning of copper from a leach solution containing 13.7 - 24 g L^{-1} Cu at ambient temperatures gave about 70 % current efficiency and a energy consumption of about 1.3 kWh/kg Cu at 47-93 A m^{-2}. Shantz and Reich [77] ran locked leaching-electrowinning tests on a copper rougher concentrate and obtained 62 % current efficiency and a energy consumption of 0.7 kWh/kg Cu at 70-80 A m^{-2}. Copper electrowinning from dilute barren copper cyanide solutions was carried out with a high surface area cathode [22-25], but no details such as copper deposition current efficiency, cyanide consumption and energy consumption are reported. Du Pont [26] has patented a process for the recovery of cyanide and copper by electrowinning from cyanide solutions in a cell in which the anolyte is separated from the catholyte by a membrane to avoid the anodic oxidation of cyanide. Acidification, ion exchange or carbon adsorption was used to concentrate the copper cyanide solutions and adjust the ratio of cyanide to copper to below 3.0 - 4.0. Copper electrowinning has been conducted at UBC using membrane cells with the effects of temperature, composition, current density being studied [28]. Solvent extraction was used to concentrate copper cyanide. Solvent extraction is more effective in the extraction of copper cyanide from dilute copper cyanide solutions than the use of acidification, ion exchange or carbon adsorption. The UBC SX-EW process may have advantages over the Du Pont process.

Copper plating from cyanide solutions has been used throughout the metal finishing industry since Elkington discovered this technology in 1840 [80]. Under the proper conditions, the metal distribution over irregularly shaped articles is excellent because of the good throwing power. Typical copper cyanide bath compositions and conditions are listed in Table 2-2. Current efficiency is a function of composition, temperature and current density.

Copper cyanide solution was used to plate copper on porous materials [121] or carbon fibres in the presence of supporting electrolyte [125].

Table 2-2 Copper cyanide bath compositions and conditions [82]

Bath Type	Strike	Rochelle	High Efficiency
Cu (g/l)	11.0	15 - 30	34 - 89
Free cyanide (g/l)	6.0	4 - 9	11 - 19
Na_2CO_3 or NaOH (g/l)	15(Na_2CO_3)	15-60 (Na_2CO_3)	22-27(NaOH)
Temperature (^0C)	41-60	55-70	60-80
Cathode Current (A/m^2)	100 - 320	160 - 650	100 - 1110
Cathode current efficiency (%)	10 - 60	30 - 70	>99

2.2.2 The Effect of Parameters on Copper Deposition

The copper current efficiency decreases with increasing mole ratio of cyanide to copper [91, 92, 124]. With increasing ratio of cyanide to copper, the equilibrium potential decreases. By Le Chatelier's principle we should expect increasing cyanide to inhibit the dissociation of copper cyanide complexes and to retard the discharge reactions. However, it has a more important effect in shifting the complex distribution towards the less active complex state ($Cu(CN)_2^- \rightarrow Cu(CN)_3^{2-} \rightarrow Cu(CN)_4^{3-}$). Therefore the copper discharge potential decreases resulting in more hydrogen evolution. The ratio of cyanide to copper close to 3 is optimum for the high efficiency electrolyte.

The equilibrium potential for H_2O/H_2 (expressed as $E(H^+/H) = -0.0591$ pH V vs. SHE) decreases with increasing pH, but pH has a relatively small effect on the redox potential for Cu^+/Cu at a pH above 9. In alkaline solution H_2O is discharged on the electrode and so the current of hydrogen evolution at a fixed potential may not be dependent on pH as expected from the change in the equilibrium potential for H_2O/H_2. The copper current efficiency may not significantly increase with increasing pH. Hydroxide or carbonate salts have to be added to get a higher pH. However, addition of carbonate and hydroxide ions is also associated with a reduction in the current for copper deposition, with the relationship being approximately linear [92, 124]. These effects are not only due to the presence of CO_3^{2-} and OH$^-$ ions, but probably to the concomitant increase in the alkali metal ion concentration and surface adsorption.

The current efficiency decreases with increasing current density. Obviously, at a higher current density and a higher polarization potential [87, 88, 91, 92], the ratio of cyanide to copper in the solution near the cathode surface is higher due to a limited diffusion rate and hydrogen evolution increases faster than copper deposition.

The cathodic current efficiency increases with increasing temperature. At higher temperatures, the copper-cyanide dissociation constant is larger and the balance shifts to the formation of lowly coordinated copper complexes $(Cu(CN)_2^-)$, which will be discussed in the next chapter, and cuprous complexes diffuse faster to the cathode surface and are more readily reduced. However, with increasing temperature, the hydrolytic decomposition of cyanide increases [91].

Agitation increases the cathodic current efficiency [92]. Due to the reduction of cuprous ions at the cathode, the ratio of copper to cyanide in the cathode boundary layer decreases resulting in a lower current efficiency. Agitation accelerates the rate of cuprous ion movement to the cathode surface and cyanide movement away from the cathode. Therefore the concentration of cuprous ions near the cathode surface increases, resulting in a higher current efficiency.

Iron and chromium in the copper-cyanide solution decrease the current efficiency [92]. Bismuth, zinc, antimony and other metals will cause a rough deposit at times [89].

The incorporation of thiocyanate and specific surface-active agents permits the deposition of bright, smooth deposits [90-98, 101-104]. Thiocyanate also increases the cathodic current efficiency [92, 94-96, 98]. It is possible that the adsorption of SCN^- at the copper cathode suppresses the discharge of H^+ (or H_2O) and therefore increases the copper cathodic current efficiency. Shivirin et al [99, 100] reported that the addition of thiocyanate had little effect on the overpotential of hydrogen evolution. It was reported that thiocyanate could be used in place of cyanide for copper plating [105].

Sodium sulphite and bisulphite have been recommended as additions to copper cyanide baths to improve the brightness of the deposits [90].

2.2.3 The Kinetics and Mechanism of Copper Deposition

The kinetics and mechanism of copper deposition from copper-cyanide solution have not been widely studied. Blanc [108] reported that the species discharged could not be free Cu^+ according to his work on the effect of alternating current. Glasstone [32] proposed the direction reduction of copper from $Cu(CN)_2^-$.

Costa [110] studied the electrochemical behaviour of copper-cyanide solutions (0.01-0.08 M CuCl and 0.06-0.93 M KCN) and proposed the following mechanism:

$$Cu(CN)_3^{2-} \rightarrow CuCN + 2CN^- \tag{2-16}$$

$$CuCN + e \rightarrow Cu + CN^- \tag{2-17}$$

The transfer coefficient was 0.38 ± 0.04 and the exchange current density was proportional to Cu^+ concentration. The curve of log I, as a function of $log[CN^-]$ exhibits a changing slope for a free CN^- concentration greater than 0.21 M. The varying slope is considered to be a result of the variation in the physical surface of the electrode rather than a change in the electrochemical process.

Lowenheim [111] thought that the direct discharge of $Cu(CN)_4^{3-}$ was more possible than the two-step discharge mechanism

$$Cu(CN)_4^{3-} \rightarrow Cu^+ + 4CN^- \xrightarrow{+e} Cu \tag{2-18}$$

Raub and Muller [112] thought that the reaction mechanism is:

$$Cu(CN)_3^{2-} \rightarrow Cu(CN)_2^- + CN^- \xrightarrow{+e} Cu \tag{2-19}$$

Bek and Zhukov [113-116] studied the deposition of copper from a solution with 0.1 M Cu^+ and a $CN^-:Cu^+$ mole ratio of 2.8-3.2 at pH 13 and thought that copper deposition results in a significant variation in the distribution of the copper-cyanide species and a significant concentration polarization. They found that $Cu(CN)_2^-$ was the discharged species and the charge transfer coefficient was 0.1 after correcting for the concentration change. They proposed the following reaction mechanism:

$$Cu(CN)_3^{2-} \rightarrow Cu(CN)_2^- + CN^- \qquad \text{at CN:Cu ratio} < 3 \tag{2-20}$$

$$Cu(CN)_4^{3-} \rightarrow Cu(CN)_2^- + 2CN^- \qquad \text{at CN:Cu ratio} > 4 \tag{2-21}$$

$$Cu(CN)_2^- + e \rightarrow Cu + 2CN^- \tag{2-22}$$

Sinitski et al. [118] reported that a distinct limiting current could be obtained in dilute copper cyanide solutions at pH 4.95. The Tafel slopes ranged from 0.130-0.165 V decade^{-1} and the transfer coefficient was 0.40 ± 0.03.

Chu and Fedkiw [122] have used the voltammetric and steady-state polarization response of a copper-disk electrode to study the kinetics of copper deposition from a cyanide bath using the solution: 0.1 M Na_2CO_3 + 0.2 M CuCN + 0.6 M NaCN and pH 12. The major species discharged was considered to be $Cu(CN)_3^{2-}$, although $Cu(CN)_4^{3-}$ is the predominant complex. The cyanide released during deposition shifts the distribution of the complexes at the surface to the coordinately saturated state and results in a decreased copper deposition rate since the discharge of $Cu(CN)_4^{3-}$ is considerably slower than that of $Cu(CN)_3^{2-}$.

Hatherley et al. [124] measured the polarization curves of copper deposition from cyanide solution. It was concluded that $Cu(CN)_2^-$ was first discharged and subsequently $Cu(CN)_3^{2-}$. $Cu(CN)_4^{3-}$ does not seem to take part in the deposition process. At a certain limiting current density these processes break down and there is a loss of cathode current efficiency.

Steponavicius et al. [127] studied the mechanism of copper deposition using linear potential sweep, linear current scan and single galvanostatic pulse methods and found that the preceding reaction for copper deposition is the dissociation of $Cu(CN)_3^{2-}$ into $Cu(CN)_2^-$ and CN^- and then $Cu(CN)_2^-$ is discharged on the cathode.

Hsu and Tran [129] studied the reduction of copper cyanide using a rotating disc and found that the electrochemical active species is $Cu(CN)_2^-$.

2.3 Electrochemical Oxidation of Cyanide

Great attention has been paid to the study of the electrochemical oxidation of CN^- in order to minimize the destruction of cyanide in metal electrowinning from cyanide solution and maximize the efficiency of the destruction of cyanide in effluent streams to meet environmental requirements [21-24, 85, 130 - 168]. The products and mechanism of cyanide

oxidation depend mainly on pH , potential and concentration. From the following redox reactions, hydrocyanic acid is more difficult to oxidize and is much less electro-active [138].

$$2HCN = (CN)_2 + 2H^+ + 2e \qquad E^0 = 0.373 \text{ V vs. SHE} \qquad (2\text{-}23)$$

$$2CN^- = (CN)_2 + 2e \qquad E^0 = -0.176 \text{ V vs. SHE} \qquad (2\text{-}24)$$
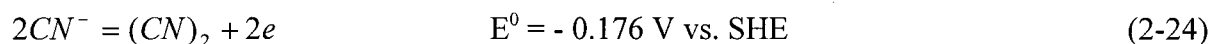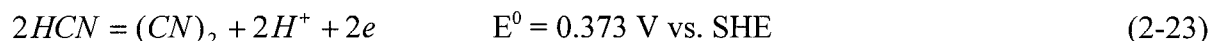
2.3.1 Cyanide Oxidation in Alkaline Solution

Under alkaline conditions, the reaction for the oxidation of cyanide is [131, 132, 149, 150, 158]:

$$CN^- + 2OH^- = CNO^- + H_2O + 2e \qquad E^0 = -0.97 \text{ V vs. SHE} \qquad (2\text{-}25)$$

Cyanate can be further oxidized at higher potentials to CO_3^{2-} and N_2 [131, 137, 158], but its current efficiency has not been reported.

$$2CNO^- + 8OH^- = 2CO_3^{2-} + N_2 + 4H_2O + 6e \qquad E^0 = -0.95 \text{ V vs. SHE} \qquad (2\text{-}26)$$
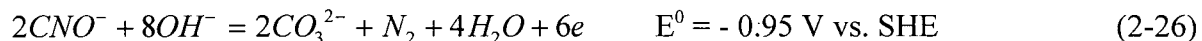
Arikado et al. [143] reported that the Tafel slope for cyanide oxidation on a graphite electrode was about 0.12 V decade^{-1} and the reaction orders were unity and zero for CN^- and OH^- respectively. Cyanide is not oxidized by atomic oxygen formed by way of oxygen evolution. The following mechanism was proposed:

$$OH^- + CN^- \xrightarrow{-2e} HOCN \xrightarrow{+OH^-} CNO^- + H_2O \qquad (2\text{-}27)$$
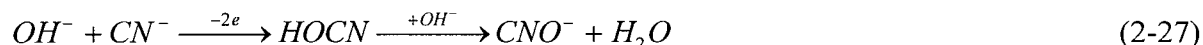
The rate of cyanide oxidation increases with increasing cyanide concentration and is independent of OH^- concentration (> 0.01 M). The discharge of cyanide ion determines the overall reaction rate. The apparent number of electrons participating in the reaction decreases from 2 to 1 with decreasing OH^- concentration (1 to 10^{-4} M) [143].

The current efficiency of cyanide oxidation depends on the anode materials, current density and concentration [156].

2.3.2 Cyanide Oxidation in Weakly Acidic, or Alkaline or Neutral Solutions

In neutral and weakly alkaline solutions (pH 7.0 - 11.7), cyanogen is the main cyanide oxidation product according to Reaction 2-24 [138, 143, 149, 150, 163]. This condition is referred to as hydroxide-starved oxidation of cyanide. Cyanogen can react subsequently with hydroxide in solution to give cyanate and cyanide:

$$(CN)_2 + 2OH^- = CNO^- + CN^- + H_2O \tag{2-28}$$

The cyanide radical can also polymerize to form paracyanogen $(CN)_n$.

Azulmin, $(HCN)_n$ is formed due to the polymerization of aqueous hydrocyanic acid [136, 149,156, 157]. Hine et al. [156] reported that azulmin formation is closely related to the ratio of CN^- to OH^-.

In neutral or slightly alkaline solutions (pH 7.0 - 8.6) [157] or in weakly alkaline carbonate-buffer solutions (pH 9.3) [149], the cyanate ion may continuously undergo hydrolysis to produce ammonium and carbonate ions ($CNO^- + 2\ H_2O \rightarrow NH_4^+ + CO_3^{2-}$).

In weakly acidic solution (pH 5.2-6.8), $(CN)_2$ is hydrolyzed to form oxamide, $(CONH_2)_2$ and oxalate, $C_2O_4^{2-}$ and NH_4^+:

$$(CN)_2 + 2H_2O = (CONH_2)_2 \tag{2-29}$$

$$(CN)_2 + 4H_2O = C_2O_4^{2-} + 2NH_4^+ \tag{2-30}$$

2.3.3 The Anodic Oxidation of Copper Cyanide

There are some reports on the anodic oxidation of copper cyanide, but most of them are about the products and phenomena of the electrolytic oxidation and are incomplete[135, 139-142, 144, 145, 147, 149-152, 156, 157, 160]. Sperry and Caldwell [135], Dart et al. [139], and Easton [141] thought that copper deposition releases free cyanide at the cathode and then the free cyanide is oxidized to cyanate at the anode. Drogen and Pasek [140] and Daubaras [151] proposed a direct oxidation route (copper cyanide complexes are directly oxidized to cyanate and cuprous ions. Tan et al. [160] believed that copper cyanide complexes are first oxidized to cyanate releasing cuprous ions, which are oxidized to copper hydroxide according to their electrolytic products.

Byerley et al. [142] observed that cuprous ions sufficient to complex 10 - 30% of total cyanide exhibited the best catalytic effect on cyanide oxidation at pH 10 - 11. Hofseth and Chapman [168] reported that the cyanide concentration can be reduced from 100 to 1 ppm in a porous flow-through reticulated vitreous carbon catalyzed by copper ions. Yoshimura and Katagiri et al. [144, 145, 147, 149, 150] measured the steady-state polarization curves at a

platinum anode in cyanide solutions containing a very small amount of copper (CN:Cu > 5) and 0.5 M K_2SO_4 as supporting electrolyte, and found that the Tafel slope was about 0.158 V decade^{-1} in a low potential region, suggesting that a simple one-electron reaction was occurring at the electrode. The current at a constant potential was proportional to the total cuprous ion concentration but it was almost independent of the total cyanide concentration. It was assumed that all of the copper exists in the form of $Cu(CN)_4^{3-}$ without checking the distribution of copper species. In fact, in the ranges of cyanide and copper concentration studied by these authors, a significant amount of copper exists in the form of $Cu(CN)_3^{2-}$ and their assumption is not appropriate. The calculated reaction order with respect to $Cu(CN)_4^{3-}$ (actually Cu(I)) was 0.9. $Cu(CN)_4^{2-}$ was detected by ESR spectroscopy. It was thought that $Cu(CN)_4^{3-}$ is oxidized to $Cu(CN)_4^{2-}$, which is the rate-determining step. The following mechanism was proposed [150]:

$$Cu(CN)_4^{3-} \rightarrow Cu(CN)_4^{2-} + e \qquad (2\text{-}31)$$

$$2Cu(CN)_4^{2-} \Leftrightarrow Cu_2(CN)_6^{2-} + 2CN^- \qquad (2\text{-}32)$$

$$Cu_2(CN)_6^{2-} \rightarrow 2Cu(CN)_2^- + (CN)_2 \qquad (2\text{-}33)$$

$$Cu(CN)_2^- + 2CN^- \rightarrow Cu(CN)_4^{3-} \qquad (2\text{-}34)$$

$$(CN)_2 + 2OH^- \rightarrow CN^- + OCN^- + H_2O \qquad (2\text{-}35)$$
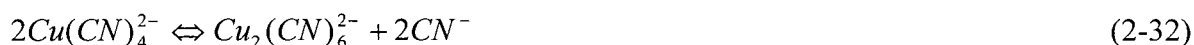
However, no kinetic data are given for alkaline copper cyanide solutions except for a polarization curve in 1 M KOH solution. The reaction products of the anodic oxidation of cyanide at 0.6 and 1.2 V vs. SCE were determined. In alkaline solutions (pH 11.8-14), the reaction can be expressed by Equation 2-25 and cyanate ion was not oxidized further.

Hine et al. [156] studied the anodic oxidation of copper cyanide on a PbO_2 -coated anode and found that only copper exhibited a catalytic effect on cyanide oxidation. The Tafel slope for the oxidation of the solution containing 1 M NaCN and 0.3 M copper was 0.070 - 0.110 V decade^{-1} in the current density range of 50 -1000 A m^{-2}. The current efficiency of cyanide oxidation decreased with decreasing total cyanide concentration at constant copper concentration. It was thought that the following reaction was occurring:

$$Cu(CN)_3^{2-} + 2OH^- = Cu(OH)_2 + 3CN^- + e \qquad (2\text{-}36)$$

Hwang et al. [157] studied the electrolytic oxidation of copper cyanide solution with CN:Cu mole ratios of 2.8 to 20 and at different pH's using a platinum anode. In strongly

alkaline solution (pH > 12), the copper-cyanide complex is oxidized directly to cyanate and copper oxide. The following reaction sequence was proposed:

$$Cu(CN)_n^{(n-1)-} + 2nOH^- = Cu^+ + nCNO^- + nH_2O + 2ne \qquad (2\text{-}37)$$

$$2Cu^+ + 2OH^- = Cu_2O + H_2O \qquad (2\text{-}38)$$

$$Cu_2O + 2OH^- = CuO + 2H_2O + 2e \qquad (2\text{-}39)$$
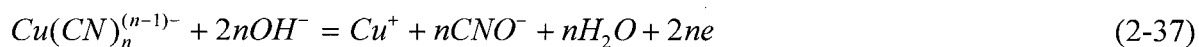
However, the potential was controlled at 0.71 and 1.2 V vs. SCE and so the oxygen evolution may have affected the coulometric measurement. Also, in their experiment, the cathode and the anode were not separated. Therefore copper deposition may have affected significantly the mole ratio of cyanide to copper during the course of the experiment. In neutral or weakly alkaline or acidic solutions, the complex does not undergo the direct oxidation, but dissociates to free cyanide due to copper deposition and then free cyanide is oxidized on the anode. Apparently the above oxidation procedure is not reasonable. If the anode and the cathode are separated, the anodic oxidation will not happen. Even if the anode and the cathode are not separated, at low CN:Cu mole ratios (e.g. 3), the free cyanide released from the cathode will immediately bond to the lowly coordinated copper cyanide complexes ($Cu(CN)_3^{2-}$ and $Cu(CN)_2^-$). Furthermore if only free cyanide is oxidized, at CN:Cu < 3, the concentration of free cyanide is so low (less than 1/1000 of the total cyanide) that the cyanide oxidation can be neglected.

Later Hwang et al. [166] adopted the direct oxidation mechanism reported by their group [157] and the catalytic mechanism by Katagiri et al. [147, 150] and reported that the Tafel slope increased from 0.040 V decade^{-1} at CN:Cu = 3 to 0.120 V decade^{-1} at CN:Cu > 10. The anodic oxidation of copper cyanide undergoes both direct oxidation and catalytic oxidation. At CN:Cu < 3, there is only the direct oxidation and at CN:Cu > 10, there is only the catalytic oxidation.

The anodic oxidation of copper cyanide resulted in the formation of copper oxide, which catalyzed the oxidation of free cyanide [159, 163, 165, 167].

From the above discussion, there are incomplete and conflicting results on the anodic oxidation of copper cyanide in alkaline solution and the information from the literature is insufficient for the present research, especially with respect to the design of an electrochemical process for Cu-CN electrowinning.

2.4 The Electrochemical Oxidation of Thiocyanate

Thiocyanic acid exists in two isomeric forms, $H - S - C \equiv N$ or $H - N = C = S$ in equilibrium with each other and thiocyanate ions exist in two tautomeric forms, $^{-}S - C \equiv N$ (I) and $S = C = N^{-}$ (II) [169]. The redox reaction is:

$$2SCN^{-} = (SCN)_2 + 2e \qquad\qquad E° = 0.77 \text{ V vs. SHE} \qquad\qquad (2\text{-}40)$$
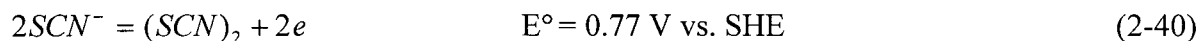
The structure of thiocyanogen is $N \equiv C - S - S - C \equiv N$. $(SCN)_2$ undergoes rapid hydrolysis in water to give SO_4^{2-}, HCN, and H^+.

The electrochemical oxidation of thiocyanate has been studied for a long time both in aqueous and non-aqueous media [130, 131, 170-204]. The products of the oxidation of thiocyanate in aqueous solution are sulphate and either cyanide or cyanate or, further, ammonium and carbonate or nitrogen depending on the pH of the solution and the anodic potential.

The oxidation of thiocyanate is irreversible. In acid solutions, the reaction can be expressed mainly by the following equation [174, 177-180, 185, 192-195, 198, 199, 203]:

$$SCN^{-} + 4H_2O = SO_4^{2-} + HCN + 7H^{+} + 6e \qquad E° = 0.515 \text{ V vs. SHE} \qquad (2\text{-}41)$$

Other products are also formed, e.g. parathicyanogen $(SCN)_x$, [177-179], a passivation film $C_6N_4S_4$, and $(SCN)_3^{-}$ [192]. The initial step of the anodic oxidation may be the removal of an electron from one thiocyanate ion [185, 192]. However, Loucka et al. [203] reported that the first step is the decomposition into sulfur and cyanide and then the sulfur is oxidized to sulphate and the oxidation of thiocyanate occurs at potentials higher than 0.7 V vs. SHE.

In basic solutions, the oxidation reaction can be expressed as: [133, 170]:

$$SCN^{-} + 8OH^{-} = SO_4^{2-} + CN^{-} + 4H_2O + 6e \qquad E° = -0.61 \text{ V vs. SHE} \qquad (2\text{-}42)$$

Gauguin [174-176] gave the following expressions for the potential of SCN⁻ oxidation: E = 0.57 - 0.058 log[SCN⁻] from pH 0 to 7 and E = 1.17 + (0.058/6) log $([H^+]^8/[SCN^-]^6)$ from pH 9 to pH 14. The potential for CN⁻ oxidation is E = 0.10 - 0.058 log [CN⁻] from pH 0 to 13 and E = 0.88 + (0.058/2) log$([H^+]^2/[CN^-])$ above pH 13.

The electrolytic conversion of thiocyanate to cyanide has been studied as a means of regenerating cyanide and minimizing the consumption of cyanide in hydrometallurgy [23, 87, 130, 170-172, 189-191, 193-195]. The conversion of thiocyanate to cyanide is never complete and depends on cyanide and thiocyanate concentrations, pH, potential, and anode materials. In 1911, Clennell [78, 170] reported that the production of cyanide rose to a maximum and then ceased. If the electrolysis was continued, the cyanide produced from thiocyanate oxidation gradually diminished and finally disappeared.

Crook et al. [171] investigated the electrolysis of thiocyanate on graphite anodes and gave results at different current densities. Without the addition of KOH, no CN⁻ was detected. This was probably because HCN was formed and volatilized at low pH. The increase in CN⁻ was proportional to the decrease in SCN⁻ and KOH.

Kern [172] found that thiocyanate in cyanide solutions reduced the consumption of cyanide in the electrolysis and was converted into cyanide to some extent.

Varentsov and Belyakova [189-191] studied the electrochemical oxidation of thiocyanate and cyanide at a ruthenium oxide or cobalt oxide coated titanium anode and graphite. They found that the relative rates of thiocyanate and cyanide oxidation depended on their concentrations and at higher concentrations of thiocyanate, more thiocyanate was oxidized and less cyanide. The graphite anode favored the oxidation of thiocyanate. However, the graphite broke down leading to contamination of the solution.

Orocon Inc. reported that thiocyanate from barren leach solutions can be oxidized to CN⁻ and sulphate on graphite fibre [23]. No current efficiency of the anodic oxidation of thiocyanate was given.

Byerley and Enns [193-195] studied the electrochemical regeneration of cyanide from thiocyanate at graphite anodes and found that the recovery of CN⁻ from thiocyanate increased with decreasing pH. At low pH thiocyanate is electrooxidized to produce cyanide ion which is immediately protonated by H^+. The acidic anode boundary layer functions to preserve cyanide from rapid electrooxidation at the anode by converting the cyanide ion into HCN, the much more difficultly oxidized neutral protonated form. The pH should be kept below 4 to realize the better conversion of thiocyanate into cyanide.

2.5 The Electrochemical Oxidation of Sulphite

The anodic oxidation of sulphite has been studied over a wide range of pH. The anodic behaviour changes with pH due to the change in the speciation of sulphite. It is important to know the distribution of the sulphite species with pH in order to understand the anodic oxidation of SO_3^{2-}.

In solution, sulphite exists in the form of SO_2 (aq), HSO_3^- and SO_3^{2-} with the following equilibria between these species [205]:
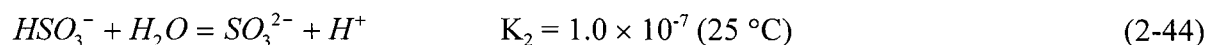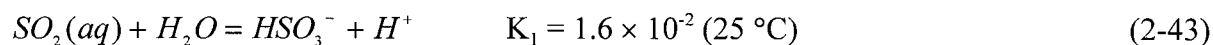
$$SO_2(aq) + H_2O = HSO_3^- + H^+ \qquad K_1 = 1.6 \times 10^{-2} \ (25 \ ^\circ C) \qquad (2\text{-}43)$$

$$HSO_3^- + H_2O = SO_3^{2-} + H^+ \qquad K_2 = 1.0 \times 10^{-7} \ (25 \ ^\circ C) \qquad (2\text{-}44)$$

SO_2 (aq), HSO_3^- and SO_3^{2-} species are predicted to predominate over the pH ranges < 1.8, 1.8 - 7 and > 7, respectively. At pH > 12, the dominant species in solution is SO_3^{2-}.

The redox reaction of sulphite -sulphate on graphite can be expressed by the following equations:

$$SO_4^{2-} + 2e + 4H^+ = H_2SO_3 + H_2O \qquad E^\circ = 0.158 \ V \ vs. \ SHE \qquad (2\text{-}45)$$

$$SO_4^{2-} + 2e + H_2O = SO_3^{2-} + 2OH^- \qquad E^\circ = -0.936 \ V \ vs. \ SHE \qquad (2\text{-}46)$$

$$S_2O_6^{2-} + 2e = 2SO_3^{2-} \qquad E^\circ = 0.037 \ V \ vs. \ SHE \qquad (2\text{-}47)$$

SO_3^{2-} cannot be reduced cathodically, while HSO_3^- (pH 6-3) may be reduced to dithionite $S_2O_4^{2-}$ [206]. The sulphite-sulphate redox systems are irreversible.

The electrochemical oxidation of sulphur dioxide or sulphite has been studied and tried as an anode depolariser to reduce the overall cell voltage in the production of hydrogen and in copper electrowinning in acid sulphate medium [207-252]. However, there are only a few reports on the electrochemical oxidation of sulphite in alkaline solutions [243, 253-255].

Sulphate and dithionate are formed during the oxidation of sulphite in alkaline and neutral solutions. The amount of dithionate produced at the anodic surface was shown to depend on operating conditions, namely the anode material, its preparation, current density, solution pH, and the presence of additives in the electrolyte. Friessner et al. [207,208] studied the oxidation of sulphite earlier and concluded that the formation of dithionate takes place at higher potentials than that of sulphate. Essin [209] reported that the addition of NH_4F increases the anodic potential and this benefits the formation of dithionate. The annealing of platinum leads to the formation of platinum oxide which favours the formation of dithionate.

Glasstone et al. [210, 211] investigated the effect of electrolysis conditions on the yield of dithionate and found that dithionate yields of up to 30 % can be obtained on nickel or gold electrodes, whereas the yield did not exceed 3% for graphite electrodes. Preliminary anodic polarization increases dithionate yield from 22 to 33%. In the current density range from 10 to 30 A/m^2, the dithionate formation rate does not change, but it decreases noticeably at below 10 A/m^2. Dithionate does not form at current densities above 300 A/m^2. Increasing temperature in the range of 18 - 60 °C had a little negative effect on dithionate formation. The sulphite concentration has no effect on the dithionate yield. The optimal pH value for the formation of dithionate is from 7 to 9.

Rozental et al. [216] reported that the oxidation of sulphite in acid media takes place at much smaller positive potentials (about 0.7 V vs. SHE) than the evolution of oxygen and concluded that the oxidation takes place via the surface oxides of platinum.

Lezhneva et al. [219] investigated the rate of the oxidation of sulphur dioxide on gold and platinum-gold alloys and found that the presence of water, cations, and anions near the metal surface sharply changes the properties of the surface oxygen compounds. Therefore, data on the properties of surface oxygen compounds obtained by electrochemical methods cannot always be used in studying the mechanism of sulphite oxidation.

Shlygin et al. [220, 221] studied the oxidation of sulphur dioxide and sulphite at a platinum electrode and concluded that the anodic oxidation of sulphur dioxide in acid and neutral solutions takes place at low potentials (0.65-1.2 V SHE) by a reversible electron-radical mechanism:

$$SO_2 + 4H_2O \Leftrightarrow H_2SO_4 + 2H_3O^+ + 2e \tag{2-48}$$

The appearance of adsorbed oxygen can completely stop the oxidation by the electron-radical mechanism at above 1.2 V vs. SHE. The electrochemical oxidation of SO_3^{2-} and HSO_3^- begins at 1.2 V vs. SHE and is irreversible. The ions cannot be oxidized by the electron-radical mechanism. Their oxidation mechanism consists in the addition of an OH radical at relatively high anodic potentials and the mechanism may be expressed by the following reactions:

$$2H_2O \rightarrow 2H_2O^+ + 2e \tag{2-49}$$

$$2H_2O^+ + 2H_2O \rightarrow 2OH + 2H_3O^+ \qquad (2\text{-}50)$$

$$SO_3^{2-} + 2OH \rightarrow SO_4^{2-} + H_2O \qquad (2\text{-}51)$$

Tarasevich et al. [239-240, 243] studied the oxidation of sulphite on platinum and carbon materials at 22 °C. The anchoring of the acidic oxides on the surface of the carbon materials decreases the reaction rate. The reaction order of the electrochemical oxidation depends on the sulphite concentration, being in all cases less than 1. This behaviour may be due to adsorption effects. At low concentrations of sulphite, the coverage is low and the reaction rate is proportional to the concentration of sulphite in the bulk solution. At high concentrations, the current is proportional to the concentration to a fractional power. In alkaline solutions, sulphite seems to be adsorbed to a lesser extent than in acid solution and the reaction is first-order up to 0.1 M. The dependence of the reaction rate on pH plays an essential role. The $\partial E/\partial pH$ value for both pyrographite and activated carbon is close to -40 mV in the range of pH 0 - 7 and becomes zero in the region of higher pH values. The $\partial E/\partial \log i$ value in the case of pyrographite amounts to ca. 150 mv decade^{-1} for pH < 7, and increases up to ca. 280 mv decade^{-1} for pH > 7. The shape of the polarization curves on the activated carbon is weakly dependent on the type of anion.

In the region of intermediate pH values, the curves exhibit two or even three Tafel slopes. The first slope in the acidic and neutral pH region is 35 to 50 mV decade^{-1}, whereas in alkaline solutions it is 60 - 70 mv decade^{-1}. The electrochemical oxidation of sulphite to sulphuric acid proceeds most likely via the mechanism involving the direct loss of an electron from the oxidized species. The dependence of the reaction rate on pH for carbon materials is due to a variation in the composition of the species which are subject to oxidation (at pH < 1.8 H_2SO_3, HSO_3^-, at pH 1.8-7, HSO_3^-, SO_3^{2-} and at pH > 7, SO_3^{2-}). The adsorbed species that are subject to oxidation undergo deprotonation (pH < 7):

$$H_2SO_3 \rightarrow HSO_{3\ ads} + H^+ \qquad (2\text{-}52)$$

$$HSO_3^- \rightarrow SO_{3\ ads}^{2-} + H^+ \qquad (2\text{-}53)$$

The slow step may involve the transfer of the first and the second electron from the adsorbed species:

$$HSO_3^{-}{}_{ads} \rightarrow HSO_3^{-} + e \qquad\qquad (2\text{-}54)$$

$$SO_3^{2-} + H_2O \rightarrow H_2SO_4^{-} + e \qquad\qquad (2\text{-}55)$$

Hunger et al. [253, 254] studied the electrochemical oxidation of sulphite (0.012 M - 0.09 M) on a graphite electrode at pH 9 and 25 °C and observed that the current gradually increased at about 0.2 V vs. SCE with increasing electrode potential. A poorly defined current density plateau was observed in the range 0.5-0.7 V vs. SCE. The onset of oxygen started at 1.5 V vs. SCE. Based on the Koutecky- Levich equation, they calculated the kinetic current at different sulphite concentrations and finally obtained reaction rate constants, reaction orders of 0.68 and 1.34, and charge transfer coefficients of 0.058 and 0.048 respectively for natural graphite and graphite impregnated with phenol. It should be noted that the Koutecky- Levich equation is valid only for the first order reaction and therefore their results are not convincing.

Brevett and Johnson [255] studied the anodic oxidation of sulphite (0.02-0.18 M) on pure and doped PbO_2 film electrodes at 25 and 65 °C in a $NaHCO_3/Na_2CO_3$ buffer (pH 10). They obtained a reaction order of -0.2 using the same method as Hunger et al. [253, 254]. The reason for their obtaining negative reaction order may be that the current was corrected by subtracting the background in the absence of sulphite which was much smaller than that in the presence of sulphite and the Koutecky- Levich equation was not valid for their calculation of the kinetic current.

Stankovic et al. [256] reported that the concentration of sulphite ions and temperature greatly influence the reaction rate. The number of transferred electrons for the slow step was nearly one.

2.6 The Electrochemical Oxidation of Methanol

The catalytic electrochemical oxidation of methanol has been widely studied for about 70 years [257-280]. The reaction in alkaline solutions can be written as:

$$CH_3OH + 8OH^{-} = CO_3^{2-} + 6H_2O + 6e \qquad E^{\circ} = -0.895 \text{ V vs. SHE} \qquad (2\text{-}56)$$
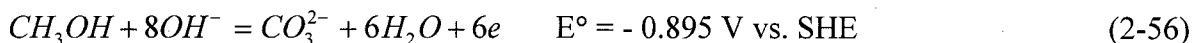
The best catalytic anode materials are platinum metals and their alloys [258, 259, 270-275]. The oxidation of methanol is mainly used in fuel cells. Methanol has been studied for use in metal electrowinning for depolarization [275-280]. Among soluble fuels, methanol is the most practical to use in an electrowinning cell. Vereecken et al. [275] used methanol for zinc electrowinning and observed its oxidation at a low potential on a platinum-activated graphite anode. The electrode potential, however, started to drift upwards after some time, and eventually the reaction shifted to oxygen evolution. Vining et al. [276, 277] proposed the use of a precious metal coated titanium anode to extend the catalytic activity of the electrode. The anode materials for an acidic electrolyte are mainly platinum-based and a RuO_2-based catalytic film on titanium. There is no report on the application of methanol electrochemical oxidation in alkaline solutions in electrometallurgy.

2.7 The Electrochemical Oxidation of Ammonia

In aqueous solutions the oxidation of ammonia to nitrogen is only possible in alkaline solutions and is dependent on the electrode materials and their pretreatment [281]. Therefore the study of ammonia oxidation was conducted in concentrated hydroxide solutions [282-291]. The reaction can be expressed as:

$$2NH_3 + 6OH^- = 6H_2O + N_2 + 6e \qquad\qquad E° = -0.74 \text{ V vs. SHE} \qquad\qquad (2\text{-}57)$$

The best catalysts are platinum metals and their alloys and these materials were studied for fuel cell application [281-289]. The anodic oxidation of ammonia was also conducted on a $Ti/TiO_2/RuO_2$ electrode [291]. Due to the slow kinetics for ammonia oxidation, chloride ion was used as a catalyst to oxidize ammonia [292, 293].

2.8 Summary

Copper and cyanide can form three stable cuprous complexes (dicyanide, tricyanide and tetracyanide) and their distribution depends on the concentrations of copper and cyanide and the mole ratio of cyanide to copper. Cupric cyanide complexes are not stable and rapidly decompose and cyanide is oxidized. Copper has a catalytic effect on the anodic oxidation of

cyanide. In alkaline solutions, cyanide is more readily oxidized than thiocyanate and the relative oxidation rates are dependent on the ratio of cyanide to thiocyanate concentration, current density, temperature and anode materials. However, the situation could be different in a copper cyanide solution. The anodic oxidation of sulphite and cyanide begins at an approximately potential. However, there are no data which afford a direct comparison. For methanol, an anode with a platinum-based film has to be used to decrease the overpotential for methanol oxidation. The anode will probably lose its catalytic effect with time. Ammonia can be readily oxidized in strongly alkaline solution at a platinum electrode. However, such a high hydroxide concentration is not suitable for the copper-cyanide system.

The copper deposition from cyanide solution has been widely reported. However, most of these reports focus on copper plating. The copper electrowinning from cyanide solution has not been studied extensively and the operating conditions should be optimized. However, some conditions used for plating can be applied to improve the efficiency of copper electrowinning. In order to obtain a high current efficiency of copper deposition, the temperature should be above 40 °C, the copper concentration should be above 50 g L^{-1} and the CN:Cu mole ratio should be around at 3. The addition of thiocyanate can improve the copper cathodic current efficiency.

There is very little information on copper electrodeposition from dilute cyanide solutions. In order to get a reasonable current efficiency of copper deposition, porous high surface area electrodes have to be used. The graphite fibre has a large surface area and has been used to remove metal ions from waste effluent efficiently. It is possible to use graphite fibre felt to deposit copper from dilute cyanide efficiently. To prevent cyanide oxidation, a membrane cell should be used.

From the above discussions, the information available in the literature is insufficient for this project and the further study must be done to develop a successful process.

The anodic and cathodic behaviour of copper cyanide is dependent on the distribution of the concentrations of copper cyanide species. The first step toward understanding the anodic and cathodic behaviour of copper cyanide is to know the distribution of copper cyanide species at different concentrations, pH's, and temperatures. The distribution of copper cyanide species can be calculated using reliable complex constants. Copper electrowinning using an alternative anode reaction in an undivided cell should be conducted

in a mini-cell to select the best sacrificial species. Finally using the best sacrificial species, copper electrowinning can be improved by changing the temperature and the compositions of the electrolyte. Therefore the anodic oxidation of the sacrificial species, copper cyanide and their mixture should be studied to (a) understand how the sacrificial species limits the anodic oxidation of cyanide and (b) provide some fundamental information to further improve the copper electrowinning process.

Although the graphite fibre felt can be used effectively to deposit copper from very dilute solution, copper is more difficult to deposit from cyanide solution. A feasibility test should first be done and then further research can be conducted to investigate the direct electrowinning on a graphite felt cathode with reference to copper concentration, mole ratio of cyanide to copper and flow rate.

3. THERMODYNAMICS OF COPPER CYANIDE

3.1 Distribution of Copper Cyanide Species

Copper cyanide species establish an equilibrium speciation (Reactions 2-1 to 2-6). The corresponding equilibrium constants selected for 25 °C are listed in Table 3-1 [38, 44, 49]. In some cases, we have to know the distribution of copper cyanide species and the equilibrium potentials for Cu(I)/Cu to understand copper deposition and cyanide oxidation at higher temperatures. However, so far the published data are inadequate for such a study. Therefore additional data must be generated by calculation. The $\Delta H°$ values for Reactions 2-1 and 2-3 to 2-6 are 128, -121.8, -46.4, -46.9 and 43.6 kJ mol^{-1} respectively, the absolute values of which are larger than 40 kJ/mole. Assuming that $\Delta H°$ is approximately constant in the range of 25 - 60 °C, we can calculate the equilibrium constant using the equation: $d\ln K/dT = \Delta H°/RT^2$ [294]. Some calculated constants are listed in Table 3-1.

Table 3-1 Equilibrium constants for copper cyanide system [38, 44, 49, 57]

Temperature(°C)	K_a	K_{sp}	β_2	$K_{2,3}$	$K_{3,4}$
25	6.17×10^{-10}	1.0×10^{-20}	1.0×10^{24}	2.00×10^5	31.63
40	1.43×10^{-09}	8.44×10^{-20}	9.47×10^{22}	8.14×10^4	12.77
50	2.40×10^{-09}	5.33×10^{-19}	2.22×10^{22}	4.69×10^4	7.317
60	3.91×10^{-9}	2.27×10^{-18}	5.61×10^{21}	2.79×10^4	4.333

The concentration distributions of these species are dependent on pH, temperature and the total concentrations of copper and cyanide. The mass balances of the copper and cyanide species are described by the following equations:

$$[Cu(I)]_{Total} = [Cu^+] + [Cu(CN)_2^-] + [Cu(CN)_3^{2-}] + [Cu(CN)_4^{3-}] \qquad (3-1)$$

$$[CN]_{Total} = [CN^-] + [HCN] + 2[Cu(CN)_2^-] + 3[Cu(CN)_3^{2-}] + 4[Cu(CN)_4^{3-}] \qquad (3-2)$$

By considering the equilibria (Reactions 2-1 to 2-6) and solving the above equations for the mass balance of these species, the distribution of copper cyanide species has been calculated. Since the exact values of the equilibrium constants used to calculate the concentration distribution are not sufficiently accurate and the parameters to calculate the activity coefficients of all the species are not available, the activity coefficients have not been considered in this study. Therefore the calculated values should be interpreted as indicating trends rather than absolute values. However, the validity of the prediction is confirmed by the experimental potential measurements reported in the next section. Figures 3-1 and 3-2 show the cyanocuprate distribution and the redox potential for Cu(I)/Cu vs. mole ratio of total cyanide to copper at pH 9 and 12. There is the following relation between the potential and the activity of cuprous ions:

$$E(Cu(I) / Cu) = E°(Cu(I) / Cu) + \frac{RT}{F} \ln(a_{Cu^+}) \qquad (3-3)$$

where E(Cu(I)/Cu) is the equilibrium potential for the Cu(I)/Cu couple, E°(Cu(I)/Cu) the standard potential (0.521, 0.520, 0.5195, and 0.519 V vs. SHE respectively for 25, 40, 50 and 60 °C, which were calculated using the data from the literature [295]). The other symbols have their common meanings. Therefore the potential reveals the activity (or concentration) of cuprous ions. The distribution of the copper cyanide species depends mainly on the mole ratio of total cyanide to copper and also on the concentration of total copper and the pH. At CN:Cu mole ratio < 3, the distribution of the cyanocuprate species depends on the CN:Cu mole ratio, and less on the concentration of copper at pH > 9. The dominant species are copper tricyanide and dicyanide, and copper tetracyanide can be neglected. At a mole ratio of cyanide to copper = 3, copper tricyanide dominates and most of copper exists in the form of tricyanide. At a mole ratio of cyanide to copper > 3, the distribution of the copper-cyanide species depends on the CN:Cu mole ratio, the total copper concentration and pH. For example, At $[Cu(I)]_{Total}$ = 0.001 M, copper tricyanide dominates and slowly decreases with increasing CN:Cu mole ratio and pH. At $[Cu(I)]_{Total}$ = 1M and CN:Cu mole ratio = 3-4, tricyanide dominates and decreases greatly with increasing CN:Cu mole ratio and slowly

with increasing pH. With further increase in the mole ratio of cyanide to copper, tetracyanide is dominant.
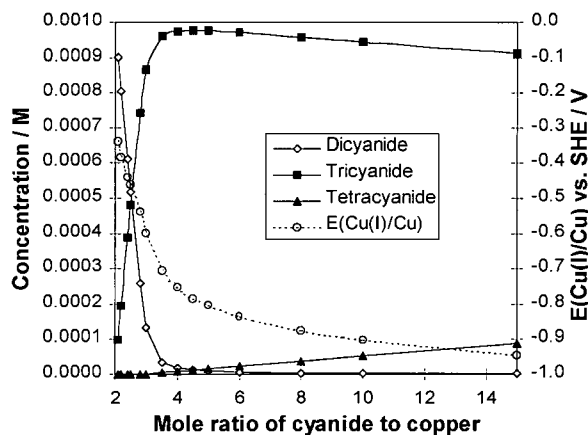
(a) $[Cu(I)]_{Total} = 0.001$ M, pH 9
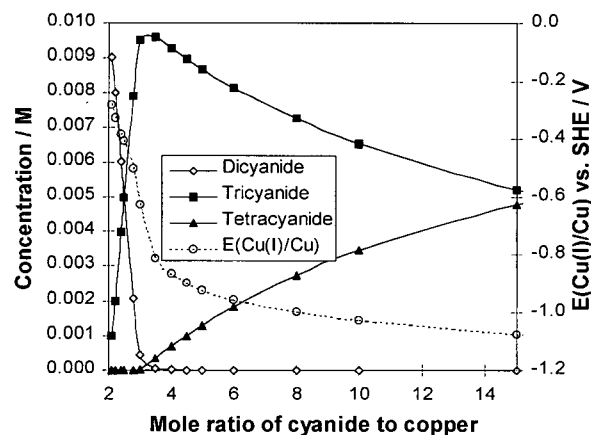
(b) $[Cu(I)]_{Total} = 0.01$ M, pH 9
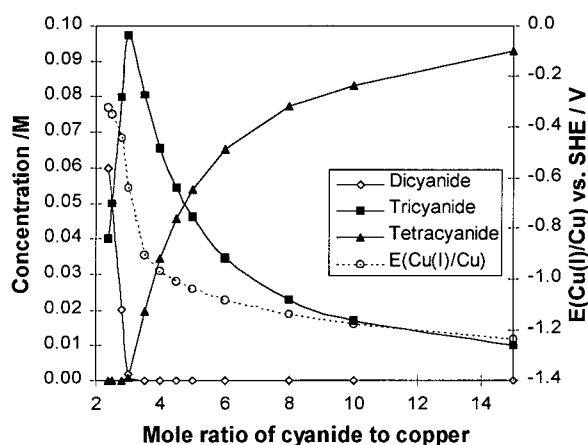
(c) $[Cu(I)]_{Total} = 0.1$ M, pH 9
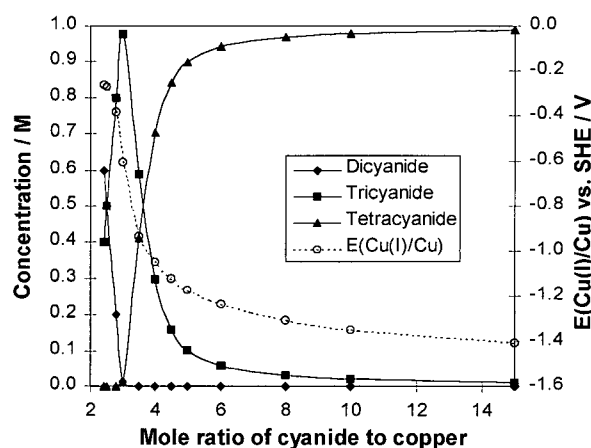
(d) $[Cu(I)]_{Total} = 1$ M, pH 9

Figure 3-1 Copper cyanide species distribution and E(Cu(I)/Cu) vs. mole ratio of cyanide to copper for various solutions at 25 °C and pH 9
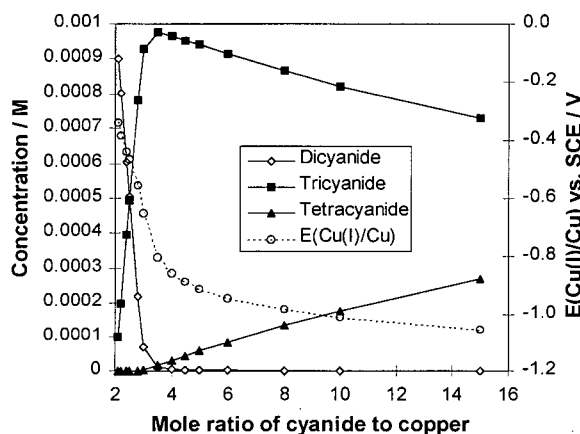
(a) $[Cu(I)]_{Total} = 0.001$ M, pH 12
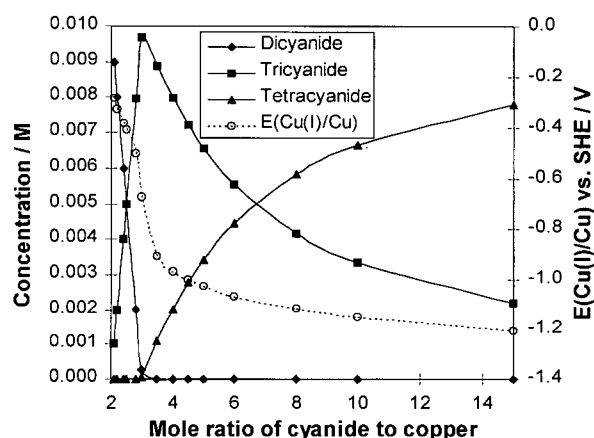
(b) $[Cu(I)]_{Total} = 0.01$ M, pH 12
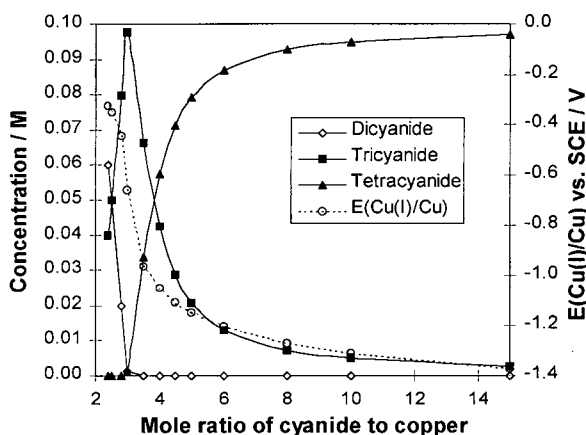
(c) $[Cu(I)]_{Total} = 0.1$ M, pH 12
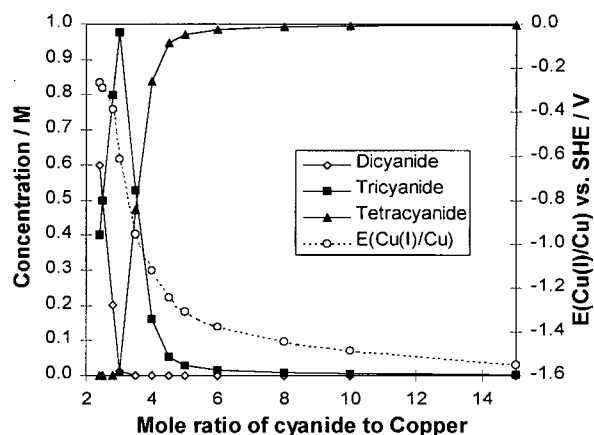
(d) $[Cu(I)]_{Total} = 1$ M, pH 12

Figure 3-2 Copper - cyanide species distribution and E(Cu(I)/Cu) vs. mole ratio of cyanide to copper for various solutions at 25 °C and pH 12.

Figure 3-3 shows the distribution of copper cyanide species vs. the mole ratio of cyanide to copper at 60 °C. Compared to Figure 3-2b and d (25 °C), at CN:Cu mole ratio < 3, the distribution of copper cyanide almost does not change. At a CN:Cu mole ratio > 3, the distribution shifts to lowly coordinated complexes to some extent with increasing temperature due to the decrease in the stability constants of copper cyanide complexes.

(a) [Cu(I)] = 0.01 M and pH 12   (b) [Cu(I)] = 1 M and pH 12
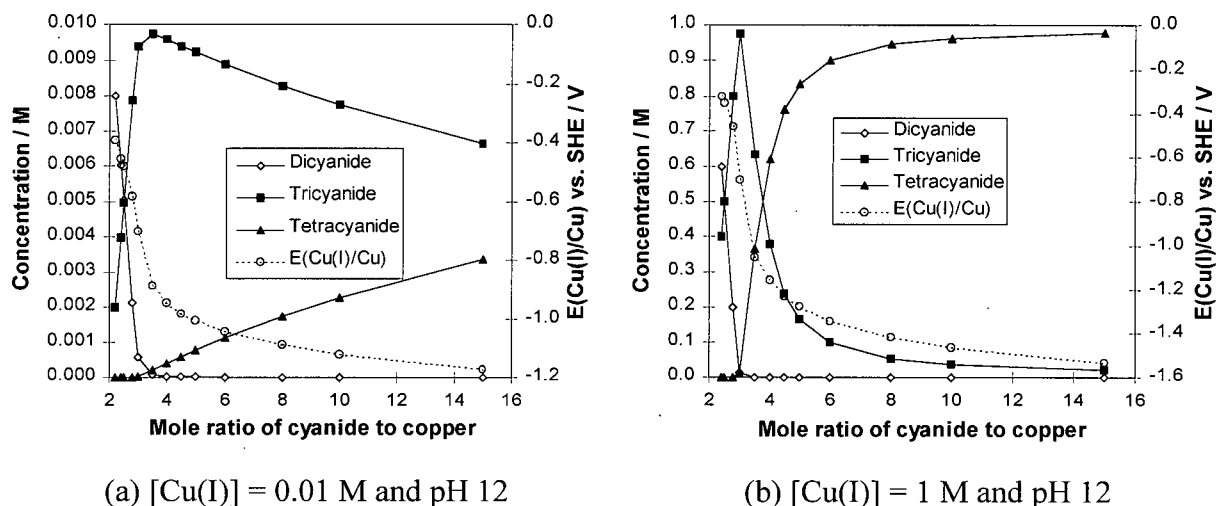
Figure 3-3 Copper cyanide species distribution and E(Cu(I)/Cu) vs. mole ratio of cyanide to copper for various solutions at 60 °C and pH 12

The redox potential for Cu(I)/Cu decreases with increasing ratio of total cyanide to copper and to some extent with increasing pH. From Figure 3-4 a, with increasing CN:Cu mole ratio, the redox potential for Cu^+/Cu decreases greatly at a CN:Cu mole ratio < 4 and decreases relatively slowly at a CN:Cu mole ratio > 4. At a CN:Cu mole ratio < about 3, the higher the total copper concentration, the higher the redox potential for Cu(I)/Cu. At a CN: Cu ratio ≅ 3, the redox potential is almost independent of the total copper concentration. At a CN:Cu mole ratio > about 3, the higher the total Cu^+ concentration, the lower the redox potential. Figure 3-4 b shows the redox potential for Cu(I)/Cu vs. pH at $[Cu(I)]_{Total}$ = 0.1 M and different CN:Cu mole ratios. The effect of pH on the redox potential depends on the CN:Cu mole ratio and pH range.

   -   Increasing pH is similar to increasing free cyanide concentration, because at a higher pH, less hydrogen ions compete for CN^- with copper to form HCN.
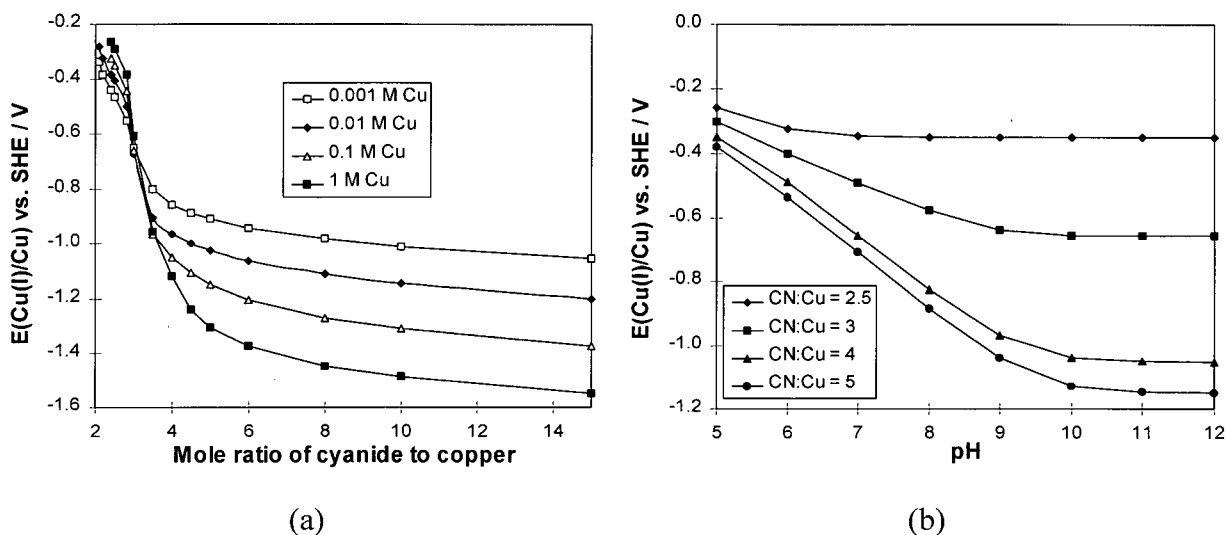
Figure 3-4 (a) E(Cu(I)/Cu) vs. mole ratio of cyanide to copper at 25 °C, pH 12 and different copper concentration and (b) E(Cu(I)/Cu) vs. pH at 25 °C, 0.1 M Cu and different mole ratios of cyanide to copper

In the direct electrowinning process for copper depletion from solutions, the cyanide concentration is maintained at a constant value and the copper concentration changes due to copper cathodic deposition. For example, copper concentration decreases from 2 g L^{-1} (or 1 g L^{-1}) to 1 g L^{-1} (or 0.5 g L^{-1}) due to copper deposition on the graphite felt electrode and the cyanide concentration is kept at 2.445 g L^{-1} (or 1.228 g L^{-1}). Therefore it is necessary to know the distribution of copper cyanide species at a constant cyanide concentration and different copper concentrations. Figures 3-5 and 6 show the concentration distribution of copper cyanide species at [CN^{-}] = 0.09442 M (2.455 g L^{-1}) and 0.04721 M (1.228 g L^{-1}) respectively. From Figure 3-5, with decreasing total copper concentration from 2 to 1.2 g L^{-1}, the concentrations of dicyanide and tricyanide decrease. However, the tetracyanide concentration increases. The calculated redox potential for Cu(I)/Cu decreases quickly. With further decrease in the total copper concentration, all copper cyanide species decrease and the redox potential for Cu(I)/Cu decreases. A similar trend is shown in Figure 3-6.

The stability of the copper-cyanide solution depends not only on the ratio of total cyanide to copper, but also on the concentrations of total copper, pH and temperature. For example, the critical cyanide concentrations for stable solutions containing 1M Cu(I) are 2.8, 2.7, 2.6 and 2.5 M for 25, 40, 50 and 60 °C respectively, and if the cyanide concentrations are

lower than the above values, the product of the equilibrium [CN⁻] and [Cu⁺] will be larger than the Ksp of CuCN and CuCN would precipitate. The product of [Cu⁺] and [CN⁻] for 0.0021 M cyanide and 0.001 M copper solution is less than the Ksp of CuCN. Therefore the solution is stable. The lower the total cyanide concentration, the lower the critical mole ratio of cyanide to copper.
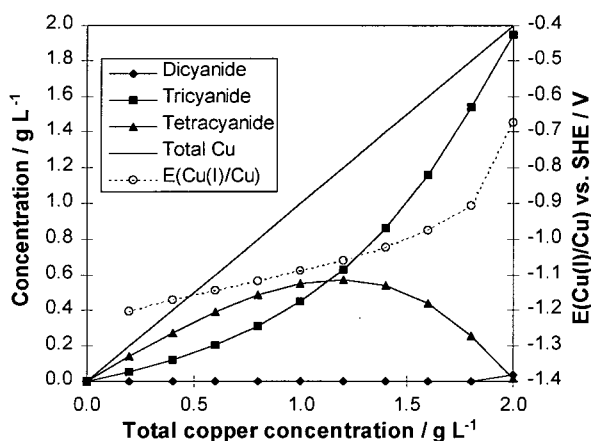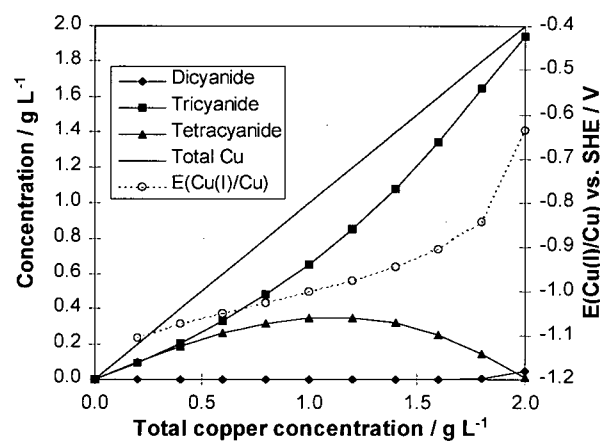
(a) 25 °C   (b) 40 °C

Figure 3-5 Copper concentrations in the form of copper complexes and the equilibrium potential vs. total copper concentration at [CN⁻] = 2.455 g L⁻¹ and [OH⁻] = 0.01 M.
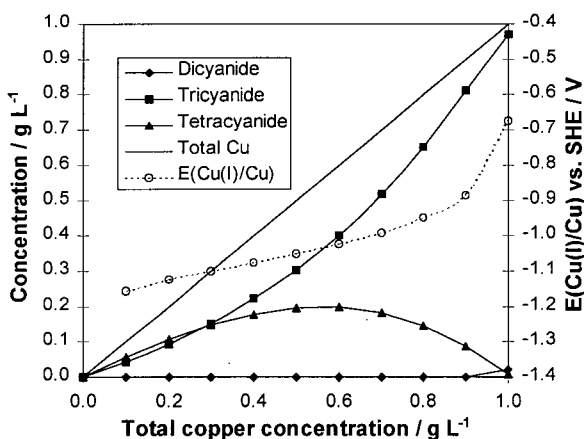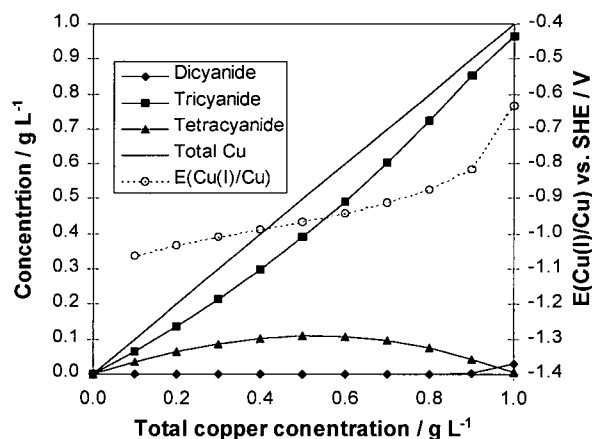
(a) 25 °C   (b) 40 °C

Figure 3-6 Copper concentrations in the form of copper complexes and the equilibrium potential vs. total copper concentration at [CN⁻] = 1.227 g L⁻¹ and [OH⁻] = 0.01 M.

3.2 The Equilibrium Potential Measurement of Copper Cyanide

The cuprous equilibrium potential can be expressed by Equation 3-3. The activity of the cuprous ion depends on the distribution of the cyanide copper species. Therefore E(Cu(I)/Cu) is a function of the copper cyanide association constants at constant temperature, pH, and the copper and cyanide concentrations. We can evaluate the validity of the calculated value using thermodynamic constants by comparing the calculated equilibrium potentials to the measured values for different compositions. It is very important to conduct the measurement of the equilibrium potentials. There are many varied reports on the potential measurement for the Cu(I)/Cu couple in copper cyanide solution [31, 32, 42, 46, 47] with different measuring methods and conditions. In this thesis, a few measurements of copper cyanide equilibrium potentials were made to confirm the calculated values in Section 3.1.

3.2.1 Experimental

Equipment: The copper cyanide solutions were placed in a 100-mL airtight water-jacketed electrolytic cell whose temperature was maintained at constant (± 0.2 °C) using a water bath circulator. The solutions were rendered free of oxygen by bubbling with highly pure argon gas which passed a FISHER OXICLEAR gas purifier to reduce oxygen to below 5 ppb. The copper electrode was a 2-mm diameter 99.999% pure copper wire which was first polished by silicon carbide sand, then washed with acetone and finally put in 0.01 M pure sodium cyanide solutions at pH 10 awaiting for use. A Solartron 1286 electrochemical interface was used to measure the potential between the copper wire and the saturated calomel reference electrode and the potential data over time were recorded by a computer. The experiment set-up is shown in Figure 3-7. The liquid junction potential, estimated by the Henderson equation (Appendix 7), is less than 2 mV and negligible.

Reagents: 99.99% sodium cyanide, 99.99% copper cyanide, standard 1 M NaOH solution and ultrapure deionized water were used to prepare the required copper cyanide solutions containing 0.01 M NaOH.
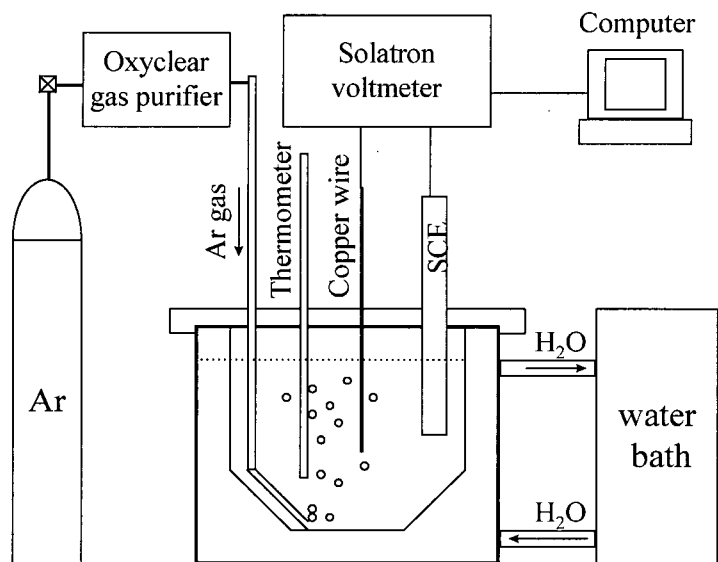
Figure 3-7 Experimental set-up for the equilibrium potential measurement

3.2.2 Results and Discussion

Any oxygen in the solution has a significant effect on the potential measurement. Figure 3-8 shows the electrode potential decreasing with continued Ar gas bubbling and stabilizing after 3 hours. In general, 3 hours were required to stabilize the potential and so the final value was taken after 3 hours. Figures 3-9 and 3-10 show both the calculated and measured potentials vs. the mole ratio of copper to cyanide at 25, 40, 50 and 60 °C for the solutions containing 0.1 M and 0.01M copper. At a CN:Cu mole ratio < 4, the measured potentials are a little higher than the calculated values and the differences between the measured and calculated potentials are in the range of 5-20 mV for 0.1 M and 10 - 25 mv for 0.01 M Cu. This difference might be caused by a trace amount of oxygen and the solution ionic strength or change in the concentration equilibrium constant. The exchange current for the lower concentration is lower than that for the higher concentration and may be easily affected by some factors such as oxygen and hydrogen ions. Therefore the difference for the solution containing 0.01 M Cu is larger than that for the solution containing 0.1 M Cu. At a CN:Cu mole ratio > 4, the difference between the calculated and measured potentials became larger. The reason could be that at 0.01 M OH⁻, the hydrogen potential is about 0.70 V vs. SHE and much higher than the potential for Cu(I)/Cu. Therefore the measured potential

might be a mixed potential. So using the measured potentials to evaluate or calculate the equilibrium constants may be inappropriate.

The equilibrium constants obtained by Rothbaum [42] and Hancock [46] using the potentials measured at CN:Cu mole ratio > 4 are less reliable in spite of the high overpotential of hydrogen on copper. The potential trend with CN:Cu mole ratio, total copper concentration and temperature is the same as that predicted by calculation. For example, at a CN:Cu mole ratio < 3, the potential decreases with increasing temperature and increases with increasing copper concentration. At a CN:Cu mole ratio = 3-4, the potential is less dependent on the temperature and concentration. At a CN:Cu mole ratio > 4, the potential increases with increasing temperature and decreases with increasing copper concentration.

The above dependence of the equilibrium potential for Cu(I)/Cu on the temperature and CN:Cu mole ratio is similar to those measured in 0.5 to 0.4 M Cu^+ solutions with CN:Cu mole ratio = 2.4 - 40 at 20 and 80 °C [42] and in 0.15 M Cu^+ solutions with CN:Cu mole ratio = 2.9 - 4.03 in the temperature range 10 to 50 °C [47]. From the above statements, it would appear that the use of the cited equilibrium constants to calculate the distribution of copper cyanide species will not result in a significant error.
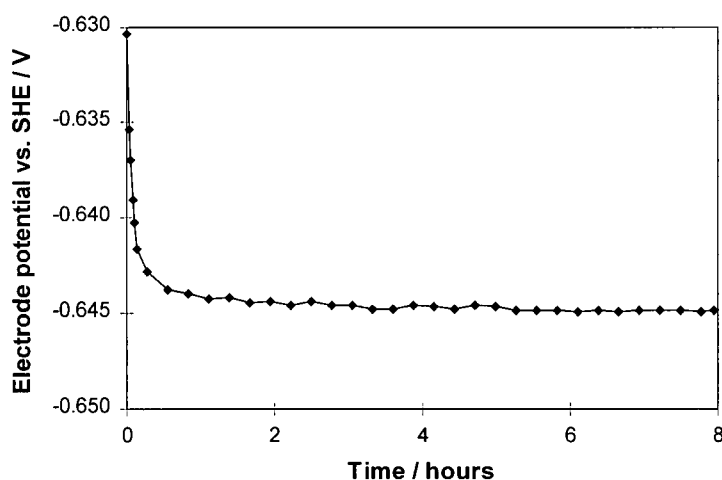
Figure 3-8 Electrode potential vs. time at 25 °C, CN:Cu mole ratio = 3 and $[Cu]_{total}$ = 0.1 M
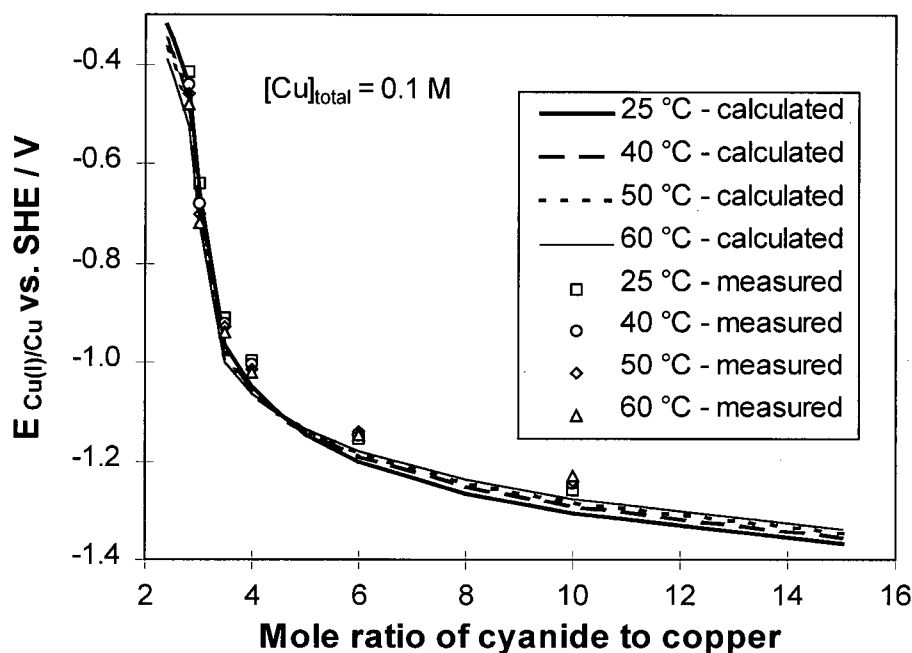
Figure 3-9 Electrode potential vs. the mole ratio of cyanide to copper at 25, 40, 50 and 60 °C, $[Cu]_{total}$ = 0.1 M and $[OH^-]$ = 0.01 M.
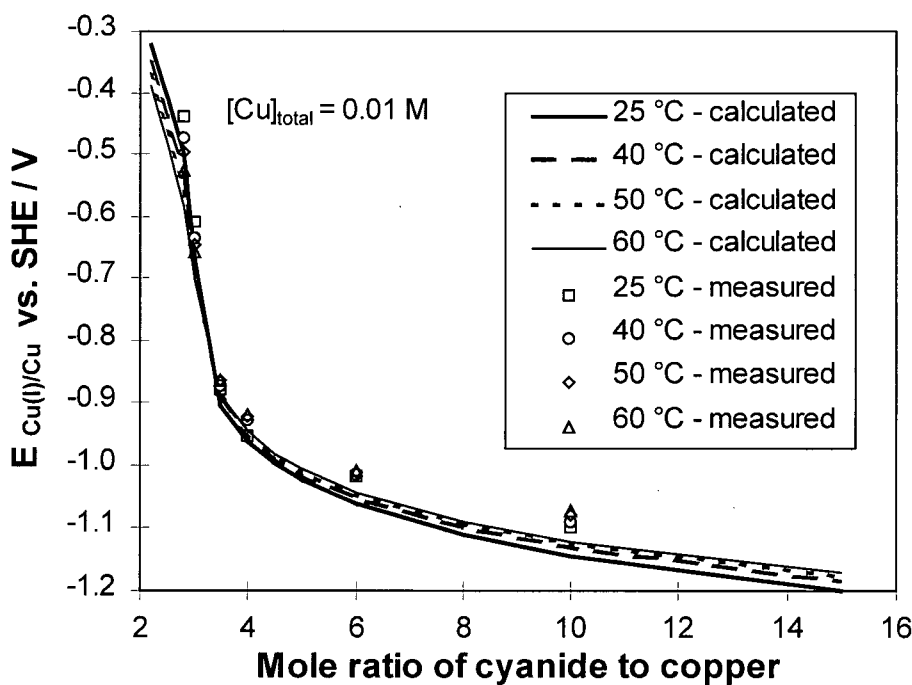
Figure 3-10 Electrode potential vs. the mole ratio of cyanide to copper at 25, 40, 50 and 60 °C, $[Cu]_{total}$ = 0.01 M and $[OH^-]$ = 0.01 M.

3.3 Potential-pH Diagrams for Copper Cyanide

In Section 3.1, the distribution of copper cyanide species has been discussed. However, since the stability of the copper cyanide species is related to the potential and pH, potential-pH diagrams are required to discuss the stability of the copper cyanide species. Potential-pH diagrams show which species are stable at a fixed species concentration, potential and pH. Because the stability of copper cyanide changes with concentration, the potential-pH diagrams for the different species concentrations should be used. The free energy data provided by Bard et al. [296] are thought to be the most reliable and therefore the free energy data for copper and cyanide are cited from this source. However, the data for copper dicyanide are questionable because its free energy was calculated from the stability constant (β_2) reported by Kappenstein and Hugel [48] which is only $10^{16.7}$ and much smaller than the formation constant (K_{sp}^{-1})(10^{20}) of CuCN. This value was discussed in Chapter 2 and considered to be unreliable. According to the free energy data of dicyanide and tricyanide reported by Bard et al. [296], $K_{2,3}$ is $10^{11.7}$, much larger than $10^{5.3}$ the value which is considered to be most reliable. Therefore in this study, the free energy data for dicyanide, tricyanide and tetracyanide have been calculated from the free energy data for Cu^+, CN^- and equilibrium constants ($\beta_2 = 10^{24}$, $K_3 = 10^{5.3}$ and $K_4 = 10^{1.5}$) of the copper cyanide complexes. The free energy data for all species are listed in Table 3-2.

Table 3-2 Gibbs free energy data for copper and cyanide species ($J\ mol^{-1}$) at 25 °C [38, 44, 49, 284]

Cu	Cu^+	Cu^{2+}	Cu_2O	CuO	$Cu(OH)_2$	$HCuO_2^-$
0	50,300	65,700	-148,100	-134,000	-359,500	-258,900
CuO_2^{2-}	H_2O	H^+	H_2	O_2	CN^-	HCN
-183900	-237178	0	0	0	166,000	113,423
CNO^-	HCNO	$(CN)_2$	CuCN	$Cu(CN)_2^-$	$Cu(CN)_3^{2-}$	$Cu(CN)_4^{3-}$
-98700	-12,100	296,300	102,126	245,291	381,035	538,471

On the basis of the change in Gibbs free energy, CuO is more stable than $Cu(OH)_2$. However, $Cu(OH)_2$ may exist or coexist with CuO. Therefore both CuO and $Cu(OH)_2$ are considered in potential-pH diagrams. Figure 3-11 shows the potential-pH diagram for the $CN-H_2O$ system assuming that CN^-, CNO^-, HCN, HCNO and $(CN)_2$ are stable, although all of them are not stable. In the high potential range, CN^- and HCN are not stable and are oxidized

in accordance with thermodynamics. However, HCN and CN⁻ are metastable and the potentials for the oxidation of HCN and CN⁻ are much higher (1.0-1.2 V) than those shown in Figure 3-11. Therefore CN⁻ and HCN are considered to be stable in the Cu-CN-H_2O potential-pH diagram. Figures 3-12 and 13 show the Cu-CN-H_2O potential-pH diagrams at the activities of all of the solute species = 1, 10^{-2}, 10^{-4} and 10^{-6} assuming CuO, Cu(OH)$_2$ and CN⁻ are stable. From these two diagrams, at the activities of all of the solute species = 1, CuCN, Cu(CN)$_3^{2-}$ and Cu(CN)$_4^{2-}$ are stable in the three regions. At the activities of all of the solute species = 0.01 and 0.0001, CuCN, Cu(CN)$_2^-$ and Cu(CN)$_3^{2-}$ are stable in the three pH regions. At the activities of all of the solute species = 0.000001, only CuCN and Cu(CN)$_2^-$ are stable. From Figure 3-14, at the activities of the copper solute species = 0.01 and the activities of cyanide species = 0.1, all copper cyanide species are stable in their corresponding pH regions. Copper cyanide species are stable in certain potential and pH regions. With increasing potential, copper cyanide will be oxidized to Cu^{2+}, CuO (Cu(OH)$_2$) and CuO$_2^-$. Cyanide can also be oxidized to cyanate from Figure 3-11. Copper cyanide complexes can be oxidized to copper oxide and cyanate from the point of view of thermodynamics.

(a)   (b)
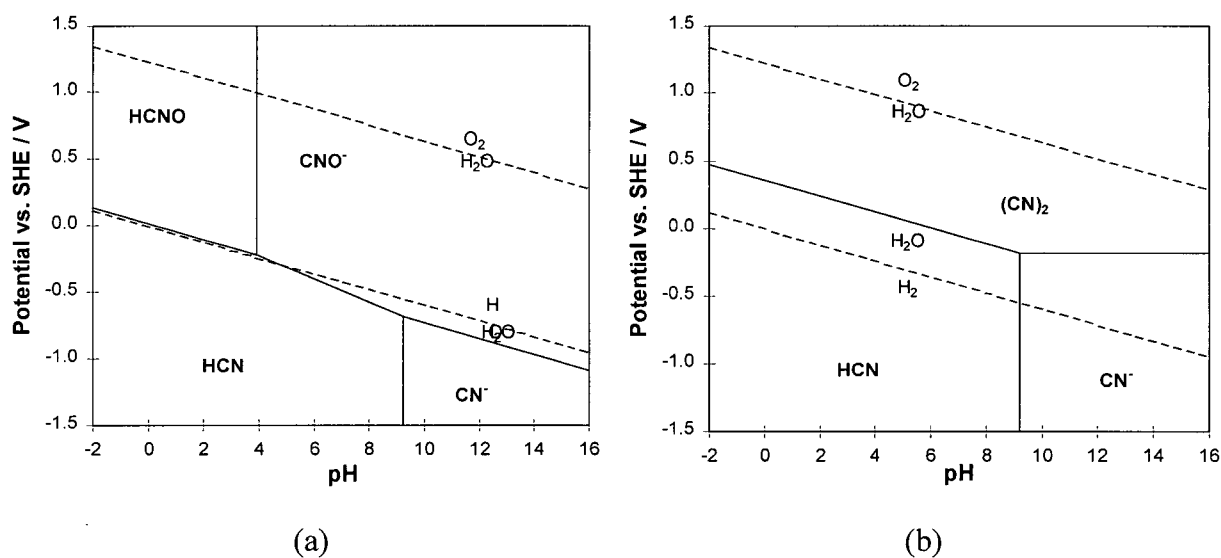
Figure 3-11 CN-H_2O potential-pH diagram at all solute species activities of 1 and P$_{(CN)2}$ = 1 atm and 25 °C. (a) assuming HCNO and CNO⁻ are stable and (b) assuming (CN)$_2$ is stable.
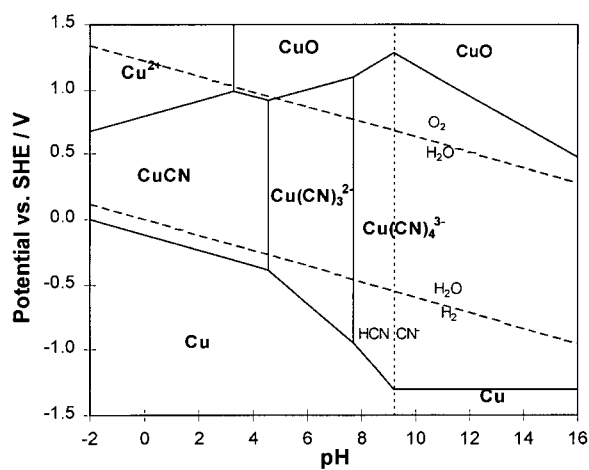
(a) Solute species activities = 1
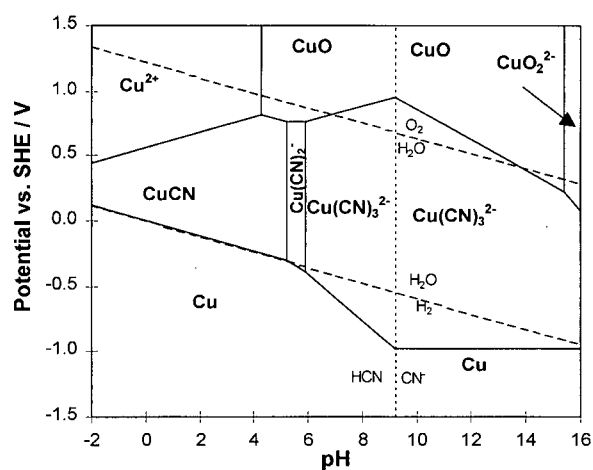
(b) Solute species activities = 10^{-2}
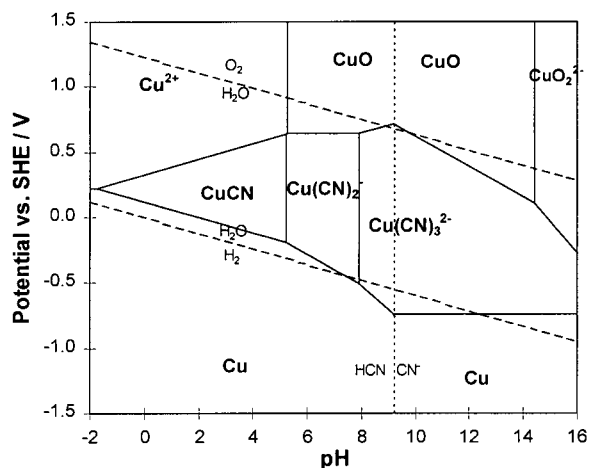
(c) Solute species activities = 10^{-4}
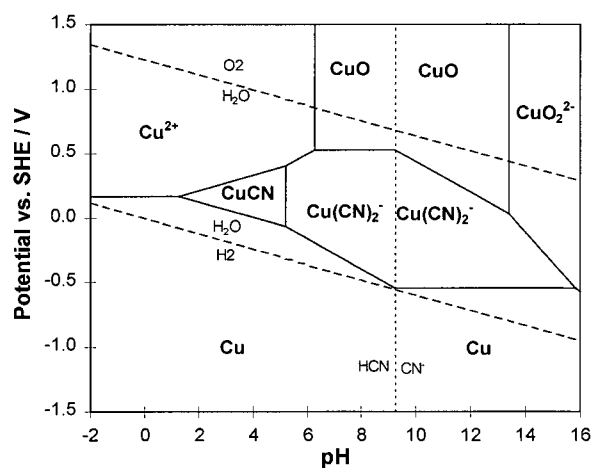
(d) Solute species activities = 10^{-6}

Figure 3-12 Potential-pH diagrams for Cu-CN-H_2O system at 25 °C and the activities of all solute species = 1, 10^{-2}, 10^{-4} and 10^{-6} considering CuO as a stable species. HCNO, CNO⁻ and $(CN)_2$ are not considered.
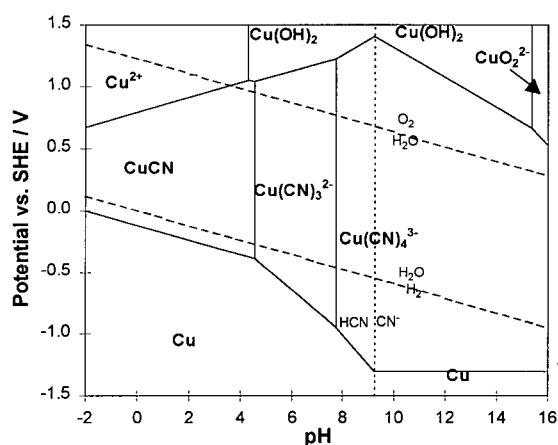
(a) Solute species activities = 1
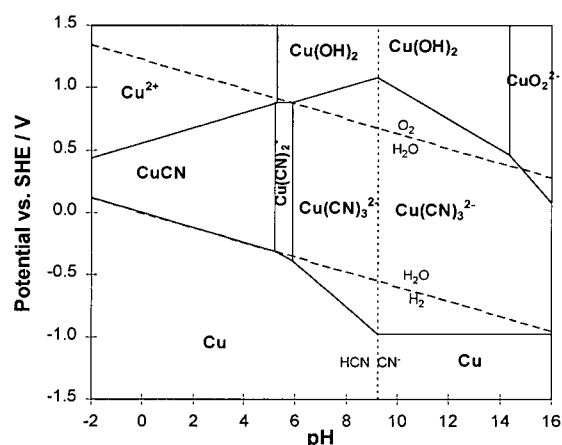
(b) Solute species activities = 10^{-2}
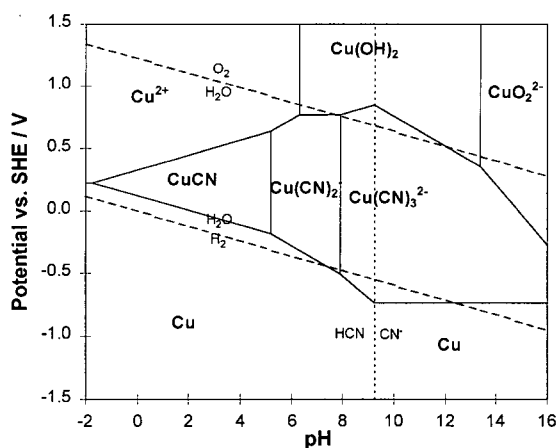
(c) Solute species activities = 10^{-4}
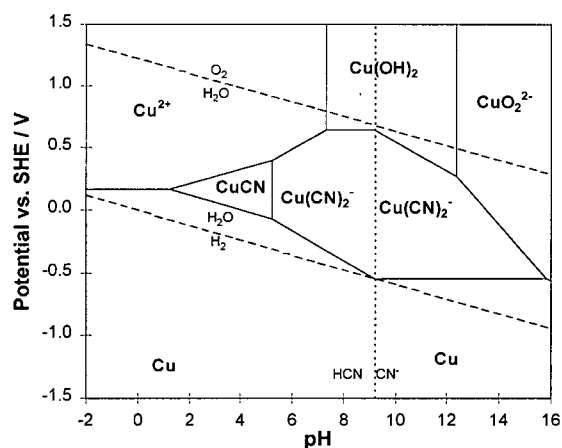
(d) Solute species activities = 10^{-6}

Figure 3-13 Potential-pH diagrams for Cu-CN-H_2O system at 25 °C and the activities of all solute species = 1, 10^{-2}, 10^{-4} and 10^{-6} considering Cu(OH)$_2$ as a stable species. HCNO, CNO$^-$ and $(CN)_2$ are not considered.
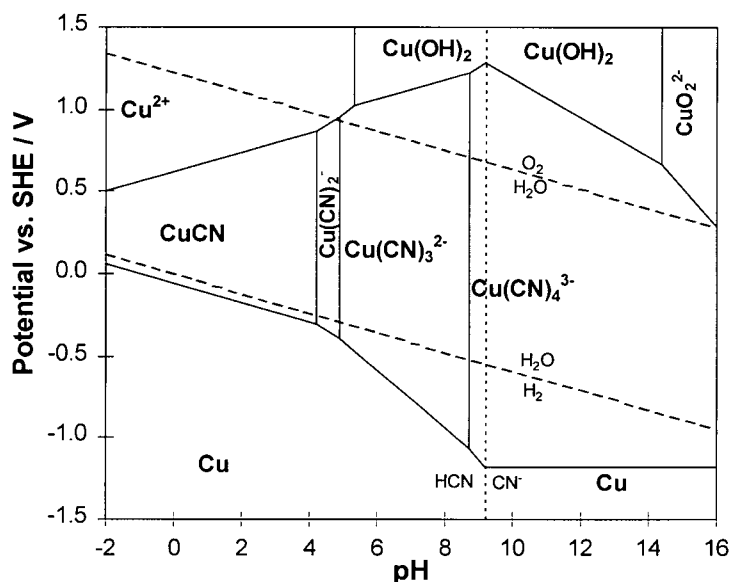
Figure 3-14 Potential-pH diagram for Cu-CN-H$_2$O system at 25 °C and solute copper species activities of 0.01 and cyanide species activities of 0.1 considering Cu(OH)$_2$ as a stable species. HCNO, CNO⁻ and (CN)$_2$ are not considered.

3.4 Summary

The distributions and equilibrium potentials of copper cyanide species are functions of the mole ratio of cyanide to copper, total cyanide concentration, pH and temperature. With increasing CN:Cu mole ratio, the distribution of copper cyanide species shifts more completely to the highly coordinated complex (Cu(CN)$_4^{3-}$) at a high cyanide concentration than that at a low cyanide concentration. The equilibrium potential for Cu(I)/ Cu decreases with increasing CN:Cu mole ratio. Increasing pH is similar to increasing free cyanide concentration. Increasing temperature results in decreasing stability constants. Therefore the distribution of copper cyanide shifts to the lowly coordinated complexes. The potential measurements have confirmed the validity of the calculated results. In the pH -potential diagrams, CuCN, Cu(CN)$_2^-$, Cu(CN)$_3^{2-}$ and Cu(CN)$_4^{3-}$ can predominate in the different pH regions. From the above discussion, it is expected that Cu deposition current efficiency decreases with increasing CN:Cu mole ratio and increases with increasing temperature. The change in the distribution of copper cyanide may affect its anodic behaviour.

4. ELECTRODEPOSITION OF COPPER ON GRAPHITE FELT FROM DILUTE CYANIDE SOLUTIONS

Porous 3-dimensional electrodes such as carbon felt and cloth, reticulated vitreous carbon and metal mesh are being used increasingly in electrochemical processing due to their high area per unit electrode volume and their moderately high mass transport characteristics. One of their applications is to recover and remove metals from dilute waste water because 2-dimensional electrodes (e. g. planar) are inefficient for this application [297-315]. No careful study on the electrodeposition of copper from dilute cyanide solution has been reported [22-25].

In this chapter, a careful study of direct electrowinning of Cu on a graphite fibre electrode is reported. Copper complexed with cyanide is much more difficult to deposit from dilute solution. Especially when the CN:Cu mole ratio is high, the equilibrium potential for the Cu(I)/Cu couple is much lower than the equilibrium potential for H^+/H_2 and so hydrogen evolution will significantly decrease the current efficiency. Graphite fibre has a high surface area, giving a maximum plating area for copper deposition and minimizing the overpotential for copper plating and the concentration polarization. Graphite also has a relatively high overpotential for hydrogen evolution which should maximize the current efficiency of copper deposition in the initial deposition stage. Therefore in this study, graphite fibre felt was used as the porous cathode.

4.1 Some Fundamental Aspects of Graphite Fibre Electrodes

Figure 4-1 shows the schematic diagram of a one-dimensional porous electrode. The electrochemical reaction takes places in the porous electrode. A consequence of electroneutrality is that the charge is conserved between the porous electrode matrix and pore-solution phases. The following equation must be applied:

$$I_s + I_l = 0 \tag{4-1}$$

where I_s is the matrix current density and I_l the solution current density.
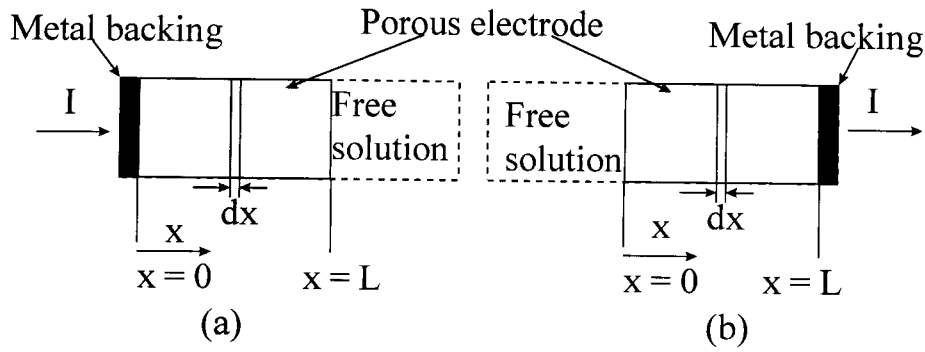
Figure 4-1 Schematic diagram of porous electrode

In the porous electrode, at x = x, the potential difference (Φ) between the solid phase (Φ_s) and the solution phase (Φ_l) is Φ_s -Φ_l. The increase in Φ (dΦ) due to the increase in the distance (dx) is:

$$d\Phi = d(\Phi_s - \Phi_l) = d\Phi_s - d\Phi_l = \frac{I_s}{\sigma}dx - \frac{I_l}{\kappa}dx \tag{4-2}$$

where σ is the effective conductivity of the solid phase and κ the effective conductivity of the solution. From Equation 4-2, the following equation can be derived:

$$\frac{I_s}{\sigma} - \frac{I_l}{\kappa} = \frac{d\Phi}{dx} \tag{4-3}$$

The increase in the solid phase (dI$_s$) or the liquid phase (dI$_l$) is due to the electrochemical reaction on the interface between the solid phase and the solution. Therefore we have:

$$dI_s = -dI_l = \mp aidx \tag{4-4}$$

where a is the specific area (m^2/m^3), i the local Faradaic current density of the electrochemical reaction on the surface (A m^{-2}) (negative for the cathodic process and positive for the anodic process) and the sign - for Figure 4-1a and the sign + for Figure 4-1b. From Equation 4-4, the following equation can be derived:

$$\frac{dI_s}{dx} = -\frac{dI_l}{dx} = \mp ai \tag{4-5}$$

From Equations 4-3 and 4-5, we have the following equation:

$$\frac{d^2\Phi}{dx^2} = \mp a(\frac{1}{\sigma} + \frac{1}{\kappa})i \tag{4-6}$$

In the case of copper deposition from cyanide solutions, the following equation can be applied:

$$i = i_{Cu} + i_H \tag{4-7}$$

$$\frac{dC_{Cu}}{dx} = \mp \frac{a i_{Cu}}{F} \tag{4-8}$$

where i the local Faradaic current density on the electrode surface, i_{Cu} copper deposition current density (A m^{-2}), i_H the hydrogen evolution current density (A m^{-2}) and C_{Cu} the copper concentration (M). The overpotential (η) can replace Φ because Φ can be expressed as (η + const.).

From the above equations, the distributions of the potential and current are non-uniform due to the resistivities of the fibre and the electrolyte. In the case of the copper deposition, the driving force ($| \Phi_s - \Phi_l |$) of copper deposition decreases locally to a value so low that copper deposition stops. In order to remove more copper, the potential difference must be increased. However, this may result in more hydrogen evolution and lower copper current efficiency. Significant hydrogen evolution can block the electrolyte from the fibre, stop copper deposition and dramatically increase the effective resistivity of the electrolyte.

Zamyatin and Bek [310] studied the effect of hydrogen evolution on gold deposition in graphite fibre felt and found that the current efficiency decreased with increasing total current (potential difference) and the deposition rate of gold first increased to a maximum value and decreased with increasing current due to hydrogen evolution. The copper deposition also depends on the electrolyte composition, temperature and flow rate (mass transfer). The maximum potential difference between the fibre and the electrolyte or the maximum current is selected by experiment with reference to the electrolyte composition and temperature. The thickness of the fibre electrode is determined by the desired extent of copper removal from the electrolyte and the maximum potential difference between the fibre and the electrolyte [297]. Beyond a certain thickness, the electrode simply adds a barren zone where no copper deposition will take place.

In the case of plating, supporting electrolytes are used to increase the conductivity to obtain a uniform copper deposition. For example, Bek and Zerebilov [125] deposited a thin layer of copper on carbon fibres using 0.01 M Cu$^+$ + 0.03 M CN$^-$ solution containing 1 M Na$_2$SO$_4$ and 0.5 M Na$_2$SO$_3$ as supporting electrolytes.

Mass transfer in graphite fibre felt is important to be able to predict the effect of flow rate (velocity) on copper deposition efficiency. There are several reports on the mass transfer

in graphite fibre [316-320]. Bek and Zamyatin [316] reported the following relations for flow-through fibre with 10 μm diameter:

$$k_m = 1.90 \times 10^{-2} u^{0.352} \quad (0.02 < Re < 0.15) \tag{4-9}$$

where k_m is the mass transfer coefficient(cm s^{-1}), u the velocity of the liquid (cm s^{-1}), Re the Reynolds number (ud/v), d the fibre diameter (cm) and v the kinematic viscosity (cm^2 s). Transformed into dimensionless form, Equation 4-7 reads

$$Sh = 6.1 Re^{0.352} \quad (0.02 < Re < 0.15) \tag{4-10}$$

where Sh is the Sherwood number (k_m d/D) and D the diffusion coefficient.

Schmal et al. [318] gave the following relation for the single fibre with 8-μm diameter:

$$Sh = 7 Re^{0.4} \quad (0.04 < Re < 0.2) \tag{4-11}$$

The above relation was consistent with the results derived from heat transfer. The Sh value for flow parallel to the fibre is 40 % lower than that for flow perpendicular to the fibre.

Kinoshita and Leach [317], Vatistas et al. [319] and Carta et al. [320] studied the mass transfer for flow-by fibre felts and their Sh numbers are smaller than that for the flow-through fibre reported by Bek and Zamyatin [316].

The compression of fibre felt also significantly changes its conductivity which depends primarily on the contact resistance between fibres. The degree of matrix compression is accounted for by the change in porosity and the matrix conductivity can be calculated approximately by the correlation [321]:

$$\sigma = 10 + 2800(1 - e/e_0)^{1.55} \text{ (S m}^{-1}) (0.68 < e/e_0 < 1 \text{ at } 20 \text{ °C}) \tag{2-12}$$

where e is the porosity of the matrix and e_0 the initial porosity of the matrix.

The conductivity of a typical aqueous electrolyte falls in the range 1 - 100 S m^{-1}. Therefore the degree of matrix compression has a significant effect on the potential distribution. Matrix compression also changes the specific electrode surface, and when the reaction is mass-transfer controlled, the compression affects the local current density by the relation of the mass transfer coefficient to the porosity [317].

Metal deposition also significantly increases the conductivity and the specific surface area of the fibre matrix and decreases the porosity of the fibre matrix. The current and potential distributions change with time.

4.2 Experimental

4.2.1 Electrolytic Cell and Experimental Set-up

Generally the main types of flow for porous electrodes are flow-through and flow-by. Flow-through was employed for this study, i.e. the flow in the fibre felt is parallel to the current flow. The graphite fibre felt supplied by the National Electric Carbon Co. has a specific surface area of 0.7 m^2 g^{-1} and a porosity of 96.5 %. SS316 stainless steel mesh was used to fix the fibre felt on two sides and conduct electricity to the fibre. Except for electrical contact parts, the stainless steel mesh was painted. The superficial cathode surface area was 12 cm^2. The catholyte was separated from the anolyte by a Du Pont Nafion 450 membrane to prevent the anodic oxidation of cyanide. The anodes were nickel sheet for oxygen evolution and TIR2000 (Ir and Ta coated titanium) for chlorine evolution and their surfaces were 6 cm^2. The electrolytic cell consisted of two parts of polycarbonate which were connected by screws and sealed by rubber. Figure 4-2 shows the schematic diagram of cell.

To start an experiment, approximately 18 liters of electrolyte in a container were preheated to about 40 °C using a water bath and then pumped to the electrolytic cell using a Cole-Parmer pump Model 7519-20A equipped with a digital variable-speed console drive for precise uniform flow rate control. The electrolytic cell was put in a water bath to maintain the electrolyte temperature at 40 °C. After the electrolyte had passed through the cell, it was pumped to a container in order to maintain a uniform flow rate. Two tubes and pumps were used to add NaOH and NaCl and circulate the anolyte. Figure 4-3 shows the schematic diagram of electrolyte flow. A coulometer was used to record the amount of charge consumed. In the case of chlorine evolution, a Bach-Simpson Ltd. PHM82 standard pH meter was used to monitor the pH of the anolyte, keeping it above 4 and avoiding the significant migration of hydrogen ions through the membrane.

A Jenway Model 5310 conductivity meter was used to measure the conductivity of the electrolyte which was placed in a 100 mL tube whose temperature was controlled by a water bath. The copper concentration in the solution was analyzed by atomic absorption and the cyanide concentration was analyzed using distillation-absorption-titration method (see

Appendix 2). The copper deposited in the graphite felt was dissolved in nitric acid and analyzed by atomic absorption.
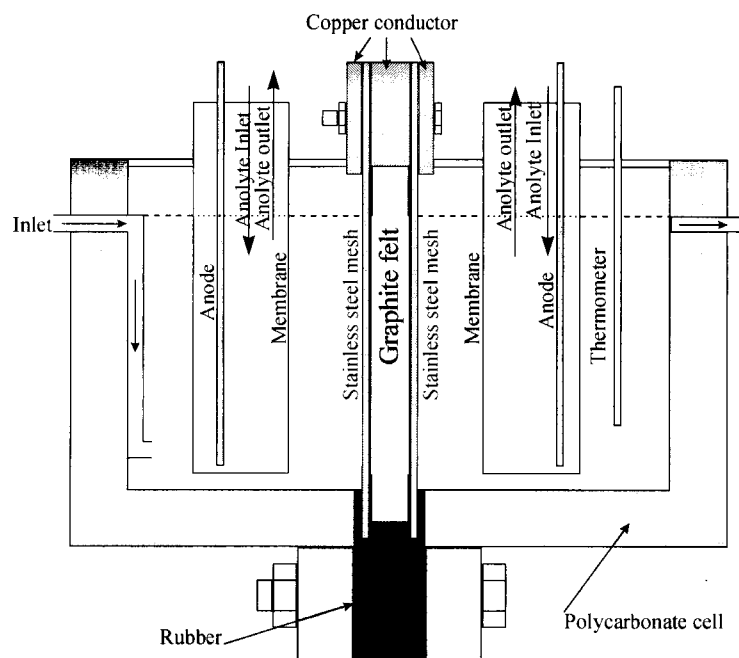
Figure 4-2 Schematic diagram of electrolytic cell (size: 18(H)×13(L)×12(W) cm)
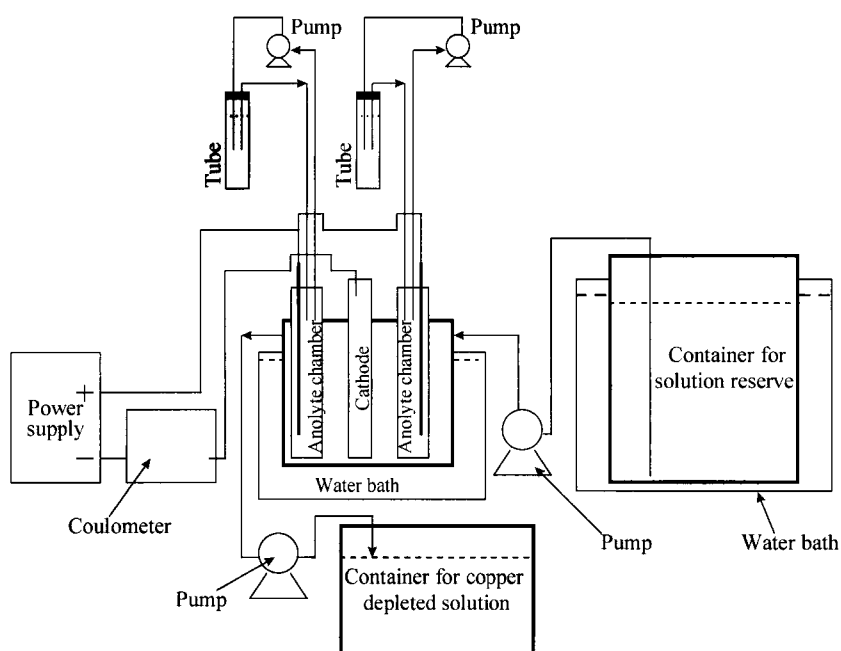
Figure 4-3 Schematic diagram of experimental set-up

4.2.2 Materials

Reagent grade sodium cyanide, copper cyanide, sodium hydroxide, sodium thiocyanate and sodium chloride were used to prepare the required synthetic solutions. Solid sodium cyanide and copper cyanide were analyzed prior to preparation of the solutions to ensure that the required compositions were achieved.

4.3 Results and Discussion

The conductivity of dilute copper cyanide solutions is expected to be low and this low conductivity significantly affects the potential and current distribution. The conductivity was therefore measured. The results are listed in Table 4-1. The conductivity is very low and will affect the potential distribution resulting in nonuniform copper deposition. From Equation 4-12, the approximate conductivities of graphite fibre felt are 10, 37, 89, 158, 241, 336 and 443 S m^{-1} respectively for 0, 5, 10, 15, 20, 25, 30 % compression. In order to increase the conductivities of the graphite felt and decrease the potential difference in the graphite felt, the compression of the graphite felt should be increased. The compression of the graphite felt also increases the specific surface area. However, when the graphite felt is compressed to some degree, the conductivity of the graphite felt is much larger than that of the solution and the further compression will not significantly affect the potential and current distribution according to Equation 4-12. If the compression is too high, the porosity becomes low and the amount of the deposited copper per unit volume becomes low. The compression mainly affects the deposition of copper when the deposition begins. When a certain amount of copper is deposited in the graphite felt, the contact resistivity between the fibres becomes negligible and the conductivity of the graphite felt becomes much higher. Therefore the selection of the degree of the compression is important. In the preliminary test, at a low mole ratio of cyanide to copper (e.g. 3), the compression had less effect on the current efficiency. At a high mole ratio of cyanide to copper, the compression had a significant effect on the current efficiency.

The reasons are: at a low mole ratio of cyanide to copper, copper is easily deposited on the graphite and then significantly increases the conductivity of the graphite and improves the surface condition. At a high mole ratio of cyanide to copper, copper is difficult to deposit

on the graphite and hydrogen evolution is dominant and the conductivity of the graphite felt does not improves greatly with time. From these tests, 25% of compression is required to get an acceptable and reproducible current efficiency. Therefore, 25% of compression was used for all the experiments. In the dilute solutions discussed, the migration of copper cyanide complexes is important, resulting in a decrease in the mass transfer toward the cathode. Also the effect of the diffuse double layer can decrease the reduction of copper complexes due to their negative charge when the potential is well below the zero-charge potential.

Table 4-1 Conductivities of copper cyanide solutions with different CN:Cu mole ratios at fixed Cu concentrations (unit: S m^{-1})*

[Cu] / g L^{-1}	Temp. (°C)	CN:Cu = 3	CN:Cu = 3.5	CN:Cu=4	CN:Cu=4.5
2	25	1.105	1.241	1.375	1.512
2	40	1.410	1.588	1.769	1.955
1	25	0.703	0.788	0.873	0.952
1	40	0.902	1.002	1.121	1.220

*[NaOH] = 0.01 M, [NaCNS] = 0.01724 and 0.00862 M respectively for 2 and 1 g L^{-1} Cu.

Copper deposition on graphite fibre was first conducted in an undivided cell in an attempt to use the anodic oxidation of thiocyanate to prevent the cyanide oxidation. However, the thiocyanate did not protect against the anodic oxidation of cyanide and the anodic oxidation current efficiency was around 100%. Therefore the catholyte was separated from the anolyte by a Du Pont Nafion 450 membrane. The anolytes were 5 M NaOH and 5 M NaCl respectively for the oxygen and chlorine evolution experiments. The current efficiency of copper deposition and the conductivities of the solution are expected to increase with increasing solution temperature. Operating copper deposition at elevated temperatures needs heating a large volume of dilute solution, resulting in significant energy consumption. However, operating at a low temperature results in a low current efficiency which increases the power consumption. A temperature range of 25-40 °C was selected for the investigation. The velocity of flow used was in the range 3-10 cm min.$^{-1}$ and the estimated mass transfer coefficient is in the range 0.55 to 1.01 ×10^{-2} cm s^{-1} according to Equation 4-10. In all the experiments, the total cyanide concentration did not change after electrowinning and the amount of the deposited copper matched closely the change of the copper concentration in the solution.

The results of copper deposition and energy consumption for oxygen evolution as anode reaction are listed in Table 4-2 (initial copper concentration = 1 g L^{-1}) and Table 4-3 (initial copper concentration = 2 g L^{-1}). In the case of chlorine evolution, the cell voltages are 0.78, 0.57 and 0.41 V higher than those in the case of oxygen evolution respectively for 30, 60 and 100 A m^{-2} and the other results are the same.

Table 4-2 Copper cathodic current efficiency and energy consumption at 40 °C and initial [Cu] = 1 g L^{-1} for experiments with oxygen evolution at anode

CN:Cu	3	3.5	4	4.5	3	3.5	4	4.5	3	3.5	4	4.5
Current Density / Am^{-2}	30	30	30	30	60	60	60	60	100	100	100	100
Flow velocity / cm $min.^{-1}$	2.97	2.97	2.97	2.97	5.93	5.93	5.93	5.93	9.83	9.83	9.83	9.83
$[Cu^+]$ / g L^{-1} (1)*	0.713	0.837	0.905	0.925	0.740	0.877	0.950	0.978	0.778	0.902	0.956	0.980
$[Cu^+]$ / g L^{-1} (2)**	0.686	0.767	0.868	0.900	0.725	0.823	0.919	0.970	0.751	0.864	0.948	0.975
C.E. / % (average)	64.2	40.0	22.4	22.0	57.4	38.6	23.2	19.6	47.0	30.8	11.7	7.5
Cell voltage / V	2.64	2.65	2.63	2.56	3.66	3.64	3.52	3.42	5.01	4.85	4.62	4.60

* The samples were taken after the solution passed the cell in the middle course of the experiments.
** The samples were taken after the solution passed the cell at the end of the experiments.

Table 4-3 Copper cathodic current efficiency and energy consumption at 40 °C and initial [Cu] = 2 g L^{-1} for experiments with oxygen evolution at anode

CN:Cu	3	3.5	4	4.5	3	3.5	4	4.5	3	3.5	4	4.5
Current Density / Am^{-2}	30	30	30	30	60	60	60	60	100	100	100	100
Flow velocity / cm $min.^{-1}$	2.97	2.97	2.97	2.97	5.93	5.93	5.93	5.93	9.83	9.83	9.83	9.83
$[Cu^+]$ / g L^{-1} (1)*	1.663	1.703	1.845	1.849	1.667	1.708	1.810	1.856	1.672	1.788	1.920	1.950
$[Cu^+]$ / g L^{-1} (2)**	1.612	1.658	1.712	1.741	1.633	1.661	1.767	1.800	1.642	1.708	1.82	1.86
C.E. / % (average)	88.6	69.4	42.9	37.6	84.4	58.4	38.0	31.6	80.6	47.4	23.2	18.0
Cell voltage / V	2.17	2.28	2.30	2.15	2.91	2.94	2.89	2.82	3.81	3.64	3.63	3.56

* The samples were taken after the solution passed the cell in the middle course of the experiments.
** The samples were taken after the solution passed the cell at the end of the experiments.

From Figure 4-4, with increasing CN:Cu mole ratio, the current efficiency decreases significantly and the energy consumption increases significantly. This is due to the fact that the lowly coordinated copper cyanide complexes (dicyanide or tricyanide is electroactive species) and the calculated equilibrium potential for Cu(I)/Cu redox couple decreased with increasing CN:Cu mole ratio (see Table 4-4). The exchange current is expected to decrease

with increasing mole ratio of cyanide to copper. The low concentration of electroactive species and the low exchange current result in a high polarization at a fixed current. Therefore at a high mole ratio of cyanide to copper, hydrogen evolution is dominant and decreases the current efficiency significantly.

Table 4-4 Distribution and potentials of copper cyanide at [OH⁻] = 0.01 M at 40 °C

[Cu] / g L^{-1}	Species & potential	CN:Cu = 3	CN:Cu = 3.5	CN:Cu = 4	CN:Cu = 4.5
1	$Cu(CN)_2^-$	3.00 %	0.17 %	0.08 %	0.05 %
	$Cu(CN)_3^{2-}$	96.51 %	92.01 %	85.30 %	79.34 %
	$Cu(CN)_4^{3-}$	0.49 %	7.82 %	14.62 %	20.61 %
	$E_{Cu(I)/Cu}$ vs. SHE / V	-0.632	-0.851	-0.907	-0.941
2	$Cu(CN)_2^-$	2.30 %	0.09 %	0.04 %	0.02 %
	$Cu(CN)_3^{2-}$	97.06 %	86.95 %	76.47 %	67.86 %
	$Cu(CN)_4^{3-}$	0.64 %	12.96 %	23.49 %	32.11 %
	$E_{Cu(I)/Cu}$ vs. SHE / V	-0.656	-0.878	-0.937	-0.974

When the ratio of the current to the flow rate was maintained constant, the current efficiency decreased with increasing current and flow rate, suggesting that the effect of flow rate on mass transfer and on current efficiency was lower than that of the current density. This phenomenon becomes more apparent when the ratio of cyanide to copper is high. The reasons are: (1) the mass transfer coefficient in graphite felt is only proportional to (flow rate)$^{0.4}$ from Equations 4-9 to 4-11. Therefore the increase in the mass transfer does not match the increase in the current density, resulting in higher concentration polarization and hence low current efficiency; (2) the charge transfer coefficient for hydrogen evolution (e.g. about 0.45 [113]) is larger than that for copper deposition (0.1 [116] or 0.38 [110]). Therefore the increase in the current density possibly results in more increase in the current density for hydrogen evolution than that for copper deposition. At a high mole ratio of cyanide to copper, the hydrogen evolution is a dominant reaction and the mass transfer has less effect on the current efficiency of copper deposition. The increase in the current results in significant hydrogen evolution and hydrogen bubbles could block the solution from contacting the graphite, resulting in a significant decrease in the current efficiency and the effective conductivity of the solution, giving a high energy consumption.

Due to the above dependence of current efficiency on CN:Cu mole ratio and current density, the conversion of Cu (I) to Cu decreases with increasing CN:Cu mole ratio and increasing current density at a fixed ratio of current density to flow velocity (Figure 4-5).
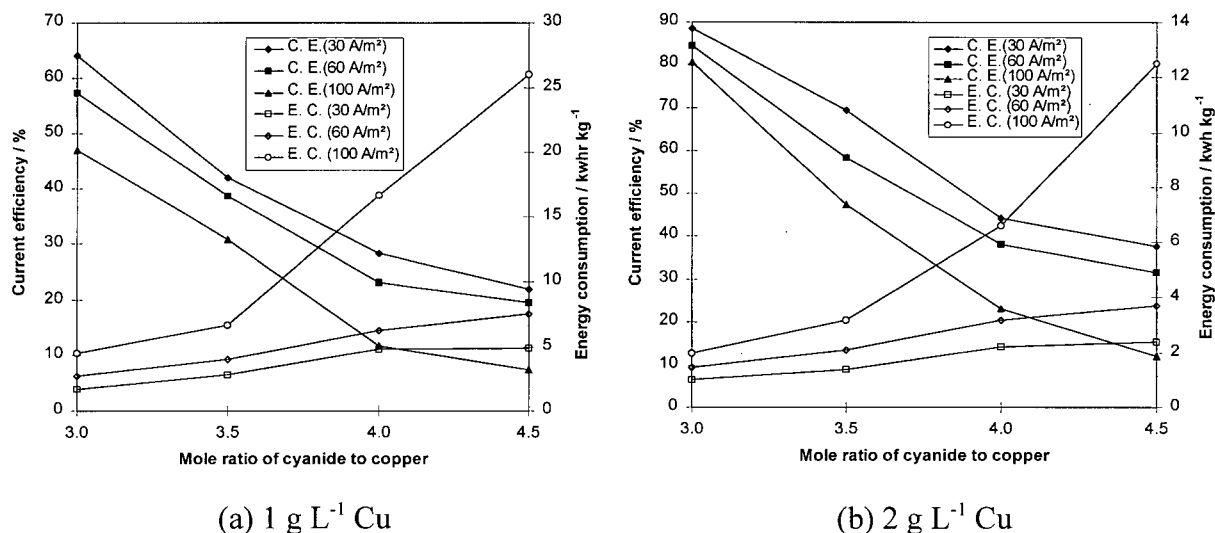
(a) 1 g L^{-1} Cu   (b) 2 g L^{-1} Cu

Figure 4-4 Current efficiency (C.E.) and the energy consumption (E.C.) of copper deposition vs. the mole ratio of cyanide to copper at different cathodic current densities and 40 °C. The electrolyte: (a) 1 g L^{-1} Cu, 0.01 M NaOH and 0.00862 M NaSCN, and (b): 2 g L^{-1} Cu, 0.01 M NaOH and 0.01724 M NaSCN. The flow velocity: 2.97, 5.93 and 9.83 cm min.$^{-1}$ respectively for 30, 60 and 100 A m^{-2}.
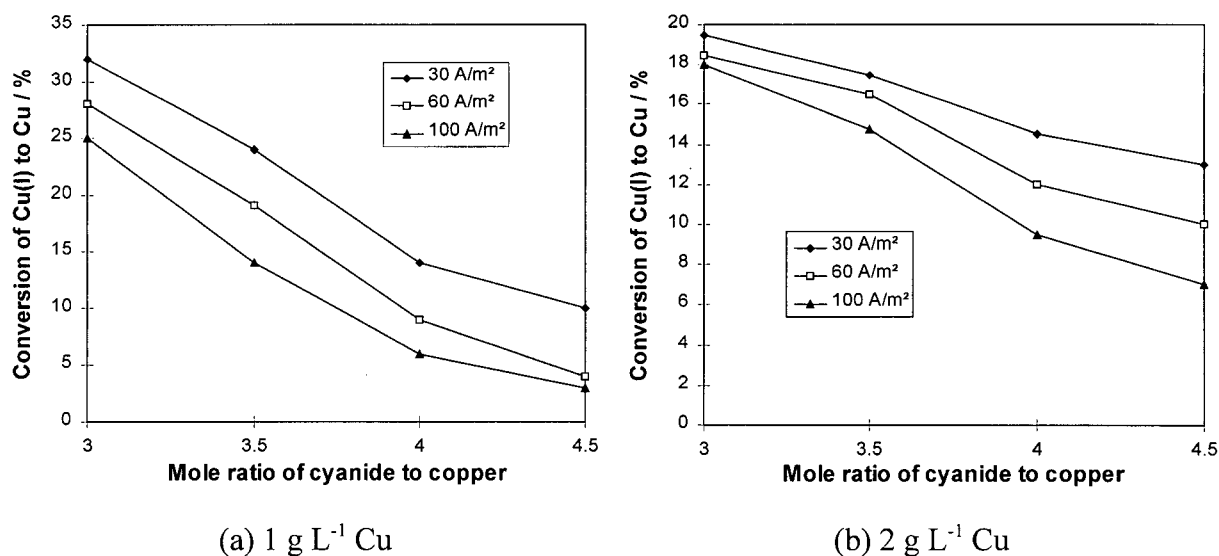
(a) 1 g L^{-1} Cu   (b) 2 g L^{-1} Cu

Figure 4-5 Conversion of Cu(I) to Cu vs. the mole ratio of cyanide to copper at different cathodic current densities and 40 °C. The electrolyte: (a) 1 g L^{-1} Cu, 0.01 M NaOH and 0.00862 M NaSCN, and (b): 2 g L^{-1} Cu, 0.01 M NaOH and 0.01724 M NaSCN. The flow velocity: 2.97, 5.93 and 9.83 cm min.$^{-1}$ respectively for 30, 60 and 100 A m^{-2}.

From Figure 4-6, the cell voltage decreased with increasing time. This is due to the increasing amount of copper deposited on the graphite fibre electrode giving improved conductivity of the graphite fibre electrode with time.
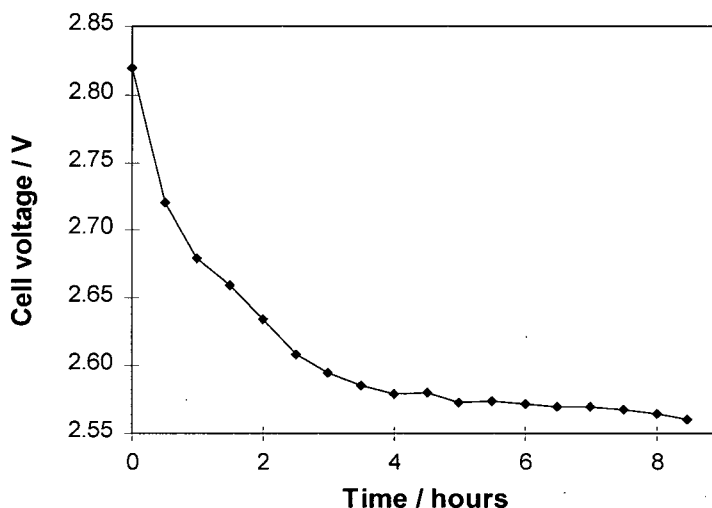
Figure 4-6 Cell voltage vs. time at the cathodic current density = 30 A m^{-2} and 40 °C. The electrolyte: 1g L^{-1} Cu, CN:Cu = 3, 0.01 M NaOH and 0.00862 M NaSCN and the flow velocity: 2.97 cm min.$^{-1}$.

From Figures 4-7, the relation between the cell voltage and the mole ratio of cyanide to copper is dependent on the current density and the copper concentration. The cell voltage is the sum of the anode potential drop, the anolyte IR drop, the membrane IR drop, the catholyte IR drop, the cathode potential drop and the hardware IR drop. At a constant potential, only the cathode potential drop and the catholyte IR drop change with CN:Cu mole ratio. According to Table 4-1, with increasing CN:Cu mole ratio, the solution conductivity increases, resulting in a decrease in the cell voltage. From Table 4-4, with increasing CN:Cu mole ratio, the redox potential for Cu(I)/Cu decreases, the concentration of dicyanide or triycyanide decreases, leading to a lower exchange current for copper reduction. Also the potential for hydrogen evolution moves negatively due to the inhibiting effect of cyanide ions on hydrogen evolution [113]. The above factors result in a decrease (more negative) in the cathode potential (i.e. an increase in the cathode potential drop) and an increase in the cell voltage at a fixed current density. Therefore the relation between the cell voltage and CN:Cu

mole ratio depends on which one (the changes in the solution IR drop and the cathode potential) is predominant.
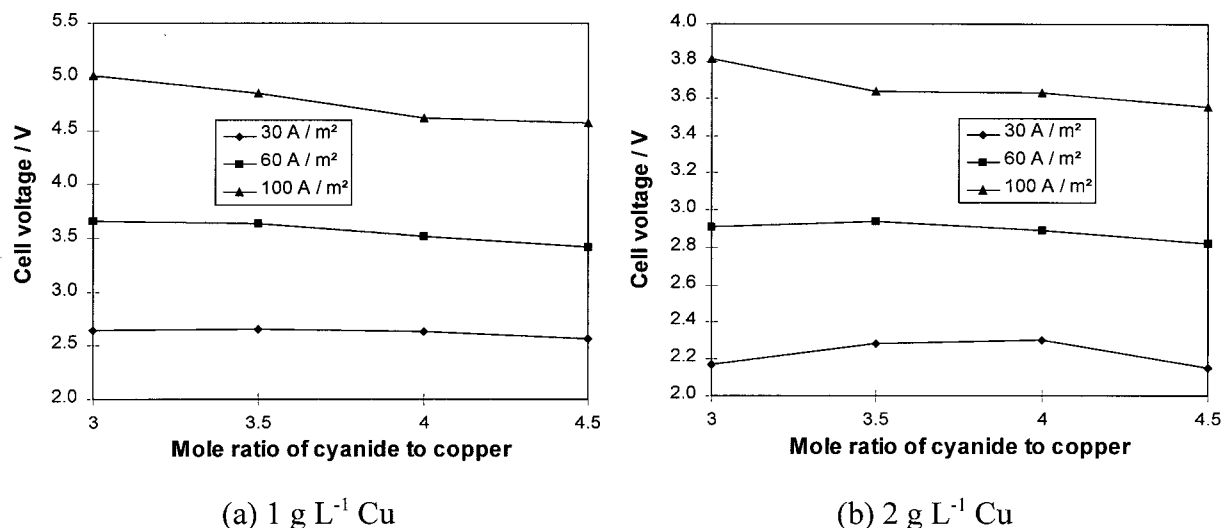
(a) 1 g L^{-1} Cu　　　　　　　　　　(b) 2 g L^{-1} Cu

Figure 4-7 Cell voltage vs. the mole ratio of cyanide to copper at different cathodic current densities and 40 °C. The electrolyte: (a) 1 g L^{-1} Cu, 0.01 M NaOH and 0.00862 M NaSCN, (b) 2 g L^{-1} Cu, 0.01 M NaOH and 0.01724 M NaSCN, the flow velocity: 2.97, 5.93 and 9.83 cm min.$^{-1}$ respectively for 30, 60 and 100 A m^{-2}.

Figures 4-8 and 4-9 show the graphite fibre felt after the deposition of copper from copper cyanide solution. Less copper was deposited where the graphite felt contacted the stainless steel mesh probably due to the shielding effect of stainless steel and the poor mass transfer because most of the solution did not pass this area. The amount of deposited copper decreased with increasing distance from the surface to the inside of the graphite due to the non-uniform potential distribution caused by the low conductivities of the solution and the graphite fibre felt. Hence there was a decrease in the driving force (polarization) of copper deposition. At a mole ratio of cyanide to copper > 4, copper was mainly deposited in a very narrow area near the surface of the graphite felt. This may be caused by the significant hydrogen evolution which greatly decreased the effective conductivity of the solution and even blocked the solution from contacting the graphite fibre. Due to the fact that no copper was deposited inside the graphite felt, the conductivity of the graphite felt was not improved.
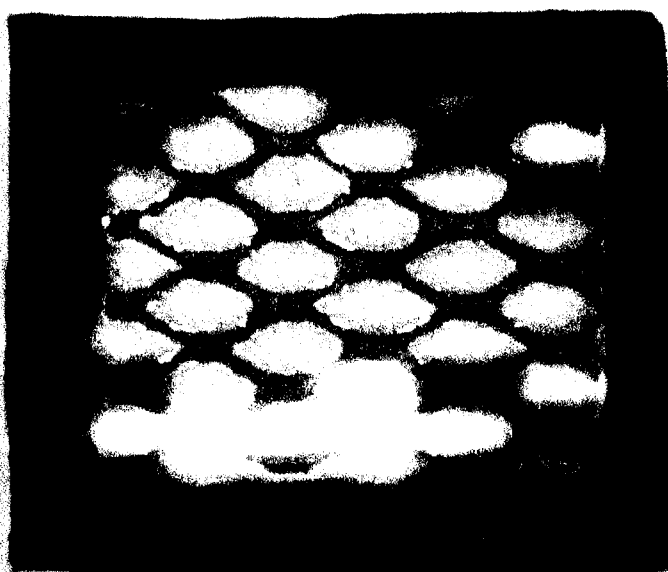
Figure 4-8 Graphite fibre felt on which copper has been deposited

Figure 4-9 Cross-section of graphite fibre felt on which copper has been deposited

From Tables 4-2 and 4-3, after the solution passed through the cell, the copper concentration in the solution taken at the end of the experiment was lower than that in the middle of the experiment. This means the current efficiency increased with time. This phenomenon is due to the increasing amount of copper deposited on the graphite giving improved conductivity of the graphite fibre electrode, the specific surface area and the surface condition. Therefore the effect of deposited copper on the current efficiency was tested using cyanide solutions with a high mole ratio of cyanide to copper. The experiments were conducted by three-cycle runs with 1g L^{-1} and 2 g L^{-1} Cu solution with an initial CN:Cu mole ratio of 3. The results are given in Table 4-5.

Table 4-5 Results of cycle run at 40 °C (the initial CN:Cu ratio = 3)

No. of cycle	1 [Cu]/C.E.	2 [Cu]/C.E.	3 [Cu]/C.E.	Average C.E.	Energy consumption
1 g L^{-1} Cu	0.76 g L^{-1} / 61 %	0.53 g L^{-1} / 58 %	0.34 g L^{-1} / 53%	57.5 %	1.8 kWh / kg Cu
2 g L^{-1} Cu	1.67 g L^{-1} / 86 %	1.38 g L^{-1} / 73 %	1.12 g L^{-1} / 68 %	78.7 %	1.15 kWh / kg Cu

After three-cycle runs, copper concentrations decreased from 1 g L^{-1} to 0.34 g L^{-1} with an average current efficiency of 57.5 % and a energy consumption of 1.8 kWh/ kg Cu and from 2 g L^{-1} to 1.1 g L^{-1} with an average current efficiency of 78.7 % and a energy consumption of 1.15 kWh/kg Cu. From Figure 4-10, the copper concentration decreased approximately linearly after every single solution pass through the graphite felt and the current efficiency decreased very little. The mole ratio of cyanide to copper increased from 3 to 9.4 and 5.5 respectively for the initial concentrations of 1 g L^{-1} and 2 g L^{-1}. Apparently for the first single pass, the current efficiency was high because copper was ready to deposit. For the second and third passes, the current efficiencies were still high because a certain amount of copper was deposited on the graphite felt, improving the conductivity of the graphite felt and increasing the specific surface. From Figures 3-5 b and 3-6 b, as expected, after the first single passes through the graphite felt, the equilibrium potential for the Cu(I)/Cu changed significantly. After the second and third passes, the equilibrium potential changed modestly, with the copper tricyanide species being always dominant. Copper deposition releases free cyanide which not only suppresses the cathodic reduction of copper (I), but also the hydrogen

evolution [113]. Therefore copper can be removed efficiently from cyanide solution even with a high CN:Cu mole ratio.
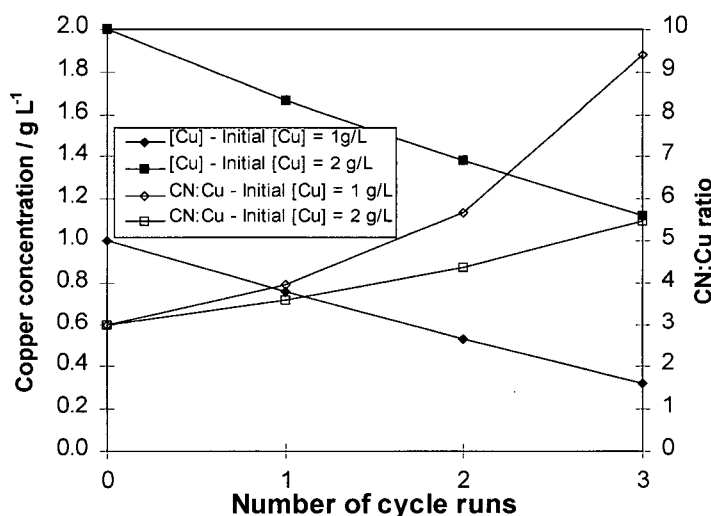
Figure 4-10 Concentration of copper vs. the number of the solution passes through the graphite felt at $[Cu]_{inital}$ = 1 and 2 g L^{-1} and 40 °C. The electrolyte: (1) 1g L^{-1} Cu, CN:Cu = 3, 0.01 M NaOH and 0.00862 M NaSCN and (2) 2 g L^{-1} Cu, CN:Cu =3, 0.01 M NaOH and 0.01724 M NaSCN, and the flow velocity: 2.97 cm min.$^{-1}$.

4.4 Summary

The current efficiency of copper deposition on a graphite felt electrode decreases with increasing CN:Cu mole ratio and current density. Due to the low conductivities of the solution and the graphite felt, the potential and current distribution of copper through the 3-dimensional electrode are not uniform. The accumulation of deposited copper with the graphite felt as the plating proceeds, significantly improves the conductivity of the graphite felt increasing the specific surface area and benefiting copper deposition. Copper can be deposited efficiently on the graphite felt from low concentration solutions event at a high CN:Cu mole ratio. Up to 60 % of the Cu can be removed efficiently from the solution. The energy requirement for copper deposition was as low as 1-2 kWh/kg Cu (1000-2000 kWh/tonne Cu) in the current range 30-100 Am^{-2}, which compares favorably with the value obtained in conventional copper electrowinning from sulphuric acid-copper sulphate solutions. The obtained results meet the requirement for industrial practice.

5. ELECTROWINNING FROM COPPER CYANIDE SOLUTION USING ALTERNATIVE ANODE REACTIONS

As discussed, copper cyanide can be extracted from dilute solutions using solvent extraction to produce a concentrated copper cyanide solution from which copper can be recovered using the copper electrowinning process. Using an alternative anodic reaction was selected as a way to prevent the anodic oxidation of cyanide and eliminate the use of a membrane cell. Thiocyanate, methanol, sulphite, and ammonia were selected as sacrificial species for addition to the electrolyte.

5.1 Experimental Apparatus and Set-up for Electrowinning

Electrowinning was carried out in a 1.5-L mini-cell made from polycarbonate. The electrolyte was circulated using a COLE-PARMER peristaltic pump at a flow rate of 0.18 L min^{-1}. The electrolyte was allowed to overflow into a 250-ml Erlenmeyer flask from which a bleed was taken periodically to remove free cyanide. CuCN, NaOH and sacrificial species were added periodically to maintain their respective concentrations due to copper deposition and the anodic consumption of NaOH and the sacrificial species. A magnetic stirrer was used to accelerate the dissolution and the mixing of CuCN, NaOH and the sacrificial species. In order to keep a constant volume of the electrolyte, deionized water was added as required. The electrolyte was heated with quartz-shielded immersion heaters connected to a temperature controller. A power supply was used to supply the current and a coulometer was used to measure the amount of electricity passed. The anode materials selected for study were TIR 2000 DSA (titanium coated with iridium and tantalum oxide) for SCN$^-$, CH_3OH, NH_3 and SO_3^{2-} and graphite only for SO_3^{2-} and SCN$^-$. SS316 stainless steel was used as the cathode material. In the case of the oxidation of SO_3^{2-}, nitrogen gas was used to prevent air oxidation. The experimental set-up is shown in Figure 5-1.

The deposited copper was recovered, washed, dried and weighed to determine the cathodic current efficiency. The current efficiencies for the oxidation of thiocyanate, methanol, ammonia and sulphite were based on the cyanide analysis (Appendix 2).

Reagent grade chemicals were used in all experiments.
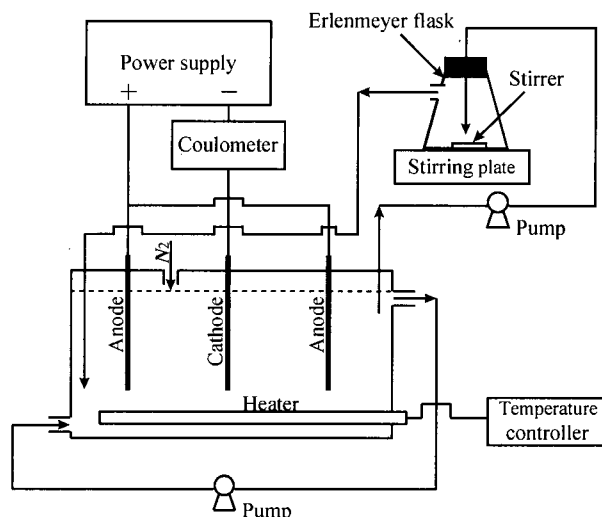
Figure 5-1 Schematic diagram of the experimental set-up

5.2 Selection of Sacrificial Materials

The anodic current efficiency was obtained using least-squares fitting according to the concentrations of the supposed oxidized species in every bleed sample and the mass balance: the amount taken out for the bleed, the amount added, and the amount in the electrolytic cell for a fixed volume of the electrolyte. Assuming a particular anodic current efficiency of cyanide, the cyanide concentration in the electrolyte can be predicted and least-squares can be used to fit the current efficiency to the measured concentration. Figure 5-2 shows the diagram of the fitted and measured concentrations of cyanide.
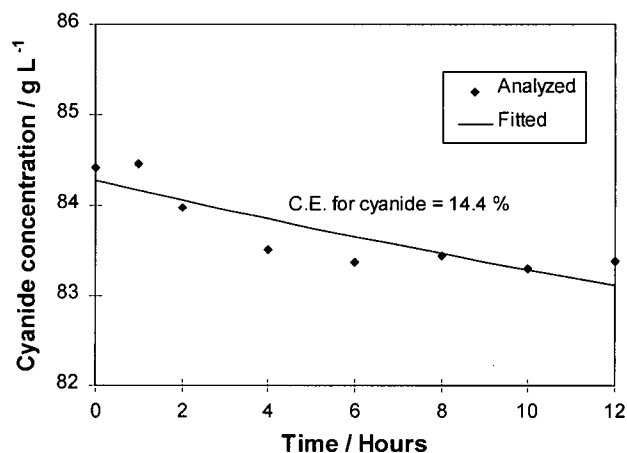
Figure 5-2 Concentration of cyanide vs. the electrolysis time for obtaining the current efficiency of cyanide oxidation at 60 °C. Electrolyte: 70 g L^{-1} Cu, CN:Cu = 3, 113 g L^{-1} Na$_2$SO$_3$, 10 g L^{-1} NaOH.

Table 5-1 Results for selection of sacrificial species at 60 °C

Additive	Anodes	current density / A m⁻²	Time / hours	Average cell voltage / V	Anodic C.E. / %	Copper C. E. /%	Anode surface condition	cathode copper condition
SCN⁻ 30 g L⁻¹	Graphite	500	13	2.26	9.10	94.6	some black coating	dendrite
SCN⁻ 30 g L⁻¹	Graphite	1000	13	2.42	6.3	95.2	some black coating	sponge dendrite
SCN⁻ 40 g L⁻¹	TIR2000	500	12	2.32	12.98	94.96	some black coating	sponge dendrite
SCN⁻ 40 g L⁻¹	TIR2000	1000	8	2.68	10.54	94.82	some black coating	sponge dendrite
CH₃OH 22.4 g L⁻¹	TIR2000	500	12	4.00	9.2	91.4	thick black coating	sponge-like dendrite
CH₃OH 22.4 g L⁻¹	TIR2000	1000	8	4.16	? 108 for CN⁻	88.1	thick black coating	strong dendrite
NH₃ 54.2 g L⁻¹	TIR2000	500	12	3.67	12.2	91.5	thick black coating and some foam	coral-like strong dendrite
NH₃ 54.2 g L⁻¹	TIR2000	1000	6	8.74	? 110 for CN⁻	82.7	thick black coating and a lot of foam	coral-like strong dendrite
Na₂SO₃ 113 g L⁻¹	TIR2000	500	12	2.18	84.5	91.7	a very little black coating	coral-like strong dendrite
Na₂SO₃ 113 g L⁻¹	TIR2000	1000	6	3.57	40	91.3	a very little black coating	coral-like strong dendrite
Na₂SO₃ 113 g L⁻¹	TIR2000	250	14	1.85	87.5	91.9	a very little black coating	small dendrite
Na₂SO₃ 113 g L⁻¹	Graphite	500	12	2.20	84.5	91.9	a very little black coating	dendrite
Na₂SO₃ 113 g L⁻¹	Graphite	250	14	1.90	86.5	92.1	a very little black coating	small dendrite

5.2.1 Thiocyanate

In the case of thiocyanate as a sacrificial species, from Table 5-1, the anodic current efficiency of thiocyanate oxidation was very low on the graphite anode and a little higher on the TIR 2000 anode. This means that thiocyanate was more difficult to oxidize on the above two anodes than copper cyanide. Both the graphite anode and the TIR 2000 anode were coated with a black solid substance, which was readily dissolved in cyanide solution or HCl solution. After dissolution of the black substance, the HCl solution became blue. Analysis showed that copper was in both the cyanide and HCl solutions. Therefore the black substance was presumed to be cupric oxide or a mixture of cupric oxide and hydroxide. No gas evolution was observed on the graphite anode, meaning there was no oxygen evolution or no

oxidation of cyanate to carbonate and nitrogen gas. At 500 A m^{-2}, on the cathode, very tight small dendrites were observed and at 1000 A m^{-2}, large dendrites like sponge coral were formed on the cathode. The current efficiency was high possibly due to the formation of coral-like copper which made the real surface area much larger than the apparent cathode surface area and the specific current density much lower than the observed value. Another reason is that thiocyanate suppresses hydrogen evolution and increases the current efficiency as reported in the literature [92, 94-96, 98].

5.2.2 Methanol

In the case of methanol as a sacrificial species, at 500 A m^{-2} the anodic current efficiency for methanol was about 9.2 % based on the cyanide analysis, but at 1000 A m^{-2} the anodic current efficiency was negative and the anodic current efficiency for cyanide was about 108%. The anodic oxidation current for cyanide was over 100% probably due to chemical oxidation by air in the presence of methanol. A little gas evolution was observed and some gas bubbles adhered to the anode surface. The gas was probably oxygen or nitrogen due either to oxygen evolution or the oxidation of cyanate to nitrogen gas. The anode was coated with a very thick layer of a black substance which dissolved readily in HCl solution which became blue. Therefore the substance was again thought to be copper oxide. Due to the thick black coating and gas bubble effects, the cell voltage became very high (4 V at the shutdown of the experiment. The formation of cupric oxide could contribute to the low consumption of cyanide and so the anodic current efficiency for methanol may be lower than the value based on analysis.

5.2.3 Ammonia

In the case of ammonia as a sacrificial species, at 500 A m^{-2} the anodic current efficiency for ammonia oxidation was 12.2 % based on the cyanide analysis. However, at 1000 A m^{-2}, the anodic current efficiency was about zero and the anodic current efficiency for cyanide was about 120 %. White foam formed around the anode and the higher the current density, the greater the foam. A black and brown substance heavily coated the anode surface and formed the passivating film. From Figure 5-3, the cell voltage increased with increasing

time of electrolysis from 2.22 to 5.41 V at 500 A m^{-2} due to increasing formation of copper oxide. The cell voltage increased from 2.89 to 19.0 V for 1000 A m^{-2} at shut-down. The black substance dissolved in cyanide and HCl solutions. However, the white brown substance did not dissolve. This substance and white foam were probably produced by the reaction of ammonia and cyanide at the anode resulting in the high consumption of cyanide (C.E. for cyanide is over 100%). At 500 A m^{-2} the cupric oxide formation could contribute to the low consumption of cyanide. Therefore the anodic current efficiency of ammonia was lower than the above value based on the cyanide analysis.

5.2.4 Sulphite

In the case of sulphite as a sacrificial species, at 500 A m^{-2} the anodic current efficiency for sulphite oxidation was about 85% both on graphite and TIR 2000 based on the cyanide analysis. However, at 1000 A m^{-2} the current efficiency decreased to 40 % at TIR 2000. This means that increasing the current results in the oxidation of more cyanide. This may be due to a change in the electrochemical kinetics of the two anode reactions at high current density. With an increasing circulating flow rate of electrolyte, the cell voltage decreased due to improved mass transfer of both copper ions to the cathode and sulphite ions to the anode. Only a very small amount of black material coated the upper side of the anode near the surface of the electrolyte. Therefore sulphite addition can effectively prevent or decrease the formation of copper oxide at the anode. From Figure 5-3, the cell voltage first increased a little and then decreased slightly with increasing time of electrolysis. The decrease in the cell voltage may be caused by the growing cathode and increasing real surface area due to the formation of the dendritic copper deposit. No gas evolution was observed on the anodes.

From the above discussion, thiocyanate, methanol and ammonia did not effectively protect against cyanide oxidation and the anode surface became coated with black copper oxide and lost its catalytic activity. Only sulphite oxidation was found to effectively limit the oxidation of cyanide. The anodic current efficiency of sulphite was the same on TIR2000 and graphite anodes. Therefore sulphite oxidation and graphite were selected as the sacrificial additive and the anode material respectively for further tests.
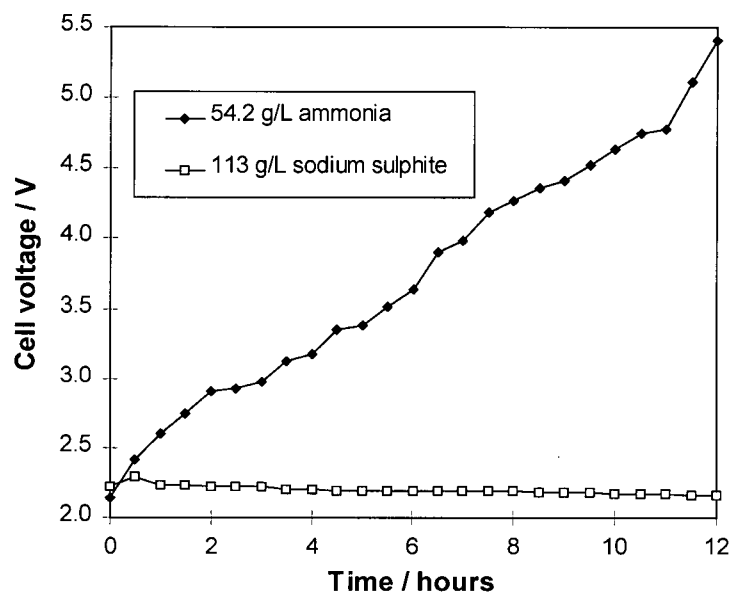
Figure 5-3 Cell voltage vs. the time of electrolysis in the presence of ammonia and sulphite as a sacrificial species at 500 A m^{-2} and 60 °C. Electrolyte: 70 g L^{-1} Cu, CN:Cu = 3, and 10 g L^{-1}.

5.3 Effect of Some Parameters on the Anodic and Cathodic Processes in the Presence of Sulphite

5.3.1 Effect of Current Density

The current density usually affects the anodic and cathodic processes significantly. Thus experiments were conducted to determine the effect of current density. Three current densities were tested and the results are listed in Table 5-2. The anodic current efficiency of cyanide decreases significantly with decreasing current density from 1000 to 500 A m^{-2}, but decreases slightly from 500 to 250 A m^{-2}. The cathodic current efficiency was almost independent of the current density. This phenomenon is probably related to the morphology of the copper deposits. At a high current density, more and larger dendrites were produced and at a low current density, fewer and smaller dendrites were obtained, resulting in approximately the same real current density.

Table 5-2 Effect of current density on the anodic current efficiency of cyanide and the cathodic current efficiency of copper at 60 ^{0}C. Electrolyte: 70 g L^{-1} Cu, CN:Cu mole ratio =3, 10 g L^{-1} NaOH and 113 g L^{-1} Na$_2$SO$_3$.

Current density / A m^{-2}	1000	500	250
C.E. for cyanide oxidation / %	59.9	14.4	12.8 ± 3
C.E. for copper deposition / %	92.2	92.0	92.1 ± 1

5.3.2 Effect of sulphite concentration

At 250 A m^{-2} solutions with 50, 63 and 113 g L^{-1} Na$_2$SO$_3$ were tested with the results being listed in Table 5-3. In this range of sulphite concentration, the anodic current efficiency of cyanide was not affected very much by sulphite concentration and the cathodic current efficiency of copper deposition was almost independent of the sulphite concentration. The sulphite concentration did not affect the morphology of the cathodic deposit. Therefore the use of 50-60 g L^{-1} Na$_2$SO$_3$ is sufficient to get a reasonable anodic current efficiency (minimum consumption of sulphite).

Table 5-3 Effect of sulphite concentration on the anodic current efficiency of cyanide and the cathodic current efficiency of copper at 60 ^{0}C and 250 A m^{-2}. Electrolyte: 70 g L^{-1} Cu, CN:Cu mole ratio =3, 10 g L^{-1} NaOH.

[Na$_2$SO$_3$] / g L^{-1}	50	63	113
C.E. for cyanide oxidation / %	13	13.2 ± 3	12.8 ± 3
C.E. for copper deposition / %	91.8	91.9 ± 2	92.1 ± 1

5.3.3 Effects of thiocyanate and mole ratio of cyanide to copper

Thiocyanate is expected to be present in the copper-cyanide electrowinning solution. The mole ratio of cyanide to copper is a very important parameter affecting the anodic and cathodic processes. Therefore experiments have been conducted on solutions with different mole ratios of cyanide to copper in the presence and absence of thiocyanate. The results are listed in Table 5-4.

Table 5-4 Results of copper electrowinning at 250 A m^{-2} and 60 °C. Electrolyte: 70 g L^{-1} Cu, CN:Cu mole ratio = 3-4.5, 63 g L^{-1} Na$_2$SO$_3$ and 10 g L^{-1} NaOH in the presence and absence of SCN$^-$.

CN:Cu mole ratio	Average cell voltage / V	Copper C. E. / %	Energy consumption / kWh kg^{-1}	Anodic C.E. for CN$^-$ / %	Anode surface	cathode copper condition
3 (no SCN$^-$)	1.92	93.1	0.873	11.3	a very little black coating	small dendrite
3 (40 g L^{-1} SCN$^-$)	1.72	95.6	0.759	11.6	a very little black coating	coral-like deposits
3.2 (no SCN$^-$)	2.05	89.2	0.968	13.8	no black coating	small dendrite
3.2 (40 g L^{-1} SCN$^-$)	1.93	93.8	0.867	14.0	no black coating	small dendrite
3.5 (no SCN$^-$)	2.08	77.85	1.13	17.9	no black coating	small dendrite
3.5 (40 g L^{-1} SCN$^-$)	1.97	89.0	0.934	18.0	no black coating	small dendrite
4 (no SCN$^-$)	2.15	40.9	2.22	37.0	no black coating	almost no dendrite
4 (40 g L^{-1} SCN$^-$)	2.08	58.8	1.49	38.8	no black coating	very small dendrite
4.5 (no SCN$^-$)	2.11	7.85	11.4	54.9	no black coating	no dendrite
4.5 (40 g L^{-1} SCN$^-$)	2.05	8.53	10.1	54.1	no black coating	no dendrite

From Figure 5-4, the cathodic current efficiency of copper deposition decreases with increasing mole ratio of cyanide to copper. At a CN:Cu mole ratio < about 3.3, the current efficiency decreases slightly with increasing mole ratio of cyanide to copper and at a CN:Cu mole ratio > 3.3, it decreases significantly with increasing CN:Cu mole ratio. From Figure 3-3, with increasing CN:Cu mole ratio, the equilibrium potential for the Cu(I)/Cu couple decreases significantly and the species of copper cyanide shifts from the lowly coordinated complexes (Cu(CN)$_2^-$ and Cu(CN)$_3^{2-}$) to the highly coordinated complex (Cu(CN)$_4^{3-}$). Therefore at a higher CN:Cu mole ratio, the discharge of copper (I) takes place at a more negative potential where more hydrogen was evolved. In another aspect, free cyanide suppresses the hydrogen evolution [113]. With increasing CN:Cu mole ratio, the hydrogen evolution should be suppressed. Increasing mole ratio of cyanide to copper has much more inhibiting effect on copper deposition than on the hydrogen evolution. Therefore the current efficiency decreases with increasing mole ratio of cyanide to copper.

Thiocyanate can increase the current efficiency of copper deposition. The effect of thiocyanate is dependent on the CN:Cu mole ratio. At a CN:Cu mole ratio = 3-3.3, the effect is small and at a CN:Cu mole ratio = 3.3 - 4.4, the effect is significant. At a CN:Cu mole ratio = 4.5, the effect is very small. At a low CN:Cu mole ratio (3-3.3), the current efficiency of copper deposition is very high and will not be improved significantly by thiocyanate. At a CN:Cu mole ratio = 4.5, the free cyanide concentration is high (about 0.5 M). Free cyanide also suppresses the hydrogen evolution significantly [113]. The effect of free cyanide on hydrogen evolution may be much higher than that of thiocyanate or the co-effect of free cyanide and thiocyanate on the hydrogen evolution is close to that of free cyanide. Therefore thiocyanate does not improve the current efficiency very much. However, thiocyanate accelerates the formation of dendrites on the cathode and produces poor quality copper. This may be another reason for the increase in copper current efficiency in the presence of thiocyanate. At a CN:Cu mole ratio = 3, the electrolyte became brown when adding CuCN, NaSCN, Na_2SO_3 and NaOH into the Erlenmeyer flask. This may be caused by an unknown reaction between thiocyanate and sulphite. The energy consumption increases slightly with increasing CN:Cu mole ratio from 3 to 3.5 and increases significantly at a CN:Cu mole ratio > 4 due to the significant decrease in the current efficiency. Since thiocyanate increases the current efficiency and the conductivity of the electrolyte, the energy consumption in the presence of thiocyanate is lower than that in its absence.

Figure 5-5 shows the anodic current efficiency of cyanide vs. CN:Cu mole ratio at 60 °C and 250 A m^{-2}. The anodic current efficiency of cyanide increases with increasing CN:Cu mole ratio. In the CN:Cu mole ratio range 3-3.2, the anodic current efficiency of cyanide increases slightly with increasing CN:Cu mole ratio. At a CN:Cu mole ratio > 3.5, the anodic current efficiency of cyanide increases rapidly with increasing CN:Cu mole ratio. At a CN:Cu mole ratio = 3, a very small amount of black copper oxide was observed on the anode and at a CN:Cu mole ratio ≥ 3.2, no precipitate was observed on the anode. This is apparently due to the fact that cyanide stabilizes copper in the form of copper(I) cyanide complex. The presence of thiocyanate does not decrease the consumption of cyanide.
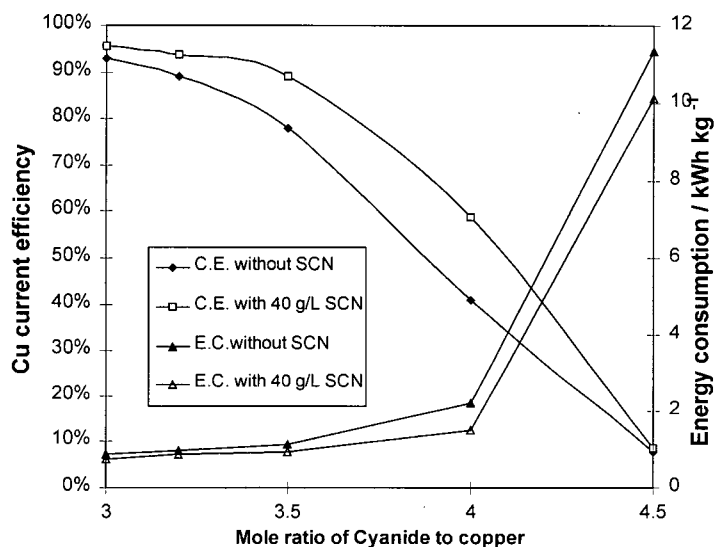
Figure 5-4 Cathodic current efficiency of copper deposition (C.E.) and power consumption (P.C.) vs. the CN:Cu mole ratio at 60 °C and 250 A m^{-2}. Electrolyte:70 g L^{-1} Cu, 63 g L^{-1} Na$_2$SO$_3$, 10 g L^{-1} NaOH, and different cyanide concentrations in the presence and absence of 40 g L^{-1} SCN^{-1}.
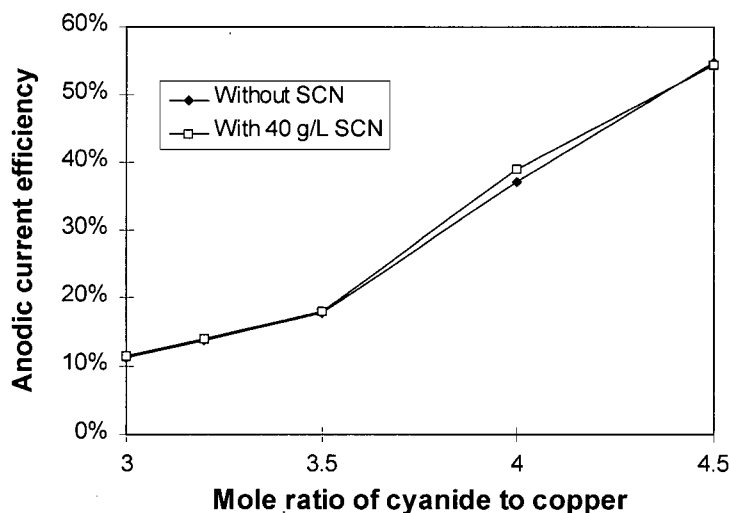
Figure 5-5 Anodic current efficiency for cyanide oxidation vs. the mole ratio of cyanide to copper at 250 A m^{-2} and 60 ^{0}C. Electrolyte:70 g L^{-1} Cu, 63 g L^{-1} Na$_2$SO$_3$, 10 g L^{-1} NaOH, and different cyanide concentrations in the presence and absence of 40 g L^{-1} SCN^{-1}.

The cell voltage vs. time of electrolysis at different CN:Cu mole ratios is shown in Figure 5-6. In the CN:Cu mole ratio range 3-4, the cell voltage first increases quickly to a certain value and then decreases with increasing time of the electrolysis. However, at a

CN:Cu mole ratio = 4.5, the cell voltage increases slowly with increasing time of electrolysis and then quite rapidly with time and exceeds the values for lower CN:Cu mole ratios, and finally reaches a maximum value and decreases slightly with time. Generally, the cell voltage increases with increasing CN:Cu mole ratio. These phenomena are probably largely related to the cathodic process. At the beginning of the electrolysis, the cathode was not covered with copper and the overpotential for hydrogen on SS 316 stainless steel is much lower than on copper and hydrogen evolution accounted for a significant part of the cathodic current. After the cathode was covered with copper, the overpotential for hydrogen evolution became larger. Therefore the cathodic potential had to move to a more negative potential to maintain a constant current, resulting in the increase in the cell voltage. This is consistent with the observations of the cathode: at the beginning, more hydrogen bubbles appeared on the cathode and after the cathode was covered with copper, the quantity of bubbles decreased and cell voltage increased. At a CN:Cu mole ratio = 3-4, the copper was ready to deposit on the cathode and completely covered the cathode in a short time.

At a CN:Cu mole ratio = 4.5, it was difficult to deposit copper on the cathode and it took a longer time (5 hours) to cover the cathode with copper completely. When the time of the electrolysis was in the range 0.5 to 4 hours, the coverage of copper was low and so hydrogen overpotential was low, the cell voltage was lower than the values with lower CN:Cu mole ratios. The deposit and its dendrites were growing with time and the distance between the cathode and the anode decreased and the real surface area became larger, resulting in a low polarization. Therefore a lower cell voltage is needed to keep a constant current.

The increase in the cell voltage with increasing mole ratio of cyanide to copper can be explained by the decrease in the redox potential for Cu(I)/Cu and the increase in the overpotential of hydrogen evolution. The increase in the CN:Cu mole ratio significantly shifts the potential for Cu(I)/Cu to more negative values and the distribution of copper cyanide shifts from the electroactive species (dicyanide or probably tricyanide) to the non-electroactive species (tetracyanide), resulting in a low exchange current. Furthermore, the increase in the CN:Cu mole ratio also increases the free cyanide concentration, which in turn increases the overpotential of hydrogen evolution [113].Therefore the cathode has to be kept at a lower potential to maintain a constant current. The increase in the mole ratio of cyanide

to copper can increase the conductivity of the electrolyte and decrease the cell voltage, but the decrease in IR in the electrolyte is smaller than the increase in the absolute value of cathode potential.
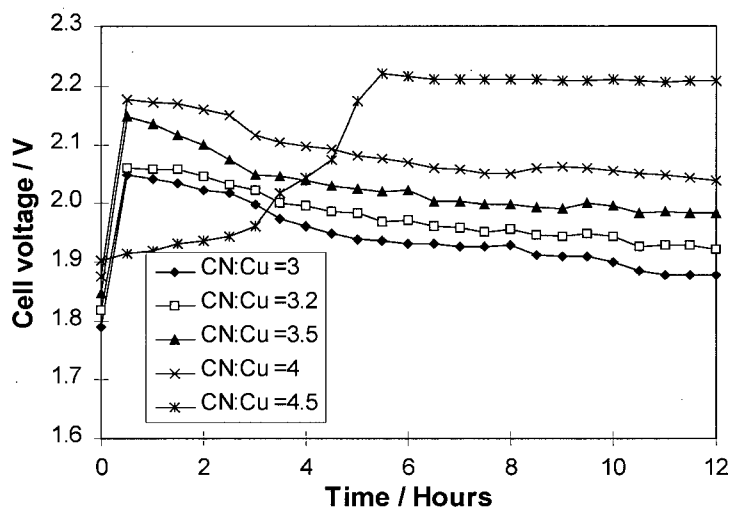
Figure 5-6 Cell voltage vs. time of electrolysis at 250 A m^{-2} and 60 °C. Electrolyte:70 g L^{-1} Cu, 63 g L^{-1} Na$_2$SO$_3$, 10 g L^{-1} NaOH, and different cyanide concentrations in the absence of SCN^{-1}.

5.3.4 Effect of Temperature

Temperature is expected to be an important factor affecting both the anodic and cathodic processes. Three temperatures (40, 50 and 60 °C) were tested and the results are given in Tables 5-4 and 5-5. The cathodic current efficiency of copper deposition decreases with decreasing temperature. The anodic current efficiency of cyanide oxidation decreases with increasing temperature and the cell voltage decreases with increasing temperature. The increase in the cell voltage was partly caused by the decrease in the conductivity of the electrolyte.

Table 5-5 Results of copper electrowinning at 250 A m^{-2} and different temperatures. Electrolytes: 70 g L^{-1} Cu, CN:Cu mole ratio = 3, 63 g L^{-1} Na$_2$SO$_3$ and 10 g L^{-1} NaOH in the presence and absence of SCN$^-$.

[SCN$^-$] / g L^{-1}	Temp. / °C	Average cell voltage / V	Copper C. E. / %	Anodic C.E. for CN$^-$ / %	Anode surface	cathode copper condition
0	50	2.12	85 ± 3	21 ± 5	a very little black coating	small dendrite
40	50	2.01	88 ± 3	20 ± 5	a very little black coating	coral-like deposits
0	40	2.20	82 ± 3	25 ± 5	a very little black coating	small dendrite
40	40	2.07	86 ± 3	25 ± 5	a very little black coating	coral-like deposits

5.4 Summary

Of four sacrificial species (sulphite, methanol, thiocyanate and ammonia), only sulphite can effectively limit the oxidation of cyanide. When the composition of the electrolyte was controlled at 50-60 g L^{-1} Na$_2$SO$_3$, 70 g L^{-1} Cu, CN:Cu mole ratio = 3-3.2, the anodic current efficiency of cyanide decreased from about 100 % to 10-20 % in the current range 250-500 A m^{-2} and the temperature range 50-60 °C. The copper deposition current efficiency was 90-96 % and the energy consumption was 0.76-1.0 kWh/kg Cu. The anodic current efficiency of cyanide increased from about 15 % to 56 % with increasing CN:Cu mole ratio from 3 to 4.5 at [Cu] = 70 gL^{-1}. With increasing current density, the anodic current efficiency of cyanide decreases greatly at the current > 500 A m^{-2} and slightly at the current < 500 A m^{-2}. The anodic current efficiency of cyanide decreases slightly with increasing temperature. The copper deposition current efficiency decreases with increasing CN:Cu mole ratio and decreasing temperature. The presence of thiocyanate increases the copper deposition current efficiency at CN:Cu mole ratio > 4. 5.

6. THE ANODIC OXIDATION OF SULPHITE ON A GRAPHITE ANODE IN ALKALINE SOLUTION

In Chapter 5, it was noted that of the additives tested only sulphite could effectively limit the oxidation of cyanide on a graphite anode. In order to further the development, it therefore is important to understand the kinetics of the anodic oxidation of sulphite on graphite. However, the anodic oxidation of sulphite in alkaline solutions has not been investigated thoroughly and the published results are inconsistent. For the purpose of using sulphite oxidation as an alternative anode reaction in copper cyanide electrowinning, the available information is inadequate and further studies on the anodic oxidation of sulphite in alkaline solution are needed. Therefore a study of the anodic oxidation of sulphite was conducted on a graphite electrode using the rotating disc technique and the potential sweep method.

6.1 Some Fundamental Aspects of Rotating Disk Electrodes

Rotating disk electrodes (RDE) have been employed for the study of a great variety of electrochemical processes due to certain advantages over other types of solid electrodes. The major advantage lies in the development of a uniform diffusion layer, the thickness of which can be calculated at a given rotational speed. So, the uniform mass transfer towards and away from the electrode surface can be changed by changing the rotational speed in a pre-determined way. RDE theory has been described by Levich [322] while a comprehensive presentation on these electrodes is discussed in two monographs by Pleskov and Filinovskii [323] and by Opekar and Beran [324]. When a rotating disk rotates in a viscous and incompressible liquid at an angular velocity ω, the liquid layer immediately adjacent to the disc surface takes part in the rotational motion. The layers not immediately adjacent to the disc must also rotate owing to the viscous forces. Using cylindrical coordinates (r, φ, z) the liquid velocity can be divided into three components: V_r - radical direction caused by centrifugal force, V_φ - azimuthal direction due to the liquid viscosity and V_z - axial direction resulting from the pressure drop. These velocity components described by the Navier-Stokes equation are a function of rotational speed, liquid viscosity, vertical distance from the disk (z)

and radial distance (r). Under these conditions: (1) the flow is non-turbulent (dV/dt = 0), (2) the flow is independent of the coordinate φ, because of axial symmetry, (3) the fluid is incompressible and the boundary is horizontal, (4) variations in the pressure in the boundary layer are dependent only on z and a sufficient angular velocity generates strong convection, so that contributions from extraneous forces are eliminated [324]. These three components can be represented by the following equations [323, 324]:

$$V_r = r\omega F(\xi) \qquad V_\varphi = r\omega G(\xi) \qquad V_z = \sqrt{r\omega} H(\xi) \tag{6-1}$$

where $\xi = (\omega/v)^{1/2} z$ - dimensionless distance from the disk surface, v is the kinematic viscosity, ω the angular velocity, r the radial distance and z the vertical distance from the disk. $F(\xi)$, $G(\xi)$ and $H(\xi)$ are dimensionless functions which have different formulae.
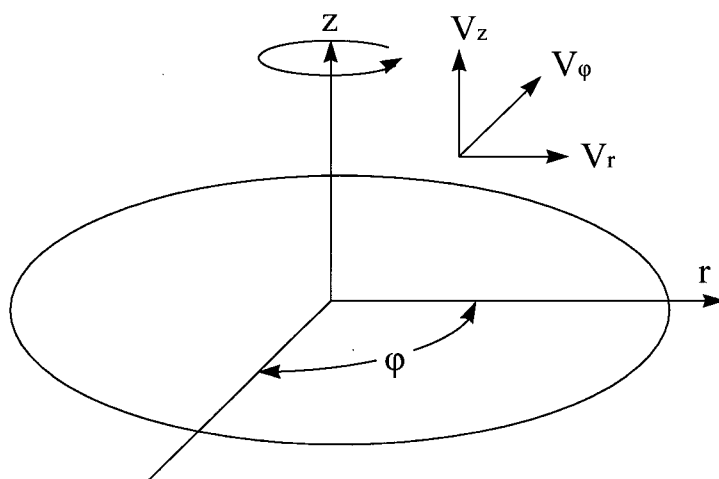
Figure 6-1 Rotating disk coordinate system used in calculations of liquid flow near the rotating disk.

The thickness of the diffusion layer (δ) depends on Schmidt number (Sc = v/D) [323]. When Sc is larger than 1000, the well-known Levich equation (Equation 6-2) has sufficient accuracy to express the thickness of the diffusion layer. For aqueous solutions, the Levich equation can be applied since Sc = v/D $\approx 10^3$.

$$\delta = 1.611(D/v)^{1/3}(v/\omega)^{1/2} = 1.611 D^{1/3} v^{1/6} \omega^{-1/2} \tag{6-2}$$

When Sc is below 1000, the following equations should be used:

$$\delta = 1.611(D/v)^{1/3}(v/\omega)^{-1/2}(1+0.3539(D/v)^{0.36}) \quad 250 < Sc < 1000 \tag{6-3}$$

$$\delta = 1.611(D/v)^{1/3}(v/\omega)^{-1/2}(1+0.3539(D/v)^{-1/3}+0.14514(D/v^{2/3}) \quad Sc > 100 \tag{6-4}$$

The above equations are based on the laminar flow condition. When the Reynolds number (Re = $\omega r^2/\nu$) exceeds a critical value, the fluid flow changes qualitatively from laminar to turbulent. Conversion is gradual. First, the edge of the disk is affected by turbulence and this gradually extends toward the center with increasing velocity of rotation. The critical Re value is 1.8-3.1×10^5 [324]. To avoid turbulence, the maximum rotational speed for 10 mm rotating disk is $(1.8$-$3.1) \times 10^5 (60\nu/2\pi r^2)$ = 17200-29600 rpm. When the disk vibrates axially or radially and the surface is uneven, turbulence appears at Re values below the critical values.

Another extreme occurs for Re $\approx$ 10, when the thickness layer becomes comparable with the dimensions of the disk and natural convection in the solution begins to play a role. Therefore the rotational speed must be much larger than $10(60\nu/2\pi r^2) \approx 1$ rpm. The thickness of the boundary layer is sufficiently smaller than the radius of the disk and Re is sufficiently large to make natural convection negligible. The rotational speed employed is usually from 100 to 6000 rpm and so the Levich equation can be accurately applied. The ratio of the diameters of the outer insulator to the electrode disc should be large enough to minimize the edge effects.

The limiting current density (i_l) for the simple reaction (O + ne = R) equals the diffusion current density (i_d) and can be expressed as

$$i_l = i_d = \frac{nFDC_b}{\delta} = 0.62nFD^{2/3}\nu^{-1/6}\omega^{1/2}C_b \qquad (6\text{-}5)$$

where n is the number of electrons transferred, F the Faraday constant (96487 A s mol^{-1}), C_b the bulk concentration (mol dm^{-3}) and D the diffusion coefficient. It should be noted that Equation 6-5 is only valid when the transport number of electroactive species i (t_i) is zero. When the transport number (t_i) is not negligible but is smaller than 0.1 and the charge number of the ionic species is equal to n, the limiting current density can be expressed by the following equation [325]:

$$i_l = \frac{nFDC_b}{\delta(1-t_i)} = \frac{0.62nFD^{2/3}\nu^{-1/6}\omega^{1/2}C_b}{(1-t_i)} \qquad (6\text{-}6)$$

From Equation 6-5, the diffusion coefficients for electrochemical species can be calculated from the slopes of the straight lines for the plot of i_l vs. $\omega^{1/2}$.

The rotating disk is a powerful tool for determining reaction order and the rate constant. There are many methods to determine the reaction order using a rotating disk and some of them are discussed in published monographs [323, 324]. The derivation of a formula which can be applied to determine the reaction order and rate constant when the limiting currents have been measured is given below.

The current density for mixed kinetics at a rotating disk electrode is determined by the heterogeneous reaction with the diffusion of the reactant and the rate of the heterogeneous reaction being equal to the diffusion rate under steady-state conditions. Therefore when the charge transfer coefficient is independent of the reactant concentration and the reverse reaction is negligible, the current density for a simple redox reaction (O + ne = R) can be expressed as:

$$i = nFk(C_s)^{n_r} \tag{6-7}$$

$$i = nFD(\frac{dC}{dx})_{surface} = nFD\frac{C_b - C_s}{\delta} = i_l(1 - \frac{C_s}{C_b}) \tag{6-8}$$

where i is the current density, n_r the reaction order, k the reaction rate constant, and C_s the electrode surface concentration. From Equations 6-7 and 6-8, we have the following equations:

$$C_s = C_b(1 - \frac{i}{i_l}) \tag{6-9}$$

$$i = nFkC_b^{n_r}(1 - \frac{i}{i_l})^{n_r} = i_k\left(1 - \frac{i}{i_l}\right)^{n_r} \tag{6-10}$$

$$\log i = \log i_k + n_r \log(1 - \frac{i}{i_l}) \tag{6-11}$$

where $i_k = nFkC_b^{n_r}$ is the kinetically controlled current. The reaction order can be calculated from the plot of log i vs. log(1-i/i$_l$) and the kinetically controlled current can be obtained from the intercept on the y-axis. The reaction order is obtained at constant ionic strength and the effects on the double layer and the activity coefficient are negligible due to the change in the reactant concentration. Furthermore, in this method it is not necessary to know the concentration of the reactant. The exchange current and Tafel slope can be obtained from the plot of i_k vs. overpotential. If $n_r = 1$ (first order), we get the Koutecky-Levich equation from Equation 6-10:

$$\frac{1}{i} = \frac{1}{i_k} + \frac{1}{i_l} \qquad (6\text{-}12)$$

Equations 6-7, 6-8, 6-11 and 6-12 are also valid for redox reactions such as O + X +ne = R when the reaction order with respect to X is zero or the concentration of X is kept at an elevated level so that there is no difference between the surface and the bulk concentration. In these cases, the kinetic expression can be reduced to Equation 6-7.

6.2 Thermodynamics of Sulphite Oxidation

As was discussed in Chapter 2, Section 2.5, sulphite exists in the form of SO_2 (aq), HSO_3^- and SO_3^{2-} in aqueous solution. SO_2 (aq), HSO_3^- and SO_3^{2-} species are predicted to predominate over the pH ranges < 1.8, $1.8 - 7$ and > 7, respectively. At pH > 12, the dominant species in solution is SO_3^{2-}. The anodic oxidation of sulphite in alkaline solution on graphite can be expressed by the following equations:

$$SO_3^{2-} + 2OH^- = SO_4^{2-} + H_2O + 2e \qquad (6\text{-}13)$$

$$2SO_3^{2-} = S_2O_6^{2-} + 2e \qquad (6\text{-}14)$$

The production of dithionate on graphite (Equation 6-14) can be neglected according to the literature [211].The standard equilibrium potentials for Equation 6-13 are -0.936 , - 0.957, -0.971, -0.985 V vs. SHE at 25, 40, 50 and 60 ^{0}C respectively obtained by calculation using reliable thermodynamics data [295, 296]. The Nernst equation for the equilibrium potential for Equation (6-13) is expressed as:

$$E = E^0 + \frac{RT}{2F} \ln\left(\frac{a_{SO_4^{2-}} a_{H_2O}}{a_{SO_3^{2-}} a_{OH^-}^2} \right) \qquad (6\text{-}15)$$

There are many methods for calculating activity coefficients in strong electrolytes such as the Guggenheim, Bromley, Meissner, Chen and Pitzer's methods [326]. Pitzer's ion-ion interaction model is good for calculating the activity coefficient of a single species in multi-component strong electrolytes [326-328] and it has been used in this study. In Pitzer's

method, the concentration is expressed in molality and so the activity of species i, is $a_i = m_i \gamma_i$. The molality of species i (m_i) has the following relationship with the molarity (C_i) [329]

$$m_i = \frac{C_j}{\rho - 0.001 \Sigma C_i M_i} \quad (6\text{-}16)$$

where ρ is the density of electrolyte. In the presence of 1 M Na_2SO_4 supporting electrolyte, m_i $\approx$ 1.02 C_i (ρ = 1.12 [330]). For convenience, the molarity replaces the molality as an approximation for calculation. The interaction of SO_3^{2-} with Na^+ and OH^- is roughly similar to that of SO_4^{2-} [328] and the activity coefficients of SO_3^{2-} and SO_4^{2-} are close [331]. Therefore the activity coefficient of SO_3^{2-} is assumed to equal to that of SO_4^{2-}. The activity coefficients of water and hydroxide ions have been calculated using Pitzer's method (see Appendix 5).

The calculated water activity, activity coefficient of hydroxide and the potential for SO_4^{2-} and SO_3^{2-} couple at 25, 40, 50 and 60 °C are listed in Table 6-1. The water activity is almost independent of the temperature and the hydroxide activity coefficient decreases slightly with increasing temperature.

Table 6-1 The activities and activity coefficients for 0.1 M Na_2SO_3, 0.25 M NaOH and 1 M Na_2SO_4 at 25, 40, 50 and 60 °C

Temperature / °C	25	40	50	60
a_w	1.03	1.03	1.03	1.03
$\gamma_{OH(I)}$	0.486	0.470	0.459	0.448
$E(SO_4^{2-}/SO_3^{2-})$ vs SHE / V	-0.822	-0.837	-0.846	-0.855

6.3 Experimental Apparatus and Set-up

An NE-150 graphite rod (impregnated with resin and carbonized at 500 °C in vacuum) from National Electric Carbon Co. was used to make a graphite rotating disk. The graphite was machined to 4 mm and tightly surrounded with a plastic shield. A spring was used to conduct the electricity from the shaft to the graphite electrode. Figure 6-2 shows the schematic diagram of the rotating disk.
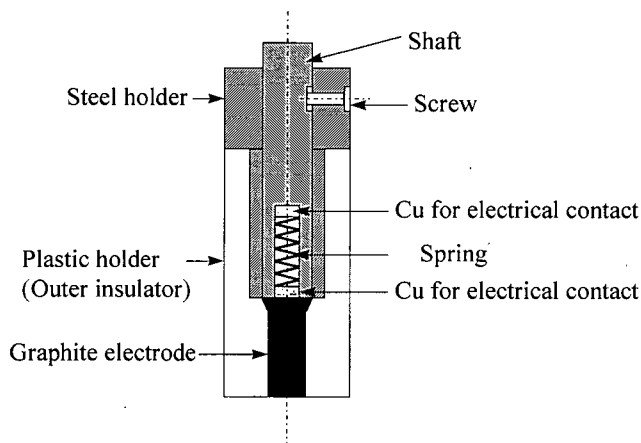
Figure 6-2 Schematic diagram of rotating disk

The electrode surface was first ground using 600-grit sandpaper, polished with 4000-grit silicon carbide sandpaper and then soft tissue paper. Finally the surface was checked under a microscope for surface smoothness. To ensure reproducible results, the electrode was first treated by cyclic voltammetry between 0 and 0.75 V vs. SCE at 100 mV s^{-1} for 30 minutes and polarized at 1mV s^{-1} until the electrode reached a stable condition. The electrode was tested in ferrous and ferric cyanide solution. The limiting current density was the same as on a Pt rotating disk from EG&G Co. and was proportional to the square root of the rotational speed. Therefore the graphite electrode was considered to be uniform.

The graphite having a 12-mm diameter was fashioned as a rotating disk for the coulometric measurements.

The rotating disc electrode system was an EG&G PARC Model 636 Electrode Rotator. The potentiostat was a SOLARTRON 1286 Electrochemical Interface. 100 mL of the solution of the required composition were placed in an EG & G water-jacketed electrolytic cell whose temperature was controlled by a water bath circulator. The experiments were carried out under an argon atmosphere to protect the sulphite from oxidation by air. The reference electrode was a FISHER saturated calomel electrode (SCE) which was connected to the cell electrolyte by an electrolyte bridge. The calomel electrode was placed in a tube containing the same electrolyte as in the cell. The temperature was kept at 25 °C using a water bath. The ohmic drop between the working electrode and the reference electrode was compensated by the current interruption technique. A schematic diagram of the

experimental set-up is shown in Figure 6-3. Except as noted, the polarization curves were generated using the potential sweeping method at 1 mV s^{-1}.
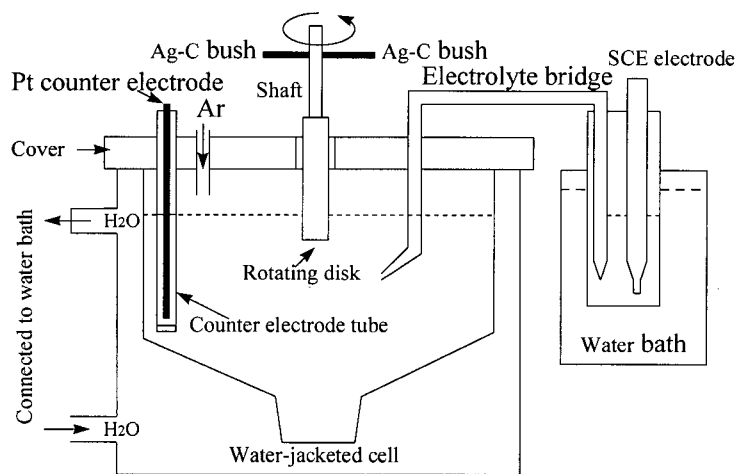
Figure 6-3 Schematic diagram of the experimental setup

A Cannon-Fenske routine viscometer (size 25) was used to measure the kinematic viscosity of the solutions studied. The experimental set-up and the measuring procedure are shown in Appendix 6. The concentration of sulphite was measured by adding an excess of standard iodine solution followed by back titration with standard thiosulphate solution (see Appendix 4).

The liquid junction potential, estimated by the Henderson equation [332] (see Appendix 7), was below 2 mV and so can be neglected. The thermal liquid junction potential was measured using two calomel reference electrodes which were placed on the two sides of an electrolyte bridge.

Reagent grade chemicals were used throughout the investigation.

6.4 Polarization Measurements

The polarization measurements were carried out at 25, 40, 50 and 60 °C in 1 M Na_2SO_4 solutions containing 0.025 to 0.5 M Na_2SO_3 and 0.025 - 0.25 M NaOH. If the applied potential was larger than about 1.0 V vs. SCE, the surface of the electrode was corroded and

became rough, affecting the current measurements (e.g. the limiting current became much lower and the current vs. potential was non-reproducible). Therefore the electrode surface was repolished for every polarization measurement to ensure reproducible results. Typical polarization curves for 0.1 M Na_2SO_3 solutions containing 0.25 M NaOH are shown in Figure 6-4 and those for 0.05, 0.2, 0.4 and 0.5 M Na_2SO_3 in Figures A-1 to A-4 in Appendix 8. The anodic oxidation of sulphite began at 0.16, 0.12, 0.08 and 0. 04 V vs. SCE for 25, 40, 50 and 60 °C respectively. Due to the presence of sulphite ions, oxygen evolution was suppressed and the corrosion of the electrode was diminished. The higher the concentration of sulphite, the greater were these effects. The oxygen evolution increases with increasing temperature. At $[Na_2SO_3] \geq 0.4$ M and 25 - 60 °C, almost no oxygen bubbles were formed and the graphite was only slightly corroded. When the current reached a limiting value, it became independent of the potential. At $[Na_2SO_3]$ = 0.05-0.4 M, the limiting current was approximately proportional to the sulphite concentration. However, the increase in the limiting current due to the increase in sulphite concentration from 0.4 to 0.5 M was much smaller than expected. The limiting current was limited probably by OH⁻ diffusion at 0.5 M Na_2SO_3.

The background current in the absence of sulphite is independent of the rotational speed (Figure A-5 in Appendix 8). However, the current measured in the presence of sulphite is sensitive to the rotational speed and the limiting current is proportional to the square root of the rotational speed. Oxygen evolution and the corrosion of graphite are greatly suppressed in the presence of sulphite. At 100 rpm (Figure 6-4), the oxygen evolution even decreased the current possibly because the oxygen bubbles were not removed efficiently. Therefore the background current in the presence of sulphite could be much smaller than that measured in the absence of sulphite and could make a negligible contribution to the total current. The background current in the absence of sulphite was inappropriate for correcting the current for the sulphite oxidation due to oxygen evolution at high potentials. The condition of the surface of the graphite electrode varied after the electrode surface was renewed each time. Therefore after the same treatment of the electrode, the values of current vs. potential scattered to some extent (±15 %). However, the limiting currents scattered less (± 2 %).
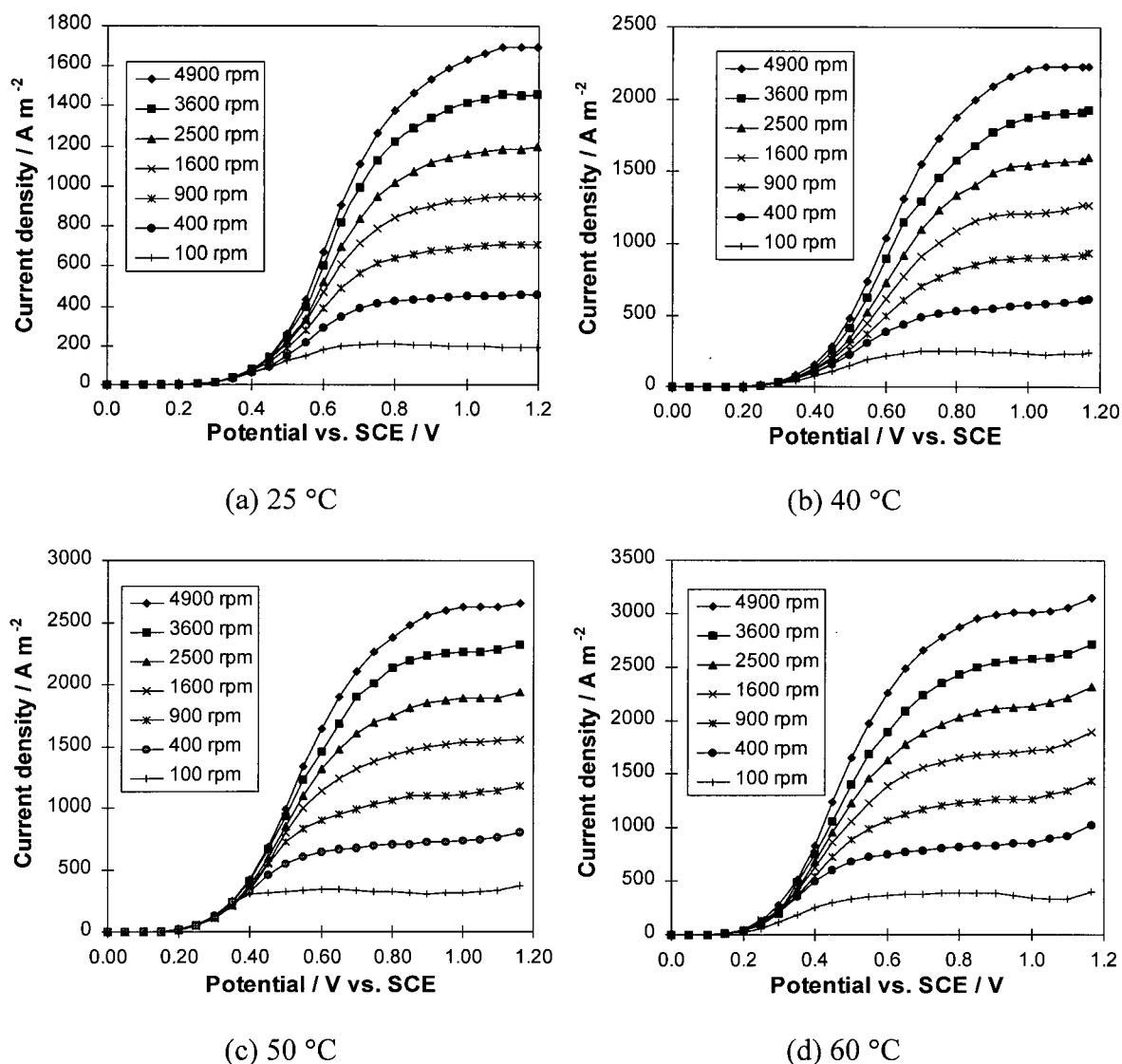
Figure 6-4 Polarization curves of sulphite oxidation using rotating disk at 25, 40, 50 and 60 °C. Electrolyte: 0.1 M Na$_2$SO$_3$, 0.25 M NaOH and 1 M Na$_2$SO$_4$.

From Figure 6-5, the polarization curves for 0.1 M Na$_2$SO$_3$ solutions containing 0.05 M NaOH are quite different from those containing 0.25 M NaOH. The current first reached a limiting value, and then increased slightly with increasing potential and finally increased with increasing potential and reached a second limiting value. Very little oxygen was evolved at potentials > 1.4 V vs. SCE. Similar polarization curves for 0.2 and 0.4 M Na$_2$SO$_3$ are shown in Figures A-6 and 7 in Appendix 8. The first limiting current increased slightly with increasing sulphite concentration from 0.1 to 0.4 M and was much smaller than the value expected for the corresponding sulphite concentration. The second limiting current (observed

at 100, 400 and 900 rpm) was proportional to the square root of the rotational speed and was a little higher than the limiting value obtained in the solution containing 0.25 M NaOH at the same sulphite concentration.

At [NaOH] = 0.05 M, the mole ratios of sulphite to hydroxide in the solution are 2, 4, 8 respectively for 0.1, 0.2 and 0.4 M Na_2SO_3. The oxidation of one sulphite ion needs two hydroxide ions according to Reaction 6-13. So the equivalent ratios of sulphite to hydroxide are 4, 8 and 16 respectively for 0.1, 0.2 and 0.4 M Na_2SO_3. So the mass transfer rates of hydroxide ions have to be 4, 8, 16 times those of sulphite ions respectively for 0.1, 0.2 and 0.4 M to maintain the alkaline condition on the electrode surface. At infinite dilution , the diffusion coefficient of hydroxide (5.26×10^{-9} m^2 s^{-1} at 25 °C) is 4.96 times that of sulphite ions (1.06×10^{-9} m^2 s^{-1}) [318].

At [Na_2SO_3] = 0.2 and 0.4 M, the current becomes so high that the mass transfer rate of hydroxide ions is not high enough to maintain the hydroxide concentration above a certain value (close to zero). Therefore the species of sulphite shifts from SO_3^{2-} to HSO_3^- and SO_2 and the properties of the surface oxygen-carbon function groups can be changed due to the proton exchange [334]. The anodic oxidation of HSO_3^- and SO_2 begins at higher potentials [240] and the change in the properties of the surface function group may result in a passivating effect. Therefore when the first limiting current appeared, the oxidized species of sulphite changed from SO_3^{2-} to HSO_3^- and SO_2 and with further increase in potential, the current increased due to the oxidation of HSO_3^- and SO_2. Finally the current reached a second limiting value related to the maximum diffusion rate of the sulphite species.

In the presence of 1 M Na_2SO_4 as supporting electrolyte, the diffusion coefficient of hydroxide ions could decrease more than that of sulphite ions and so the ratio of the diffusion coefficients may be lower than 4. Therefore two limiting currents for the solution containing 0.1 M Na_2SO_3 and 0.05 M NaOH appeared. This could be the same as that observed for the solution containing 0.5 M Na_2SO_3 and 0.25 M NaOH because the mole ratio of sulphite to NaOH (2) is the same.

At [NaOH] = 0.05 and 0.25 M, the polarization curves measured in the solutions containing 0.1 M, 0.2 and 0.4 M Na_2SO_4 at 400 rpm are shown in Figure 6-6. Compared to the polarization curves with the same sulphite concentrations, we can see: (1) at a current < about 380 A m^{-2}, the current for 0.05 M NaOH is almost the same as that for 0.25 M NaOH,

(2) at a current density > about 380 A m^{-2}, with further increase in potential, the current densities for 0.05 M NaOH are lower than those for 0.25 M NaOH. This phenomenon may be related to the limited mass transfer of hydroxide which should be the same at a constant concentration of hydroxide and rotational speed.

At a current density < about 380 A m^{-2}, when the concentrations of hydroxide at the surface for all the solutions are above a certain value (probably pH > 9). The sulphite on the surface exists only in the form of SO_3^{2-} which is discharged on the anode and the reaction order with respect to OH$^-$ is zero. Hence, the current is dependent only on the potential and the concentration of sulphite. At a current density > about 380 A m^{-2}, the concentration of hydroxide at the surface for solutions with 0.05 M NaOH becomes so low that HSO_3^- and SO_2 increase on the electrode surface and SO_3^{2-} decreases, which decreases the current density. However, the concentration of hydroxide at the surface for the solutions with 0.25 M NaOH is still high and the concentration of SO_3^{2-} does not decrease due to the shift of the sulphite species from SO_3^{2-} to HSO_3^- and SO_2.

The second limiting current for the solution with 0.05 M NaOH is larger than that for the solution with 0.25 M NaOH and the ratios of the former to the later are 1.08, 1.12 and 1.18 respectively for 0.1, 0.2 and 0.4 M Na$_2$SO$_4$. The reason could be: (1) the decrease in the concentration of hydroxide from 0.25 to 0.05 M decreases the viscosity of the solution and weakens the interaction of ions, resulting in a higher diffusion coefficient and a higher diffusion limited current, (2) the anode reaction consumes hydroxide and even generates hydrogen ions which diffuse to the bulk solution and react with SO_3^{2-} in the diffuison layer to form HSO_3^-. The diffusion coefficient of HSO_3^- (1.33 × 10^{-9} m^2 s^{-1} at infinite dilution [318]) is larger than that of SO_3^{2-} (1.06 × 10^{-9} m^2 s^{-1}at infinite dilution [330]). The concentration gradient of SO_3^{2-} is increased, resulting in a larger limiting current. This effect increases with increasing sulphite concentration because more hydrogen ions are generated at a constant hydroxide concentration in the bulk solution and therefore the ratio of the limiting currents increases with sulphite concentration.
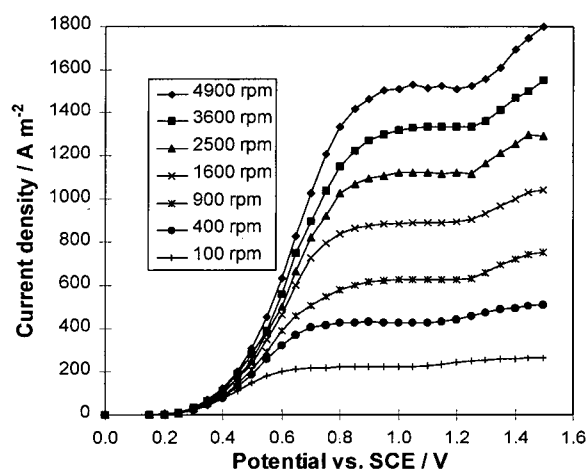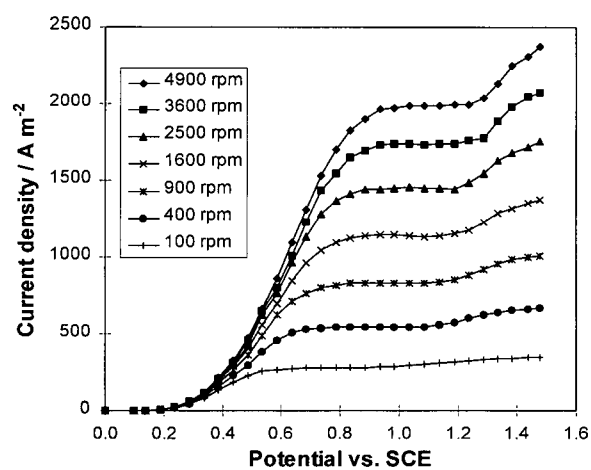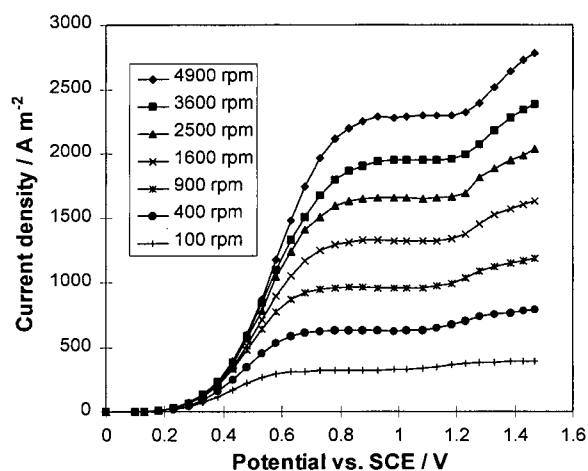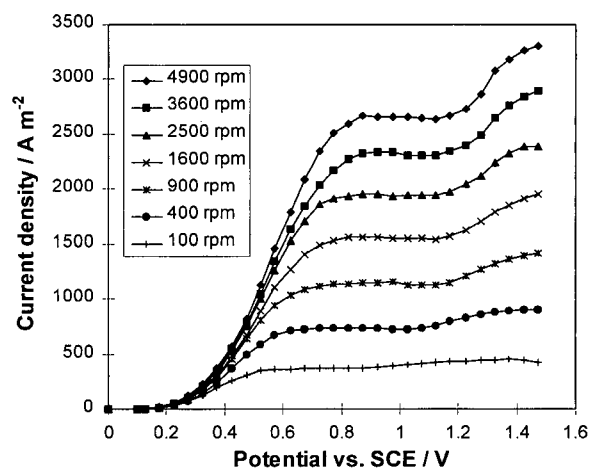
Figure 6-5 Polarization curves of sulphite oxidation using rotating disk at 25, 40, 50 and 60 °C. Electrolyte: 0.1 M Na_2SO_3, 0.05 M NaOH and 1 M Na_2SO_4.
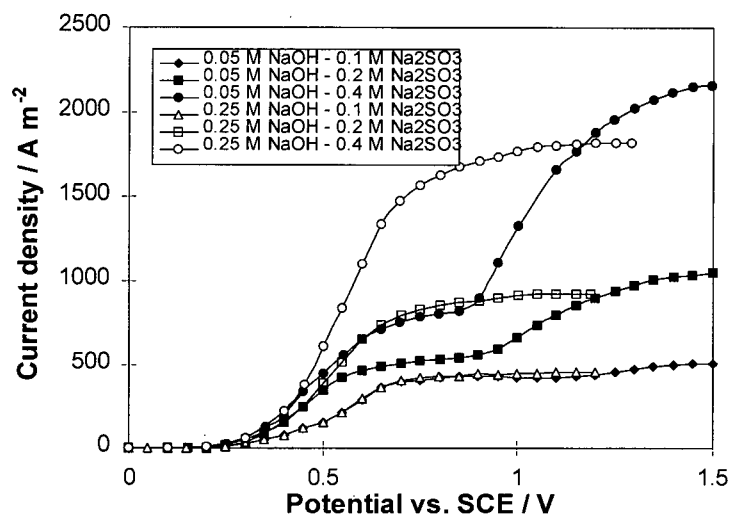
Figure 6-6   Comparison of the polarization curves with different sulphite and hydroxide concentrations at 25 °C and 400 rpm.

6.5 Coulometric Measurements

Controlled potential coulometry was used to determine the number of the electrons transferred (n) for the anodic oxidation of the sulphite ion. The electrode potentials were controlled at 0.6 and 0.9 V vs. SCE to avoid oxygen evolution and corrosion of the graphite. The results are given in Table 6-2. In all cases, the number of the electrons transferred per one sulphite ion ranges from 1.92 to 1.98. This means that almost all of the sulphite was oxidized to sulphate in two-electron reaction. Hence the oxidation of sulphite to dithionate can be neglected. Potential and temperature had almost no effect on the products of the anodic oxidation of sulphite. These results are in agreement with those reported by Glasstone and Hickling [211].

Table 6-2 Number of the electrons transferred for the anodic oxidation of sulphite

Concentration of sulphite / mol dm^{-3}	Potential / V vs. SCE	Temperature / °C	Number of electrons transferred (n) per sulphite ion
0.1	0.6	25	1.94 ± 0.03
0.1	0.9	25	1.98 ± 0.02
0.1	0.6	60	1.93 ± 0.03
0.1	0.9	60	1.97 ± 0.03
0.4	0.6	25	1.92 ± 0.04

6.6 Reaction Order

For the anodic oxidation of sulphite, the concentrations of sulphite and hydroxide can affect the reaction rate. Therefore the kinetics were first studied by changing the concentration of one species while the potential and the concentrations of the other species were maintained constant. When the potential and pH were maintained constant, the current increased with increasing sulphite concentration, indicating that the rate-controlling step involved sulphite ions. However, when the potential and sulphite concentration were maintained constant, the current was independent of pH, suggesting that the reaction order with respect to hydroxide is zero. Therefore only the sulphite concentration affects the rate of the sulphite oxidation and the kinetic expression for the anodic oxidation of sulphite ions can be reduced to Equation 6-7 over the pH range studied (11.9-13). In the mixed control region, Equation 6-11 can be applied to calculate the reaction order with respect to sulphite. The data (current vs. potential) scattered to some extent due to the inherent surface variability after the electrochemical conditioning. The data in Figures 6-4 were generated with some variation of surface condition and therefore cannot be used directly to calculate the reaction order. For the present experiments, the stability of the graphite surface was maintained by limiting the potential range of the experiments (0 - 0.7 V vs. SCE).

Figure 6-7 shows the polarization curves measured on the same electrode surface in the potential range of 0 - 0.7 V vs. SCE and in a solution containing 0.1 M Na_2SO_3, 0.25 M NaOH and 1 M Na_2SO_4. Using the data shown in Figure 6-7, the plot of log i vs. $\log(1-i/i_l)$ at 25 °C is a straight line (Figure 6-8). According to Equation 6-11, the slope of the line (i.e. the reaction order) and the intercepts on the log i axis ($\log i_k$) were calculated by least squares fitting and are given in Table 6-3. The reaction order with respect to the sulphite ion is 1. For the first order reaction, Equation 6-12 can be applied and the plot of 1/i vs. $1/i_l$ is a straight line and the intercept on the 1/i axis is $1/i_k$. From Figure 6-9, the plots of 1/i vs. $1/i_l$ are linear and the slopes are 1. The intercepts of the plot of log i vs. log $(1-i/i_l)$ are the same as - log of the intercepts of the plots of 1/i vs. $1/i_l$ at the same potential (see Table 6-2). This means that the reaction order is 1 and therefore the two methods match very well. The same results have been obtained in solutions 0.4 M Na_2SO_3, 0.25 M NaOH and 1 M Na_2SO_4. They are shown in Figures 6-10 and 6-11 and Table 6-4. The reaction order with respect to the sulphite ion at

40, 50 and 60 °C was measured at potentials below 0.65 V vs. SCE and was still one. The results at 40, 50 and 60 °C for 0.1 M Na_2SO_3 are shown in Figure A-8.
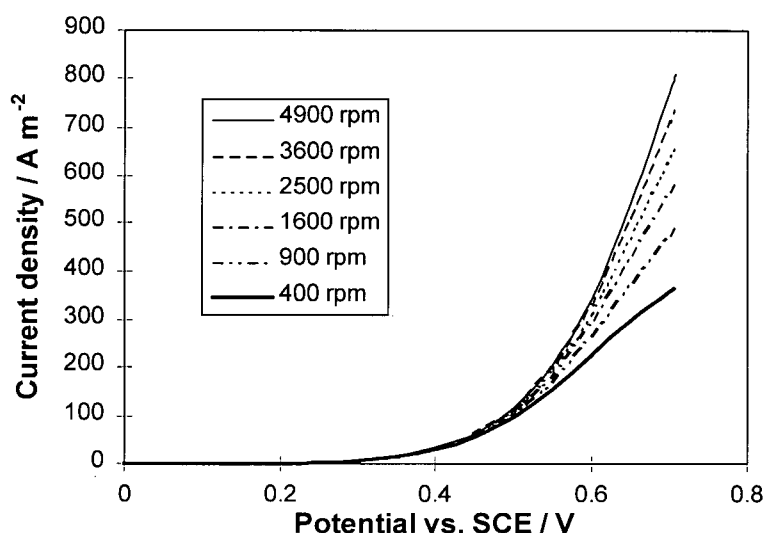
Figure 6-7 Polarization curves of sulphite oxidation using rotating disk at 25 °C. Electrolyte: 0.1 M Na_2SO_3, 0.25 M NaOH and 1 M Na_2SO_4.

Table 6-3 Reaction order and kinetic current calculated using different methods for 0.1 M Na_2SO_3.

Potential vs. SCE/ V	0.50	0.55	0.60	0.65	0.70
Slope of the plot of Log i vs. Log(1-i/i_l)	1.05	1.01	1.01	1.01	0.99
Intercepts of the plot of Log i vs. Log(1-i/i_l), i.e. i_k / A m^{-2}	2.08	2.35	2.62	2.90	3.14
Slope of plot of 1/i vs. 1/i_l	1.04	1.01	1.00	1.01	1.00
- Log (intercepts of plot of 1/i vs. 1/i_l), i.e. i_k / A m^{-2}	2.08	2.35	2.62	2.90	3.14
Log (i/(1-i/i_l)), i.e. i_k / A m^{-2}	2.06	2.33	2.61	2.89	3.15

Table 6-4 Reaction order and kinetic current calculated using different methods for 0.4 M Na_2SO_3.

Potential vs. SCE/ V	0.50	0.55	0.60	0.65	0.70
Slope of the plot of Log i vs. Log(1-i/i_l)	1.04	1.04	1.00	1.00	1.03
Intercepts of the plot of Log i vs. Log(1-i/i_l), i.e. i_k / A m^{-2}	2.64	2.90	3.19	3.39	3.62
Slope of plot of 1/i vs. 1/i_l	1.03	1.01	1.01	1.02	1.03
- Log (intercepts of plot of 1/i vs. 1/i_l), i.e. i_k / A m^{-2}	2.64	2.90	3.19	3.39	3.62
Log (i/(1-i/i_l)), i.e. i_k / A m^{-2}	2.65	2.92	3.21	3.42	3.63
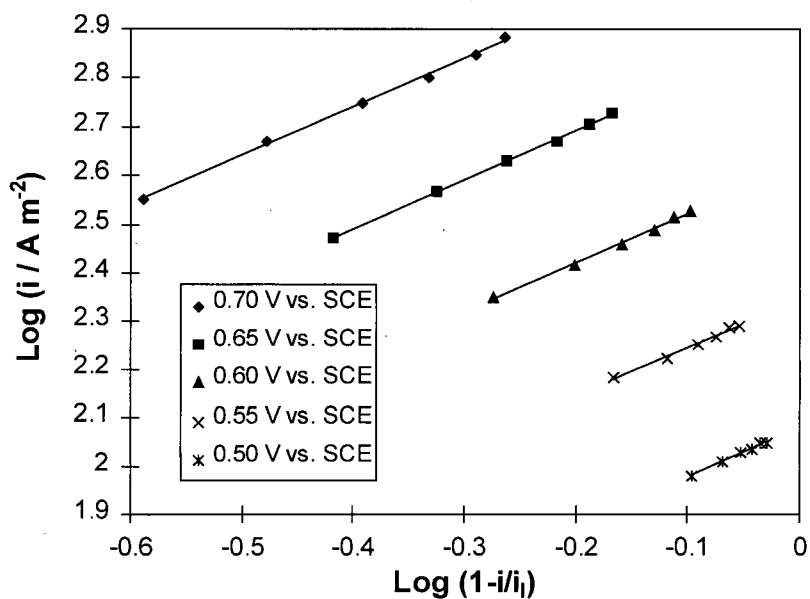
Figure 6-8 Log i vs. Log(1-i/i$_l$) at constant potential and 25 °C. Electrolyte: 0.1 M Na$_2$SO$_3$, 1 M Na$_2$SO$_4$ and 0.25 M NaOH.
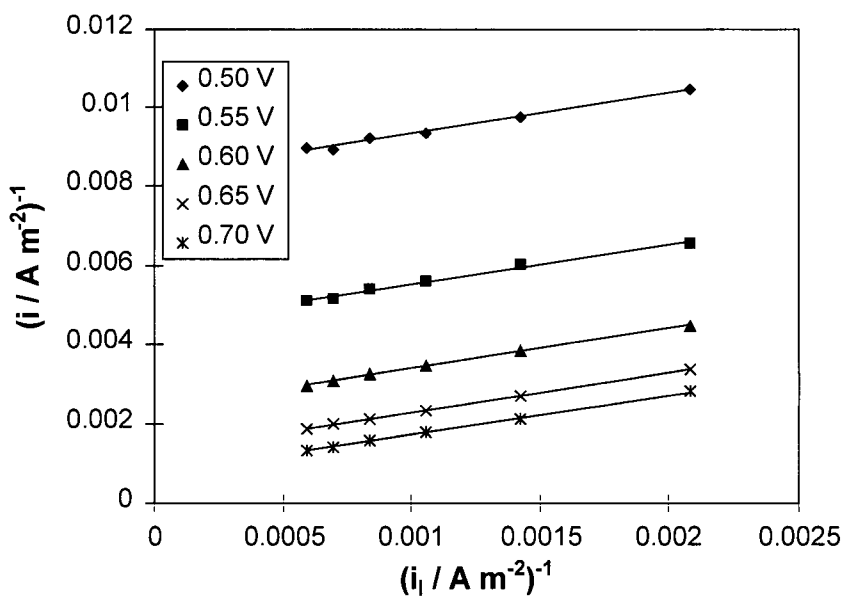
Figure 6-9 1/i vs. 1/i$_l$ at constant potential (V vs. SCE) 25 °C. Electrolyte: 0.1 M Na$_2$SO$_3$, 1 M Na$_2$SO$_4$ and 0.25 M NaOH.
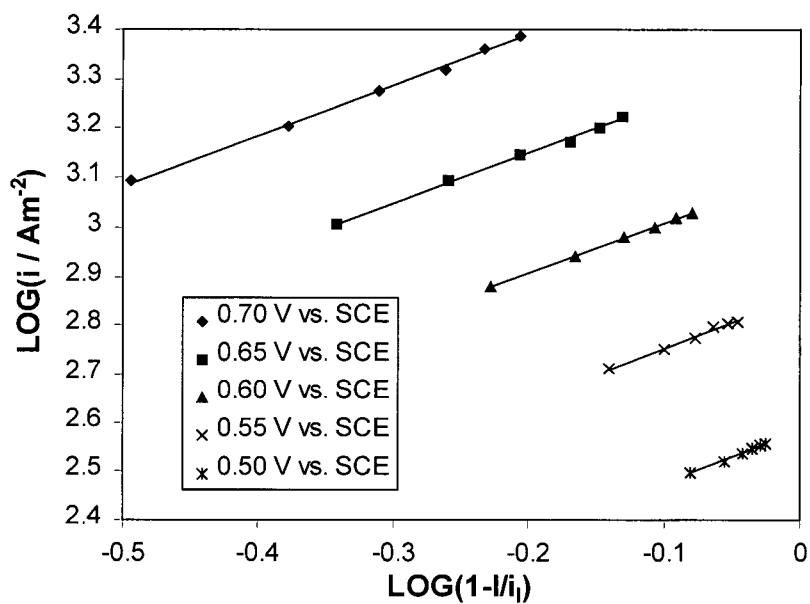
Figure 6-10 Log i vs. Log(1-i/i_l) at constant potential and 25 °C. Electrolyte: 0.4 M Na_2SO_3, 1 M Na_2SO_4 and 0.25 M NaOH.
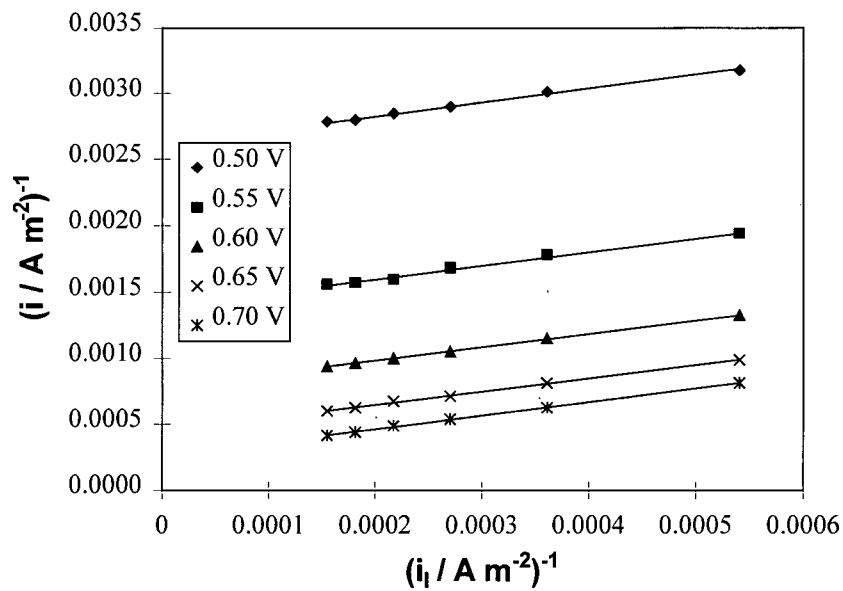
Figure 6-11 1/i vs. 1/i_l at constant potential (V vs. SCE) 25 °C. Electrolyte: 0.4 M Na_2SO_3, 1 M Na_2SO_4 and 0.25 M NaOH.

In the low polarization region, the current is small and therefore the concentrations at the electrode and in the bulk are the same. In this case, only Equation 6-7 is needed to analyze the kinetics. Equation 6-8 is not required because the mass transfer is not important. Therefore the reaction order was not calculated using the slope of the plot of log i vs. log (1-i/i_l), rather it was calculated from the plot of log i as a function of the sulphite concentration. The plots of log(i) vs. log[SO_3^{2-}] at 0.2 and 0.4 V vs. SCE at 25 °C are shown in Figure 6-12. At 0.4 V vs. SCE, the reaction order was close to 1. At 0.2 V vs. SCE, the reaction order was below 1 and appeared to be nonlinear with increasing reactant concentration. This nonlinearity could be caused by the variable adsorption of sulphite ions on the graphite electrode surface.
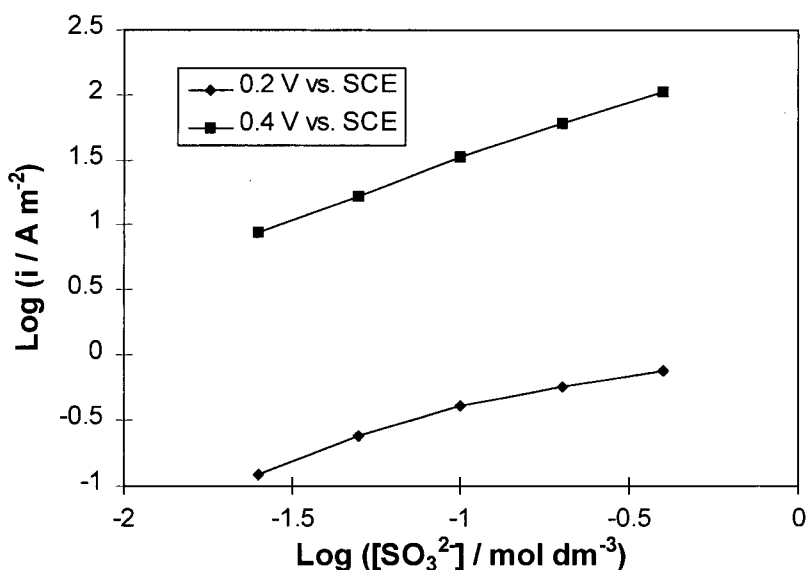
Figure 6-12 Log i vs. log [SO_3^{2-}] at 25 °C and 4900 rpm. Electrolyte: 1 M Na_2SO_4 and 0.25 M NaOH.

If the reaction order is 1, the plot of log (i /(1-i/i_l)) (corrected for the difference in concentration of sulphite between the bulk electrolyte and that at the electrode surface) vs. potential should be a straight line. At low current, (1-i/i_l) is close to 1 and the concentration difference can be neglected. The plots of log (i /(1-i/i_l)) vs. potential at 25, 40, 50 and 60 °C are shown in Figure 6-13. The corrected current (i/(1-i/i_l)) is the same as the kinetic current (i_k) calculated using the above methods (see Table 6-2). There are two Tafel slopes. The first Tafel slope at low potentials was 0.059 -0.066 V decade^{-1} and the charge transfer coefficient

was about 1. The second Tafel slope at high potentials was 0.19-0.22 V decade^{-1} with the charge transfer coefficient being in the range of 0.29 - 0.31. The Tafel slopes for the different potentials ranges and temperatures are listed in Table 6-5.

Table 6-5 Tafel slopes (V decade^{-1}) for the different potential ranges at 25, 40, 50 and 60 °C

Temperature	25 °C	40 °C	50 °C	60 °C
Low potential range (vs. SCE / V)	0.16 - 0.25	0.11 - 0.22	0.08 - 0.18	0.04 - 0.15
Tafel slopes for low potential range	0.059	0.061	0.064	0.066
High potential range (vs. SCE / V)	0.4 - 0.7	0.38 - 0.66	0.38 - 0.64	0.36 -0.64
Tafel slopes for high potential range	0.19	0.20	0.21	0.22

The first Tafel slope (0.060 V decade^{-1}) corresponds to a nonlinear reaction order (less than 1) at low potential (0.16 -0. 25 V vs. SCE) and the second Tafel slope corresponds to a first order reaction at high potentials (0.4 - 0.7 V vs. SCE) at 25 °C. This information suggests that there are two reaction mechanisms.

The change in Tafel slope, hence in the mechanism was not due to the potential-dependent change in the nature of electrode surface because after electrochemical conditioning, the electrode surface was stable over the potential range 0 - 0.7 V vs. SCE. For example, at 25 °C, the background current was almost constant over the potential range 0 - 0.6 V vs. SCE, but the change in the Tafel slope happened between 0.3 - 0.4 V vs. SCE (see Figure 6-13). The Tafel slope change could be due to the following: at low potential, the oxidation of the adsorbed sulphite was dominant and at high potential, the oxidation of unadsorbed sulphite was dominant. Tarasevich et al. [240, 243] reported that the first Tafel slope was 0.060 - 0.070 V decade^{-1} and the reaction order obtained by the change of sulphite concentration was close to 1, However, these authors did not give the other Tafel slope.
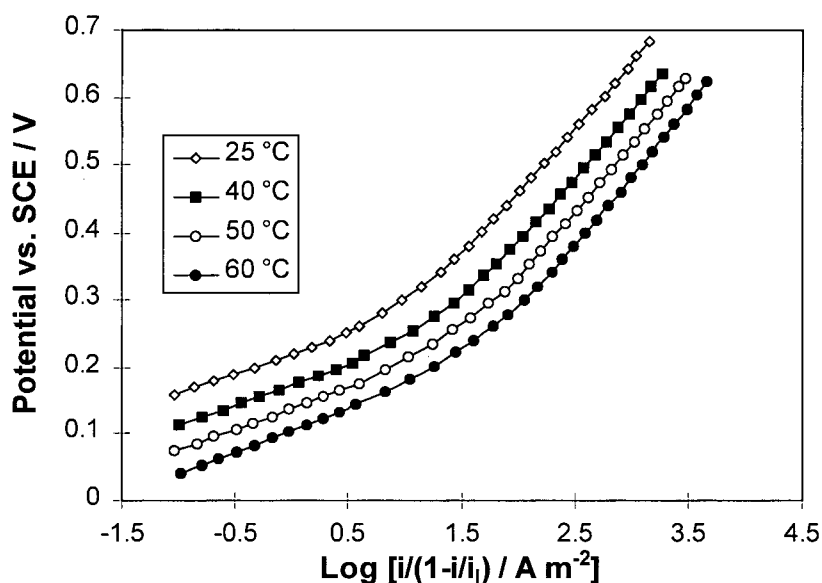
Figure 6-13 Potential vs. log $((i/(1-i/i_l))$ at different temperatures. Electrolyte: 0.1 M Na_2SO_3, 1 M Na_2SO_4 and 0.25 M NaOH.

6.7 Effect of pH

The effect of pH was studied by changing the sodium hydroxide concentration in the electrolyte containing 1 M Na_2SO_4. However, the electrolyte contained 1 M Na_2SO_4 and the pH measurement was not accurate because the electrolyte had a large background concentration of Na_2SO_4. Therefore the activity coefficient of OH⁻ was calculated by Pitzer's model (see Appendix 5). Figure 6-14 shows the polarization curves in 0.1 M Na_2SO_3 solution with different concentrations of hydroxide. The plots of the current (corrected for the difference of concentration between the electrode surface and the bulk solution) vs. pH are shown in Figure 6-15. The current at a constant potential appears to be almost independent of pH. Therefore the reaction order with respect to OH⁻ is almost zero. This result is consistent with those reported by Tarasevich et al. [240, 243] and means that the rate-controlling step does not involve OH⁻.
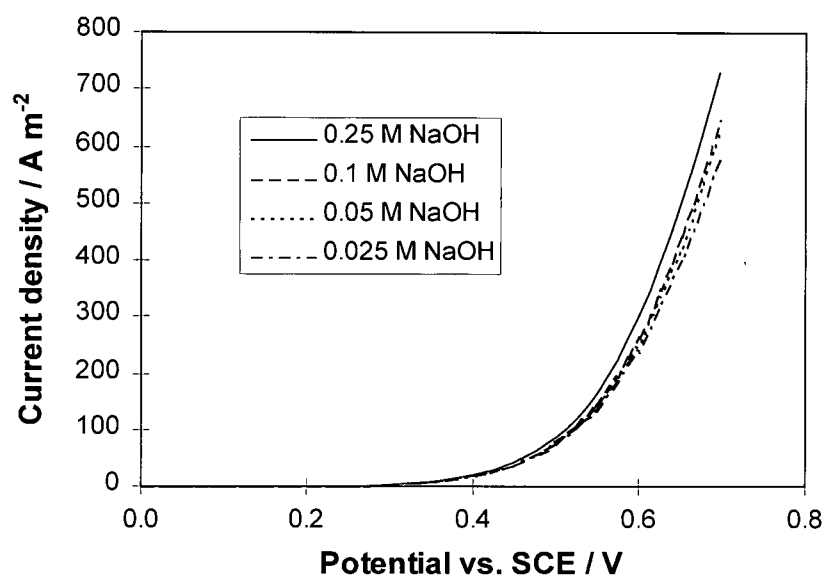
Figure 6-14 Polarization curves at different hydroxide concentrations and 25 °C. Electrolyte: 0.1 M Na$_2$SO$_3$ and 1 M Na$_2$SO$_4$.
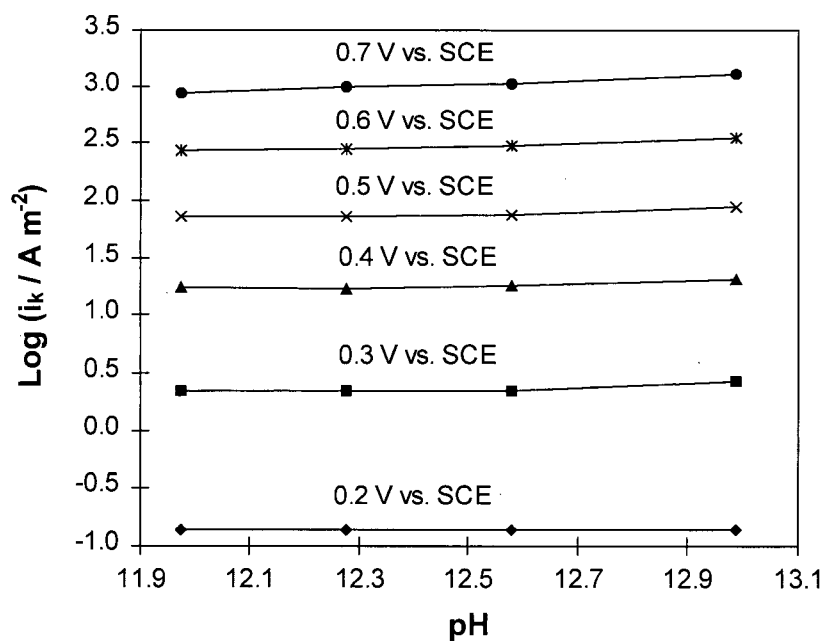
Figure 6-15 Effect of pH on sulphite oxidation at different potentials and 25 °C.
    Electrolyte: 0.1 M Na$_2$SO$_3$, 1 M Na$_2$SO$_4$ at variable pH

6.8 Calculation of Activation Energy for the Kinetic Current

At a constant potential, the following equation can be written:

$$\text{Log } i_k = \text{constant} + \frac{U_a^{\ddagger}(E)}{2.303RT} = \text{constant} + \frac{U^{\ddagger} - \alpha_a FE}{2.303RT} \qquad (6\text{-}17)$$

Where $U_a^{\ddagger}(E)$ is the activation energy at potential E, $U^{\ddagger}$ the activation energy at potential = 0, α_a the anodic charge transfer coefficient and R the gas constant. The activation energy can be calculated from the slope of the plot of log i_k vs. 1/T (Figure 6-16). The slopes of these linear plots were calculated by least squares fitting. The activation energy decreases quickly with increasing potential at low potentials and finally behaves linearly with potential at potentials > 0.4 V vs. SCE. This is due to a change in the reaction mechanism which results in a change in the charge transfer coefficient.
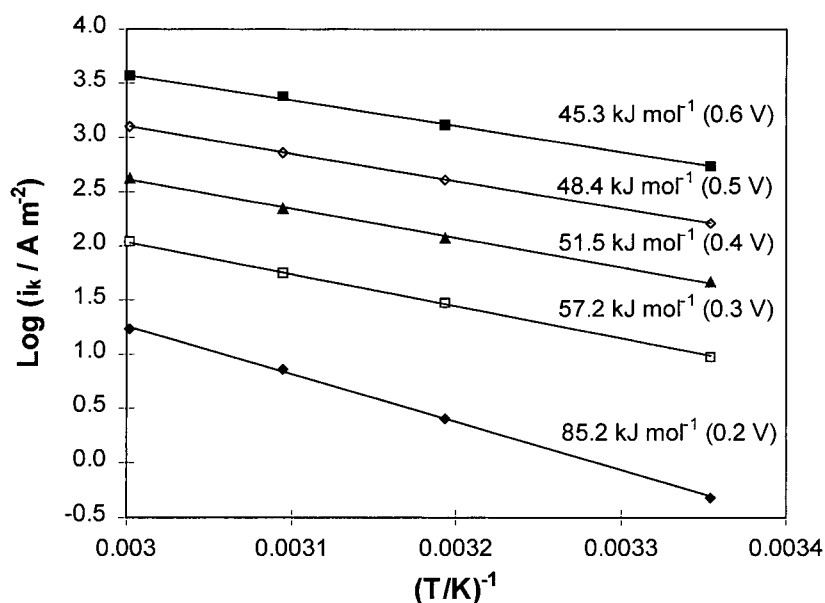
Figure 6-16 Log i_k vs.1/T at different potentials (V vs. SCE). Electrolyte: 0.1 M Na_2SO_3, 1 M Na_2SO_4 and 0.25 M NaOH.

6.9 Diffusion Coefficient Estimation

The plots of diffusion current vs. rotational speed at different temperatures are shown in Figure 6-17. These plots permit the calculation of the diffusion coefficients of SO_3^{2-} using

the slopes of the lines and Equation 6-4. The slopes were calculated using least squares fitting. The kinematic viscosity values for 0.05 M Na2O3, 0.25 M NaOH and 1M Na_2SO_4 were 1.345, 0.982, 0.818 and 0.695 × 10^{-6} m^2 s respectively for 25, 40, 50 and 60 °C. The diffusion coefficients at 25, 40, 50 and 60 C were 5.6, 8.6, 9.99 and 12.4 × 10^{-10} m^2 s^{-1} respectively. The diffusion coefficient obtained at 25 °C ($5.6 × 10^{-10}$ m^2 s^{-1}) is much lower than the value at infinite dilution ($1.06 × 10^{-9}$ m^2 s^{-1}) [330]. This difference could be caused by the high ionic strength (above 3.1 M) where the ion-ion interaction is significant and the kinematic viscosity is 35 % greater than that for water, decreasing the diffusion coefficient. The coefficient at 25 °C is close to the values ($6 - 7×10^{-10}$ m^2 s^{-1} in 0.5 M Na_2SO_4) reported by Hunger et al. [254]. At infinite dilution, the diffusion coefficient has the following temperature dependence:

$$Log\ D = constant - \frac{E_a}{2.303RT} \qquad (6\text{-}18)$$

where D is the diffusion coefficient, Ea the diffusion activation energy, R the gas constant, T the absolute temperature.

The diffusion activation energy calculated from the slope of the log plot of diffusion coefficient vs. 1/T (Figure 6-18) is 18 kJ $mole^{-1}$.
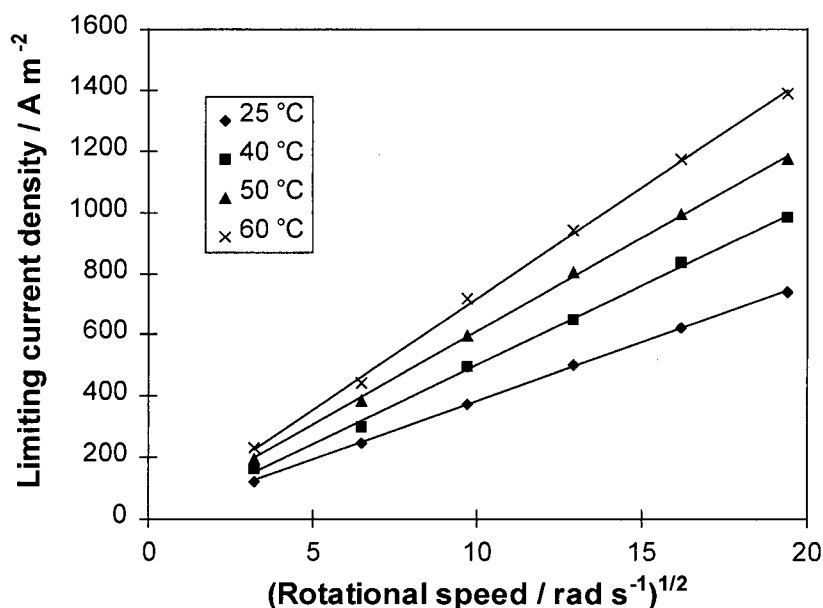
Figure 6-17 Diffusion current density vs. the square root of rotational speed at different temperatures. Electrolyte: 0.05 M Na_2SO_3, 1M Na_2SO_4, 0.25 M NaOH.
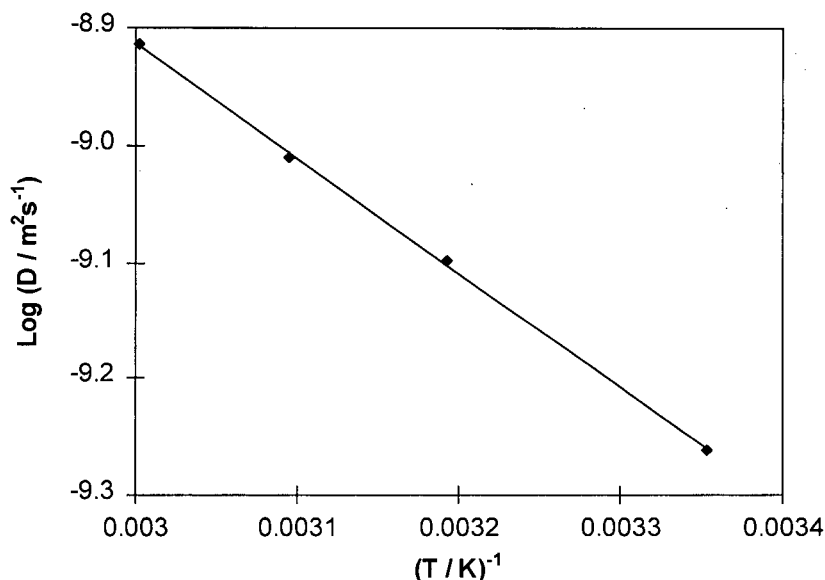
Figure 6-18 Log plot of diffusion coefficient vs.1/T.

6.10 Potential Sweep Study

The potential sweep method was used to study the anodic oxidation of sulphite. Figure 6-19 shows the cyclic voltammograms after subtraction of the background current for different scan rates. There is no negative current corresponding to the reduction of the oxidized products (or intermediates) and the oxidation of sulphite is therefore irreversible. The peak current density (i_p) is given by the following equation for the irreversible reaction [333]:

$$i_p = (2.99 \times 10^5) n(\alpha)^{1/2} C_b D^{1/2} v^{1/2} = B v^{1/2} \tag{6-19}$$

where n is the number of transferred electrons, α the rate-controlling step charge transfer coefficient, C_b the bulk reactant concentration, D the diffusion coefficient, v the potential scan rate and B $= (2.99 \times 10^5) n(\alpha)^{1/2} C_b D^{1/2}$. The peak current is proportional to the square root of the potential scan rate. The plot of i_p vs. $v^{1/2}$ gave a linear relationship (Figure 6-20). The slope (B) was calculated by least squares fitting. The following relationship obtains:

$$\left| E_p - E_{p/2} \right| = \frac{1.857 RT}{\alpha F}$$

(6-20)

where E_p is the peak potential and $E_{p/2}$ the potential when $i = i_p/2$.

From the above equation we obtain an apparent charge transfer coefficient of 0.33 which is close to that (0.30-0.31) calculated using the Tafel slope at high potentials. The total number of the electrons transferred is 1.98, 1.98, 2.00, 1.98 by combination of B, C_b, α_a, D at 25, 40, 50 and 60 °C respectively. This number corresponds to the stoichiometry indicated by Equation 6-13.
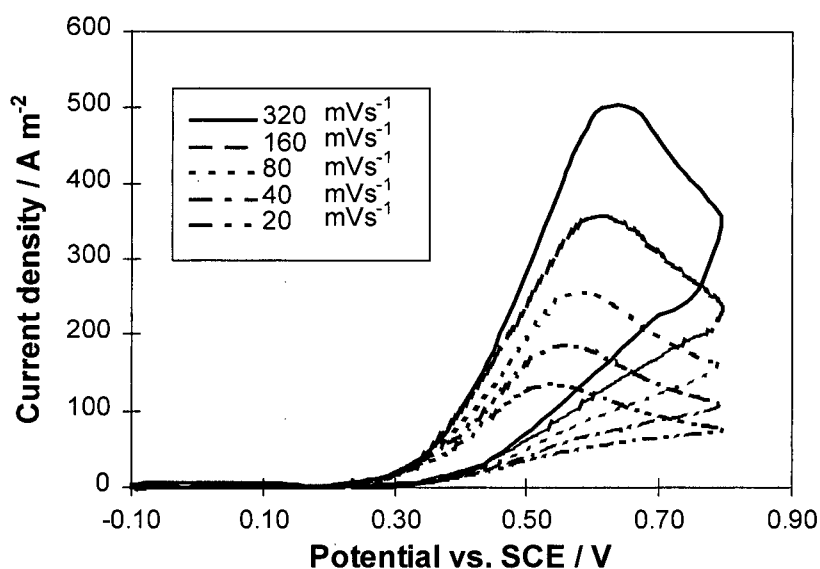
Figure 6-19 Voltammograms at different scan rates at 25 °C. Electrolyte: 0.1 M Na_2SO_3, 1 M Na_2SO_4, 0.25 M NaOH.
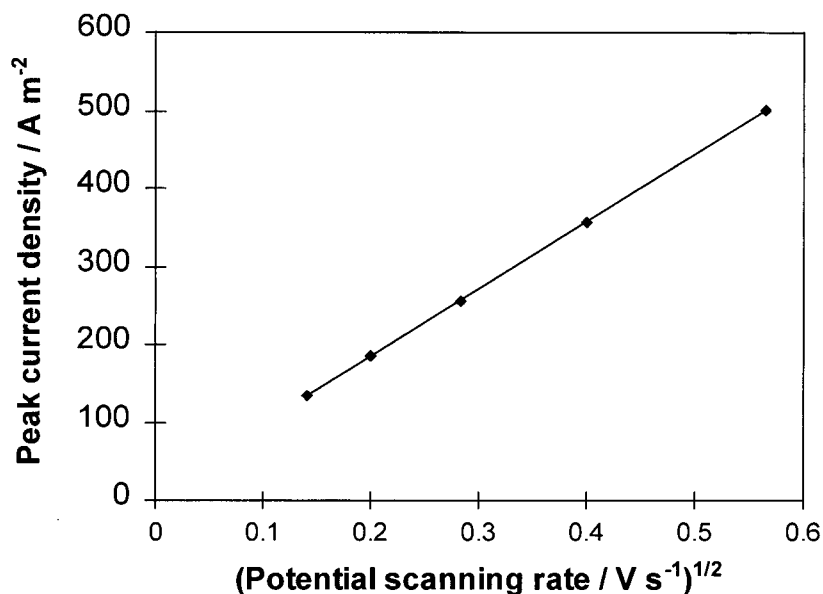
Figure 6-20 Peak current vs. potential scan rate at 25 °C. Electrolyte: 0.1 M
Na_2SO_3, 1 M Na_2SO_4 and 0.25 M NaOH.

6.11 Possible reaction mechanism

From Figure 6-13, there are two Tafel regions. The first one is 0.059 -0.066 V decade[-1] from 25 to 60 °C at low potentials and the second is 0.19-0.22 V decade[-1] at higher potentials. The corresponding charge transfer coefficients are 1 and 0.3 respectively. These values suggest a change in the reaction mechanism or in the rate-controlling step. The reaction order at low potentials is below 1 and nonlinear. It decreases slightly with increasing sulphite concentration indicating that the adsorbed sulphite could begin to be oxidized at low potentials. There are no peaks corresponding to the adsorption in the voltammograms. This means that only a very small amount of sulphite adsorbs on the electrode surface. Tarasevich et al. [239] studied the adsorption and electrooxidation of sulphite on platinum using radioactive tracers. They found that SO_3^{2-} was weakly adsorbed on the surface and the amount of adsorbed SO_3^{2-} did not change over the potential range -0.24 - 0. 26 V vs. SCE. It decreased to zero with increasing potential from 0.26 to 0.56 V vs. SCE at 22 °C. In the present study, it was found that SO_3^{2-} begins to be oxidized on a graphite anode at 0.16 V vs. SCE at 25 °C and the Tafel slope was a constant value of 0.060 V decade[-1] over the potential range 0.16 - 0.25 V vs. SCE. With further increase in potential, the Tafel slope increased with

increasing potential. When the potential exceeded 0.4 V vs. SCE, the Tafel slope remained at 0.19 V decade^{-1} and was independent of the potential.

The above phenomenon can be explained as follows: (1) at 0.16 -0.25 V vs. SCE, the adsorbed SO_3^{2-} is oxidized and the coverage of adsorbed SO_3^{2-} is independent of potential and therefore the Tafel slope (0.060 V decade $^{-1}$) is independent of the potential and the reaction order with respect to SO_3^{2-} is below 1 and nonlinear; (2) at 0.25 - 0.4 V vs. SCE, the coverage of adsorbed SO_3^{2-} decreases with increasing potential. Therefore the Tafel slope increases with increasing potential; (3) at potential > 0.4 V, the amount of adsorbed SO_3^{2-} is negligible and the direct oxidation of unadsorbed SO_3^{2-} dominates. Thus the Tafel slope becomes independent of the potential and the reaction order with respect to SO_3^{2-} become unity. The reaction order with respect to OH^- ions is almost zero. This means that the rate-controlling steps for the two Tafel slope regions do not involve OH^-. There are numerous carbon oxide surface groups on graphite [243, 334] and sulphur could be bound to these surface groups during the adsorption. In accordance with the these phenomena, the following reaction mechanism is proposed:

At low potentials (< 0.25 V SCE), sulphite first adsorbs on the graphite, then loses the first electron, finally undergoing oxygen transfer and losing the second electron. For example,

Step 1 : $SO_3^{2-} \Leftrightarrow SO_3^{2-}{}_{(ad.)}$

Step 2: $SO_3^{2-}{}_{(ad.)} \Leftrightarrow SO_3^{\cdot}{}_{(ad.)} + e$

Step 3: $SO_3^{\cdot}{}_{(ad.)} \rightarrow SO_3^{\cdot}$

Step 4: $SO_3^{\cdot} + 2OH^- \rightarrow SO_4^{2-} + H_2O + e$
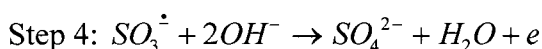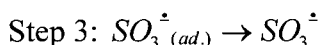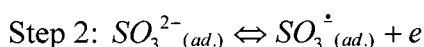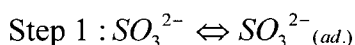
Considering the theory of multistep electrode reactions [335, 336], if step 1 is rate-controlling, the current should be independent of potential. If step 2 is rate-controlling, the Tafel slope should be above 0.059 V decade^{-1} at 25 °C (because the charge transfer coefficient < 1). If step 4 is the rate-controlling step, the Tafel slope should be around 0.040 V decade^{-1} at 25 °C and the reaction order with respect to OH^- ions should be 1 or more. If step 3 is rate-controlling, the Tafel slope is 0.059 V decade^{-1} at 25 °C. The reaction order with respect to OH^- ions could be zero. Looking at the experimental results, Step 3 could be rate-controlling.

At high potentials (> 0.4 V vs. SCE), sulphite first loses one electron, subsequently undergoes oxygen transfer and loses the second electron.

Step 1: $SO_3^{2-} \rightarrow SO_3^{\cdot} + e$

Step 2: $SO_3^{\cdot} + 2OH^- \rightarrow SO_4^{2-} + H_2O + e$
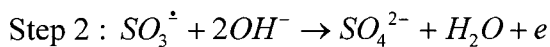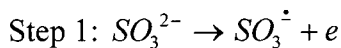
The charge transfer coefficient is only about 0.3, suggesting that the loss of the first electron is the rate-controlling step. This is in agreement with the reaction order with respect to sulphite ions. The reaction order with respect to hydroxide ions is zero, suggesting that the rate-controlling step does not involve hydroxide ions. Therefore step 1 could be the rate-controlling step at high potentials. It should be noted that a small amount of $SO_3^{\cdot}$ could combine to form dithionate and therefore the number of the electrons transferred is slightly below 2.

6.12 Summary

At low potentials (e.g. < 0.25 V vs. SCE at 25 °C), the reaction order for the oxidation of sulphite is below 1 and decreases with increasing sulphite concentration. The Tafel slope is 0.059 -0.065 V decade^{-1} in the temperature range 25-60 °C. At high potentials (> 0.4 V vs. SCE), the reaction order with respect to sulphite ions is 1 up to 0.4 M sulphite and the Tafel slope is 0.19 - 0.21 V decade^{-1}. The reaction order with respect to hydroxide ions is close to zero at surface pH > about 9.

The activation energy for the kinetic current decreases from 85.2 kJmol^{-1} at 0.2 V vs. SCE to 45.3 kJmol^{-1} at 0.6 V vs. SCE. The diffusion coefficients of sulphite ions were obtained and shown to have an activation energy of 18 kJ mol^{-1}.

Sulphite oxidation in alkaline solution appears to undergo a radical-electron mechanism. At low potentials, the adsorbed sulphite oxidation is dominant and at high potentials, the sulphite ions are oxidized directly on the electrode surface. The loss of the first electron from sulphite ions appears to be the rate-controlling step at high potentials.

7. ANODIC OXIDATION OF COPPER CYANIDE ON A GRAPHITE ANODE IN ALKALINE SOLUTION

To decrease the consumption of cyanide, it is important to understand the anodic oxidation of copper cyanide. However, the information available is inadequate and further studies are needed. Therefore a study of the anodic oxidation of copper cyanide was conducted using the rotating disk technique.

7.1 Experimental Apparatus and Set-up

The graphite rotating disk was the same as described in Section 6.3. To ensure reproducible results, the electrode was first treated by cyclic voltammetry between 0 -0.75 V vs. SCE in 0.25 M NaOH and 1M Na_2SO_4 solution at 100 rpm for 30 minutes and polarized at 1 mV s^{-1} until the electrode reached a stable condition. Graphite having diameters of 12 and 24 mm was fashioned as a rotating disk for coulometric measurements. A pyrolytic graphite rotating disk having a diameter of 4 mm and a platinum electrode having a diameter of 5 mm were made by the EG & G Co.

The rotating disk electrode system was an EG & G PARC Model 636 Electrode Rotator. The potentiostats were Model SOLARTRON 1286 and PARC 273A electrochemical Interface. Argon gas was first bubbled through the solution and the experiments were conducted under an argon atmosphere to avoid the possible effect of the air. The experimental set-up was the same as shown in Figure 6-3. The polarization curves were generated using the potential sweep method at 1 mV s^{-1} as noted.

A LEYBOLD MAX 200 XPS instrument was used to analyze the anode precipitate. A Siemens diffractometer D50000 was used to obtain the X-ray diffraction pattern of the precipitate. Samples of the anode precipitate for XPS and X-ray diffraction were placed in a bottle filled with Ar gas to protect against oxidation by air.

The stopped-flow technique and spectrometry using a SHIMADZU Model UV-2401PC UV spectrometer were employed to detect the cupric cyanide species. NaCN and $CuSO_4$ solutions were injected into a T -tube in one second and well mixed, finally entering the quartz cell for UV detection. The experimental set-up is shown in Figure 7-1.
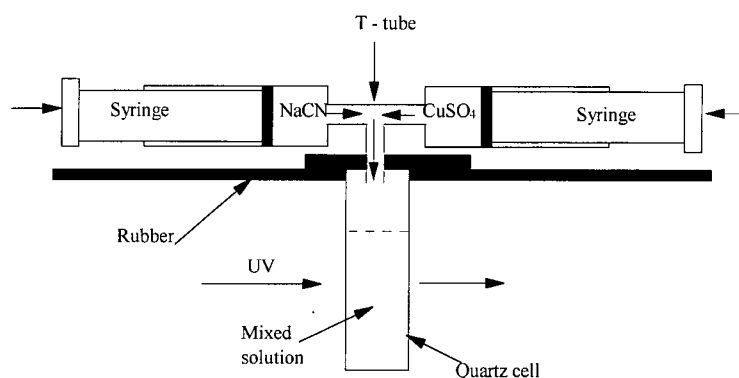
Figure 7-1 Schematic diagram for detection of cupric cyanide species

The kinematic viscosity of the solution was measured using a Cannon-Fenske routine viscometer (size 25) (see Appendix 6).

The liquid junction potential for a dilute copper cyanide solution was calculated by the Henderson equation (see Appendix 7). The liquid junction for concentrated copper cyanide was not considered because there are no data for copper cyanide species and the mobilities of copper cyanide species are expected to be close to that of sodium ion. The thermal liquid junction potential was measured using two calomel reference electrodes which were placed on the two sides of an electrolyte bridge.

The cyanide concentration was measured using the distillation-absorption-titration procedure (see Appendix 2). The copper concentration was measured by oxidizing copper cyanide to cupric nitrate using concentrated nitric acid and titration with EDTA (see Appendix 3).

Reagent grade chemicals were used in all the experiments.

7.2 Polarization Measurements and Identification of the Precipitate

7.2.1 Anodic Behaviour for Dilute Copper Cyanide Solution

To develop an understanding of the anodic oxidation of copper cyanide, the study of the electrode kinetics was first carried out in dilute copper cyanide solution in the presence of an excess of inert supporting electrolyte. As a result, all the observed potential difference was

concentrated on the electrode solution interface and available for affecting the actual rate of the electrode reaction.

The polarization measurements were conducted at 25, 40, 50 and 60 °C in alkaline solution with different concentrations of cyanide, copper and sodium hydroxide. As copper oxide and hydroxide were precipitated on the electrode surface during the polarization measurement, the electrode surface was repolished after every polarization to ensure reproducible results. The polarization curves for 0.05 M cyanide and a CN:Cu mole ratio of 3 at 25, 40, 50 and 60 °C are shown in Figure 7-2. The anodic oxidation of copper cyanide can be divided into three potential regions. In the first region (approximately 0 - 0.4 V vs. SCE), no precipitate was formed on the electrode. In the second region (approximately 0.4 - 0.6 V vs. SCE), copper oxide and hydroxide were formed on the electrode surface and the current increased sharply with increasing potential. In the third region (about > 0.6 V SCE), the oxygen was evolved.

The behavior of current vs. potential was dependent on the temperature and the rotational speed. At 25 °C (Figure 7-2a), when the rotational speed was 100 rpm, the current reached a limiting value and did not decrease with increasing potential. However, when the rotational speed was above 100 rpm, the current reached a maximum value and then decreased with increasing potential. At 40 °C (Figure 7-2b), when the rotational speed was below 1600 rpm, the current did not decrease with potential. When the rotational speed was above 2500 rpm, the current reached a maximum value, then stabilized and finally decreased with increasing potential. At 50 and 60 °C (Figure 7-2c and d), the current did not decrease with increasing potential. This anodic oxidation behaviour of copper cyanide is related to the precipitation of copper oxide.

From the cyclic voltammetry (Figure 7-3), the effect of the precipitation of the copper oxide was dependent on the applied potential. At 25 °C and 100 rpm (Figure 7-3a), when the potential was swept from 0 to 0.55 V vs. SCE and then back to 0 V vs. SCE, the current for the negative-going sweep was larger than that for the positive-going sweep. This means that the precipitate had a catalytic effect on the anodic oxidation of copper cyanide. When the potential was swept from 0 to 0.60 V vs. SCE and then back to 0 V vs. SCE, the current for the negative-going sweep was smaller than that for the positive-going current. This indicates that the precipitate had a passivating effect on the anodic oxidation of copper cyanide. The

change in the catalytic properties of copper oxide may be caused by the adsorption of oxygen produced in the electrode reaction. The cyclic voltammetry at 40 °C and 100 and 1600 rpm (Figure 7-3b) shows again the catalytic effect of the precipitate of copper oxide.

From Figure A-9 (Appendix 8), the precipitated copper oxide has a much more pronounced catalytic effect on the cyanide oxidation than the graphite and copper ions in the solution.

From the XPS analysis of the precipitate (Figures A-9 and A-10 in Appendix 8), the precipitate was found to be copper oxide. The curve fitting of the XPS spectrum (Figures A-11 and A-12 in Appendix 8) confirmed that the precipitate was a combination of copper oxide and copper hydroxide. The contents of CuO and $Cu(OH)_2$ on the surface were respectively about 50 % at 25 °C and 70 % at 60 °C. So the ratio of CuO to $Cu(OH)_2$ in the precipitate increased with increasing temperature.

The precipitation of copper oxide and hydroxide suggests that copper cyanide can be oxidized to copper oxide and cyanate. The onset of the precipitation of copper oxide depends on the CN:Cu mole ratio and potential. At low rotational speeds, the onset of the precipitation of copper oxide appears at lower potentials than at high rotational speeds leading to higher currents. The reason could be that at the same potential, the CN:Cu mole ratio at the electrode surface for a low rotational speed is lower than that at the high rotational speed, also the lowly coordinated copper cyanide complexes are less stable than the highly coordinated complexes and are easier to oxidize to copper oxide and cyanate. The onset of the formation of copper oxide occurs at higher potentials at a higher CN:Cu mole ratio from the polarization measurement.

In the third region (potentials > about 0.6 V vs. SCE), a gas was evolved, which could be oxygen or nitrogen due to the further oxidation of cyanate. The current did not change uniformly with increasing rotational speed because the film of copper oxide on the graphite was formed irregularly. Even part of it dropped from the electrode. The coating of CuO significantly increases the oxygen evolution (see Figure A-14 in Appendix 8). The current decreased with increasing potential after it reached a maximum value because the oxide film became loosely adherent on the graphite. In fact, some of it dropped from the electrode due to the oxygen evolution. In the absence of copper cyanide, the polarization curves for the electrode with precipitated copper oxide in the case of the solution containing 0.05 M cyanate

were almost the same as those without cyanate. This suggests that the evolution of oxygen was dominant.

Increasing the CN:Cu mole ratio (decreasing [Cu]) results in a change in the anodic behaviour of copper cyanide (Figures A-15 to A-18 in Appendix 8). The polarization curves for the solutions with CN:Cu mole ratios of 3.5 and 4 are similar to those for the solution with a CN:Cu mole ratio of 3. The difference is that the onset of the precipitation of copper oxide begins at a higher potential. However, at CN:Cu mole ratios of 6 and 12, there were no well defined limiting currents because the precipitation of copper oxide began at about 0.6 V vs. SCE and oxygen is ready to be evolved on the copper oxide, affecting the oxidation of copper cyanide. At a CN:Cu mole ratio of 6 (25 to 50 °C) or 12, the precipitated oxide was not tightly adherent to the graphite. Therefore the evolution of oxygen was not catalyzed significantly by the copper oxide as observed at lower mole ratios of cyanide. However, at a CN:Cu mole ratio of 6 and 60 °C the current increased continually with increasing potential because the copper oxide was relatively well deposited on the electrode and catalyzed significantly the evolution of oxygen.

Decreasing hydroxide concentration also leads to the change in the anodic behaviour of copper cyanide (see Figure A-19 to A-24 in Appendix 8).

At [OH⁻] = 0.05 M, the polarization curves for 0.05 CN⁻ solutions with CN:Cu mole ratios of 3, 4 and 12 are shown in Figures A-19 to A-21 (Appendix 8) respectively. The anodic behaviour of the copper cyanide solution can be divided into the three potential regions similar to those with 0.25 M NaOH. However, the formation of copper oxide and oxygen evolution was suppressed.

At [OH⁻] = 0.01 M, the polarization curves for 0.05 M CN⁻ solutions with CN:Cu mole ratios of 3, 4 and 12 are shown in Figures A-22 to A-24 respectively. The formation of copper oxide and oxygen evolution was significantly decreased. At CN:Cu mole ratio = 12, almost no copper oxide was formed.

Comparing the anodic behaviour of copper cyanide with 0.25 M NaOH (Figure 7-2, 7-11 and 7-13), 0.05 M NaOH (Figures A-19 to A-21) and 0.01 M NaOH (Figures A-22 to A-24), hydroxide and copper concentrations affect the anodic oxidation of copper cyanide significantly in some potential regions and the effect of hydroxide concentration is dependent

on copper concentration because the anodic behaviour is related to the distribution of copper cyanide species, as discussed in Sections 7-4 and 7-5.
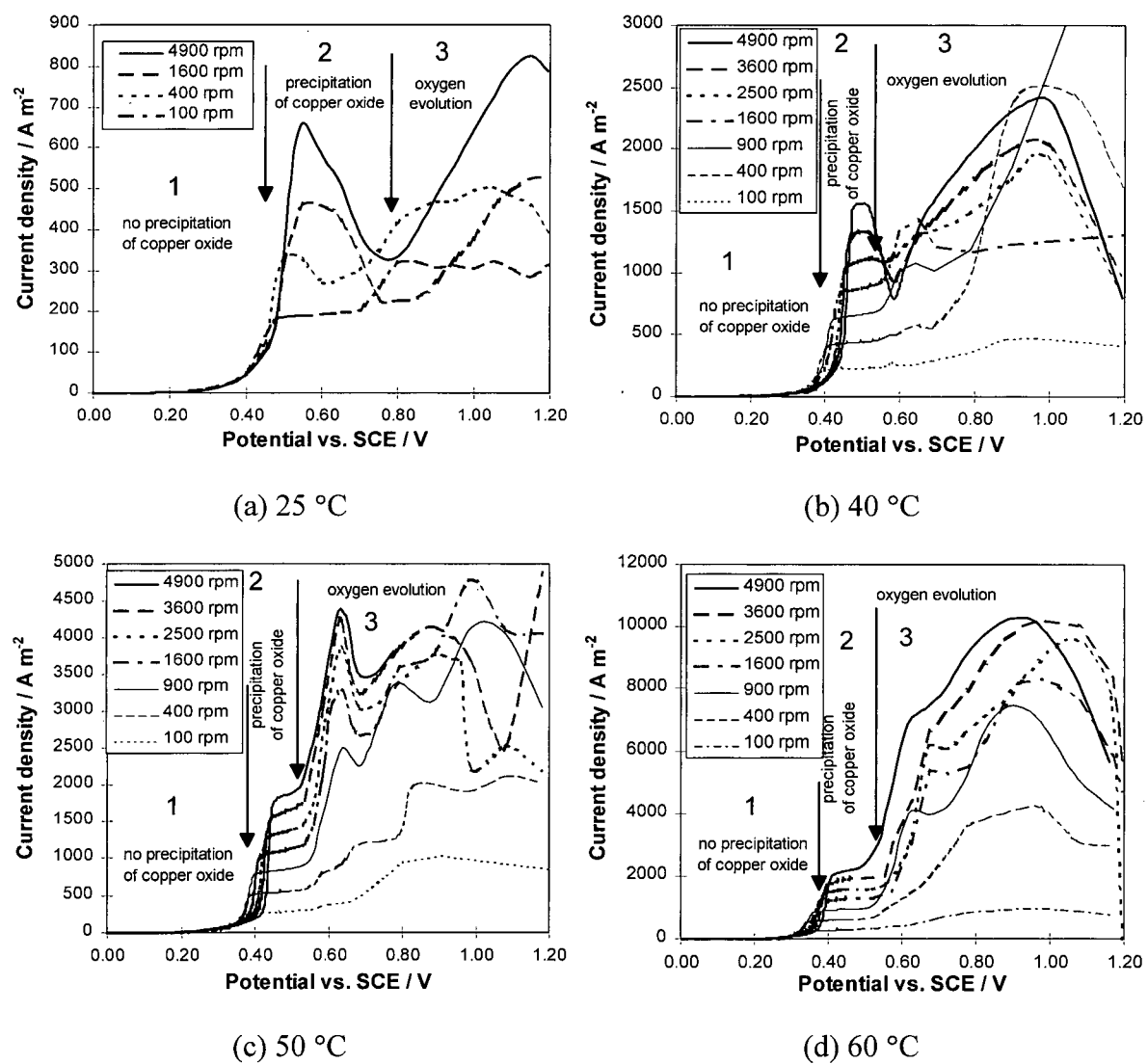
Figure 7-2 Polarization curves at different rotational speeds and temperatures. Electrolyte: 0.05 M CN⁻, CN:Cu = 3, 0.25 M NaOH and 1 M Na$_2$SO$_4$.
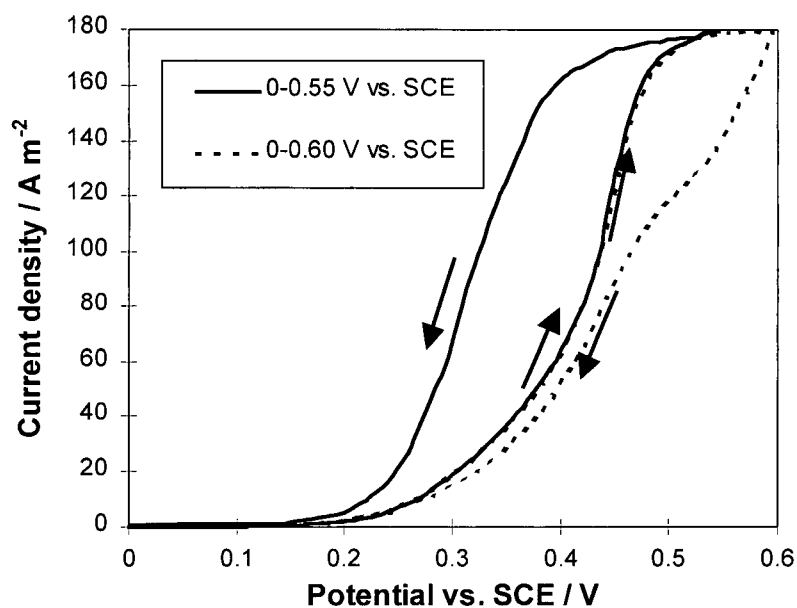
(a) 25 °C and 100 rpm
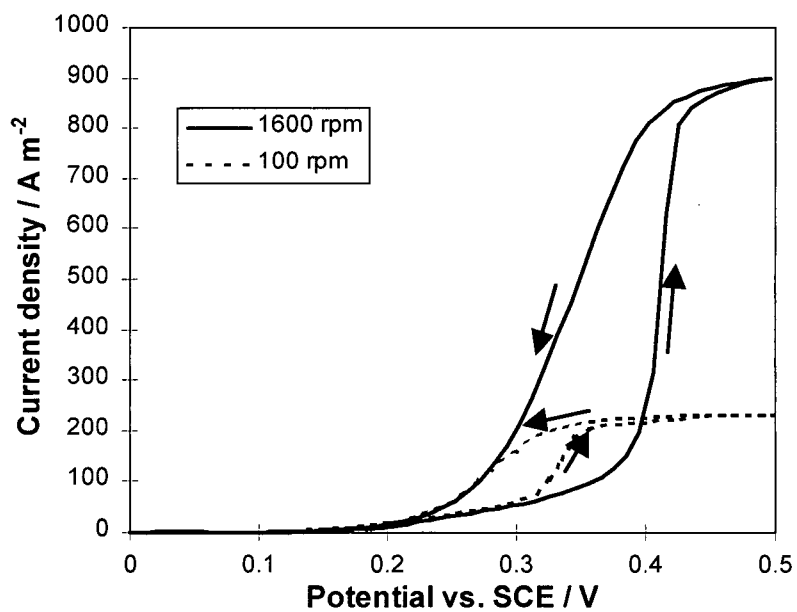
(b) 40 °C, 100 rpm and 1600 rpm

Figure 7-3 Cyclic voltammetry at 25 and 40 °C. Electrolyte: 0.05 M CN⁻, CN:Cu = 3, 0.25 M Na_2SO_4 and 1 M Na_2SO_4.

7.2.2 Anodic Behavior of Concentrated Copper Cyanide Solution

In order to obtain a reasonable copper deposition efficiency, the copper cyanide concentration should be controlled around 1 M. Therefore the study of the anodic oxidation of copper cyanide was also conducted for a high concentration copper cyanide solution.

The anodic behaviour for 0.5 M CN⁻ (Figure A-25 in Appendix 8) was quite different from that for 0.05 M CN⁻ (Figure 7-2). The current also did not increase as expected from the increase in copper cyanide concentration. The precipitation of copper oxide resulted in a significant passivation. Oxygen evolution was suppressed significantly.

From Figure 7-4, at [CN⁻] = 3 M, a CN:Cu mole ratio of 3, [OH⁻] = 0.25 and [Na_2SO_4] = 0.5 M, the anodic oxidation of copper cyanide can be described by the three potential regions. In the first region, anodic oxidation proceeded without the formation of copper oxide. In the second region, copper oxide was precipitated, resulting the passivation of the electrode. When the electrode was coated with copper oxide by sweeping the potential of the electrode to 0.48 V vs. SCE (Figures 7-4b, c and d), there was no distinct peak and the current was lower at potentials below about 0.4 V vs. SCE. Hence the decrease in the current was due to the formation of copper oxide. In the third region (> about 1.0 V vs. SCE), several bubbles were observed. The precipitation of copper oxide on the electrode increased significantly the resistance between the graphite and the solution. The IR drop at 1.0 V vs. SCE was over 1.0 V, which was estimated from the difference between the potentials measured by a potentiostat (using current interruption technique) and a multimeter.

According to the X-ray diffraction patterns of the anode precipitate produced at 25 and 60 °C (Figures A-26 and A-27 in Appendix 8), the precipitates were defined as a combination of copper hydroxide and copper oxide. At 25 °C, there was no distinct peak corresponding to CuO and so most of the precipitate was $Cu(OH)_2$. At 60 °C, there were only small peaks corresponding to the strongest peaks of CuO, and $Cu(OH)_2$ was dominant. $Cu(OH)_2$ is supposed to be have less catalytic effect on cyanide oxidation. Compared to Figure 7-2 (0.05 M CN⁻, a CN:Cu mole ratio of 3), the current did not increase, and even decreased although the concentration of copper cyanide increased by 59 times. This may be related to the composition of the anode precipitate. More than half of the anode precipitate produced in 0.05 M CN⁻ solution with a CN:Cu mole ratio of 3 was CuO, which had a good

catalytic effect on the oxidation of copper cyanide. However, from the X-ray diffraction patterns, we can predict that the amount of CuO in the precipitate produced in 3 M CN⁻ solution with a CN:Cu mole ratio of 3 is very small and the precipitate exhibited a poor catalytic effect on the oxidation of copper cyanide. It is also possible that the concentration of copper cyanide is so high that it poisoned the catalytic properties of copper oxide and suppressed the evolution of oxygen significantly possibly due to the significant adsorption of copper cyanide species.

When the cyanide concentration was increased from 3 to 3.5 M, the anodic behavour of copper cyanide became different (Figure 7-5). At 25 °C, the copper oxide was precipitated at all rotational speeds. However, at 50 and 60 °C, there was a little copper oxide (a spiral black line) formed on the electrode only at 1600 and 4900 rpm. There was no copper oxide at 100 and 400 rpm. The formation of copper oxide resulted in an increase or decrease or auto-oscillation in the current due to the change in the condition of the electrode (passivation and activation possibly related to the formation and dissolution of copper oxide) with increasing potential. At 60 °C and potentials > 0.45 and 0.54 V vs. SCE respectively for 100 rpm and 400 rpm, a significant amount of bubbles was evolved. These gas bubbles immediately dissolved when the current was turned off. The gas was thought to be cyanogen because the graphite was not corroded and oxygen was not readily evolved. The current became so high that the mass-transfer rate of hydroxide was lower than the rate of cyanogen generation and cyanogen gas was formed.

When the cyanide concentration was increased to 4 M (Figure 7-6), no anode precipitate was formed on the electrode. At 40 °C (100 and 400 rpm), 50 and 60 °C (100 - 1600 rpm), when the potential exceeded a certain value (shown in Figure 7-6), large bubbles (1-4 mm diameter) were rapidly evolved, resulting in a sharp increase in the current. Large bubbles formed and broke down resulting in the irregular change in the current with potential. The bubbles dissolved rapidly after the current was turned off and the graphite was not seriously corroded and so the gas was believed to be cyanogen. The rapid evolution of large bubbles significantly changed the mass transfer on the rotating disk. Thus the current changed irregularly with increasing rotational speed. At a high rotational speed, the bubbles evolved on the electrode were removed rapidly, having less chance to combine and form

large bubbles. The high rotational speed also increases the mass transfer of hydroxide to the electrode and reduces the formation of cyanogen.

The formation of copper oxide is related to the pH of the solution. Therefore a decrease in hydroxide concentration should affect the anodic oxidation of copper cyanide. Figure 7-7 shows the polarization curves for the solution with 3 M CN⁻, a CN:Cu mole ratio of 3, 0.05 M NaOH and 0.5 M Na$_2$SO$_4$. At 25 °C, a thin film of copper oxide was precipitated, resulting in changes in the current with the potential. Compared to the anodic behaviour of copper cyanide in the solution with 0.25 M NaOH (Figure 7-4), the current was much smaller and much less copper oxide was formed on the electrode. At 40 °C, the current vs. potential for 1600 and 4900 rpm was still similar to that at 25 °C. However, at 100 and 400 rpm, the current increased continuously to a maximum value and then decreased slightly. At 50 °C and 100 rpm, some gas was evolved at 0.38 V vs. SCE and there was almost no copper oxide formed on the electrode. At 400-4900 rpm, a very small amount of copper oxide was precipitated on the anode. At 60 °C, the gas bubbles were observed at potentials > 0.29 and 0.32 V vs. SCE for 100 and 400 rpm and no copper oxide was formed.

Figure 7-8 shows the polarization curves for the solution with 4 M CN⁻, 1 M Cu⁺, 0.05 M OH⁻ and 0.5 M Na$_2$SO$_4$. Compared to the anodic behaviour of copper cyanide at 0.25 M OH⁻ (Figure 7-6), the evolution of cyanogen began at a relatively lower potential, leading to the difference in the current. The potential for the rapid evolution of large cyanogen bubbles increased with increasing rotational speed because the high rotational speed increased the hydroxide mass transfer and so suppressed the formation of large cyanogen bubbles. At 100 or 400 rpm, the bubbles of cyanogen were not removed efficiently, resulting in the oscillation of the current. The rapid evolution of large bubbles significantly affected the mass transfer. Therefore the current for a low rotational speed was even larger than that for the higher rotational speed in some potential region.

The increase in the concentration of hydroxide should suppress the formation of cyanogen and promote the formation of copper oxide. When the concentration of hydroxide increased to 0.5 M and the concentrations of cyanide, copper and sodium sulphate were kept at 4 M, 1M and 0.5 M respectively, the anodic behaviour of copper cyanide (Figure 7-9) became quite different from that for the solutions with 0.25 and 0.05 M NaOH (Figures 7-6 and 8). A thin film of copper oxide was precipitated on the anode at the potential > a certain

value (shown in Figures 7-28 a and b). The evolution of massive gas bubbles considered to be cyanogen was only observed at 100 and 400 rpm for 50 °C, and 100 to 1600 rpm for 60 °C.

(a) 25 °C

(b) 40 °C

(c) 50 °C

(d) 60 °C
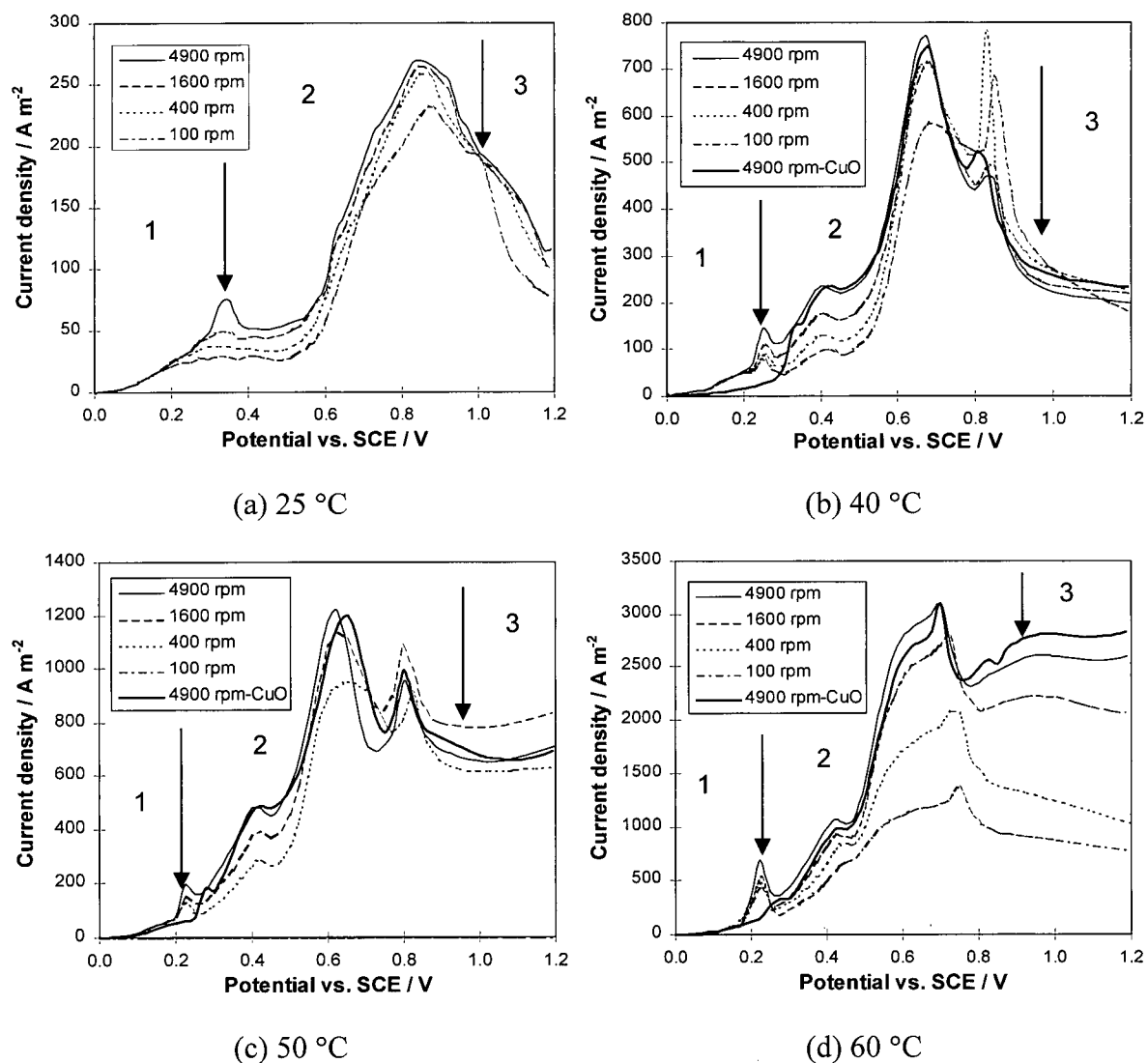
Figure 7-4 Polarization curves at different rotational speeds and temperatures. Electrolyte: 3 M CN⁻, CN:Cu mole ratio = 3, 0.25 M NaOH and 1 M Na₂SO₄. Keys: 1 - no precipitation of copper oxide, 2 - precipitation of copper oxide and 3 - evolution of oxygen.
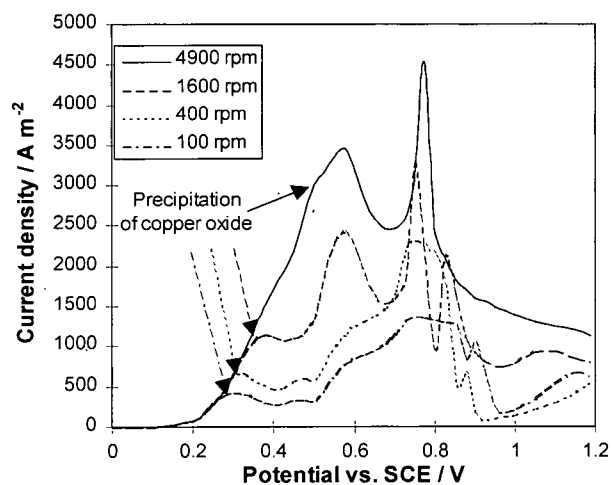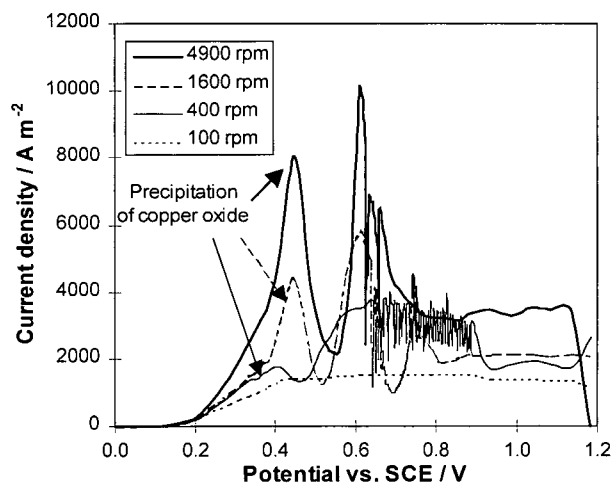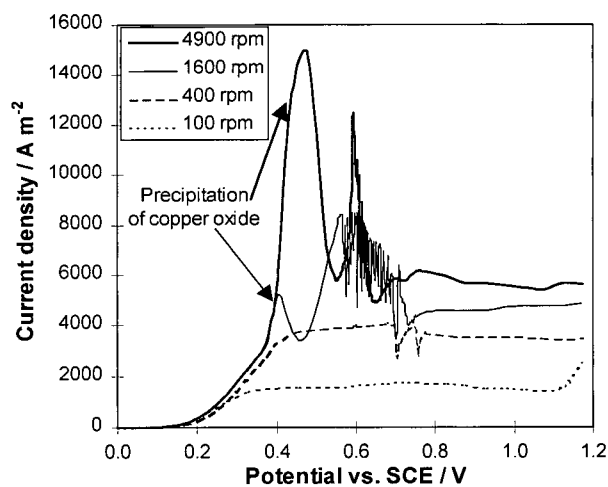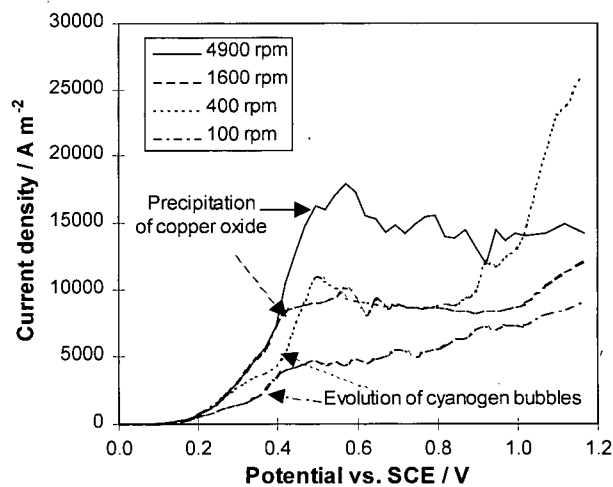
Figure 7-5 Polarization curves at different rotational speeds and temperatures. Electrolyte: 3.5 M CN⁻, CN:Cu mole ratio = 3.5, 0.25 M NaOH and 0.5 M Na$_2$SO$_4$.
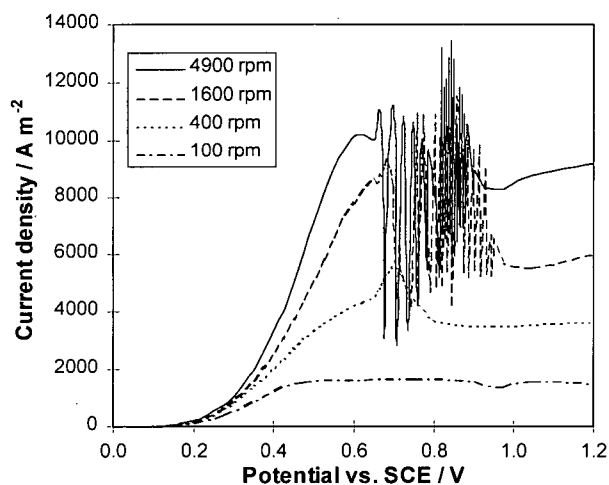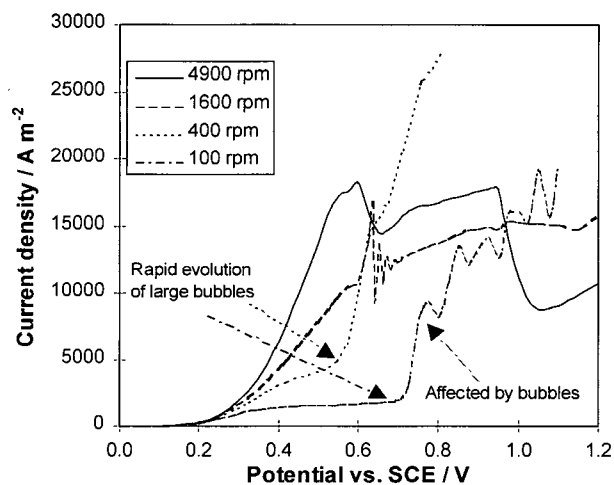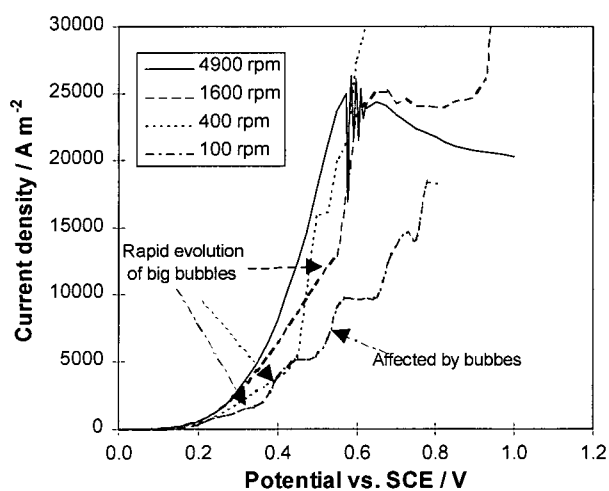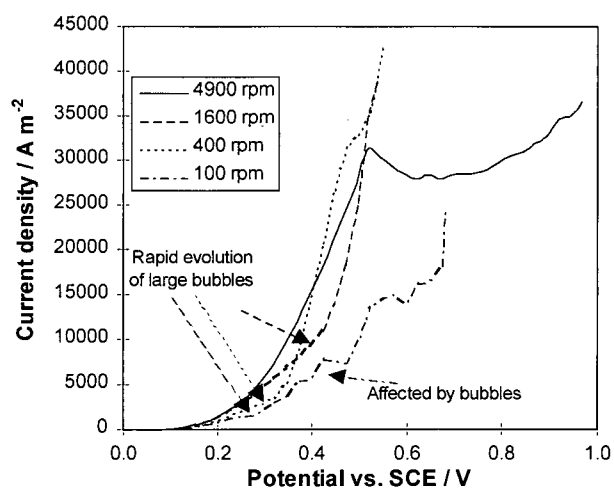
Figure 7-6 Polarization curves at different rotational speeds and temperatures. Electrolyte: 4 M CN⁻, CN:Cu mole ratio = 4, 0.25 M NaOH and 0.5 M Na₂SO₄.
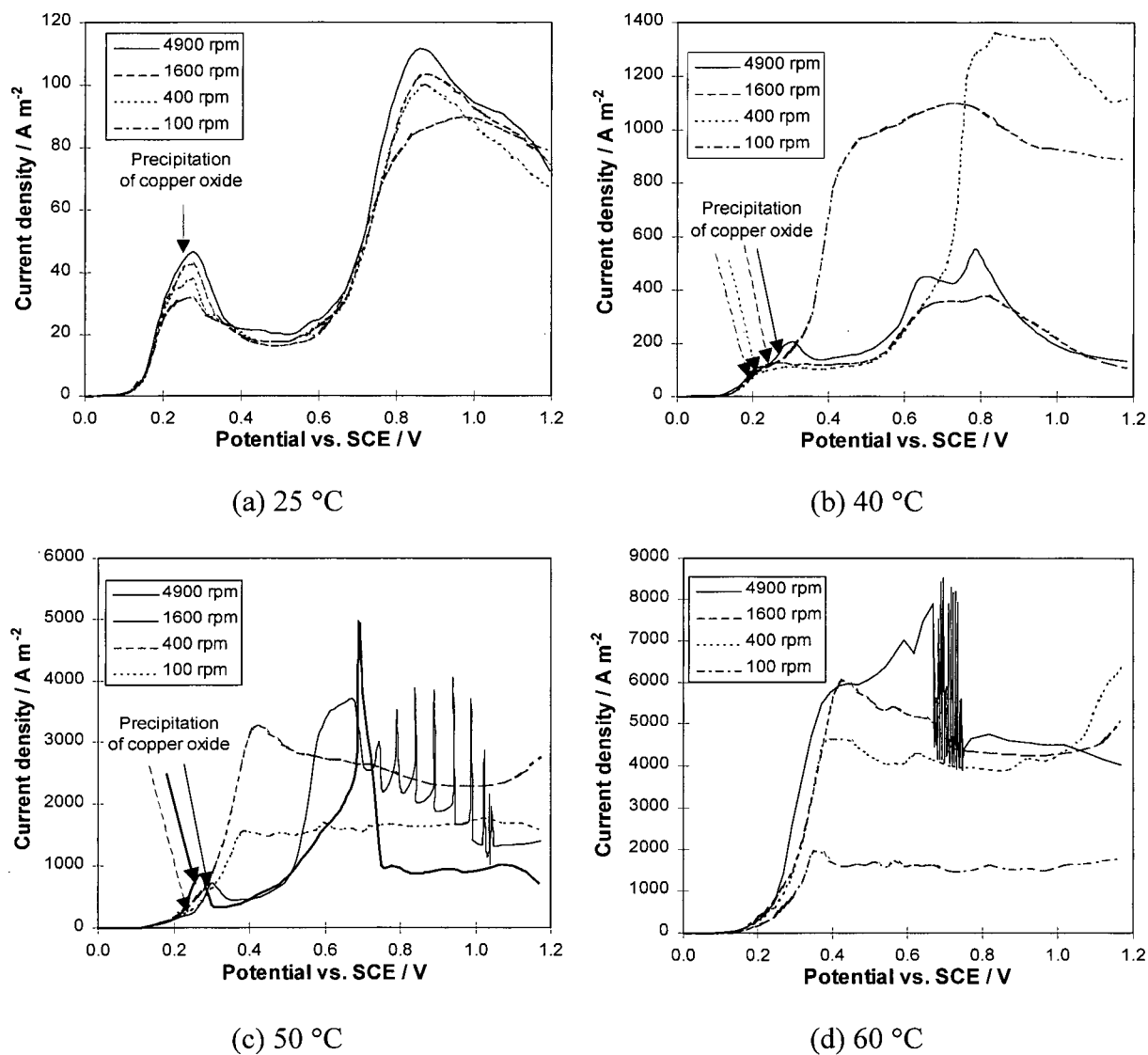
Figure 7-7 Polarization curves at different rotational speeds and temperatures. Electrolyte: 3 M CN⁻, CN:Cu mole ratio = 3, 0.05 M NaOH and 0.5 M Na₂SO₄
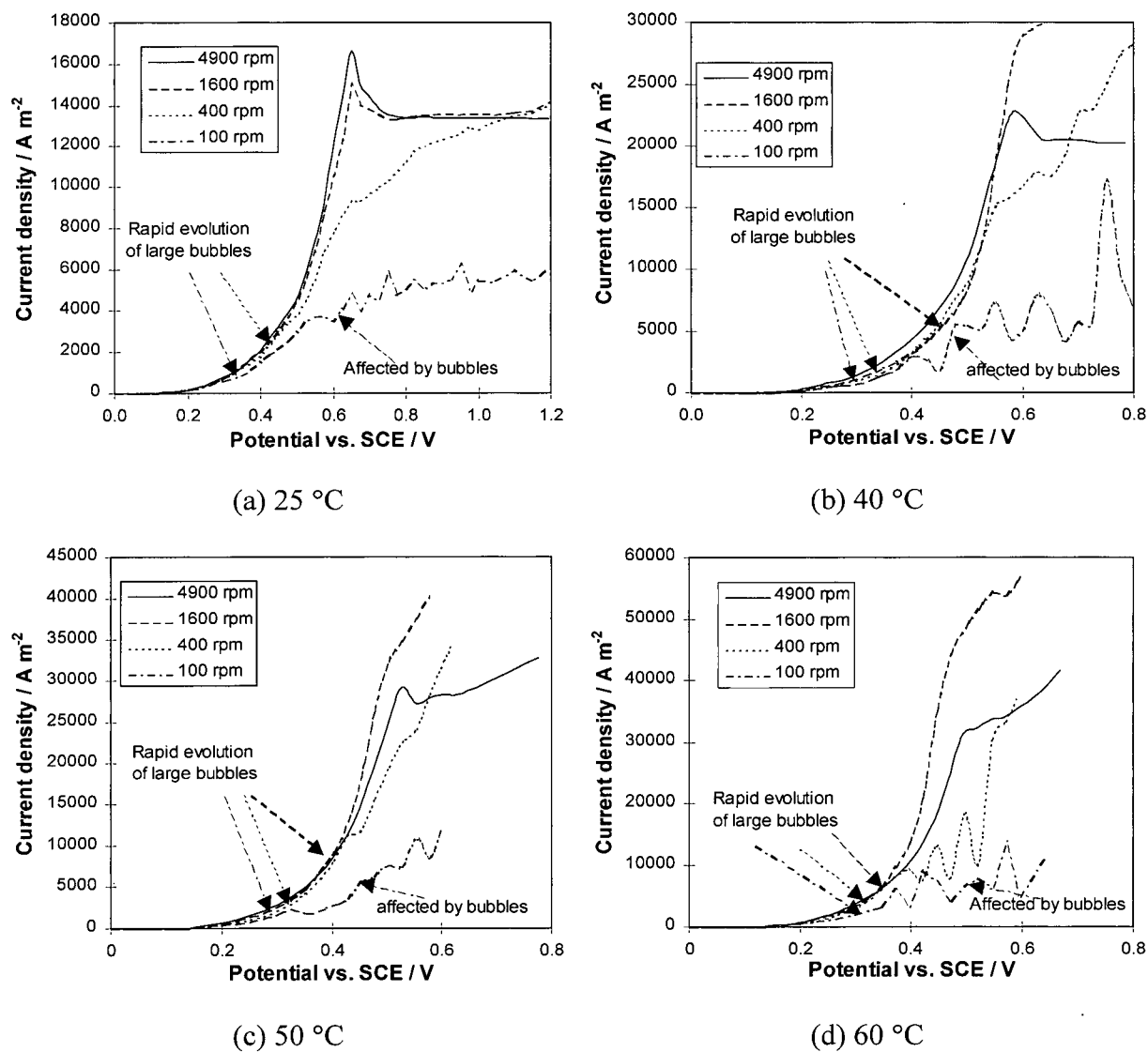
Figure 7-8 Polarization curves at different rotational speeds and temperatures. Electrolyte: 4 M CN⁻, CN:Cu mole ratio = 1, 0.05 M NaOH and 0.5 M Na$_2$SO$_4$
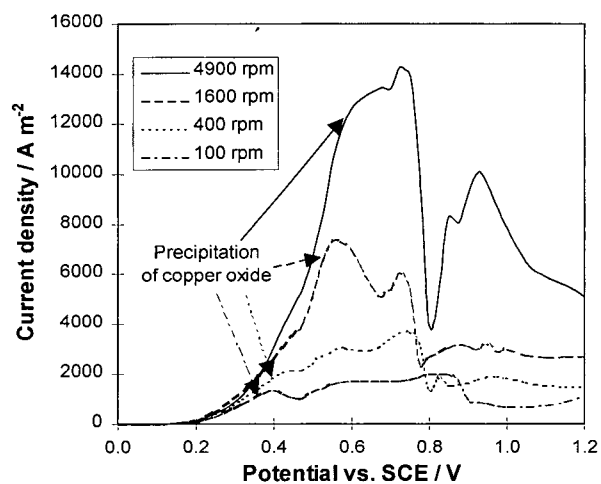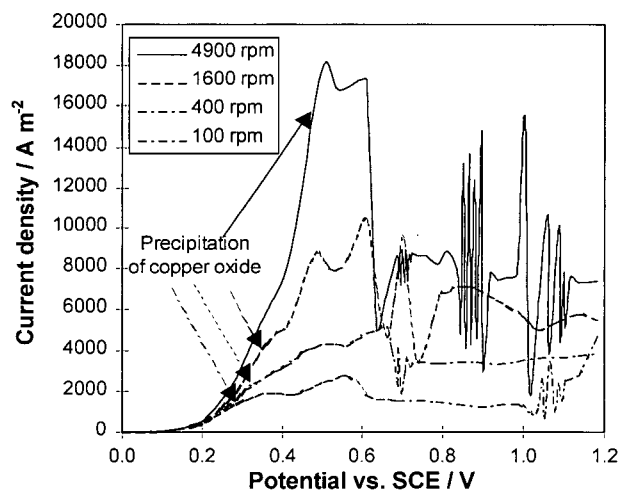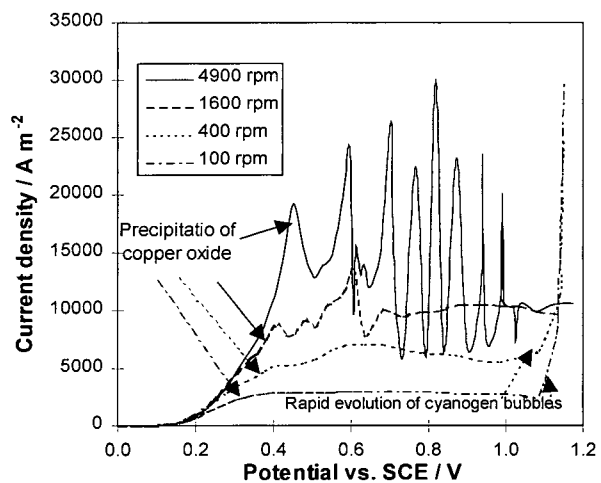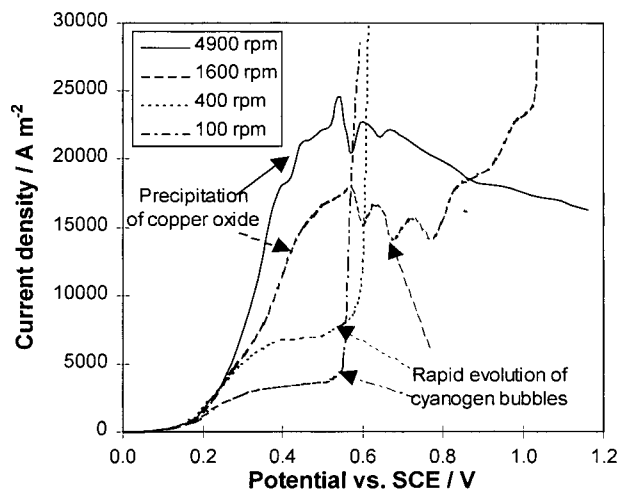
Figure 7-9 Polarization curves at different rotational speeds and temperatures. Electrolyte: 4 M CN⁻, CN:Cu mole ratio = 1, 0.50 M NaOH and 0.5 M Na_2SO_4

7.3 Coulometric Measurement

From the literature review, it appears that the stoichiometry for the anodic oxidation of copper cyanide has not been carefully studied and the results are incomplete and conflicting. In this study, controlled potential coulometry was used to determine the stoichiometry of the anodic oxidation of copper cyanide per Faraday. The anode potential was controlled at values to minimize the rates of side reactions such as oxygen evolution. The working electrode (anode) was separated from the counter electrode (the cathode) to minimize the effect of the change in the CN:Cu mole ratio due to copper deposition at the cathode. The volume of the catholyte was only about 1-2 cm^3 and its initial concentration of NaOH was 10 times that of the anolyte. The evolution of hydrogen caused a high concentration of hydroxide which can be transported to the anode compartment to maintain the concentration of hydroxide in the anolyte whose pH was monitored. The results are given in Table 7-1. Tests 1-4 show the amount of oxidized cyanide and copper (I) per Faraday at 0.05 M CN^-, a CN:Cu mole ratio = 3, 0.25 M NaOH and 1 M Na_2SO_4.

If the reaction of the anodic oxidation proceeds according to the following reaction:

$$Cu(CN)_3^{2-} + 8OH^- = 3CNO^- + Cu(OH)_2 + 3H_2O + 7e \qquad (7\text{-}1)$$
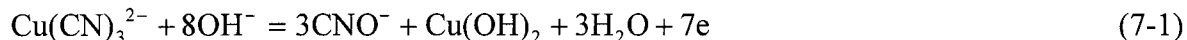
the amounts of cyanide and Cu(I) ion oxidized per Faraday are 0.429 and 0.143 mole respectively. The corresponding values of these tests are close to the values indicated by Reaction 7-1. Therefore the anodic reaction of copper cyanide under these conditions can be expressed approximately by Reaction 7-1. The current efficiencies for this reaction were found to be 99.8, 102, 103, 105 % respectively at 25, 40, 50 and 60 °C. Tests 5 - 9 show the amount of oxidized cyanide to copper per Faraday at 0.05 M CN^-, CN:Cu mole ratio = 4, 0.25 M NaOH and 1 M Na_2SO_4. Tests 5 - 8 were conducted at the potential where the current reached the limiting current at 100 rpm.

If the reaction for the anodic oxidation proceeds as follows:

$$Cu(CN)_4^{3-} + 10OH^- = 4CNO^- + Cu(OH)_2 + 4H_2O + 9e \qquad (7\text{-}2)$$
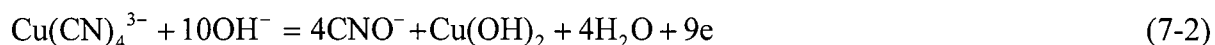
the amounts of oxidized cyanide and copper (I) ions per Faraday electricity are 0.444 and 0.111 mole respectively. The amount of cyanide oxidized per Faraday is a little higher than 0.444 and the amount of copper (I) oxidized is a little lower than 0.111 mole. Therefore the anodic reaction of copper cyanide under these conditions can be expressed approximately by

Reaction 7-2. The current efficiencies for this reaction were found to be 99.5, 100, 103, 105 % respectively at 25, 40, 50 and 60 °C. When the potential was controlled at a value where no copper oxide was formed (Test 9), the amount of cyanide oxidized per Faraday is 0.505 mol F^{-1}. The reaction can be expressed as follows:

$$CN^- + 2OH^- = CNO^- + H_2O + 2e \qquad (7\text{-}3)$$

Tests 10-13 show the amount of cyanide to copper oxidized per Faraday at 0.05 M CN^-, CN:Cu mole ratio = 12, 0.25 M NaOH and 1 M Na_2SO_4. The amount of cyanide oxidized was very close 0.5 mol F^{-1}, i.e. cyanide is oxidized to cyanate. When the concentration of hydroxide was 0. 01 M NaOH, the amount of cyanide oxidized was still close to 0.5 mol F^{-1} (Tests 14 -17).

Table 7-1 Amount of cyanide and copper (I) oxidized per Faraday at 100 rpm and different CN:Cu mole ratios and hydroxide concentrations

No.	Composition of solution	Temperature / °C	Potential vs. SCE / V	cyanide oxidized / mol F^{-1}	copper oxidized / mol F^{-1}
1	0.05 M CN^-,	25	0.5	0.435	0.126
2	0.01667 M Cu^+	40	0.5	0.443	0.136
3	CN:Cu = 3	50	0.48	0.445	0.139
4	0.25 M NaOH	60	0.46	0.439	0.159
5	0.05 M CN^-,	25	0.5	0.447	0.102
6	0.0125 M Cu^+	40	0.5	0.449	0.106
7	CN:Cu = 4	50	0.48	0.467	0.110
8	0.25 M NaOH	60	0.46	0.470	0.110
9		25	0.3	0.505	0
10	0.05 M CN^-,	25	0.45	0.508	0
11	0.0125 M Cu^+	40	0.45	0.509	0
12	CN:Cu = 12	50	0.45	0.510	0
13	0.25 M NaOH	60	0.45	0.512	0
14	0.05 M CN^-,	25	0.6	0.510	0
15	0.0125 M Cu^+	40	0.6	0.511	0
16	CN:Cu = 12	50	0.6	0.512	0
17	0.01 M NaOH	60	0.6	0.515	0

Table 7-2 lists the coulometric results for the solution with high concentrations of copper cyanide using the controlled current method (400 A m^{-2}). For the solution with 3 M CN^- and 1 M Cu^+, at [OH^-] = 0.25 M, the anodic current efficiency for cuprous ions is almost that expected from Reaction 7-1 and the cyanide current efficiency is slightly lower than that

expected from Reaction 7-1, possibly due to the evolution of oxygen. At $[OH^-] = 0.1$ M, the current efficiency for cuprous ions became much lower and the current efficiency for cyanide increased to about 100 %. For the solution with 4 M CN^- and 1M Cu^+, the cyanide current efficiencies were almost 100 % and the current efficiencies for cuprous ion were zero. Therefore the stoichiometry of the anodic oxidation of copper cyanide is dependent on the solution composition, temperature and potential.

Table 7-2 Amount of cyanide and copper (I) oxidized per Faraday at 400 A m^{-2}, 100 rpm different CN:Cu mole ratios and hydroxide concentrations

No.	Composition of solution	Temperature / °C	Cyanide oxidized / mol F^{-1}	Copper oxidized / mol F^{-1}
1	3 M CN^-, 1 M Cu^+ CN:Cu = 3	50	0.412	0.135
2	0.25 M NaOH	60	0.408	0.138
3	3 M CN^-, 1 M Cu^+ CN:Cu = 3	50	0.498	0.034
4	0.10 M NaOH	60	0.501	0.037
5	4 M CN^-, 1 M Cu^+ CN:Cu = 4	50	0.492	0
6	0.25 M NaOH	60	0.496	0
7	4 M CN^-, 1 M Cu^+ CN:Cu = 4	50	0.498	0
8	0.10 M NaOH	60	0.503	0

7.4 Effect of CN:Cu Mole Ratio

The polarization curves for the anodic oxidation of copper cyanide with different CN:Cu mole ratios and a constant cyanide concentration (0.05 M) are given in Figure 7-10. They show that copper has a significant catalytic effect on cyanide oxidation. At a CN:Cu mole ratio of 3, the anodic oxidation of copper cyanide began at 0.090, 0.045, 0.016 and 0.00 V vs. SCE respectively for 25, 40, 50 and 60 °C. At a CN:Cu mole ratio ≥ 4, the anodic oxidation of copper cyanide began at 0.170, 0.145, 0.115, 0.085 respectively for 25, 40, 50 and 60 °C. The lower the mole ratio of cyanide to copper, the lower the potential for the onset of the formation of copper oxide. When the CN:Cu mole ratio exceeded 6, no well-

defined limiting current was obtained because oxygen was evolved before the current reached a limiting value. The plot of potential vs. log (current density) for 25 and 60 °C is shown in Figure 7-11 and that for 40 and 50 °C in Figure A-28 (Appendix 8). The condition of the surface of the graphite electrode varied after the electrochemical conditioning due to the inherent surface variability. The data for Figure 7-10 were generated with some variation in the surface condition because every measurement was conducted on a renewed electrode surface. However, the data for Figure 7-11 were generated on the same electrode surface by limiting the potential well below the value at which copper oxide began to precipitate. Therefore the data for Figure 7-11 cannot compared directly to those in Figure 7-10. This explanation will also be applied in the next paragraphs.

Although there is no correction for the concentration difference between the bulk and the surface solution, at low potentials, the current was much lower than 10 % of the limiting current. Thus the concentration difference can be neglected. When the concentration difference became significant, the formation of copper oxide began and the current increased sharply. When copper oxide was precipitated on the anode, even at a constant potential, the current kept increasing. At a CN:Cu mole ratio of 3, the Tafel slope was about 0.12 V decade^{-1}. At a CN:Cu mole ratio $\geq$ 4, two Tafel slope ranges appear with the first Tafel slope being about 0.060 V decade^{-1} and the second one about 0.17-0.20 V decade^{-1}. From Figure 7-12, there is only one well-defined Tafel slope on a pyrolytic graphite electrode at a CN:Cu mole ratio $\geq$ 4 and the current at a CN:Cu mole ratio of 3 was larger than those at a CN:Cu mole ratio $\geq$ 4. Therefore the anodic behaviour of copper cyanide is dependent on the anode materials.

The increase from 3 to over 4 in the CN:Cu mole ratio resulted in a significant change in the potential vs. log (current) curves (Figures 7-11 and 7-12). This can be due to a change in the discharged species. At a constant potential and cyanide concentration, the current at a CN:Cu mole ratio of 6 (lower copper concentration) is larger than that at a CN:Cu mole ratio of 4 (higher copper concentration) and the current at a CN:Cu mole ratio of 4 is larger than that at a CN:Cu mole ratio of 12. This phenomenon should be due to the change in the concentration of the discharged species as confirmed in Section 7.6.

When the concentration of copper was fixed at 0.00833 M and the cyanide concentrations were fixed at 0.025, 0.05, 0.1, 0.2 and 0.4 M (the corresponding CN:Cu mole

ratios were 3, 6, 12, 24 and 48 respectively), the anodic behaviour of copper cyanide changed with cyanide concentration (Figure 7-13 for 25 and 60 °C and Figure A-29 (Appendix 8) for 40 and 50 °C). At [CN⁻] = 0.025 M (a CN:Cu mole ratio of 3), the plots of potential vs. log (current density) are linear. At [CN⁻] ≥ 0.05 M (a CN:Cu mole ratio ≥ 6), similar to Figure 7-11, there are two Tafel slopes in the plots of potential vs. log (current density).

The curves for potential vs. log (current density) are parallel to each other, but do not shift uniformly with increasing concentration of cyanide. Therefore probably the discharged species is not free cyanide ions, but one copper cyanide species. From the plots of potential vs. log (current density) on a pyrolytic graphite electrode (Figure 7-14), the Tafel slope for 0.025 M CN⁻ (a CN:Cu mole ratio of 3) is a little different from those for higher cyanide concentrations. However, at a CN:Cu mole ratio ≥ 6, the Tafel slopes are the same and the curves are parallel to each other and shift non-uniformly with increasing cyanide concentration.

From Figure 7-15, the increase in cyanide concentration from 3 to 4 M results in a significant increase in the current density. At [CN⁻] = 3 (i.e. a CN:Cu mole ratio of 3), the current is much lower than those for 3.5 and 4 M CN⁻ due to the passivation effect of the precipitation of copper oxide at a lower potential (0.2 V vs. SCE). From the plots of potential vs. log (current density) (Figure 7-16), at [CN⁻] = 3 M, there is a Tafel slope of 0.10 V decade⁻¹. However, at [CN⁻] = 3.5 and 4 M, there are two Tafel slopes, the first one being 0.66 V decade (RT/F) and the second 0.16 V decade⁻¹. The second Tafel slope appears to increase slightly with increasing potential probably due to the concentration change of cyanide on the surface. The results at 25, 40 and 50 °C are similar.

(a) 25 °C

(b) 40 °C

(c) 50 °C

(d) 60 °C

Figure 7-10 Effect of the mole ratio of cyanide to copper on cyanide oxidation -current vs. potential on a graphite rotating disk at 4900 rpm and different temperatures. Electrolytes: 0.05 M CN⁻, CN:Cu mole ratio = 3, 4, 6, 12 and no copper, 0.25 M NaOH and 1 M Na_2SO_4.

(a) 25 °C   (b) 60 °C
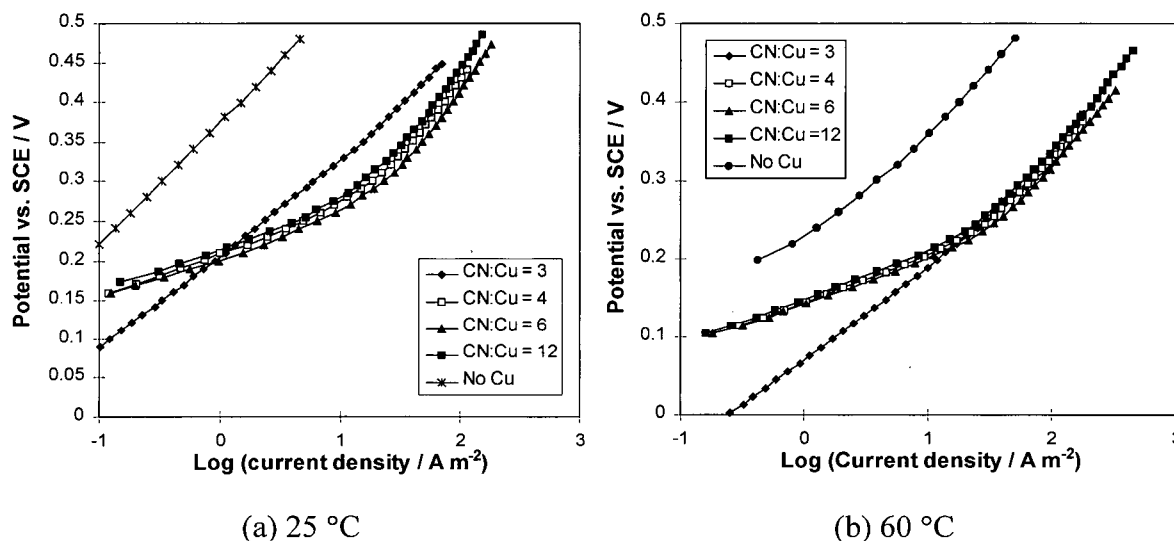
Figure 7-11 Effect of the mole ratio of cyanide to copper on cyanide oxidation - potential vs. log (current density) on a graphite rotating disk at 4900 rpm (25 and 60 °C). Electrolytes : 0.05 M CN⁻, CN:Cu mole ratio = 3, 4, 6, 12 and no copper, 0.25 M NaOH and 1 M Na₂SO₄.
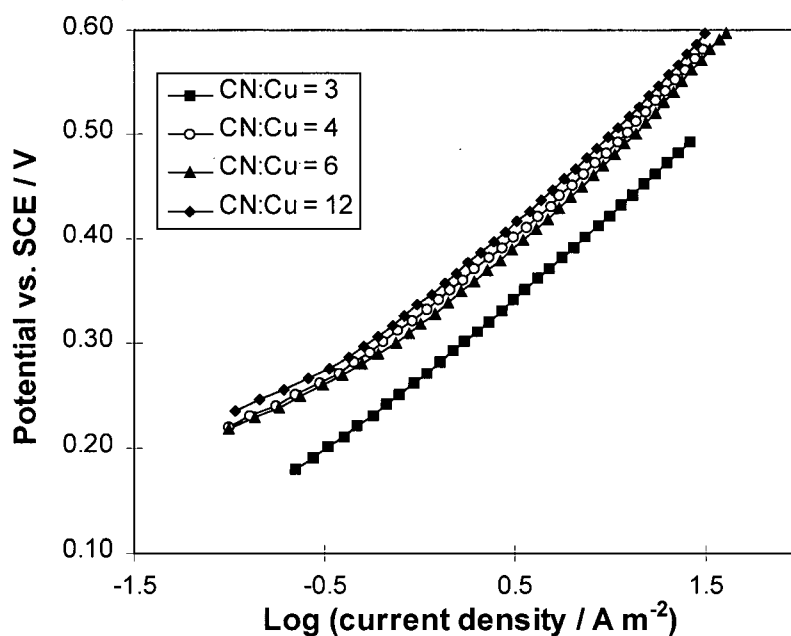
Figure 7-12 Effect of the mole ratio of cyanide to copper on cyanide oxidation - potential vs. log current density on a pyrolytic graphite rotating electrode at 4900 rpm and 25 °C. Electrolytes : 0.05 M CN⁻, CN:Cu mole ratio = 3, 4, 6, 12 and 0.25 M NaOH and 1 M Na₂SO₄.

(a) 25 °C   (b) 50 °C
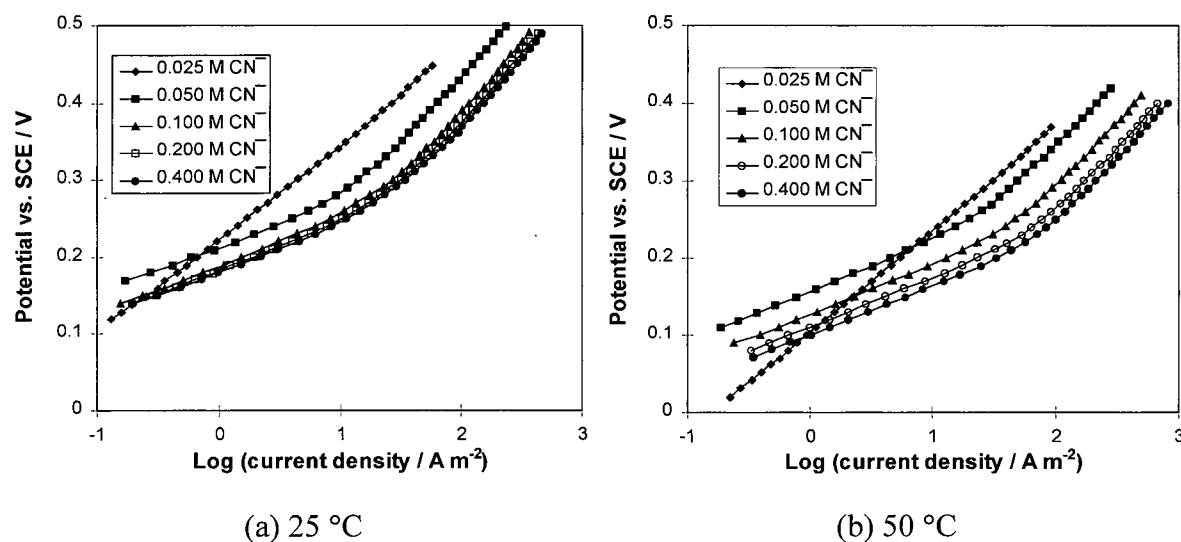
Figure 7-13 Effect of the mole ratio of cyanide to copper on cyanide oxidation - potential vs. log (current density) on a graphite rotating disk at 4900 rpm (25 and 60 °C). Electrolytes : $[Cu^+]$ = 0.00833, $[CN^-]$ = 0.025, 0.05, 0.1, 0.2 and 0.4 M, 0.25 M NaOH and 1 M Na_2SO_4.
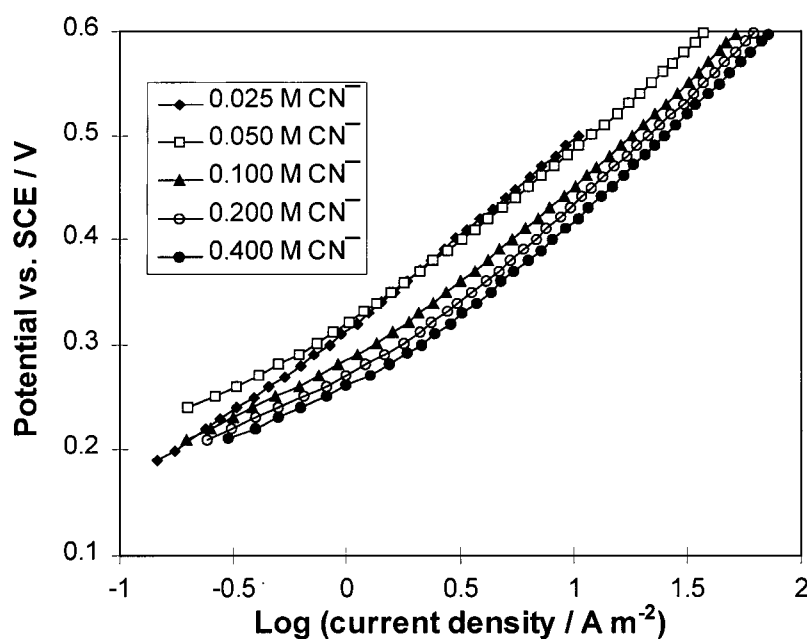
Figure 7-14 Effect of the mole ratio of cyanide to copper on cyanide oxidation - potential vs. log (current density) on a pyrolytic graphite rotating disk at 4900 rpm and 25 °C. Electrolytes : $[Cu^+]$ = 0.00833 M, $[CN^-]$ = 0.025, 0.05, 0.1, 0.2 and 0.4 M, 0.25 M NaOH and 1 M Na_2SO_4.
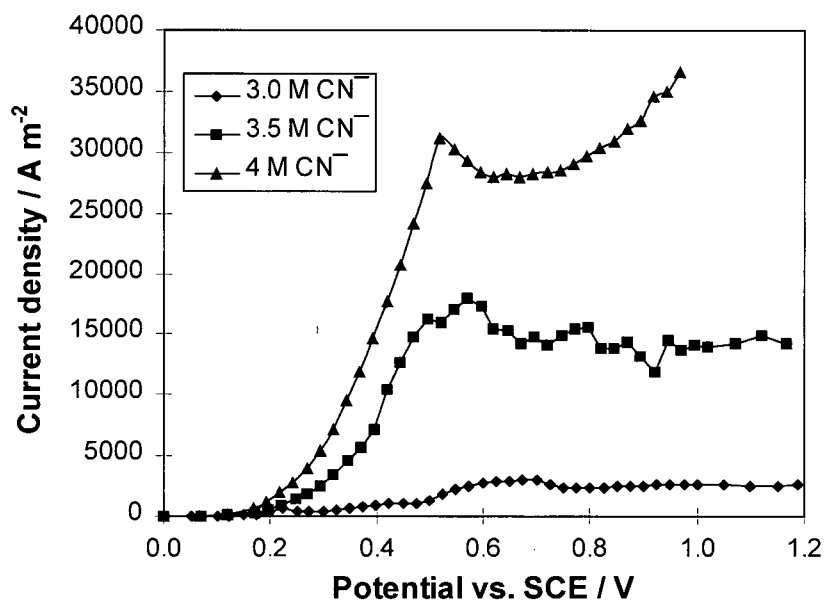
Figure 7-15 Effect of the mole ratio of cyanide to copper on cyanide oxidation - current vs. potential on a graphite rotating disk at 4900 rpm and 60 °C. Electrolytes : 1 M Cu^+, $[CN^-]$ = 3, 3.5 and 4 M, 0.25 M NaOH and 0.5 M Na_2SO_4.
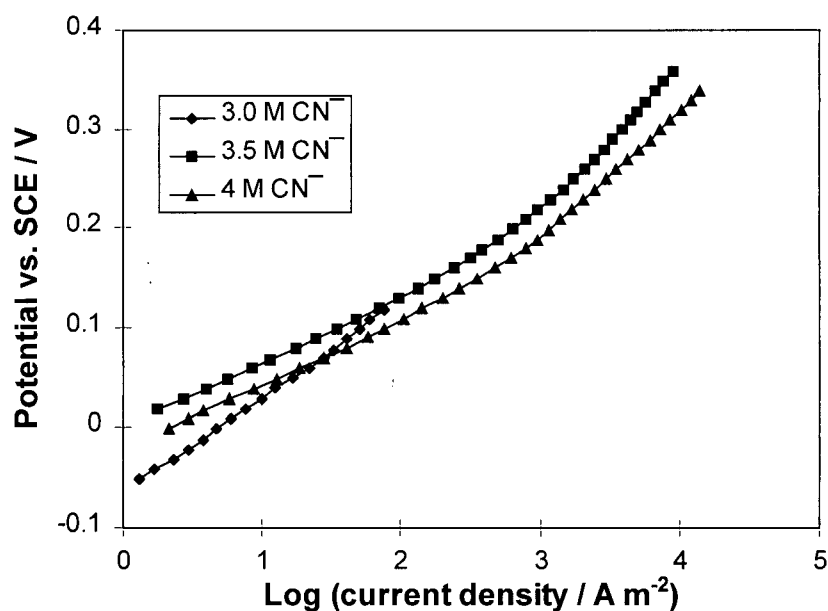
Figure 7-16 Effect of the mole ratio of cyanide to copper on cyanide oxidation - potential vs. log (current density) on a graphite rotating disk at 4900 rpm and 60 °C. Electrolytes : 1 M Cu^+, $[CN^-]$ = 3, 3.5 and 4 M, 0.25 M NaOH and 0.5 M Na_2SO_4

7.5 Effect of pH

At a CN:Cu mole ratio of 3, and [CN$^-$] = 0.05 M, the concentration of hydroxide significantly affects the anodic behaviour of copper cyanide (Figure 7-17). In the low polarization region, with decreasing concentration of hydroxide, the Tafel slope decreases from 0.130 to 0.060 V decade^{-1} and the current decreases at a constant potential (Figure 7-18 for 25 and 60 °C and Figure A-30 for 40 and 50 °C (Appendix 8)). This suggests that the rate-controlling step changes or the mechanism changes. In the high polarization region, copper cyanide is oxidized to copper oxide and cyanate. The current is sensitive to the hydroxide concentration and does not reach a well-defined limiting value at low hydroxide concentration. This means that hydroxide ions are involved in the rate-controlling step. The results obtained on pyrographite (Figure 7-19) and Pt rotating disks (Figure A-30 in Appendix 8) are similar.

At a CN:Cu mole ratio of 4, [CN$^-$] = 0.05 M, the effect of pH on the anodic oxidation depends on the applied potential (Figure 7-20, and Figure 7-21 and Figure A-32 (Appendix 8)). In the low polarization region, pH has little effect on the anodic oxidation of cyanide. The Tafel slope was independent of pH and the current decreased slightly with decreasing pH. Similar results were obtained on pyrolytic graphite (Figure 7-22). This means that hydroxide is not involved in the rate-controlling step.

In the high polarization region (> about 0.5-0.6 V vs. SCE), copper cyanide was oxidized to copper oxide and cyanate with the current depending greatly on the hydroxide concentration. Generally, the current decreases with decreasing hydroxide concentration. At 25 °C and a potential > 0.65 V vs. SCE, the current for 0.25 M NaOH was below that for 0.05 M NaOH due to passivation (possibly the adsorption of the oxygen). The oxygen evolution and the formation of copper oxide decreased significantly with decreasing concentration of hydroxide. Therefore the current is dependent on the concentration of hydroxide and hydroxide is involved in the rate-controlling step.

From Figures 7-23, 7-24 and Figure A-33, the effect of pH at a CN:Cu mole ratio = 12 is similar to that at CN:Cu mole ratio = 4. In the low polarization region (< about 0.5 V SCE), the current was slightly affected by pH and the Tafel slope was independent of pH. The results obtained on a pyrolytic graphite electrode (Figure 7-25) also show that pH has

almost no effect on the anodic oxidation of copper cyanide at a potential < 0.6 V vs. SCE. At a potential > about 0.5 V vs. SCE (Figure 7-23), pH affected the current. The difference between the currents for 0.25 and 0.05 M OH⁻ is relatively small and the difference between the currents for 0.25 (or 0.05) and 0.01 M OH⁻ is significant. At 25 and 40 °C, the current for 0.25 M OH⁻ was even lower than that for 0.05 M OH⁻ in one potential region possibly because the evolution of oxygen diminished the oxidation of copper cyanide.

At a CN:Cu mole ratio of 3 and [CN⁻] = 3 M, the effect of the hydroxide concentration was dependent on the temperature (Figure 7-26). At 25 °C, the current decreased with decreasing concentration of hydroxide and the anodic oxidation of copper cyanide was affected by the precipitation of copper oxide on the electrode.

At the temperature ≥ 40 °C, in the initial potential region the current decreased with increasing concentration of hydroxide. In the higher potential region, the currents for 0.50 M OH⁻ was larger than that for 0.25 M OH⁻. However, in some potential regions, the current for 0.05 M OH⁻ was larger than that for 0.25 M OH⁻ or even 0.50 M OH⁻. This phenomenon is probably related to the fact that the amount of the precipitated copper oxide for 0.05 M OH⁻ decreased significantly with increasing temperature, resulting in the less passivation of the electrode. At 60 °C, there was almost no precipitate on the electrode at 0.05 M OH⁻, but at 0.25 or 0.50 M OH⁻, a thick copper oxide film was formed, leading to the difference in the anodic behaviour.

From Figure 7-27, at 0.25 and 0.50 M OH⁻¹, the Tafel slope was about 0.10 V decade⁻¹. At 0.05 M OH⁻, there were two Tafel slopes, the first being about 0.66 V decade⁻¹ and the second one 0.11 V decade⁻¹. The change in pH could result in a change in the discharged species or the rate-determining step.

At a CN:Cu mole ratio of 4 and [CN⁻] = 4 (Figure 7-28), in the lower polarization region (< 0.50 V vs. SCE), the current was slightly affected by the change in the concentration of hydroxide. At potentials > about 0.5 V vs. SCE, the concentration of hydroxide significantly affected the behaviour of the anodic oxidation of copper cyanide.

At [OH⁻] = 0.5 M, when the current increased to a certain value, the mole ratio of cyanide to copper on the surface became low, but the hydroxide concentration on the surface was still high and reacted with cupric ions to form copper cyanide, resulting in passivation of the anodic oxidation of cyanide. At [OH⁻] = 0.05 M, when the current became so high that

the pH on the surface was low and $(CN)_2$ gas was formed. At $[OH^-]$ = 0.25 M, the anodic behaviour of copper cyanide is between those at $[OH^-]$ = 0.5 and 0.05 M. From the plot of potential vs. log (current density) (Figure 7-29) in the low polarization region, the current decreases slightly with decreasing hydroxide concentration.

From the above discussion, we can see that the anodic behaviour of copper cyanide is a function of the total cyanide concentration, the mole ratio of cyanide to copper, hydroxide concentration and temperature.

(a) 25 °C

(b) 40 °C

(c) 50 °C

(d) 60 °C
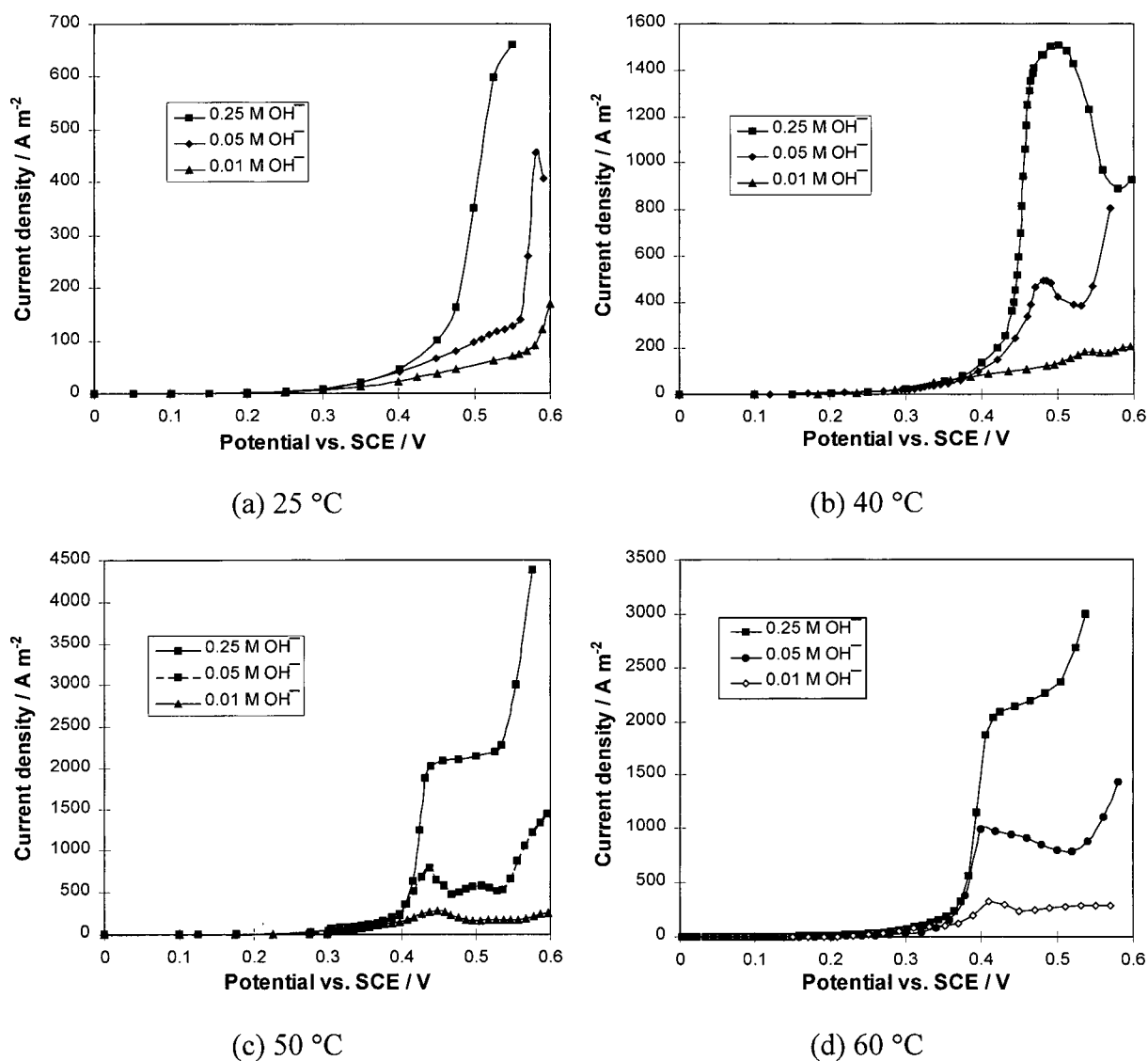
Figure 7-17 Effect of pH on cyanide oxidation - current vs. potential on a graphite rotating disk at 4900 rpm and different temperatures. Electrolytes : 0.05 M CN$^-$, a CN:Cu mole ratio of 3, $[OH^-]$ = 0.25, 0.05 and 0.01M and 1 M Na_2SO_4.
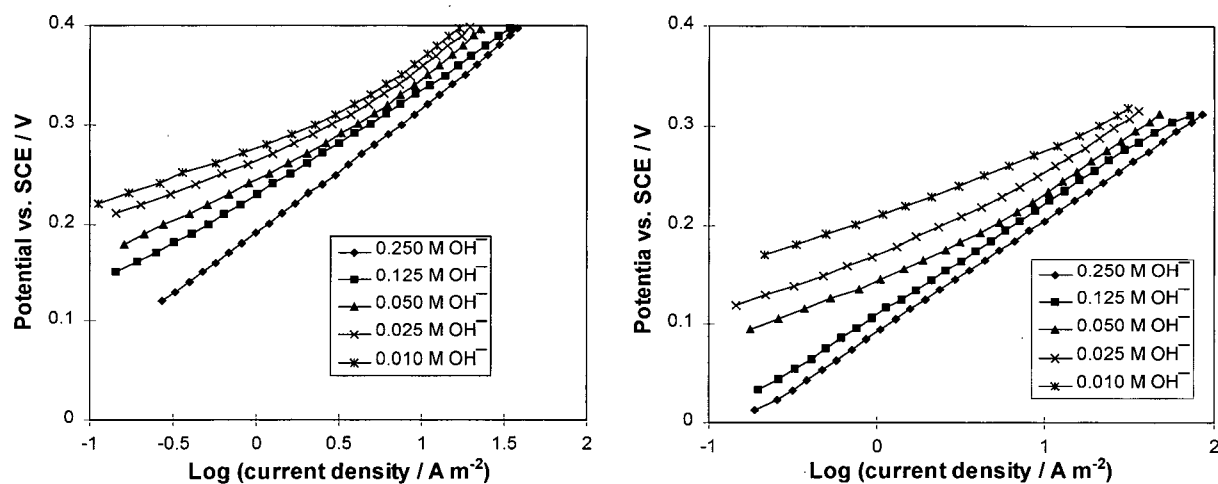
Figure 7-18   Effect of pH on cyanide oxidation - potential vs. log (current density) on a graphite rotating disk at 4900 rpm (25 and 60 °C). Electrolytes : 0.05 M CN⁻, a CN:Cu mole ratio of 3, [OH⁻] = 0.25, 0.125, 0.05, 0.025 and 0.01M and 1 M Na₂SO₄.
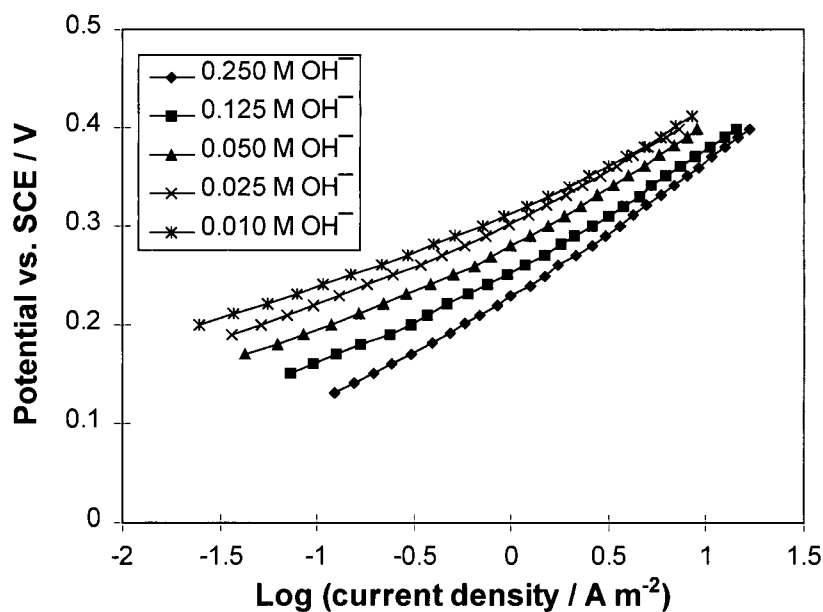
Figure 7-19   Effect of of pH on cyanide oxidation - potential vs. log (current density) on a pyrolytic graphite rotating disk at 4900 rpm and 25 °C. Electrolytes : 0.05 M CN⁻, a CN:Cu mole ratio of 3, [OH⁻] = 0.25, 0.125, 0.05, 0.025 and 0.01M and 1 M Na₂SO₄

(a) 25 °C

(b) 40 °C

(b) 50 °C

(b) 60 °C
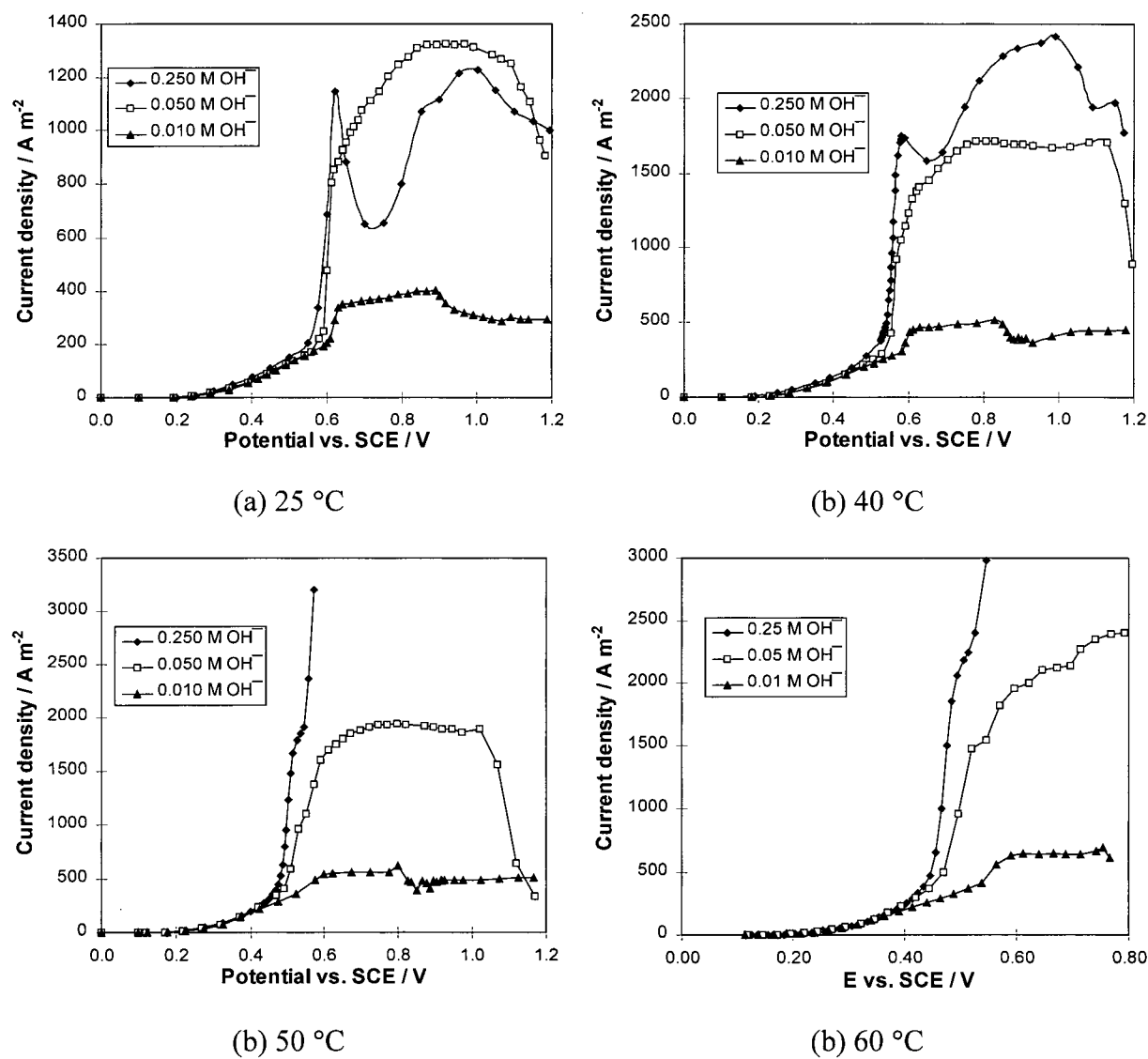
Figure 7-20 Effect of pH on cyanide oxidation - current vs. potential on a graphite rotating disk at 4900 rpm and different temperatures. Electrolytes : 0.05 M CN⁻, a CN:Cu mole ratio of 4, [OH⁻] = 0.25, 0.05, and 0.01M and 1 M Na₂SO₄.

(a) 25 °C

(b) 60 °C
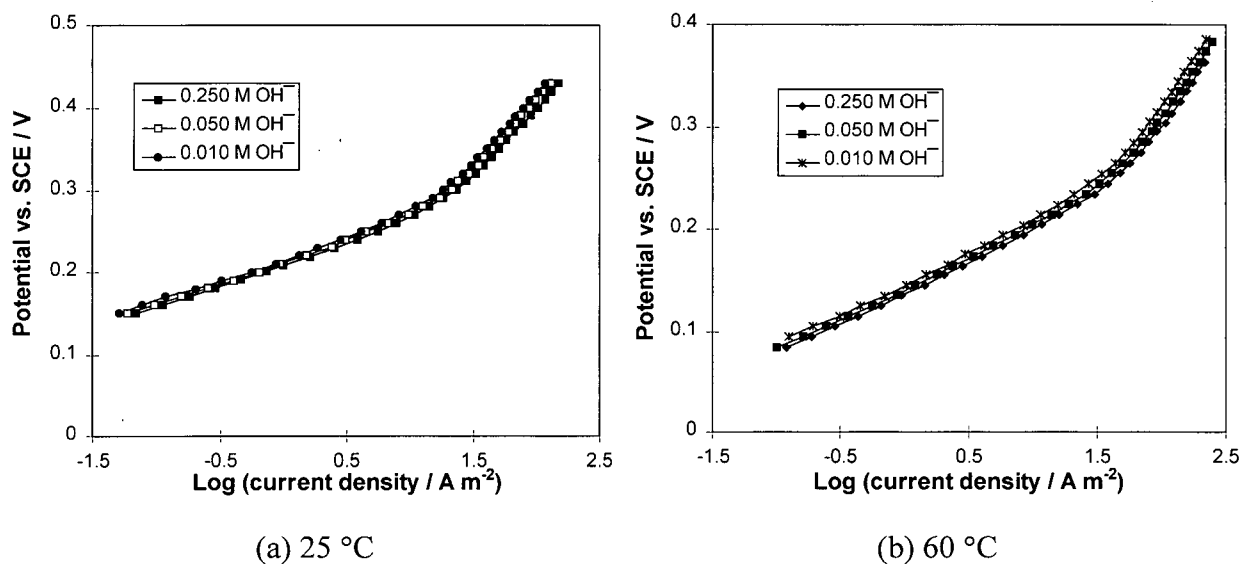
Figure 7-21 Effect of pH on cyanide oxidation - potential vs. log (current density) on a graphite rotating disk 4900 rpm (25 and 60 °C). Electrolytes : 0.05 M CN⁻, a CN:Cu mole ratio of 4, [OH⁻] = 0.25, 0.05, and 0.01M and 1 M Na₂SO₄.
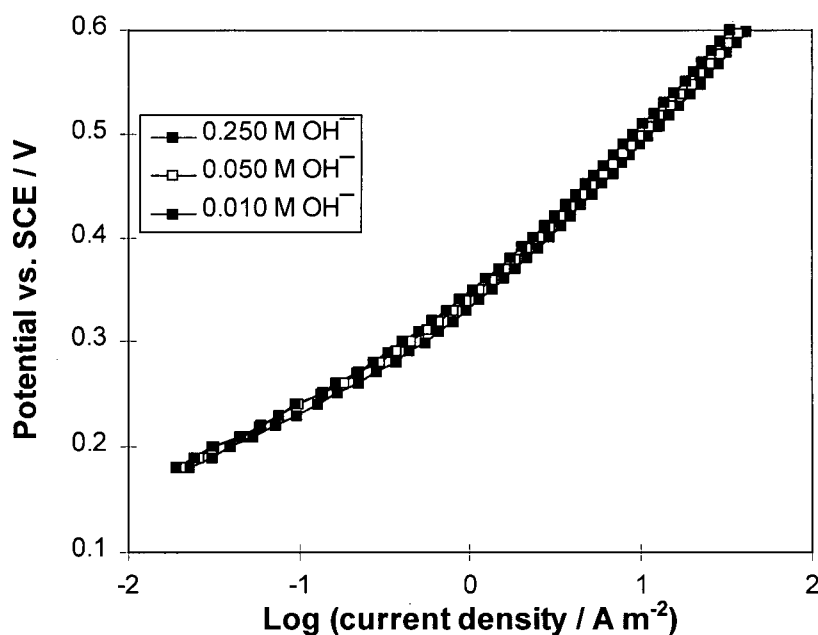
Figure 7-22 Effect of pH on cyanide oxidation - potential vs. log (current density) on a pyrolytic graphite rotating disk at 4900 rpm and 25 °C. Electrolytes : 0.05 M CN⁻, a CN:Cu mole ratio of 4, [OH⁻] = 0.25, 0.05, and 0.01M and 1 M Na₂SO₄.
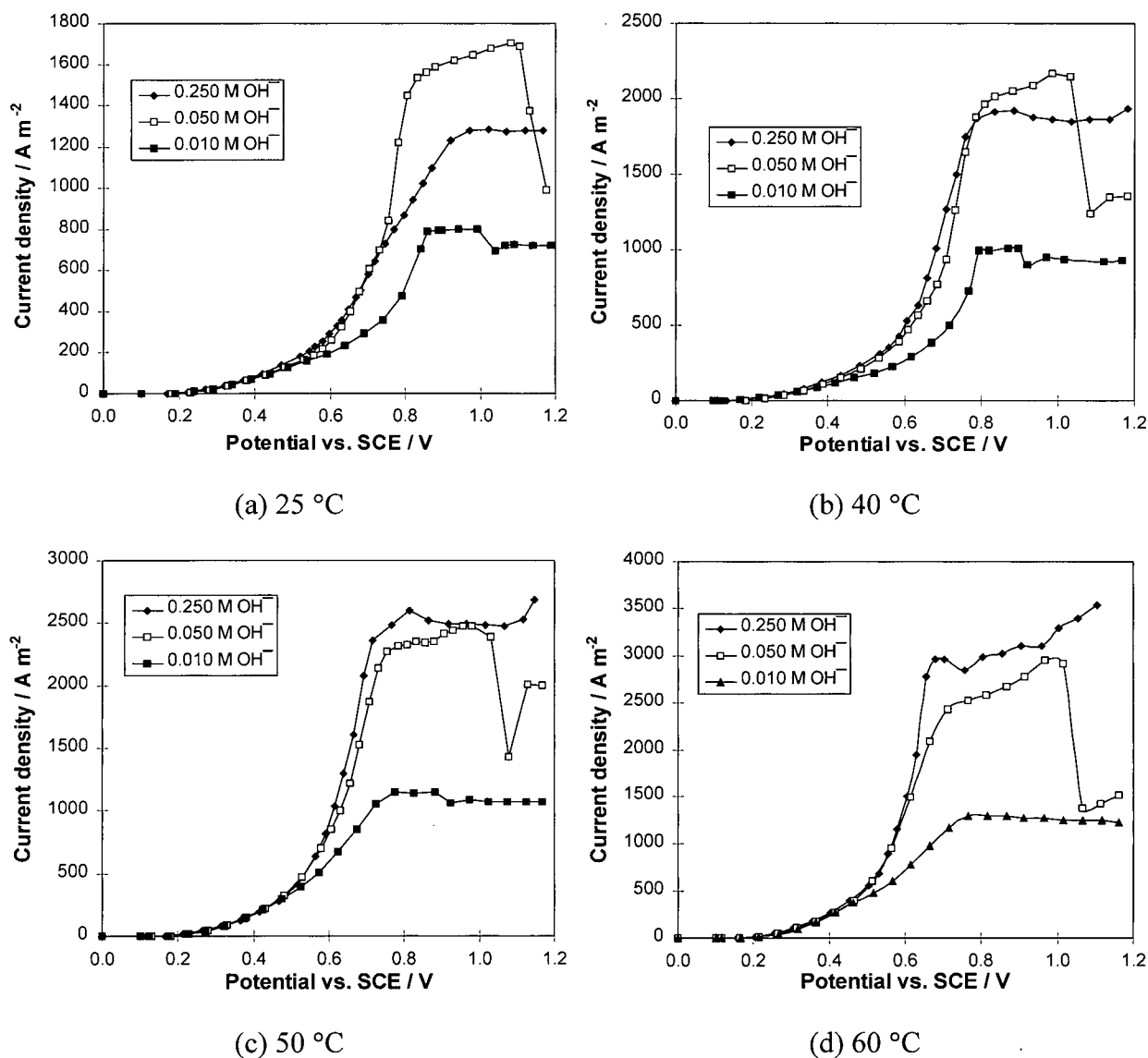
Figure 7-23 Effect of pH on cyanide oxidation - current vs. potential on a graphite rotating disk at 4900 rpm and different temperatures. Electrolytes : 0.05 M CN⁻, a CN:Cu mole ratio of 12, [OH⁻] = 0.25, 0.05, and 0.01M and 1 M Na₂SO₄.

(a) 25 °C   (b) 60 °C
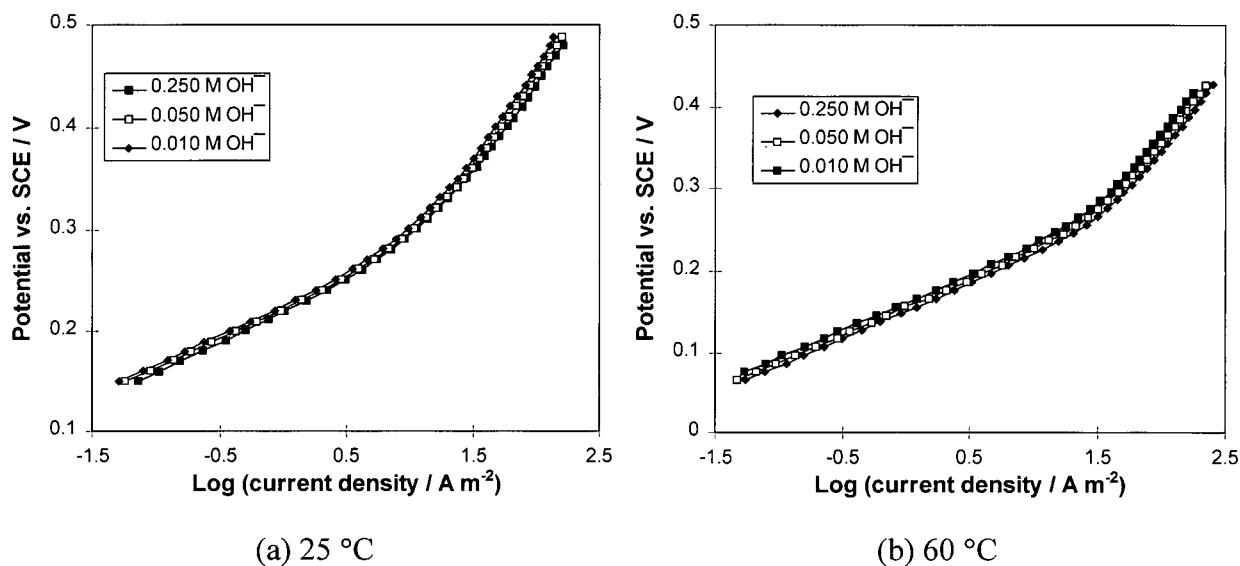
Figure 7-24   Effect of pH on cyanide oxidation - potential vs. log (current density) on a graphite rotating disk at 4900 rpm (25 and 60 °C). Electrolytes : 0.05 M CN⁻, a CN:Cu mole ratio of 12, [OH⁻] = 0.25, 0.05 and 0.01M and 1 M Na$_2$SO$_4$.
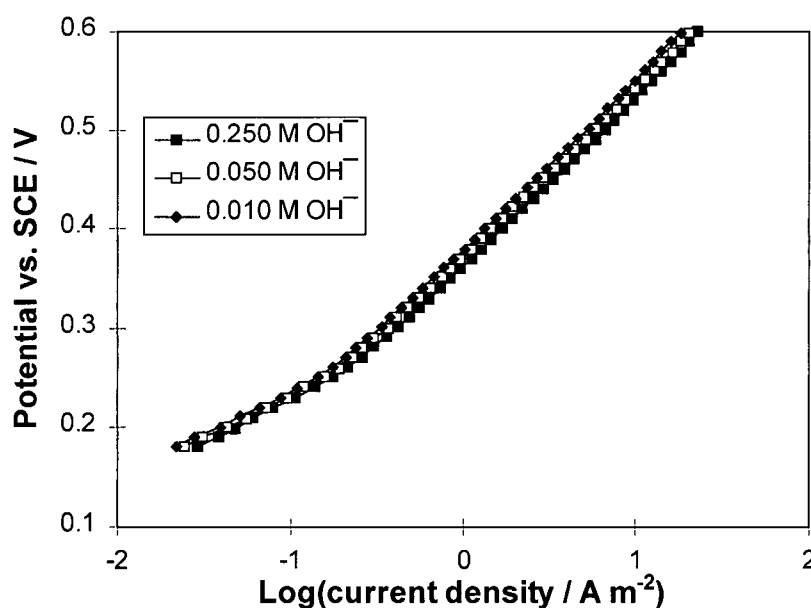
Figure 7-25   Effect of pH on cyanide oxidation - potential vs. log (current density) on a pyrolytic graphite rotating disk at 4900 rpm and 25 °C. Electrolytes : 0.05 M CN⁻, a CN:Cu mole ratio of 12, [OH⁻] = 0.25, 0.125, 0.05, 0.025 and 0.01M and 1 M Na$_2$SO$_4$.
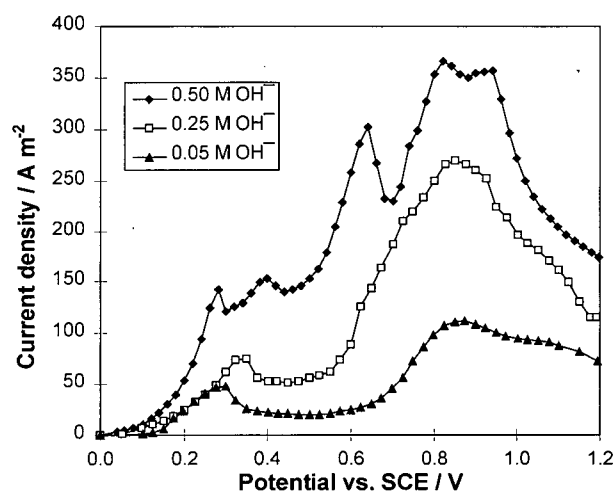
(a) 25 °C
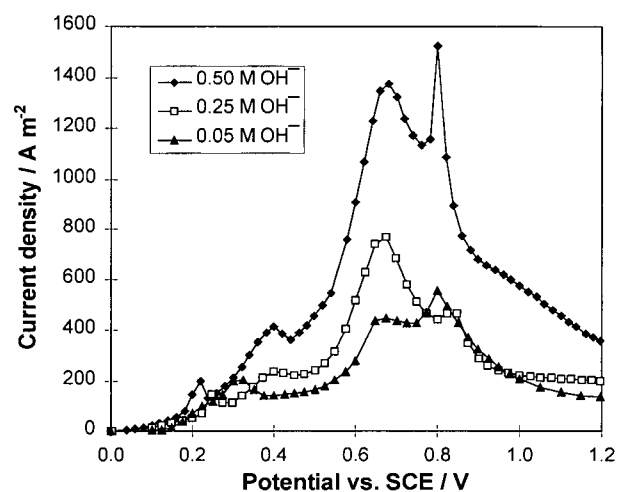
(b) 40 °C
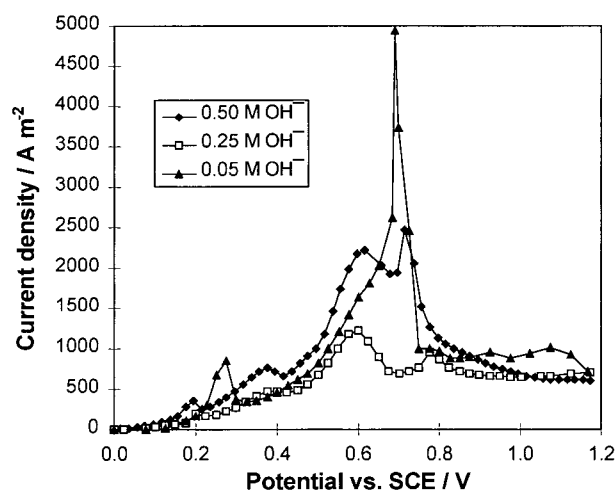
(c) 50 °C
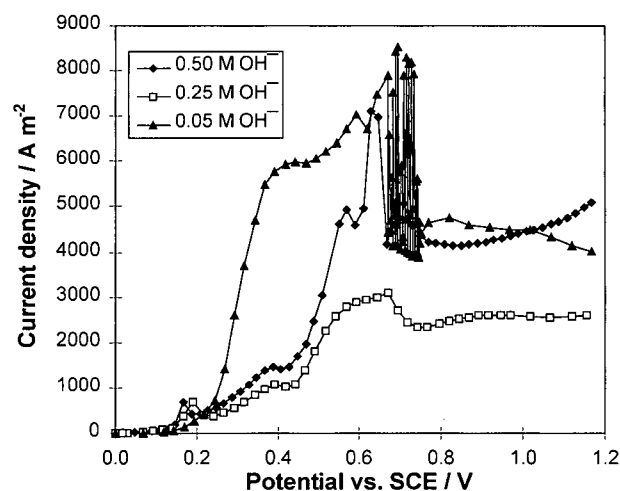
(d) 60 °C

Figure 7-26 Effect of pH on cyanide oxidation - the plot of the current vs. the potential on a graphite rotating disk at 4900 rpm and different temperatures. Electrolytes : 3 M CN⁻, a CN:Cu mole ratio of 3, 0.50, 0.25 and 0.05 M OH⁻ and 0.5 M Na_2SO_4.
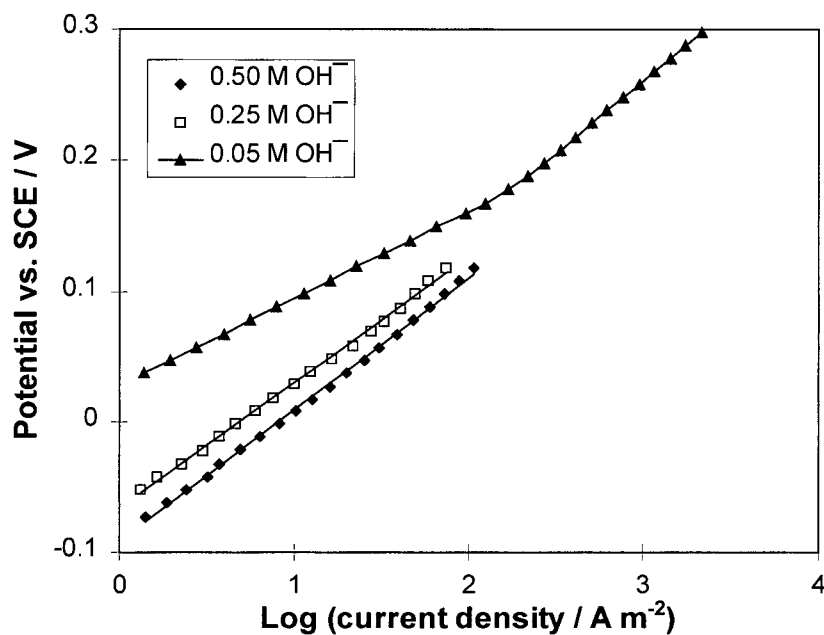
Figure 7-27   Effect of pH on cyanide oxidation - potential vs. log (current density) on a graphite rotating disk at 4900 rpm and 60 °C. Electrolytes : 3 M CN⁻, a CN:Cu mole ratio of 3, 0.50, 0.25, and 0.05 M OH⁻ and 0.6 M Na₂SO₄.
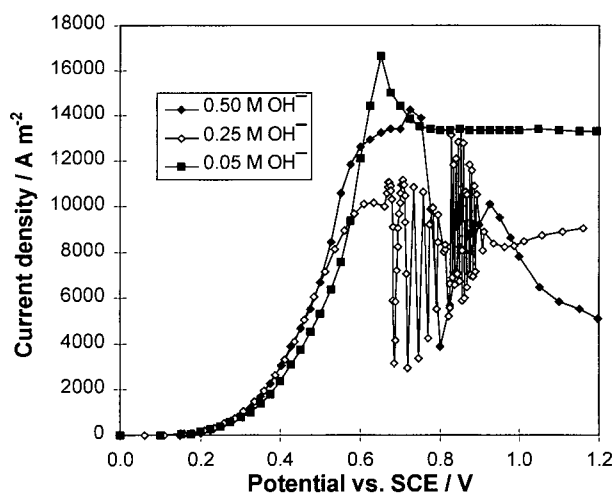
(a) 25 °C   (b) 40 °C
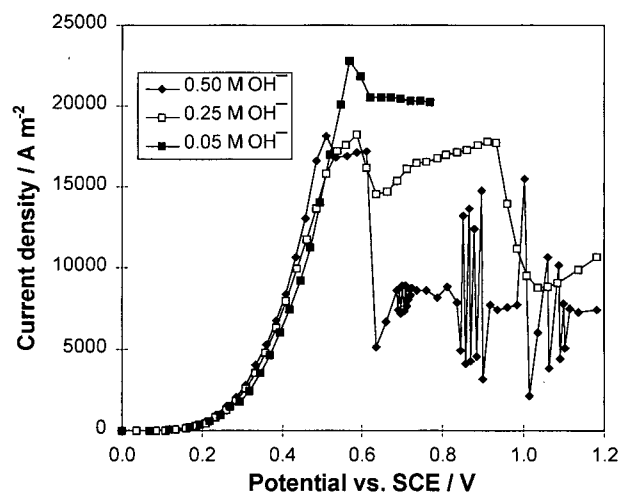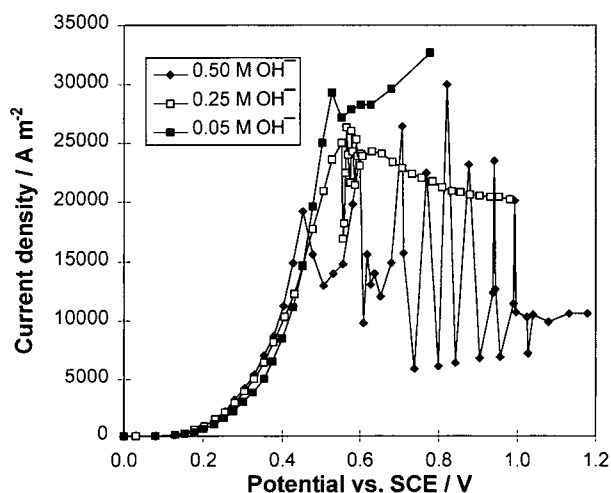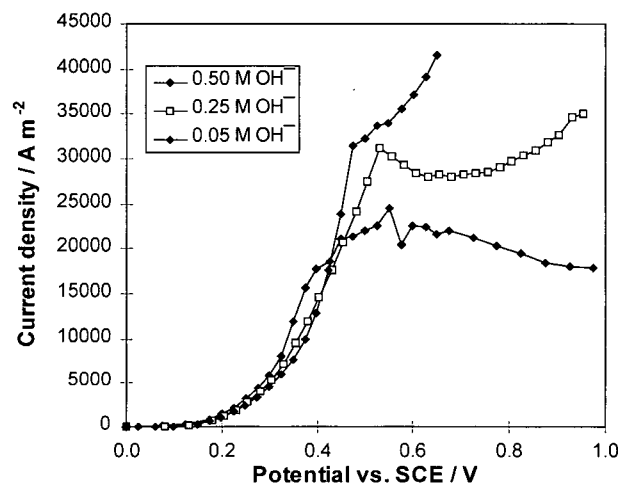
(c) 50 °C   (d) 60 °C
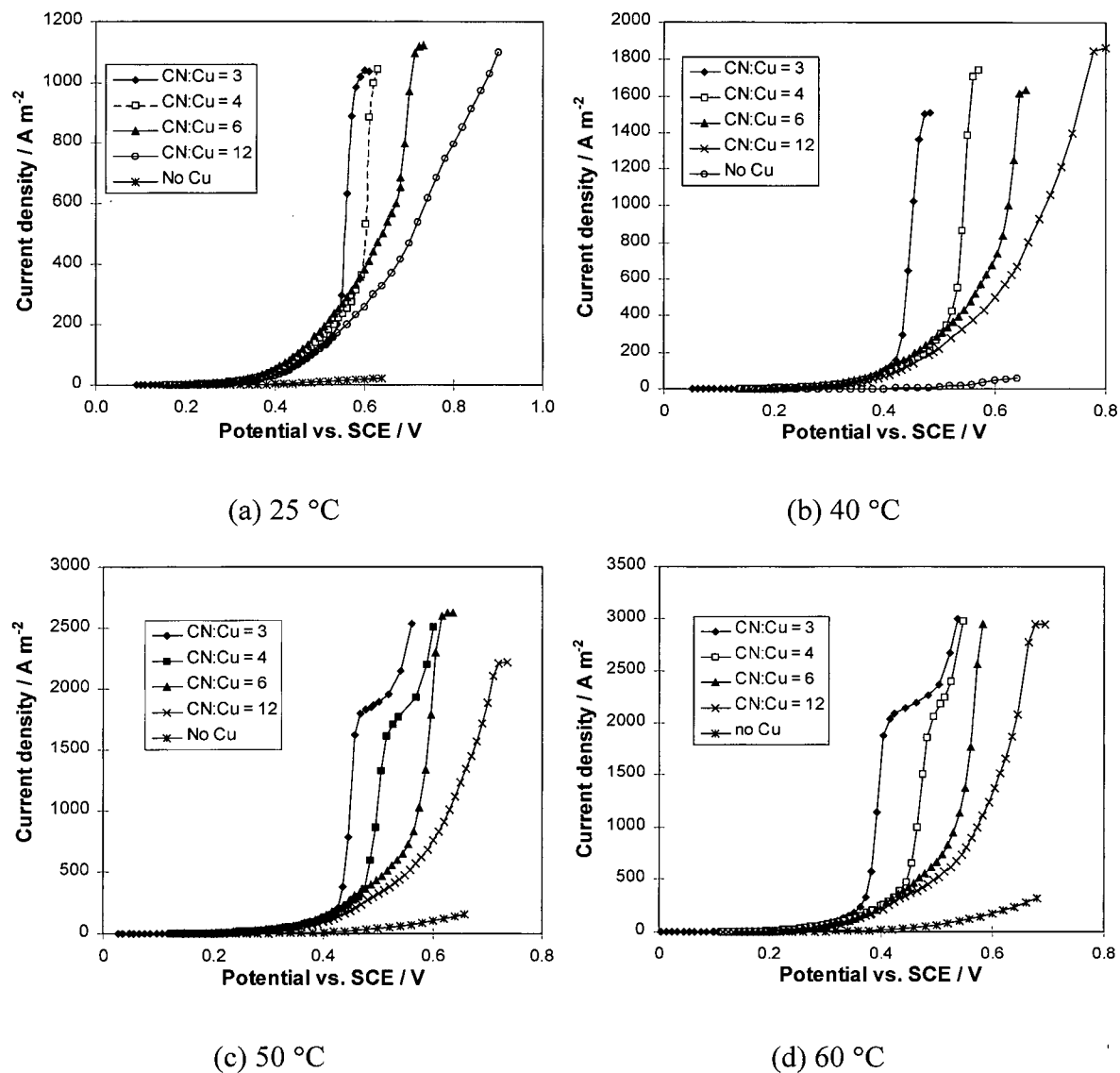
Figure 7-28 Effect of pH on cyanide oxidation - current vs. potential on a graphite rotating disk at 4900 rpm and different temperatures. Electrolytes : 4 M CN⁻, a CN:Cu mole ratio of 4, [OH⁻] = 0.5 and 0.25 and 0.05 M and 0.5 M Na₂SO₄.
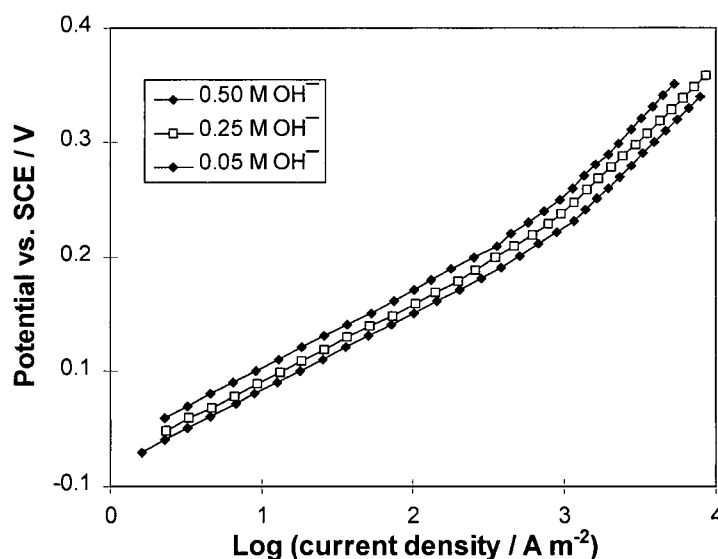
Figure 7-29 Effect of pH on cyanide oxidation - potential vs. log (current density) on a graphite rotating disk at 60 °C. Electrolytes : 4 M CN⁻ , a CN:Cu mole ratio of 3, [OH⁻] = 0.50, 0.25 and 0.05 M and 0.5 M Na₂SO₄.

7.6 Reaction Order

In order to determine which of the copper cyanide species is discharged at the electrode surface, the reaction order with respect to copper cyanide species was calculated by changing the copper cyanide concentration and the mole ratio of cyanide to copper and measuring the current vs. concentration of copper cyanide species at a constant potential. The concentrations of copper cyanide species ($Cu(CN)_2^-$, $Cu(CN)_3^{2-}$ and $Cu(CN)_4^{2-}$) were calculated by solving the mass balance equations (Equations 3-1 and 3-2) related to Reactions 2-3 to 2-6.

At a CN:Cu mole ratio of 3, the polarization curves were measured in the cyanide concentration range 0.025 - 0.2 M and the temperature range 25 to 60 °C. The current increased uniformly with increasing concentration of copper cyanide and the Tafel slope remained at about 0.120 V decade^{-1} (Figure A-34 in Appendix 8). This means that the kinetic parameters do not change with changing concentration. About 97 % of the copper exists in the form of $Cu(CN)_3^{2-}$ and its concentration is proportional to the concentration of the total copper cyanide. The concentrations of CN^-, $Cu(CN)_2^-$ and $Cu(CN)_4^{2-}$ are very low and do not increase uniformly with increasing concentration of the total copper cyanide. The plots of log (current) vs. log (concentrations of tricyanide) at constant potentials gave straight lines having slopes 0.97-0.99 (Figure 7-30). This suggests that the reaction order with respect to tricyanide is one. Therefore $Cu(CN)_3^{2-}$ could be discharged at the electrode forming $Cu(CN)_3^-$. The same results were obtained on a pyrolytic graphite rotating disk (Figures A-35 and A-36 in Appendix 8).

From Figures 7-13 and 7-14, at [Cu] = 0.00833 M, the increase in cyanide concentration from 0.025 M (a CN:Cu mole ratio of 3) to 0.05 M (a CN:Cu mole ratio of 6) resulted in a change in the Tafel slope. This means that the discharged species or the rate-controlling step changed. However, when the concentration of cyanide increased from 0.05 to 0.4 M, the Tafel slope did not change. The polarization curves shifted and were almost parallel to each other. This shift could be due to a change in the concentration of some copper cyanide species. The current at a constant potential was almost proportional to the concentration of $Cu(CN)_4^{3-}$ but not the other copper cyanide species. At 25 °C, the plots of log current vs. log($[Cu(CN)_4^{3-}]$) at 0.2 and 0.4 V vs. SCE gave straight lines having slopes of

0.96 and 1.0 respectively (Figure 7-31). The slopes obtained on a pyrolytic graphite rotating disk at 0.4 and 0.6 V vs. SCE were 1.01 and 0.98 (Figure 7-32). The results at 40, 50 and 60 ^{0}C are the same.

| (a) 25 °C | (b) 60 °C |
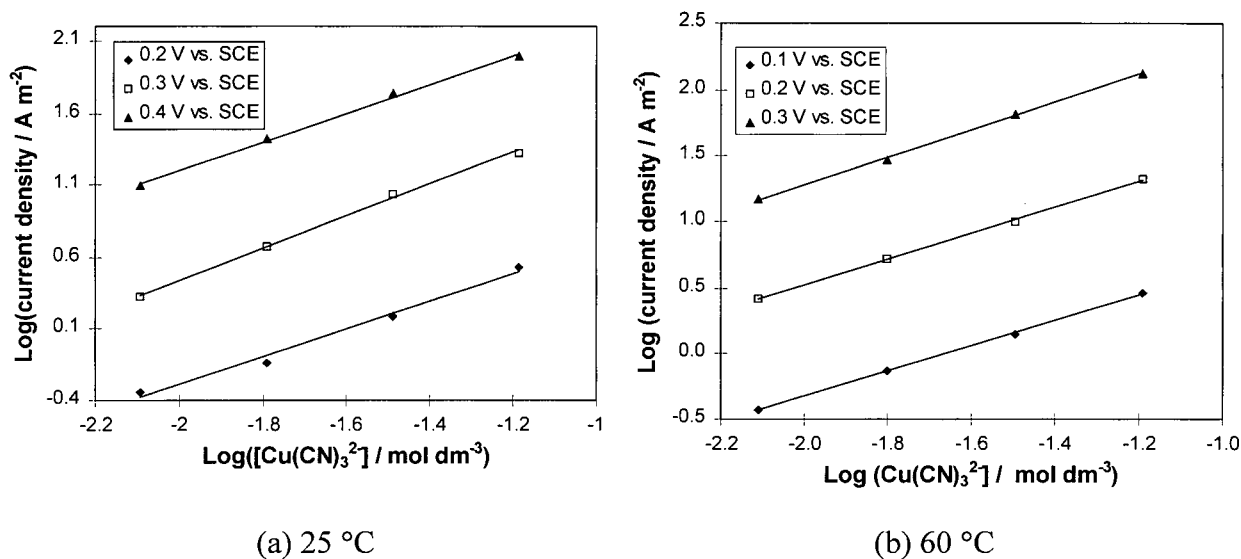
Figure 7-30 Plots of log (current density) vs. log ([Cu(CN)$_3^{2-}$]) on a graphite rotating disk at 4900 rpm (25 and 60 °C). Electrolytes: [CN$^-$] = 0.025, 0.05, 0.1 and 0.20 M, a CN:Cu mole ratio = 3, [OH$^-$] = 0.25 M and 1 M Na$_2$SO$_4$.
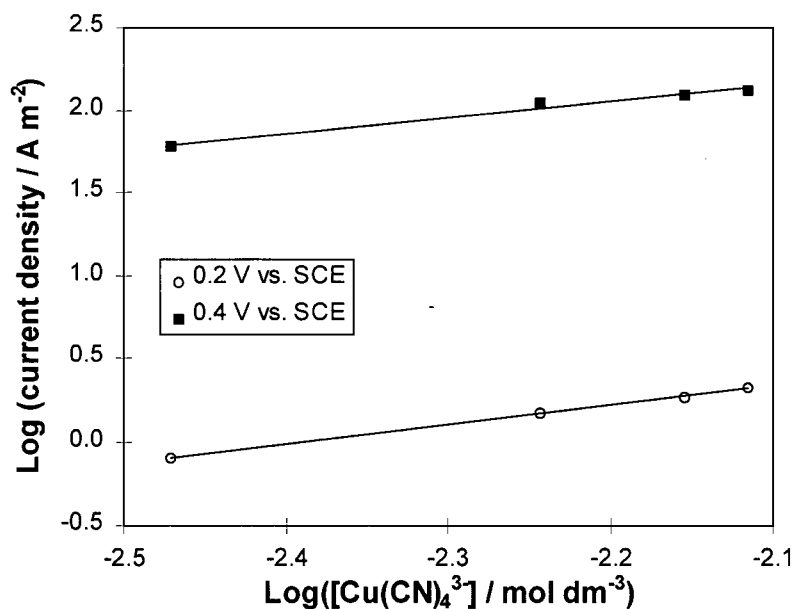
Figure 7-31 Plots of log (current density) vs. log ([Cu(CN)$_4^{2-}$]) on a graphite rotating disk at 4900 rpm and 25 °C. Electrolytes : [CN$^-$] = 0.05, 0.1, 0.20 and 0.40 M, [Cu$^+$] = 0.00833 M, [OH$^-$] = 0.25 M and 1 M Na$_2$SO$_4$.
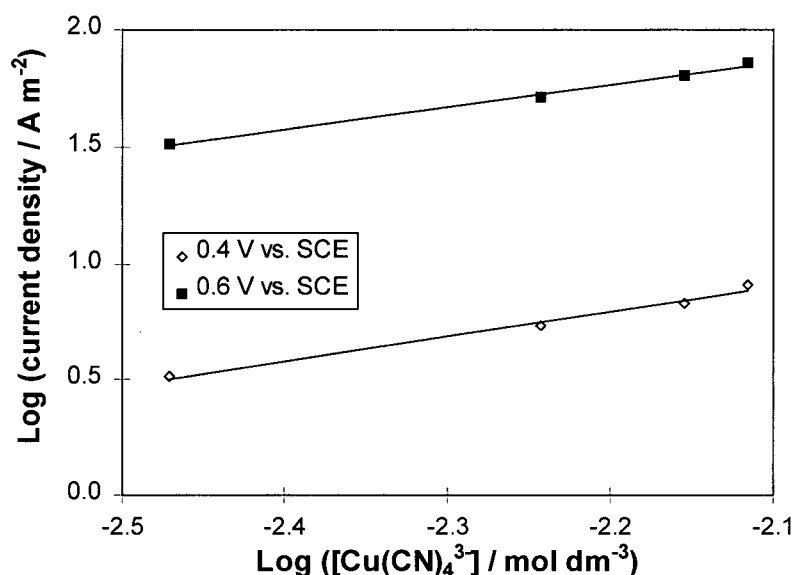
Figure 7-32 Plots of log (current density) vs. log ($[Cu(CN)_3^{2-}]$) on a pyrolytic graphite rotating disk at 4900 rpm and 25 °C. Electrolytes : $[CN^-]$ = 0.05, 0.10, 0.20 and 0.40 M, $[Cu^+]$ = 0.0833, $[OH^-]$ = 0.25 M and 1 M Na_2SO_4.

Figure 7-33 shows the plots of log (current density) vs. log ($[Cu(CN)_4^{2-}]$) when the total cyanide concentration was kept at 0.4 M and the copper concentration was changed. The slopes of the curves were 0.96 and 0.93 respectively for 0.2 and 0.4 V vs. SCE, which correspond to the two Tafel slope ranges. The reaction order with respect to $Cu(CN)_4^{3-}$ obtained on a pyrolytic graphite electrode was 1.0. Yoshimura et al. [144] studied the anodic oxidation of copper cyanide on platinum and thought that almost all of the copper exists in the form of $Cu(CN)_4^{3-}$. They plotted log current vs. log $[Cu]_{Total}$ and obtained a slope of 0.9. However, from our calculation, 32 -24 % of the copper exists in the form of $Cu(CN)_3^{2-}$ in the concentration range studied and the concentration of $Cu(CN)_4^{3-}$ is not exactly proportional to the total copper concentration. The plot of log $[Cu(CN)_4^{3-}]$ vs. log $[Cu]_{Total}$ gave a slope of 0.901. Therefore the corrected reaction order with respect to $Cu(CN)_4^{3-}$ should be 0.99 for Ref. 144.

From Figure 7-11 and 7-12, at $[CN]_{total}$ = 0.05 M, the polarization curves for CN:Cu mole ratios of 4, 6, and 12 are very close and the current for a CN:Cu mole ratio of 6 ($[Cu]$ = 0.00833 M) at a constant potential is even larger than that for a CN:Cu mole ratio of 4 ($[Cu]$

= 0.0125 M). This is because the concentration of $Cu(CN)_4^{3-}$ for a CN:Cu mole ratio 6 is larger than that for a CN:Cu mole ratio of 4.

The reaction order with respect to the copper cyanide species was also calculated by changing the total copper cyanide concentration and keeping CN:Cu mole ratio at 48. At this mole ratio, most of copper exists in the form of $Cu(CN)_4^{3-}$. The current is almost proportional to the concentration of $Cu(CN)_4^{3-}$, but not to that of $Cu(CN)_3^{2-}$. The plots of log(current) vs. log($[Cu(CN)_4^{3-}]$) gave straight lines having slopes of 1.1 and 1.0 respectively at 0.2 V and 0.4 V vs. SCE. The reaction order measured on a pyrolytic graphite electrode was 1.0.

The reaction order with respect to hydroxide was determined by changing the hydroxide concentration. From Figures 7-18 and 7-19, at a CN:Cu mole ratio of 3, the Tafel slope changes with hydroxide concentration and the rate-controlling step or the reaction mechanism changes. From Figures 7-21, 7-22, 7-24 and 7-25, in the low polarization region, at a CN:Cu mole ratio $\geq$ 4, the current changes only slightly with hydroxide concentration and the reaction order with respect to hydroxide is close to zero. Thus the rate-controlling step does not involve hydroxide.
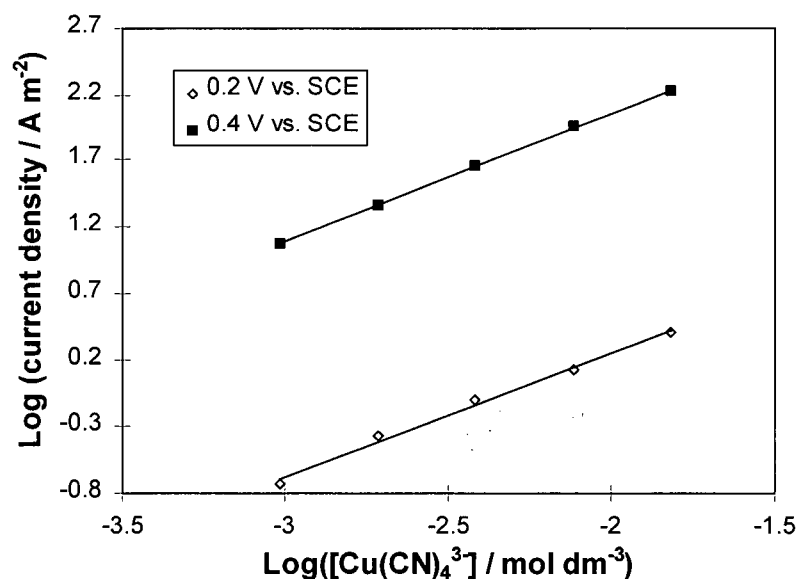
Figure 7-33 Plots of log (current density) vs. log ($[Cu(CN)_3^{2-}]$) on a graphite rotating disk at 4900 rpm and 25 °C. Electrolytes : $[CN^-]$ = 0.40 M, $[Cu^+]$ = 0.0167, 0.00833, 0.00417, 0.00208, 0.00104 M, $[OH^-]$ = 0.25 M and 1 M Na_2SO_4.

7.7 Reaction Between Cyanide and Copper(II)

The reaction between cyanide and Cu(II) ions produces $Cu(CN)_4^{2-}$ ions which have a violet color and rapidly decompose into cyanogen and a copper cyanide species [58-73]. The conditions in the literature reports are different from those in this study and the results cannot be compared. Therefore the experiments on the reaction between cyanide and Cu(II) were conducted to understand the phenomena observed in this study. Mixing sodium cyanide and $CuSO_4$ gave a transient violet color which disappeared in less than one second. Using UV spectroscopy and stop-flow technology a transient species was detected at 535 nm which was assumed to belong to $Cu(CN)_4^{2-}$ [49].

Figures 7-34 and 7-35 show the absorbance vs. time at 535 ± 3 nm when 2.5 cm^3 of 0.05 M cyanide solutions with 0.25 and 0.05 M OH$^-$ were mixed with 0.4 cm^3 of 0.05 M copper sulphate solution. From Figure 7-36, the decomposition rate of $Cu(CN)_4^{2-}$ was decreased when the concentration of cyanide was increased to 1 M. The plot of (1/absorbance) vs. time (Figure 7-37) is a straight line giving a reaction order with respect to $Cu(CN)_4^{2-}$ of two. The selection of the time range for Figure 7-37 is based on the fact that at the time < 6.5 s, the concentration of $Cu(CN)_4^{2-}$ was too high to be proportional to the absorbance and at the time > 9 s, the concentration of $Cu(CN)_4^{2-}$ was too small and was interfered by the environment.
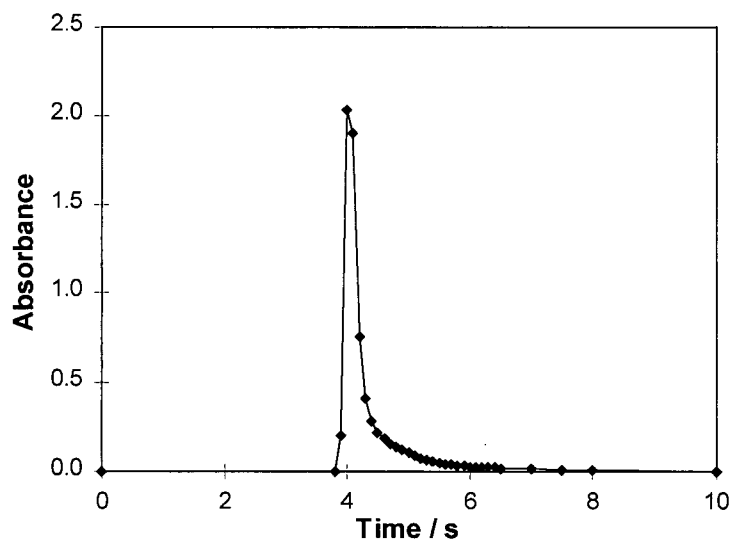
Figure 7-34 Absorbance vs. time when 2.5 cm^3 of 0.05 M cyanide solution with 0.25 M OH$^-$ were mixed with 0.4 cm^3 of 0.05 M copper sulphate solution at 25 °C.
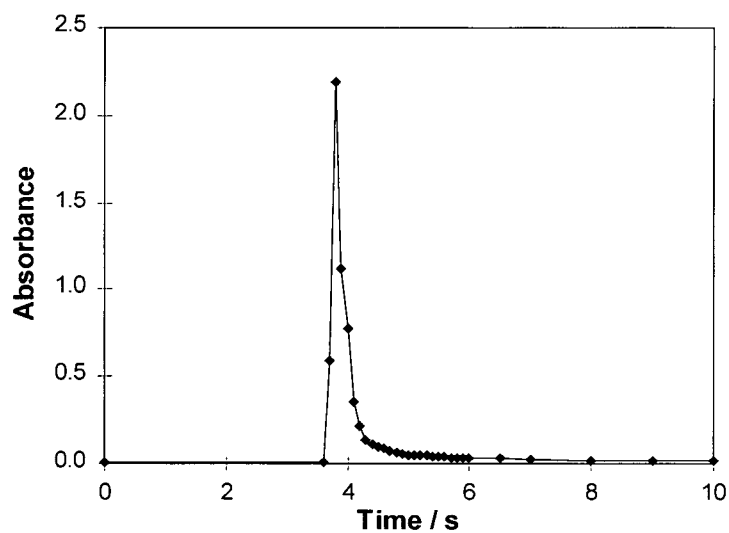
Figure 7-35 Absorbance vs. time when 2.5 cm³ of 0.05 M cyanide solution with 0.05 M OH⁻ were mixed with 0.4 cm³ of 0.05 M copper sulphate solution at 25 °C.
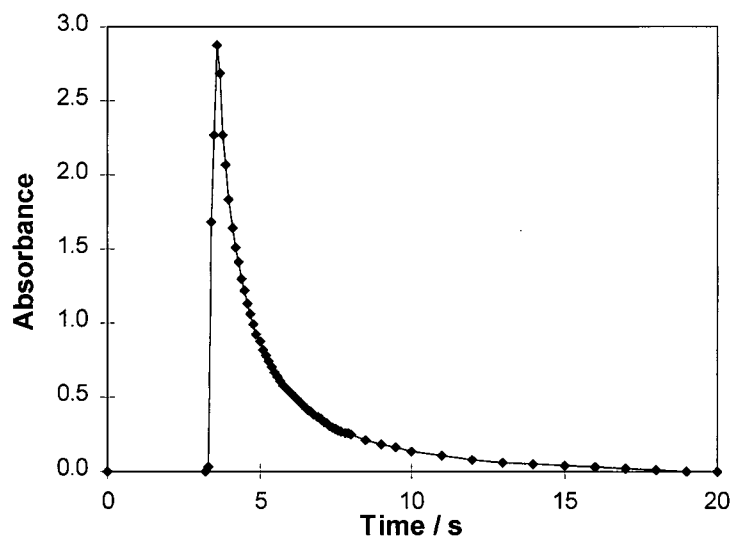
Figure 7-36 Absorbance vs. time when 2.5 cm³ of 1 M cyanide solution with 0.25 M OH⁻ were mixed with 0.4 cm³ of 0.05 M copper sulphate solution at 25 °C.
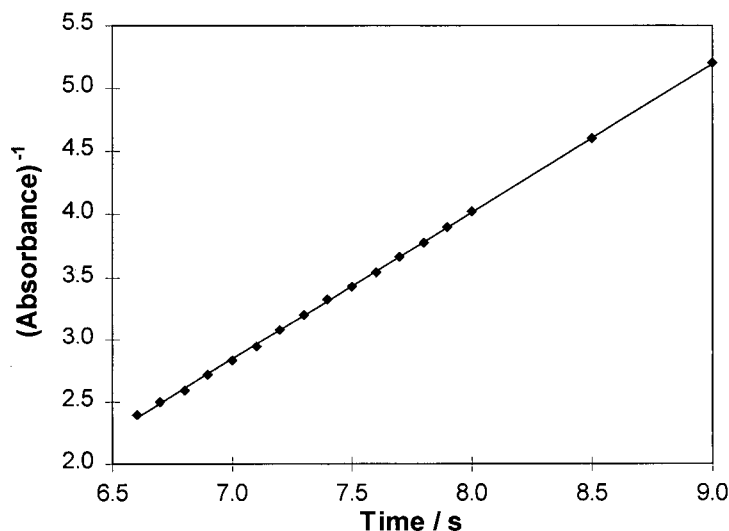
Figure 7-37 The plot of (absorbance)$^{-1}$ vs. time when 2.5 cm^3 of 1 M cyanide solution with 0.25 M OH$^-$ were mixed with 0.4 cm^3 of 0.05 M copper sulphate solution at 25 °C.

0.1 M CuSO$_4$ solution was also gradually added to 0.05 M sodium cyanide solutions with 0.25 M NaOH and 0.01 M NaOH. In the case of the solution containing 0.25 M NaOH at 25 °C, after CuSO4 was added to the reactor, the local solution became blue and black. Then the whole solution became purple, this colour disappearing in less than one second. When the amount of copper added made the mole ratio of cyanide to copper exceed about 2.85, the whole solution became a light blue, which colour gradually disappeared. No purple color was observed. At a mole ratio of cyanide to copper < 2.75, blue Cu(OH)$_2$ began to precipitate upon the further addition of cupric ions. At 50 °C, the precipitate had a mixed color of black, brown and blue. Apparently cupric ions reacted with cyanide ions and formed cupric cyanide which decomposed into cuprous cyanide and cyanogen. Cupric ions also reacted with hydroxide to form copper hydroxide or oxide.

When only a small amount of cupric ions was added, the mole ratio of cyanide to copper and free cyanide was high and the reaction between cyanide and cupric ions was favored. When a large amount of cupric ions was added, the concentration of free cyanide became so low due to the formation of very stable cuprous complexes that the reaction between cupric ion and hydroxide is favored.

When the concentration of sodium hydroxide was decreased to 0.01 M, no blue precipitate was observed. After the addition of cupric ions, a local yellowish color appeared

which became purple and disappeared in one second. When the mole ratio of cyanide to copper was below 1.6, a white precipitate appeared and the pH decreased to 4-4.3 due to the consumption of hydroxide ions in the reaction between cyanide and cupric ion:

$$2Cu^{2+} + CN^- + 2OH^- = 2Cu(I) + CNO^- + H_2O \qquad (7\text{-}4)$$
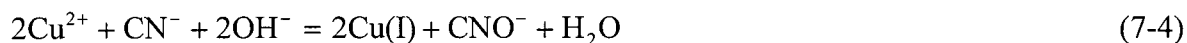
Upon further addition of cupric ions, more white precipitate was produced. The white precipitate was apparently CuCN.

In the light of the above observations, the phenomenon of the anodic oxidation of copper becomes easy to understand. At a low potential, the current is low and the mole ratio of cyanide to copper on the surface is high, preventing the precipitation of copper oxide due to the oxidation of copper cyanide. When the potential exceeds a critical value and the current is so high that the mole ratio of cyanide to copper is low, the oxidation of copper cyanide produces copper oxide. When the copper concentration is low, the potential needs to be higher to make the current reach a critical value where the mole ratio of cyanide to copper on the surface becomes low enough to favour the precipitation of copper oxide. Decreasing the hydroxide concentration suppresses the formation of copper oxide from the viewpoint of both thermodynamics and kinetics. This is in agreement with the results on the anodic oxidation of copper cyanide.

7.8 Cyclic Voltammetry

Using cyclic voltammetry, we can evaluate the reversibility of the anodic oxidation of copper and know the stability of the intermediate products. During the positive potential scanning, cuprous cyanide species are oxidized to cupric cyanide species which may be reduced during the negative potential scanning. The scanning rate was kept above 10 V s^{-1} to avoid the precipitation of copper oxide and the maximum potential was below 1 V vs. SCE to avoid the significant evolution of oxygen. Figure 7-38 shows the cyclic voltammetry of the solution containing 0.05 M CN$^-$, 0.01666 M Cu and 0.25 M NaOH at 25 °C after subtraction of the background current. There was no reduction current during the negative-going scanning. The anodic oxidation of copper cyanide seems to be irreversible. The chemical reaction of the oxidized copper cyanide species is too fast to be detected during the

negative scanning. By increasing the mole ratio of cyanide to copper and decreasing the pH, there was still no reduction current during the negative potential scanning.
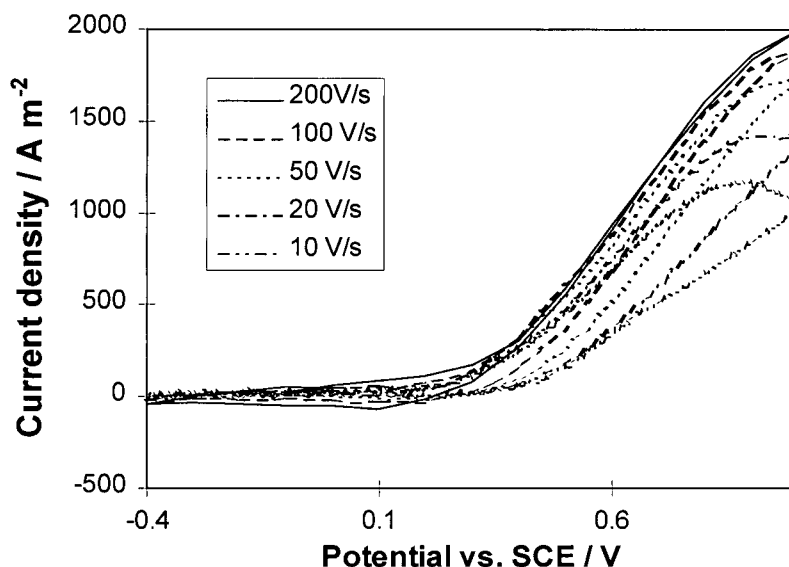
Figure 7-38 Cyclic voltammetry at 25 °C. Electrolyte: 0.025 M CN⁻, CN:Cu mole ratio =3, 0.25 M NaOH and 1 M Na$_2$SO$_4$.

7.9 Possible Reaction Mechanism

At a CN:Cu mole ratio = 3 and [OH⁻] = 0.25 M, over 97 % of the copper exists in the form of Cu(CN)$_3^{2-}$ and the current is proportional to the concentration of Cu(CN)$_3^{2-}$ but not the concentrations of Cu(CN)$_2^{-}$ and Cu(CN)$_4^{3-}$. This suggests that Cu(CN)$_3^{2-}$ can be discharged and oxidized to Cu(CN)$_3^{-}$ at the electrode. Cu(CN)$_3^{-}$ is unstable and decomposes to form cyanogen. Cyanogen reacts with hydroxide to produce cyanate.

When the electrode potential exceeded a certain value, copper oxide was formed on the electrode (both on the graphite and the outer insulator) and the current increased sharply to a limiting value.

Copper oxide or hydroxide can be formed by three ways: (1) copper cyanide decomposes into free cyanide and cuprous ions which are oxidized to copper oxide on the anode, (2) copper cyanide is oxidized to free cyanide and cupric ions which react with hydroxide to form copper oxide and (3) cuprous cyanide is oxidized to cupric cyanide which reacts with hydroxide to form copper oxide. The formation of copper oxide on the outer

insulator means that cupric species diffuse to the surface of the outer insulator and react with OH⁻ to form copper oxide and hydroxide. The most likely mechanism is: the cuprous complex ($Cu(CN)_3^{2-}$) is oxidized to cupric complex ($Cu(CN)_3^-$) and some of the cupric complex decomposes to form cyanogen. Some of it reacts with hydroxide to form hydroxide on the anode and a small amount diffuses to the surface of the outer insulator to form copper oxide. The mechanism of the anodic oxidation of cyanide at high potentials is different from that at low potentials.

With decreasing concentration of hydroxide, the current and the Tafel slope decrease. This means that hydroxide affects the rate-controlling step. The decrease in the Tafel slope from 0.12 V to 0.060 V decade^{-1} means the rate-controlling step changes or even the mechanism changes. At high hydroxide concentration, the thermodynamic stability of the copper (I) species is relatively low and the species are more easily oxidized. With decreasing hydroxide concentration, the electrochemical stability of $Cu(CN)_3^{2-}$ increases and copper cyanide becomes less electrochemically activated.

As the CN:Cu mole ratio increases, the current and Tafel slope also decrease at low potentials. The Tafel slope decreases to about 0.060 V decade^{-1} when the mole ratio exceeds 4 at [CN⁻] = 0.05 M. This means that the rate-controlling step or the reaction mechanism changes. With further increase in potential, the second Tafel slope (0.160 to 0.200 V decade^{-1}) appeared. The current at a constant potential is proportional to the concentration of $Cu(CN)_4^{3-}$ and but independent of the concentration of hydroxide. The discharged species are not sensitive to hydroxide ion and therefore it is unlikely that $Cu(CN)_3^{2-}$ is discharged. $Cu(CN)_4^{-3}$ is most likely to be discharged at the electrode.

At [OH⁻] = 0.01 M and a constant potential, the ratio of the current measured in 0.05 M CN⁻ solutions with CN:Cu mole ratios of 3 and 4 is close to the mole ratio of $Cu(CN)_4^{3-}$ of the solutions. Therefore the discharged species could transfer from $Cu(CN)_3^{2-}$ and $Cu(CN)_4^{3-}$ to $Cu(CN)_4^{3-}$ with decreasing hydroxide concentration. At high hydroxide concentration, $Cu(CN)_3^{2-}$ is discharged much faster than $Cu(CN)_4^{3-}$ and the current contributed by $Cu(CN)_4^{3-}$ can be neglected compared to that of $Cu(CN)_3^{2-}$. With decreasing hydroxide concentration, the discharge of $Cu(CN)_3^{2-}$ is suppressed and the discharge of $Cu(CN)_4^{3-}$ maintains the constant rate and becomes the dominant discharged species.

The amount of copper oxide formed decreases with increasing CN:Cu mole ratio and decreasing hydroxide concentration. No copper oxide formed at the outer insulator at a CN:Cu mole ratio >3.5 or [OH⁻] < 0.05 M. When copper oxide was precipitated on the electrode, with decreasing hydroxide concentration, the current decreases with decreasing hydroxide concentration. The higher the CN:Cu mole ratio, the less the effect of hydroxide, the higher the potential for the precipitation of copper oxide and the more stable the copper (I) species.

The following possible mechanisms are proposed:

(1) In the low potential region (< about 0.4 V vs. SCE):

At a CN:Cu mole ratio = 3 and a high concentration of hydroxide (0.25 M OH⁻)

Step 1 $Cu(CN)_3^{2-} \rightarrow Cu(CN)_3^{-} + e$

Step 2 $2Cu(CN)_3^{-} \rightarrow 2Cu(CN)_2^{-} + (CN)_2$

Step 3 $(CN)_2 + 2OH^{-} \rightarrow CNO^{-} + CN^{-} + H_2O$
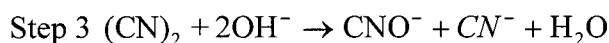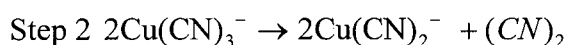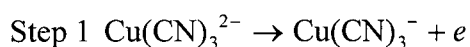
Step 1 could be the rate-controlling step from a Tafel slope of 0.12 V decade⁻¹ [335, 336] and the discharge of $Cu(CN)_4^{3-}$ is negligible compared to $Cu(CN)_3^{2-}$. Step 1 is catalyzed by hydroxide ions. Hydroxide ions might be weakly bound to $Cu(CN)_3^{2-}$ to form a surface complex such as $Cu(CN)_3^{2-}OH^{-}$ which is more readily discharged on the anode. With decreasing pH, the above reaction is suppressed probably due to the decrease in the surface complex concentration, the current decreases, and the discharge of $Cu(CN)_4^{3-}$ becomes the dominant anodic reaction.

Increasing CN:Cu mole ratio has a similar effect because it shifts the distribution of copper cyanide species from lowly coordinated complexes to a highly coordinated complex $(Cu(CN)_4^{3-})$ and probably also suppresses the formation of a surface complex (such as $Cu(CN)_3^{2-}OH^{-}$). The critical value for the CN:Cu mole ratio depends on the total copper cyanide concentration because the distribution of copper cyanide species is dependent on cyanide concentration. For example, at [CN⁻] = 0.05 M, when a CN:Cu mole ratio > about 4, the discharge of $Cu(CN)_4^{3-}$ is dominant. However, at [CN⁻] =3.5, when CN:Cu mole ratio ≥ 3.5, the discharge of $Cu(CN)_4^{3-}$ becomes dominant.

When the dominant discharged species is $Cu(CN)_4^{3-}$, the anodic reaction probably consists of the following steps according to the observed kinetics:

Step 1 $Cu(CN)_4^{3-} \underset{k_{-1}}{\overset{k_1}{\Leftrightarrow}} Cu(CN)_4^{2-}{}_{(ads)} + e$

Step 2 $Cu(CN)_4^{2-}{}_{(ads)} \underset{k_{-2}}{\overset{k_2}{\Leftrightarrow}} Cu(CN)_4^{2-}$

Step 3 $2Cu(CN)_4^{2-} \rightarrow 2Cu(CN)_3^{2-} + (CN)_2$

Step 4 $(CN)_2 + 2OH^- \rightarrow CNO + CN^- + H_2O$
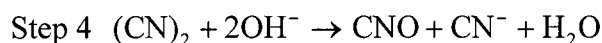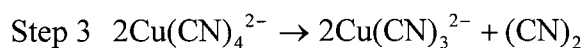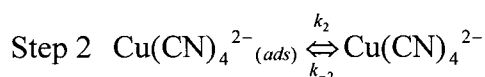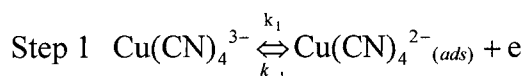
The adsorption rate for the coverage of $Cu(CN)_4^{2-}$, $(d\theta/dt)$, can be expressed by the following equation:

$$\frac{d\theta}{dt} = k_1(1-\theta)[Cu(CN)_4^{3-}] - k_{-1}\theta - k_2\theta + k_{-2}(1-\theta)[Cu(CN)_4^{2-}] \qquad (7\text{-}5)$$

where θ is the coverage of $Cu(CN)_4^{2-}$ on the electrode, k_1 the rate constant for the electrochemical adsorption, k_{-1} the rate constant for the electrochemical desorption, k_2 the rate constant for the chemical desorption and k_{-2} the rate constant for the chemical adsorption.

At steady state, $d\theta/dt = 0$ and if $\theta \approx 0$ and $k_{-1} \gg k_{-2}$, the following equation can be obtained from Equation 7-5:

$$\theta = \frac{k_1[Cu(CN)_4^{3-}]}{k_{-1} + k_2} \qquad (7\text{-}6)$$

In the initial low potential region, if $k_{-1} \gg k_2$, the following equation can be obtained:

$$\theta = \frac{k_1}{k_{-1}}[Cu(CN)_4^{3-}] = \frac{k_{0,1}\exp(\alpha FE / RT)}{k_{0,-1}\exp(-(1-\alpha)FE / RT)} = \frac{k_{0,1}}{k_{0,-1}}\exp(\frac{FE}{RT}) \qquad (7\text{-}7)$$

where α is the charge transfer coefficient, $k_{0,1}$ and $k_{0,-1}$ the rate constants respectively for oxidation and reduction at $E = 0$ and $k_1 = k_{0,1}\exp(\alpha FE/RT)$ and $k_{-1} = k_{0,-1}\exp(-(1-\alpha)FE/RT)$.

Reaction rate $= k_2\theta$ \qquad (7-8)

$$i = Fk_2\theta = \frac{Fk_2 k_{0,1}}{k_{0,-1}}[Cu(CN)_4^{3-}]\exp(\frac{FE}{RT}) \qquad (7\text{-}9)$$

From Equation 7-9, the reaction order with respect to $Cu(CN)_4^{3-}$ is one and the Tafel slope is RT/F(about 0.06 V decade^{-1}). Therefore the above assumption is consistent with the experimental results.

When the potential increases to a value where $k_{-1} \ll k_2$, from Equation 7-6, the coverage of the adsorbed $Cu(CN)_4^{2-}$ can be expressed as:

$$\theta = \frac{k_1[Cu(CN)_4^{3-}]}{k_2} \tag{7-10}$$

$$i = Fk_2\theta = Fk_1[Cu(CN)_4^{3-}] = Fk_{0,1}[Cu(CN)_4^{3-}]\exp(\frac{\alpha FE}{RT}) \tag{7-11}$$

From the above equation, the reaction order with respect to $Cu(CN)_4^{3-}$ is one and the Tafel slope is $RT/\alpha F$. This is consistent with the experiment results. It should be pointed out that Step 3 involves some elementary reactions. From the plot of log(current density) vs. potential (or potential vs. log (current density) according to Equations 7-9 and 7-11, we can calculate $Fk_2k_{0,1}[Cu(CN)_4^{3-}]/k_{0,-1}$ and $Fk_{0,1}[Cu(CN)_4^{3-}]$. Therefore $k_{0,-1}/k_2$ can be calculated from the above values. At $[CN^-] = 0.1$ M, CN:Cu mole ratio = 12 and 25 °C, $Fk_2k_{0,1}[Cu(CN)_4^{3-}]/k_{0,-1}$ and $Fk_{0,1}[Cu(CN)_4^{3-}]$ are about 8.33×10^{-4} and 0.546 A m^{-2} respectively. So $k_{0,-1}/k_2$ is 726 and k_{-1}/k_2 is 726 exp(-(1-α)FT/RT). At potentials < 0.20 V vs. SCE, k_{-1}/k_2 is above 10 and so the Tafel slopes are about 0.060 V decade^{-1}. At a potential > 0.35 V vs. SCE, k_{-1}/k_2 is below 1/10 and the Tafel slope is about 0.171 V decade^{-1} ($\alpha = 0.35$). Equation 7-6 can be rearranged as:

$$\theta = \frac{(k_1/k_{-1})[Cu(CN)_4^{3-}]}{1+k_2/k_{-1}} = \frac{(k_{0,1}/k_{0,-1})[Cu(CN)_4^{3-}]\exp(FE/RT)}{1+(k_2/k_{0,-1})\exp((1-\alpha)FE/RT)} \tag{7-12}$$

$$i = Fk_2\theta = \frac{F(k_2k_{0,1}/k_{0,-1})[Cu(CN)_4^{3-}]\exp(FE/RT)}{1+(k_2/k_{0,-1})\exp((1-\alpha)FE/RT)} \tag{7-13}$$

From the above equation, the reaction order with respect to $Cu(CN)_4^{2-}$ is one at any potential.

Figure 7-39 shows the plots of potential vs. log (current density) using data measured and predicted using Equation 7-13. The predicted data are consistent with the data measured at a potential < 0.45 V vs. SCE. However, at potentials > 0.45 V, the measured data appear to deviate from the predicted value. This is because at potentials > 0.45 V, the assumptions are not valid and the difference in the copper concentration between the bulk solution and the surface is not negligible. The current is so high that the coverage of $Cu(CN)_4^{2-}$ cannot be neglected and the chemical desorption determines the whole reaction rate. $Cu(CN)_4^{2-}$ is much less adsorbed on a pyrolytic graphite electrode. Therefore there appears to be only one well-defined Tafel slope.

With further increase in potential, the current reaches a critical value and the CN:Cu mole ratio on the electrode surface decreases to such a low value that copper oxide or hydroxide is precipitated on the anode. From the standpoint of thermodynamics, dicyanide

and tricyanide are less stable and more readily oxidized to copper oxide and cyanide. The effect of the precipitated copper oxide on the anodic oxidation of copper cyanide depends on the applied potential, temperature and total cyanide concentration.

At $[CN^-]$ = 0.05 M and a temperature > 40 ^{0}C, copper oxide catalyzes the oxidation of copper cyanide. At a temperature < 40 ^{0}C, copper oxide has a limited catalytic effect on the cyanide oxidation. It may even exhibit an inhibiting effect at a potential > 0.6 V vs. SCE. At $[Cu^+]$ = 1M and $[CN^-]$ = 3 M, the formation of copper oxide or hydroxide significantly inhibits the anodic oxidation of copper cyanide. This may be related to the properties of the precipitated copper oxide and to the adsorption of copper cyanide.

The oxidation of free cyanide was catalyzed by cupric oxide formed on the electrode because in the absence of copper, the anodic current of free cyanide on the copper oxide-coated anode is significantly higher than that on the anode without copper oxide. Cu(III) species such as Cu_2O_3 can be produced in the potential range studied [341-345]. For example, Cu(III) oxide phase was stabilized at approximately 0.48 V vs. SCE and 0 °C in alkaline solution [341]. The oxidation of the Cu(II) species began at about 0.35 V vs. SCE and 24 °C in 1 M NaOH [343] and the intrinsic redox potential for Cu(III)/Cu(II) in the solid oxide is 0.42 V vs. SCE at pH 14 and 20 °C [344]. It is possible for Cu(III) to form on the surface and catalyze the cyanide oxidation as was suggested by Wells and Johnson [157]. Oxygen evolution was also catalyzed possibly by the formation and decomposition of Cu_2O_3 [345]. The reaction procedure can be expressed by the following set of possible reactions:

Step 1 $Cu(CN)_n^{-(n-1)} \rightarrow Cu(CN)_n^{-(n-2)}{}_{(ads)} + e$ (n =2, 3, 4)

Step 2 $Cu(CN)_n^{-(n-2)}{}_{(ads)} + 2OH^- \rightarrow nCN^-{}_{(ads)} + Cu(OH)_2 (or\ CuO + H_2O)$

Step 3 $Cu(CN)_n^{-(n-1)} \rightarrow Cu(CN)_n^{-(n-2)} + e$

Step 4 $Cu(CN)_n^{-(n-2)} = Cu(CN)_{(n-1)}^{-(n-2)} + 1/2(CN)_2$

Step 5 $CN^-{}_{(ads)} + 2OH^- \xrightarrow{\text{Catalyzed by copper oxide}} CNO^- + H_2O$
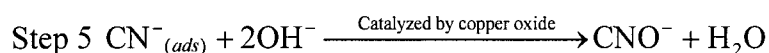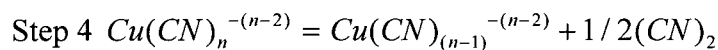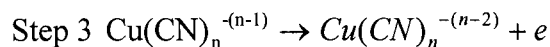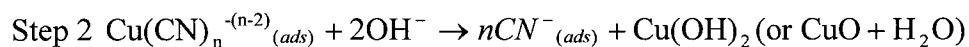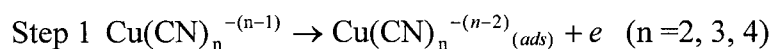
With decreasing pH and increasing mole ratio of cyanide to copper, Step 1 (n = 2 and 3), Step 2, Step 3 (n = 3) and Step 5 are suppressed. This results in a decrease in the current and it is in agreement with the experimental results. At a high CN:Cu ratio and low pH, no copper oxide is formed. The catalysis of copper oxide was prevented with increasing the potential and the copper cyanide concentration.
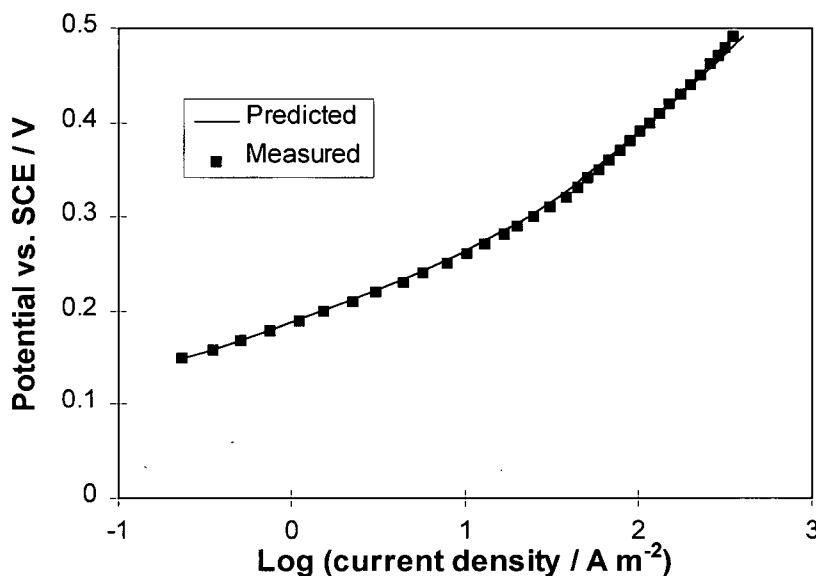
Figure 7-39 Plots of potential vs. log (current density) using data measured and predicted using Equation 7-12 at 25 ^{0}C. Electrolyte: 0.1 M CN⁻, CN:Cu mole ratio = 12, 0.25 M NaOH and 1 M Na_2SO_4.

7.10 Diffusion Coefficient Estimation

In the presence of a large amount of supporting electrolyte, the limiting current for a simple electrochemical reaction on the rotating disk can be expressed by Equation 6-5. The diffusion coefficients can be calculated from the slopes of the straight lines for the plots of i_l vs. $\omega^{1/2}$. In this study, when the current reaches the limiting value, cuprous cyanide is oxidized to cupric cyanide which undergoes two further reaction paths. One is that cupric cyanide reacted with hydroxide to produce copper oxide or hydroxide and free cyanide which is further oxidized to cyanate. Another is that cupric cyanide species diffuse from the surface and rapidly decompose to form cyanogen and lower coordinated copper cyanide. The diffusion of cupric species to the bulk solution has the following effect on the limiting current: (1) the decomposition in the diffusion layer results in the shift of the distribution to the formation of the lowly coordinated copper (I) complex and affects the concentration gradient of copper cyanide species and affects the limiting current; (2) the undecomposed cupric species during the diffusion bring cyanide to the bulk resulting in the decrease in the limiting current.

From the coulometric measurement, at a CN:Cu mole ratio = 3 and $[OH^-]$ = 0.25 M, the anodic oxidation of copper cyanide can be expressed as Reaction 7-1, i.e. the oxidation of one complex gave 7 electrons and $Cu(CN)_3^{2-}$ is completely oxidized to cyanate and copper oxide. So the amount of cupric cyanide reaching the bulk solution is very small. Otherwise more cyanide and less cuprous ions are oxidized. The decomposition of cupric cyanide (mainly $Cu(CN)_3^-$) produces $Cu(CN)_2^-$, which does not affect the concentration of $Cu(CN)_3^{2-}$ in the diffusion layer according to the calculation at CN:Cu < 3.

The plots of the limiting current vs. $\omega^{1/2}$ for 0.05 M CN^- and a CN:Cu mole ratio = 3 (Figure 7-40) are linear. The slopes were calculated using least-squares fitting. At CN:Cu = 3, 97 % of copper and cyanide exist in the form of $Cu(CN)_3^{2-}$ and the calculated diffusion coefficients can be assumed to be that of $Cu(CN)_3^{2-}$. The diffusion coefficients for $Cu(CN)_3^{2-}$ at 40, 50 and 60 ^0C were found to be 1.05×10^{-9}, 1.29×10^{-9} and 1.52×10^{-9} m^2 s^{-1} respectively. The diffusion activation energy is 16.6 kJ/mole. From the activation energy and Equation 6-18, the predicted diffusion coefficient at 25 ^0C is 0.76×10^{-9} $m^2 s^{-1}$.
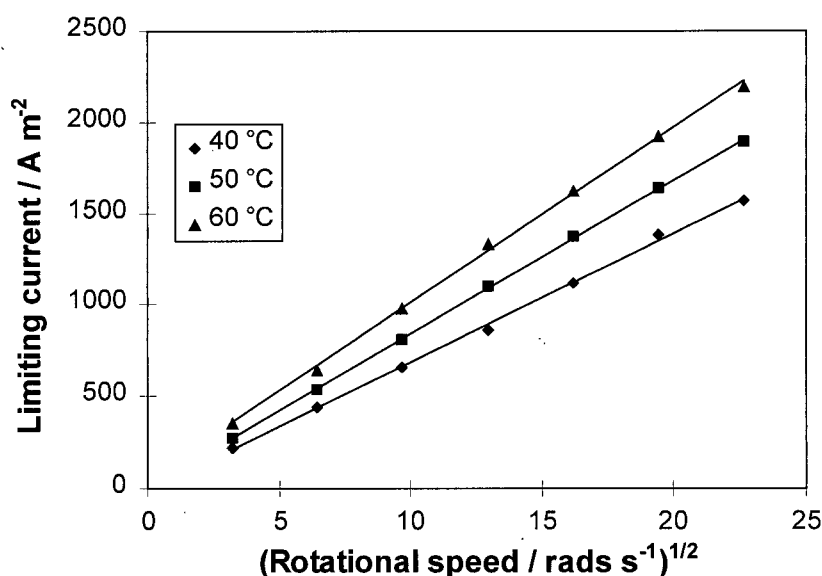
Figure 7-40 Limiting current vs. rotational speed at 40, 50 and 60 °C. Electrolyte: 0.05 M CN^-, CN:Cu mole ratio = 3, 0.25 M NaOH and 1 M Na_2SO_4.

When the mole ratio of cyanide to copper is very large, $Cu(CN)_4^{3-}$ is dominant and is oxidized to $Cu(CN)_4^{2-}$ which diffuses from the surface and decomposes to form $Cu(CN)_3^{2-}$

and cyanogen. $Cu(CN)_3^{2-}$ reacts with free cyanide to regenerate $Cu(CN)_4^{3-}$. Therefore the observed limiting current is larger than that expected from the Levich equation.

7.11 Activation Energy Calculation for the Kinetic Current

At a constant potential, Equation 6-17 can be applied. The activation energy can be calculated from the slope of the plot of log i vs. 1/T. The slopes of these linear plots were calculated by least-squares fitting. When the mole ratio of cyanide to copper is 3 and the concentration of hydroxide is 0.25 M, the discharged species is $Cu(CN)_3^{2-}$. From the calculation, the concentration of $Cu(CN)_3^{2-}$ is almost constant in the temperature range of 25 to 60 ^0C and the change in the concentration of $Cu(CN)_3^{2-}$ does not need to be considered for the activation energy calculation. At $[CN^-]$ =0.05 M, a CN:Cu mole ratio = 3, $[OH^-]$ = 0.25 M, the plots of log i vs. 1/T and the activation energies are shown in Figure 7-41.
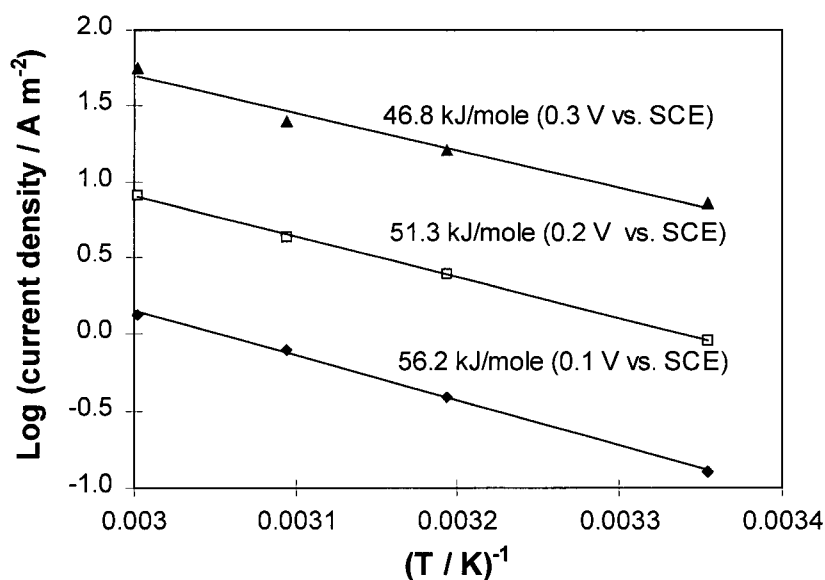
7-41   Activation energy calculation- plot of log (current density) vs. 1/T at constant potentials. Electrolyte: 0.05 M CN^-, CN:Cu mole ratio = 3, 0.25 M NaOH and 1 M Na_2SO_4.

7.12 Summary

The electrochemical kinetic behavior of copper cyanide is dependent on CN:Cu mole ratio, pH and total cyanide concentration. At low potentials (roughly 0 to 0.4 V vs. SCE), cuprous cyanide is oxidized to cupric cyanide complexes which produce cyanogen, which in turn reacts with hydroxide to form cyanate. At a CN:Cu mole ratio = 3 and [OH$^-$] = 0.25 M, the Tafel slope is about 0.12 V decade^{-1} and the reaction order with respect to Cu(CN)$_3^{2-}$ is one. Cu(CN)$_3^{2-}$ is discharged at the electrode. The current and Tafel slope decrease with decreasing hydroxide concentration and so hydroxide is involved in the rate-determining step. Increasing CN:Cu mole ratio also results in the change in the anodic behaviour of copper cyanide. When the CN:Cu mole ratio is larger than a certain value which depends on the total cyanide concentration, e. g. about 4 at [CN$^-$] = 0.05 M and 3.5 at [CN$^-$] = 3.5 M, a Tafel slope of about 0.06 V decade^{-1} was observed over the potential range 0.1 - 0.25 V vs. SCE. A second Tafel slope of about 0.17 -0.20 V decade^{-1} was noted over the higher potential range.

This change is related to the change in the distribution of copper cyanide species which in turn depends on the total cyanide concentration. The current is proportional to the concentration of cuprous tetracyanide and almost independent of the total cyanide concentration. pH has little effect on cyanide oxidation. Cu(CN)$_4^{3-}$ is discharged at the electrode.

In the middle potential region (roughly 0.4 to 0.6 V vs. SCE), copper oxide is precipitated on the electrode. Copper cyanide is oxidized to copper oxide and cyanate. The potential for the precipitation of copper oxide is dependent on CN:Cu mole ratio and temperature. The higher the mole ratio of cyanide to copper, the higher the potential for the precipitation of copper oxide. However, when cyanide concentration was high and hydroxide concentration was low, no copper oxide was precipitated, but cyanogen gas was evolved.

The current decreases with decreasing hydroxide concentration and the rate-controlling step involves hydroxide. The catalysis of copper oxide precipitated decreases with increasing copper cyanide concentration.

The anodic behaviour of copper cyanide could be compared to that of sulphite and the mixture of sulphite and copper cyanide to understand how sulphite can limit the oxidation of cyanide.

8. ANODIC OXIDATION OF MIXED COPPER CYANIDE AND SULPHITE IN ALKALINE SOLUTION

The anodic behaviour of sulphite and copper cyanide has been discussed in Chapters 6 and 7 when they are in the solution separately. The anodic behaviour of mixed sulphite and copper cyanide solution is presented in this Chapter. The objective of this study has been to understand how sulphite is oxidized as a sacrificial species while protecting the cyanide from oxidation. The study was conducted using the rotating disk technique.

8.1 Experimental Apparatus and Set-up

The graphite rotating disk was the same as described in Section 6.3. The electrode treatment was the same as in Chapter 7. Graphite rod having 12- and 24-mm diameters was fashioned as rotating disks for coulometric measurements. The working electrode (anode) was separated from the counter electrode (the cathode) to minimize the effect of the change in the CN:Cu mole ratio due to copper deposition at the cathode. The volume of the catholyte was only about 1-2 cm^3 and the initial concentration of hydroxide was ten times that in the anolyte. The evolution of hydrogen built a high concentration of hydroxide which can be transported to the anode compartment to maintain the concentration of hydroxide in the anolyte. The pH of the anolyte was monitored.

The rotating disk electrode system was an EG & G model 636 Electrode Rotator. A SOLARTRON 1286 Electrochemical Interface was used as the potentiostat. Except as noted, the polarization curves were generated at a scanning rate of 1 mV s^{-1}. The experimental set-up was the same as shown in Figure 6-3.

The liquid junction potential was not considered since the concentration of hydroxide is not very high and the mobilities of the ions of sulphate, sulphite and copper cyanide species are close to that of the sodium ion. The thermal liquid junction potential was measured using two calomel reference electrodes which were placed on the two sides of an electrolyte bridge.

Samples were taken for cyanide analysis (Appendix 2) and sulphite analysis (Appendix 4). The copper concentration was measured by oxidizing copper cyanide to cupric

nitrate using concentrated nitric acid and titrating with EDTA (see Appendix 3). The analysis of copper in the anodic precipitate was conducted by dissolving the precipitate in nitric acid and titrating with EDTA.

Reagent grade chemicals were used throughout all the experiments.

8.2 Anodic Behaviour of Mixed Sulphite and Copper Cyanide Solution

8.2.1 Anodic Behaviour of Dilute Copper Cyanide Solution with Sulphite

The anodic oxidation of mixed sulphite and copper cyanide has been studied as a function of temperature, the mole ratio of cyanide to copper, sulphite concentration and hydroxide concentration. Figure 8-1 shows the polarization curves of the solution with 0.05 M CN^-, a CN:Cu mole ratio of 3, 0.4 M Na_2SO_3, 0.25 M NaOH and 1 M Na_2SO_4.

At 25 and 40 °C, the current first increased and then decreased sharply to a minimum value with the formation of copper oxide on the anode. With further increase in potential, the current increased again. At a potential > about 0.8 V vs. SCE, some gas bubbles were observed on the anode. They were believed to be due to oxygen evolution. The passivation is probably due to the precipitation of copper oxide and the adsorption of oxygen. A very thin layer of copper oxide was precipitated on the graphite but not on the outer insulator.

When only copper cyanide was present in the solution, copper oxide was precipitated both on the graphite and the outer insulator with the amount of copper oxide being much larger. Therefore sulphite can reduce cupric ions to cuprous ions and decrease the extent of copper oxide formation.

At 50 °C, the polarization curves (Figure 8-1c) became different. At 100 rpm, the current increased to a limiting value, which was approximately the sum of copper cyanide and sulphite limiting currents when they are present separately in the solution. At 400 and 1600 rpm, the current first increased and then decreased to a minimum value with the precipitation of copper oxide. At a potential > 0.64 V vs. SCE, the current rose sharply to a limiting value and the electrode surface was reactivated. At a potential > 1.0 V vs. SCE, bubbles were observed and the current decreased sharply. Oxygen evolution passivated the electrode surface.

At 60 °C, the anodic behaviour for 100 and 400 rpm is similar to that for 100 rpm at 50 °. However, at 1600 rpm, the polarization curve was still similar to that at 50 °C. This dependence of the anodic behaviour on the rotational speed is due to the difference in the composition at the electrode surface at different rotational speeds. The difference in the compositions of the electrolyte can affect the precipitation of copper oxide and evolution of oxygen and finally the electrochemical properties.

From Figure 8-2, it can been seen that the passivation decreased with increasing potential scan rate. At 5 mV/s, the current increased to a maximum and decreased with the precipitation of copper oxide finally increasing to a limiting value. At 10 and 20 mV/s, the current increased continuously to a limiting value. This current was related to the ratio of the precipitated copper oxide to copper hydroxide.

From the polarization curves on the electrode with and without pre-coated copper oxide (Curves 1 and 2 in Figure 8-3) in the solution containing both copper cyanide and sulphite, the copper oxide had an inhibiting effect on the oxidation of copper cyanide and sulphite. However, in comparing the polarization curves containing only sulphite (Curves 3-5) in Figure 8-3, the copper cyanide oxide did not show a large inhibiting effect on the oxidation of sulphite. Therefore the passivation might be caused by the adsorption of copper cyanide species in the presence of sulphite or concomitant effect of copper cyanide and sulphite. In comparing three polarization curves respectively for (1) mixed sulphite and copper cyanide, (2) sulphite and (3) copper cyanide (Figure 8-4), it can been seen that copper catalyzed the oxidation of sulphite.

The anodic behaviour for 0.2 M and 0.1 M Na_2SO_3 was shown in Appendix 8 (Figures A-37 and A-38) is different from that for 0.4 M Na_2SO_3. More copper oxide was formed and more oxygen evolved. In the potential range 0.6 -1.0 V vs. SCE, the current did not change significantly with decreasing sulphite concentration from 0.4 to 0.1 M. The decrease in the sulphite concentration resulted in an increase in oxygen evolution.

When the mole ratio of cyanide to copper increased from 3 to 4 ([Cu^+] decreased from 0.0167 to 0.0125 M) at [CN^-] = 0.05 M, the polarization curves were different (Figures A-39 to A-40 in Appendix 8). The difference is due to the change in the distribution of copper cyanide species.

The precipitation of copper oxide affected the anodic oxidation of sulphite and copper cyanide. The concentration of hydroxide was decreased to 0.05 M from 0.25 M to see its effect on the anodic behaviour of sulphite and copper cyanide. Figure 8-5 shows the polarization curves for the solution with 0.05 M CN^-, 0.0167 M Cu^+ (CN:Cu = 3), 0.4 M Na_2SO_3 , 0.05 M NaOH and 1 M Na_2SO_4. The current first increased smoothly with increasing potential. When the potential was larger than a certain value (dependent on the rotational speed), it rose rapidly to a limiting value and then decreased slightly with increasing potential. At the potential > about 0.70 V vs. SCE, the current increased slightly and became stable around 1.0 V vs. SCE. No visible copper oxide was formed.

From Figure 8-6, at a potential < about 0.30 V vs. SCE, the sulphite oxidation did not seem to be catalyzed by the oxidation of copper cyanide. However, at a potential > about 0.3 V vs. SCE, the current increased rapidly and the sulphite oxidation was catalyzed by the oxidation of copper cyanide. The potential for the sharp increase in the current for mixed sulphite and copper cyanide is almost the same as that for copper cyanide. At a potential > about 0.9 V vs. SCE, the current did not increase as expected from the further oxidation of sulphite species (HSO_3^- or SO_2) possibly because the oxidation of SO_3^{2-}, but not HSO_3^{2-} and SO_2, was ready to be catalyzed by the oxidation of copper cyanide and the electrode surface was passivated for the oxidation of HSO_3^- and SO_3^{2}.

When the sulphite concentration decreased from 0.4 M to 0.2 M, copper oxide and hydroxide was precipitated on the electrode. Hence the anodic behaviour (see Figure A-42 in Appendix 8) became quite different.

The anodic behavior for 0.05 M CN^-, 0.0125 M Cu^+ (CN:Cu = 4), 0.4 M Na_2SO_3 and 1 M Na_2SO_4 (Figure A-43 in Appendix 8) was similar to that for CN:Cu = 3 (Figure 8-5). The current first increased smoothly and then rose rapidly to a maximum value. When the concentration of sulphite was decreased to 0.2 M, the anodic behaviour (Figure A-44 in Appendix 8) was similar to that for 0.4 M Na_2SO_3 (Figure A-44). However, when the concentration of sulphite was decreased to 0.1 M, the anodic behaviour (A-45 in Appendix 8) was different due to the formation of copper oxide. From Figure 8-7, it appears that sulphite oxidation was catalyzed by the oxidation of copper cyanide at a potential > about 0.35 V vs. SCE.
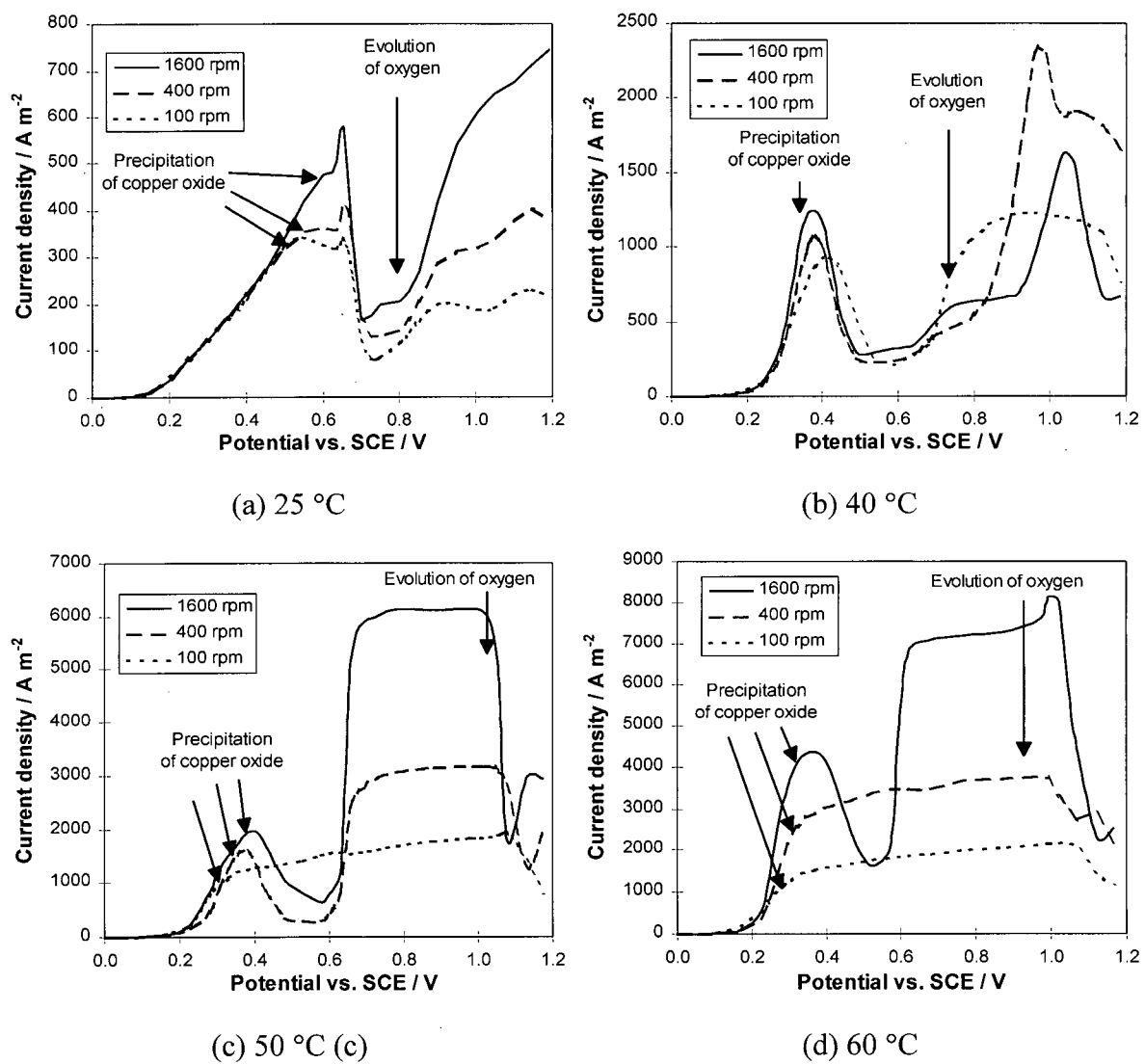
Figure 8-1 Polarization curves at different temperatures. Electrolyte: 0.05 M CN⁻, 0.0167 M Cu⁺ (CN:Cu mole ratio = 3), 0.25 M NaOH, 0.4 M Na₂SO₃ and 1 M Na₂SO₄
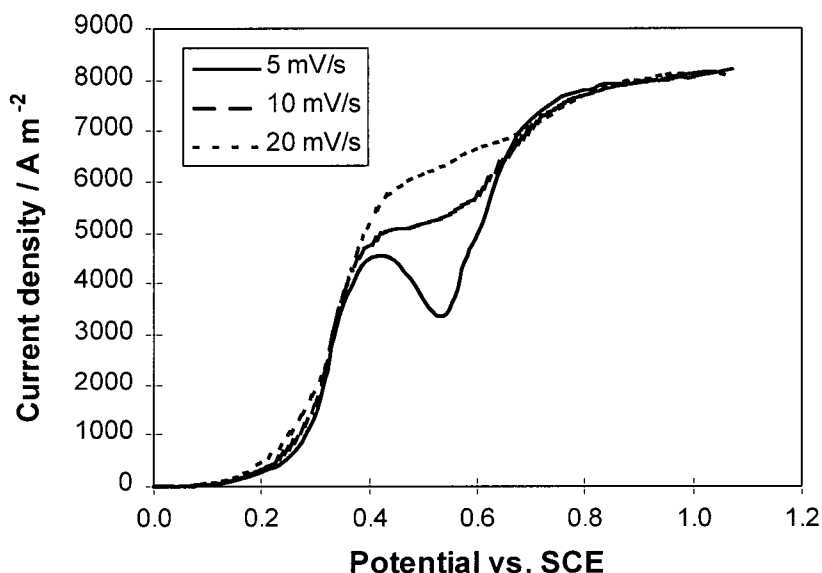
Figure 8-2 Effect of potential scanning rate on the anodic behaviour of mixed sulphite and copper cyanide at 4900 rpm and 60 °C. Electrolyte: 0.05 M CN⁻, 0.0167 M Cu⁺ (CN:Cu mole ratio = 3), 0.25 M NaOH, 0.4 M Na_2SO_3 and 1 M Na_2SO_4.
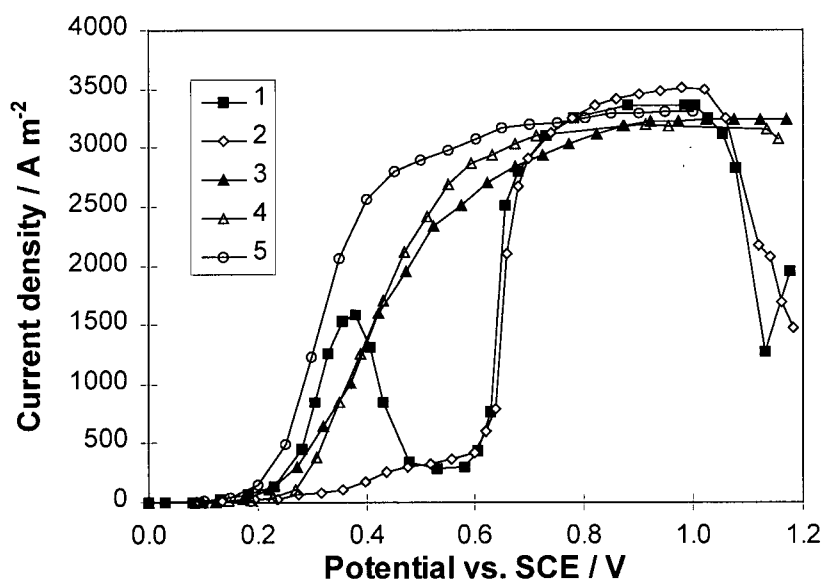
Figure 8-3 Polarization curves for (1) 0.05 M CN⁻, 0.0167 M Cu⁺ and 0.4 M Na_2SO_3, (2) the same composition as (1), the electrode coated with copper oxide at 0.5 V vs. SCE for 10 minutes in the same solution. (3) 0.4 M Na_2SO_3, (4) 0.4 M Na_2SO_3 on the electrode coated with copper oxide in the same solution as (1), and (5) 0.4 M Na_2SO_3 on the electrode coated with copper oxide from 0.05 M CN⁻ and 0.0167 M Cu⁺ at 400 rpm and 60 °C. Supporting electrolyte: 0.25 M NaOH and 1 M Na_2SO_4.
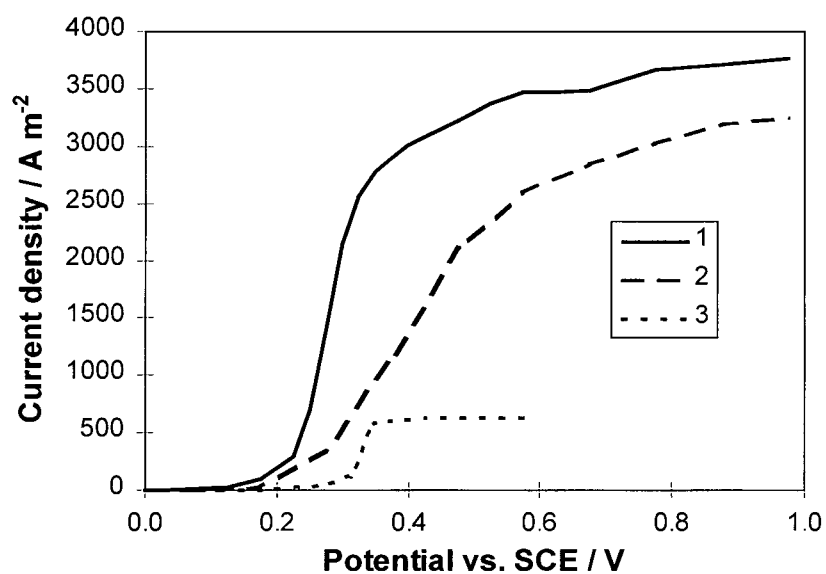
Figure 8-4 Polarization curves for (1) 0.05 M CN^-, 0.0167 M Cu^+ (CN:Cu mole ratio = 3) and 0.4 M Na_2SO_3, (2) 0.4 M Na_2SO_3 and (3) 0.05 M CN^- and 0.0167 M Cu^+ at 400 rpm and 60 °C. Supporting electrolyte: 0.25 M NaOH and 1 M Na_2SO_4.
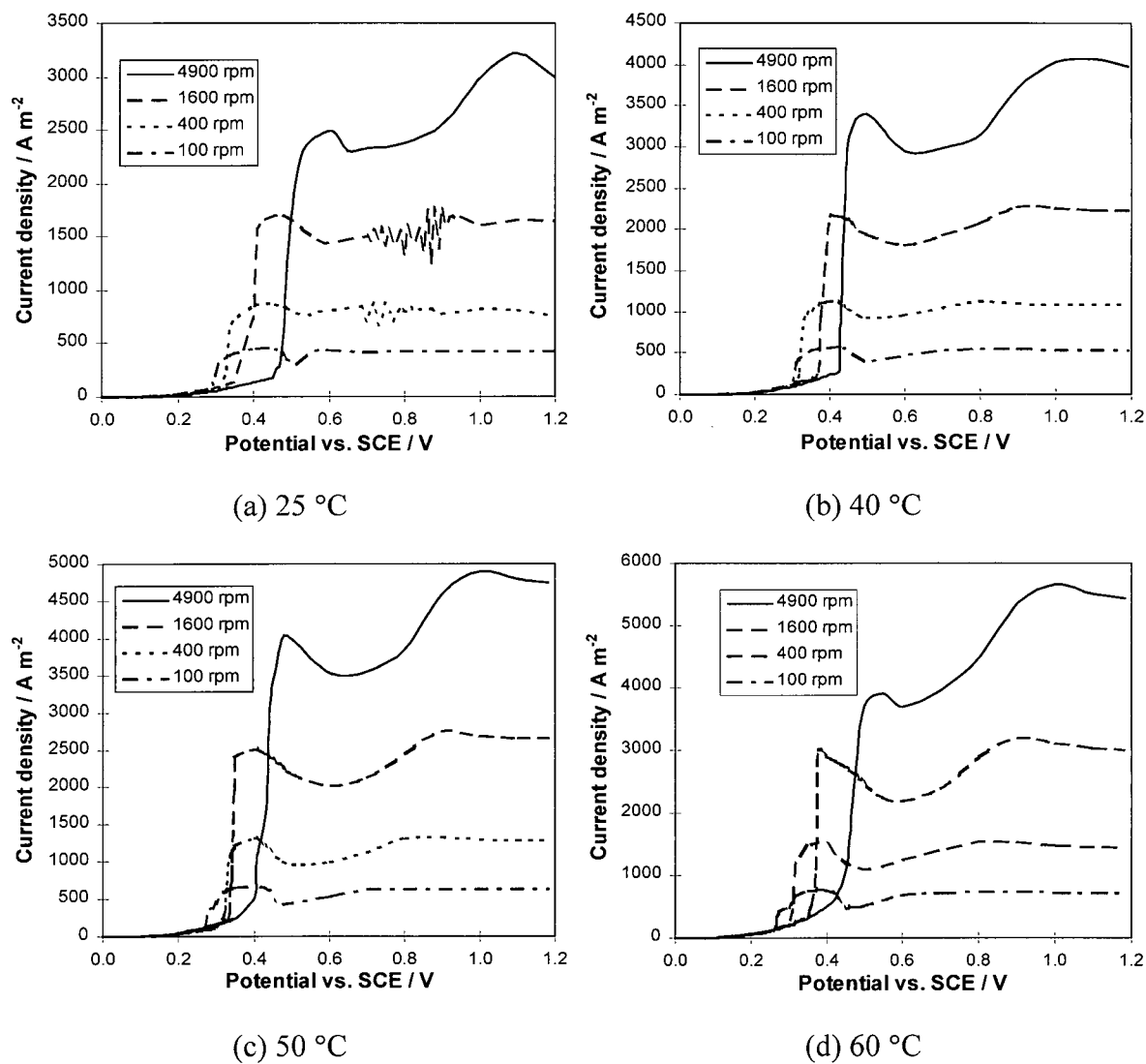
Figure 8-5 Polarization curves at different temperatures. Electrolyte: 0.05 M CN⁻, 0.0167 M Cu⁺ (CN:Cu mole ratio = 3), 0.05 M NaOH, 0.4 M Na_2SO_3 and 1 M Na_2SO_4.
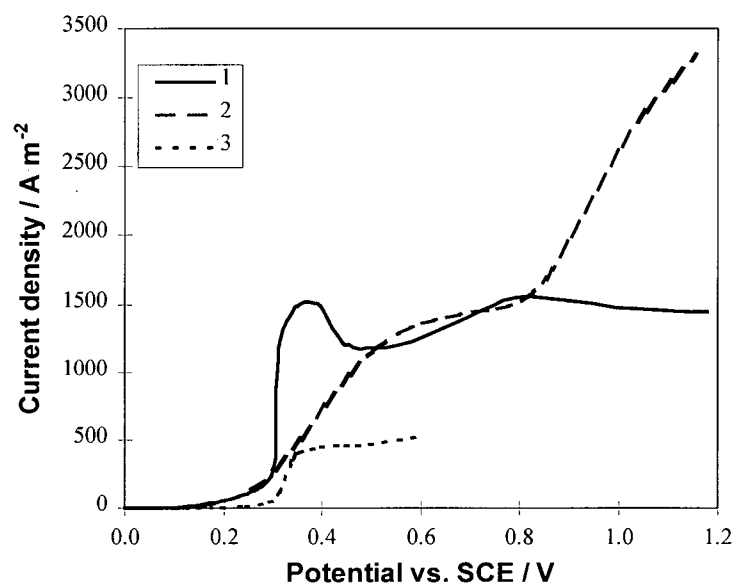
Figure 8-6 Polarization curves for (1) 0.05 M CN⁻, 0.0167 M Cu⁺ (CN:Cu mole ratio = 3) and 0.4 M Na_2SO_3 , (2) 0.4 M Na_2SO_3 and (3) 0.05 M CN⁻ and 0.0167 M Cu⁺ at 400 rpm and 60 °C. Supporting electrolyte: 0.05 M NaOH and 1 M Na_2SO_4.
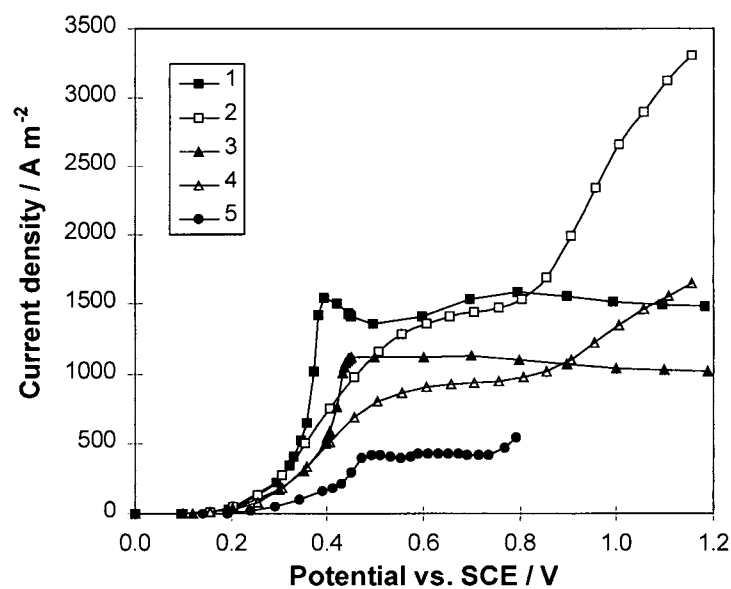
Figure 8-7 Polarization curves for (1) 0.05 M CN⁻, 0.0125 M Cu⁺ and 0.4 M Na_2SO_3 , (2) 0.4 M Na_2SO_3, (3) 0.05 M CN⁻, 0.0125 M Cu⁺ and 0.2 M Na_2SO_3, (4) 0.2 M Na_2SO_3 and (5) 0.05 M CN⁻ and 0.0125 M Cu⁺ at 400 rpm and 60 °C. Supporting electrolyte: 0.05 M NaOH and 1 M Na_2SO_4.

8.2.2 Anodic Behaviour of Concentrated Copper Cyanide Solution with Sulphite

The polarization curves for the solution with 3 M CN⁻, 1 M [Cu⁺] and 0.5 M Na$_2$SO$_3$ and 0.25 M NaOH are shown in Figure 8-8. At 25 °C, the current first increased and then decreased slightly with the precipitation of copper oxide. At a potential > about 0.52 V vs. SCE, the current increased to a peak value and decreased rapidly. The second passivation is probably due to oxygen adsorption. At 40 °C, the polarization curves at 400 and 1600 rpm were similar to those at 25 °C. However, at 100 rpm, the current reached a limiting value and became independent of potential. The oxide formed in the potential range 0.38 to 0.5 V vs. SCE was dissolved when the current was at its limiting value. This is why the current did not decrease with potential after the current sharply increased to a limiting value.

This dependence of the anodic behaviour on the rotational speed is related to the composition of the reactive species on the surface of the electrode. At a potential > about 0.5 V vs. SCE, the current increased sharply with increasing potential and was almost independent of the rotational speed. Therefore the concentration of hydroxide on the electrode surface decreased with decreasing rotational speed. At 100 rpm, the concentration of hydroxide was so low that the formation of copper oxide was not favored. Even copper oxide was more readily reduced by sulphite ions and dissolved. Therefore a second passivation was not observed. At 400 and 1600 rpm, the concentration of hydroxide on the surface was still high and the formation of copper oxide was still favored. With increasing potential, the second passivaion appeared probably due to the adsorption of oxygen.

At 50 °C and 100 rpm, the current increased continuously to a limiting value and no copper oxide was formed on the electrode. At 400 rpm, the anodic behaviour of current vs. potential was similar to that at 100 rpm and 40 °C. At 1600 rpm, the anodic behaviour was still similar to that at 50 °C. At 60 °C and a rotational speed of 100 or 400 rpm, the current increased continuously to a limiting value and became independent of the potential. The anodic behaviour at 1600 rpm was similar to that at 100 rpm and 40 °C.

The anodic oxidation of sulphite and cyanide increases with increasing temperature much faster than the diffusion of the hydroxide ion. Therefore even at a higher rotating speed, the hydroxide concentration on the surface of anode is so low that no copper hydroxide was formed and the current reached a limiting value.

Figure 8-9 shows the plots of the current vs. time at different potentials at 400 rpm. At 25 °C and 0.4 V vs. SCE, the current first decreased rapidly and then slowly and finally became stable. A thin layer of copper oxide was precipitated on the anode. At 0.60 V vs. SCE, the current increased to a certain value and then became stable. No copper oxide was precipitated on the electrode. At 0.80 V vs. SCE, the current decreased to a limiting value and became stable with no copper oxide appearing on the anode. It should be noted that at 25 °C and 0.80 V vs. SCE, the current densities in Figure 8-9a do not match those in Figure 8-8a. This can be explained by: (1) the current obtained in Figure 8-9a was obtained using the controlled potential method. When the potential was applied, the instantaneous current reached a value where the concentration of hydroxide on the electrode surface was low so that copper oxide was not formed and the current was stabilized at a limiting value; (2) the current in Figure 8-8a was generated by a potential scan at 1 mV s^{-1} and so the current never reached a value at which copper oxide was readily reduced and dissolved. Hence it passivated the electrode surface.

At 40 °C (Figure 8-9b), the results are similar to those at 25 °C (8-9a). At 50 °C and 0.3 V vs. SCE, the current decreased and became stable. At 0.4 V vs. SCE, the current density increased and then decreased and was finally stabilized. The current was much higher than those in Figures 8-8 b. The reason for this behaviour is the same as discussed for 25 °C. At a potential > 0.60 V vs. SCE, the current is the same as that obtained using a potential scan rate of 1 mV s^{-1}. At 60 °C and 0.2 or 0.3 V vs. SCE, the current decreased, then increased to a certain value and was stabilized. At a potential > 0.4 V vs. SCE, the current decreased or increased to a limiting value and became stable. The current in Figure 8-9d is the same as that in Figure 8-8d.

The precipitation of copper oxide affected the anodic behaviour. Hence the concentration of hydroxide was decreased to investigate the effect of pH on the anodic behaviour. Figures 8-10 and 8-11 show the polarization curves for the solution containing 0.1 and 0.05 M NaOH. The passivation did not appear because there was no precipitate on the anode.

Figure 8-12 shows the polarization curves for mixed sulphite and copper cyanide solution, sulphite solution and copper cyanide solution with 0.25 M NaOH at 60 °C. Sulphite oxidation appears to be catalyzed by copper cyanide oxidation. The oxidation of copper

cyanide also seems to be affected by sulphite. From Figure 8-13, when the hydroxide concentration decreased to 0.05 M, the oxidation of copper cyanide and sulphite was significantly catalyzed by each other. The increase in sulphite concentration from 0.2 to 0.4 M resulted in the increase in the current. However, its limiting value is much smaller than that expected from the increase in the concentration possibly because the pH on the electrode was so low that the speciation of sulphite shifted from SO_3^{2-} to HSO_3^- and SO_2 which were less active.

When the concentration of cyanide increased from 3 to 3.5 M and the concentrations of the other species were maintained constant, the polarization curves (Figure 8-14) became different and no passivation was observed. At 25 °C, the current increased with increasing potential and then reached a limiting value and became independent of the potential. At 40, 50, and 60 °C, there was no limiting current and no passivation. At 50 and 60 °C, when the potential exceeded 0.4 V vs. SCE, a significant amount of bubbles was observed at 100 and 400 rpm. The bubbles were rapidly dissolved in two seconds after turning off the current. The graphite was not corroded. At such a high current, sulphite only limited a part of the cyanide oxidation and pH on the electrode surface was so low that the rate of the production of $(CN)_2$ was higher than the rate of the reaction between $(CN)_2$ and OH^-. Therefore $(CN)_2$ bubbles were evolved.

Figure 8-15 shows the polarization curves for mixed sulphite and copper cyanide solution, copper cyanide and sulphite. The current for mixed copper cyanide and sulphite is higher than that for copper cyanide or sulphite. So the oxidation of both sulphite and copper cyanide contributed to the total anodic current.

Figure 8-16 shows the polarization curves for the solution with 4 M CN^-, 1 M Cu^+, 0.5 M Na_2SO_3 and 0.25 M NaOH. The current increased continuously with increasing potential. When the current exceeded a certain value (depending on the rotational speed), a layer of bubbles was formed on the graphite. With increasing potential, the bubbles became larger and had a significant effect on the mass transfer. Thus the current increased significantly. Due to the formation of the bubble layer, the IR drop was even larger than 1 V.

Figure 8-17 shows the polarization curves for mixed sulphite and copper cyanide solution, copper cyanide and sulphite. The current for mixed copper cyanide and sulphite was

a little higher than that for copper cyanide. So the oxidation of sulphite did not contribute very much to the total anodic current.

(a) 25 °C

(b) 40 °C

(c) 50 °C

(b) 60 °C
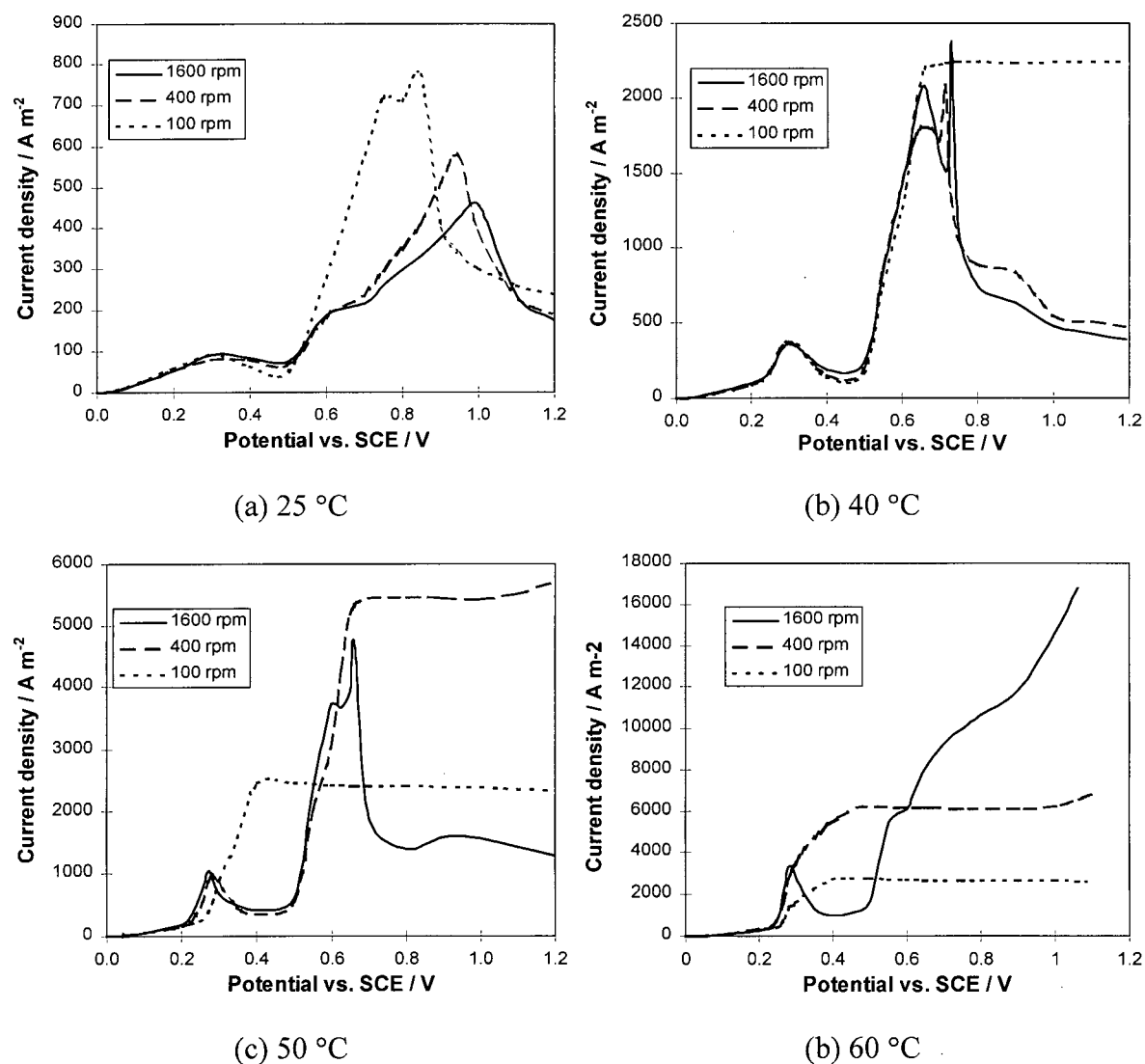
Figure 8-8 Polarization curves at different temperatures. Electrolyte: 3 M CN⁻, 1 M Cu⁺, 0.25 M NaOH, 0.5 M Na₂SO₃.
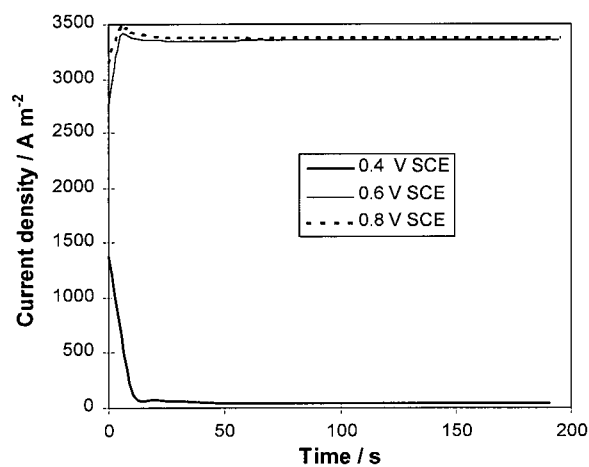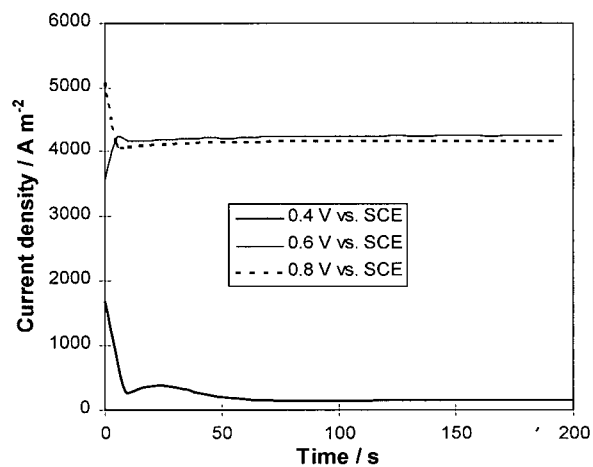
(a) 25 °C

(b) 40 °C
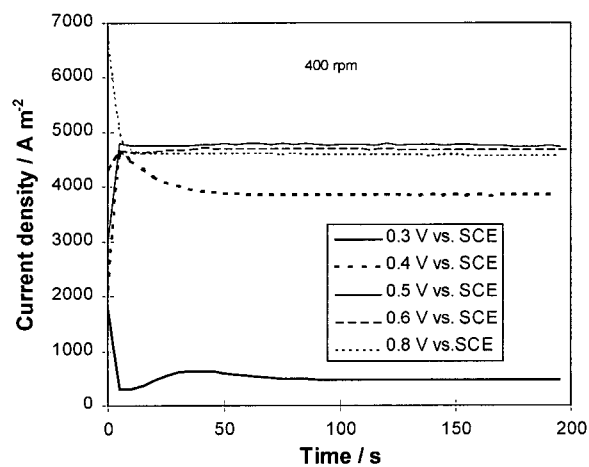
(c) 50 °C
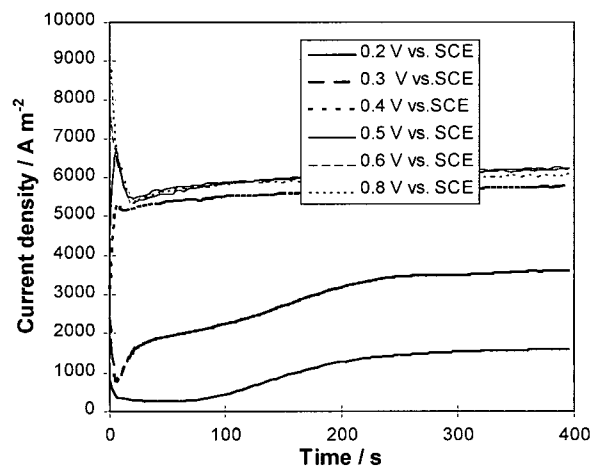
(d) 60 °C

Figure 8-9 Current density vs. time at constant potential, 400 rpm and different temperatures. Electrolyte: 3 M CN^-, 1 M Cu^+, 0.25 M NaOH, 0.5 M Na_2SO_3.
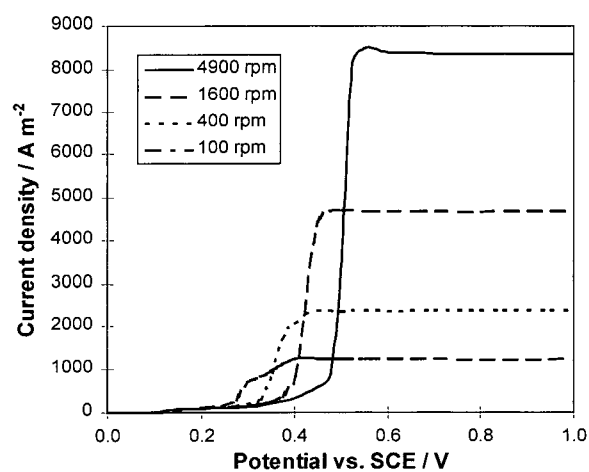
(a) 25 °C (a)
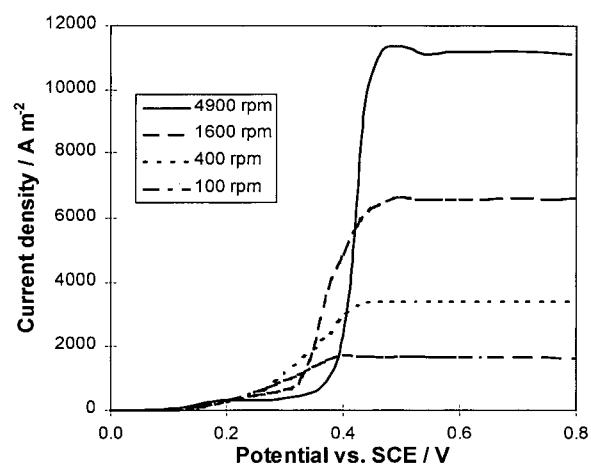
(b) 40 °C
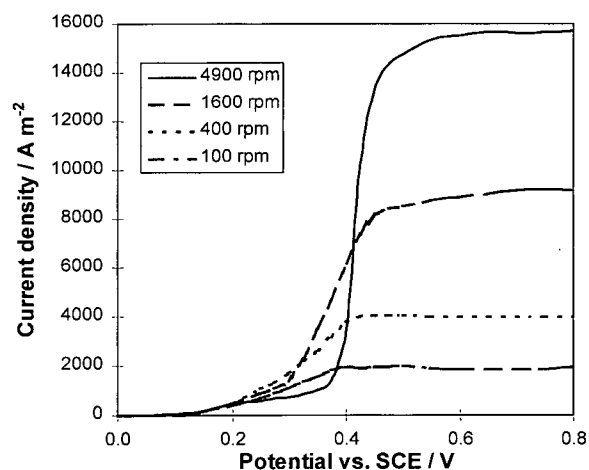
(c) 50 °C
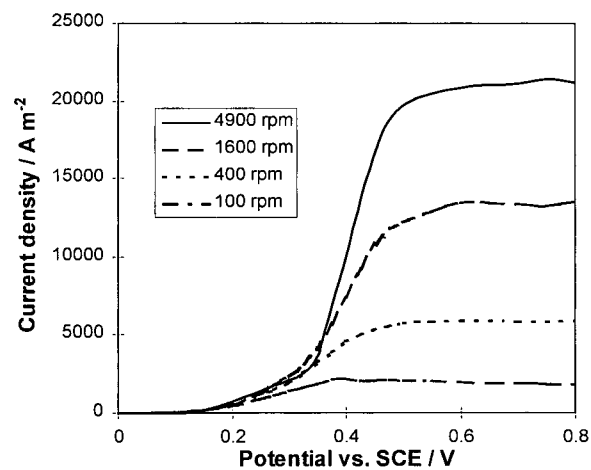
(d) 60 °C

Figure 8-10 Polarization curves at different temperatures. Electrolyte: 3 M CN⁻, 1 M Cu⁺, 0.1 M NaOH, 0.5 M Na$_2$SO$_3$.
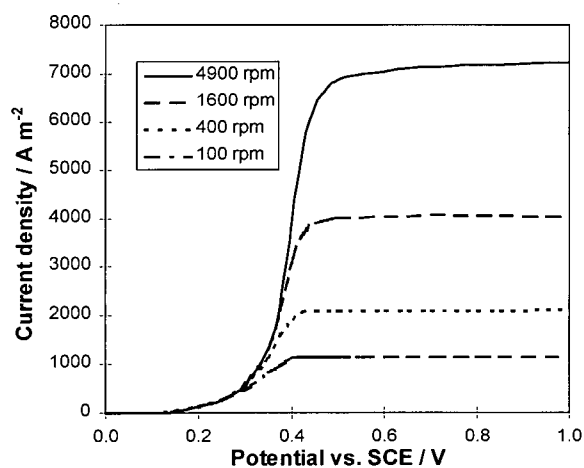
(a) 25 °C
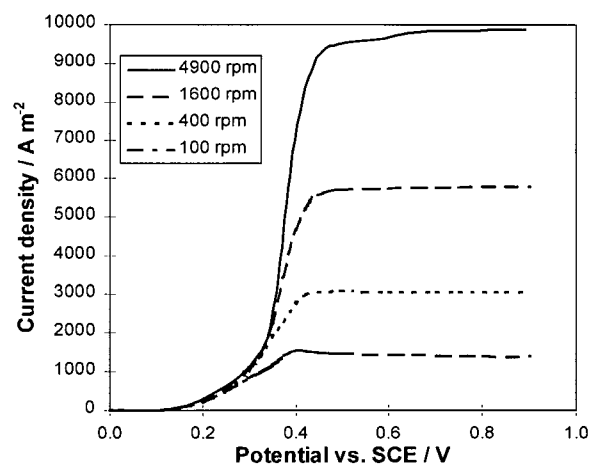
(b) 60 °C
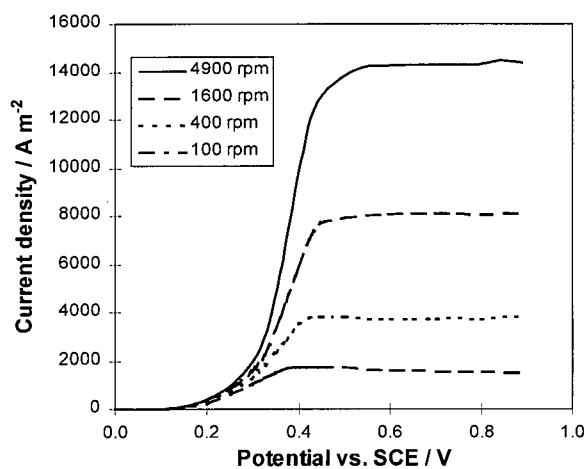
(c) 50 °C
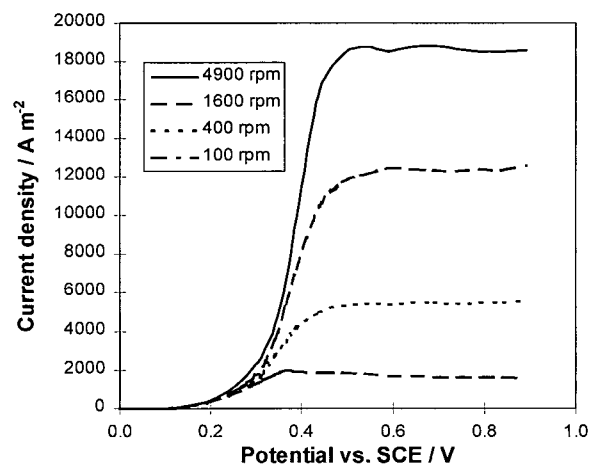
(d) 60 °C

Figure 8-11 Polarization curves at different temperatures. Electrolyte: 3 M CN⁻, 1 M Cu⁺, 0.05 M NaOH, 0.5 M Na₂SO₃.
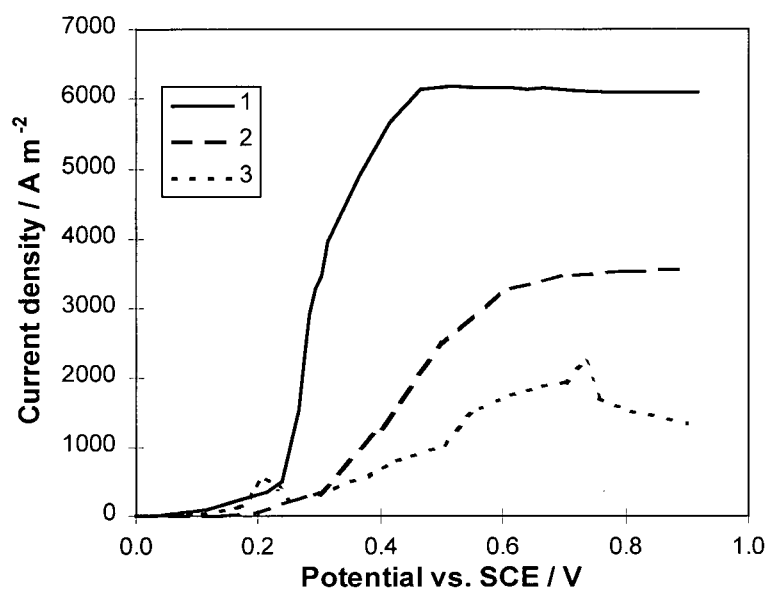
Figure 8-12 Polarization curves for (1)3 M CN⁻, 1 M Cu⁺ (CN:Cu mole ratio = 3), 0.25 M NaOH and 0.5 M Na$_2$SO$_3$, (2) 0.5 M Na$_2$SO$_3$, 0.25 M NaOH and 1 M Na$_2$SO$_4$ and (3) 3 M CN⁻, 1 M Cu⁺, 0.25 M NaOH and 0.5 M Na$_2$SO$_4$ at 400 rpm and 60 °C.
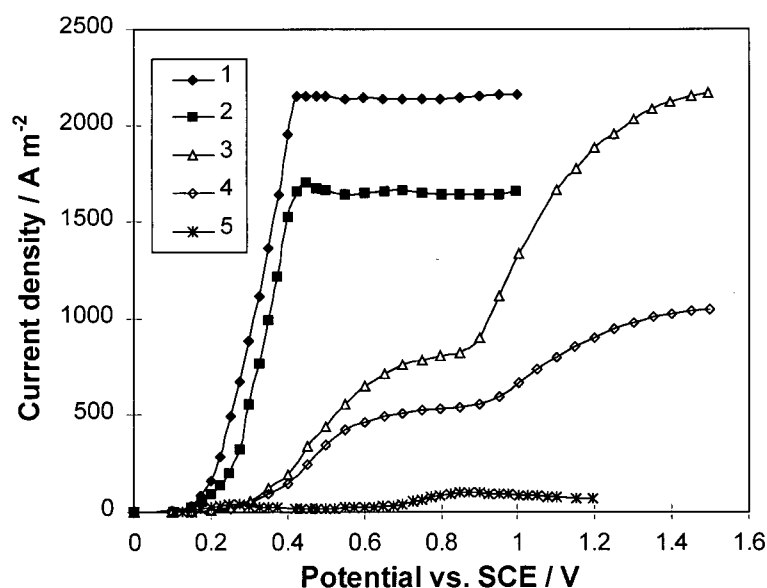
Figure 8-13 Polarization curves at 400 rpm and 25 °C for (1) 3 M CN⁻ + 1 M Cu⁺ + 0.4 M Na$_2$SO$_3$ + 0.1 M Na$_2$SO$_4$ (2) 3 M CN⁻ + 1 M Cu⁺ + 0.2 M Na$_2$SO$_3$ + 0.3 M Na$_2$SO$_4$, (3) 0.4 M Na$_2$SO$_3$ + 1 M Na$_2$SO$_4$, (4) 0.2 M Na$_2$SO$_3$ + 1 M Na$_2$SO$_4$ (5) 3 M CN⁻ + 1 M Cu⁺ + 0.5 M Na$_2$SO$_4$ at [NaOH] = 0.05 M NaOH.
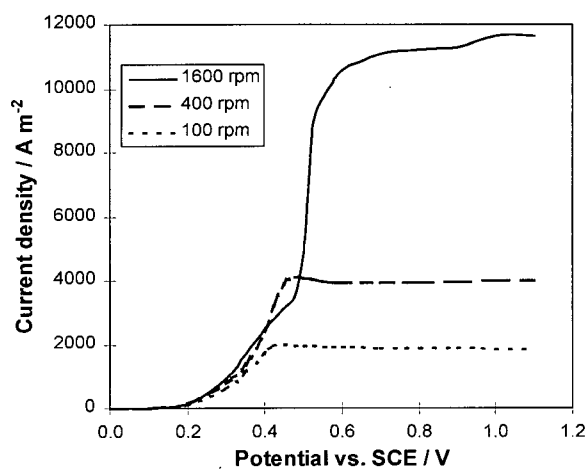
(a) 25 °C
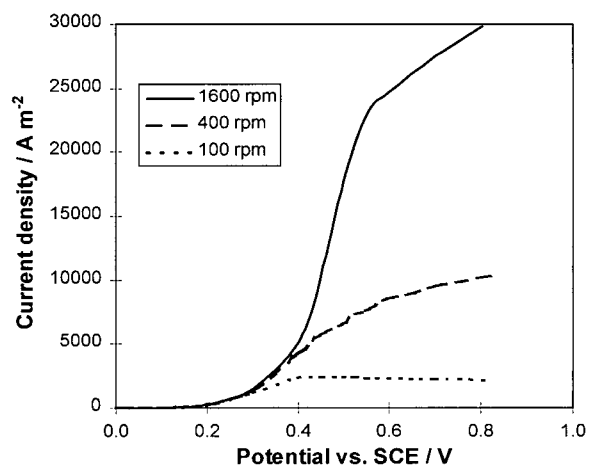
(b) 40 °C
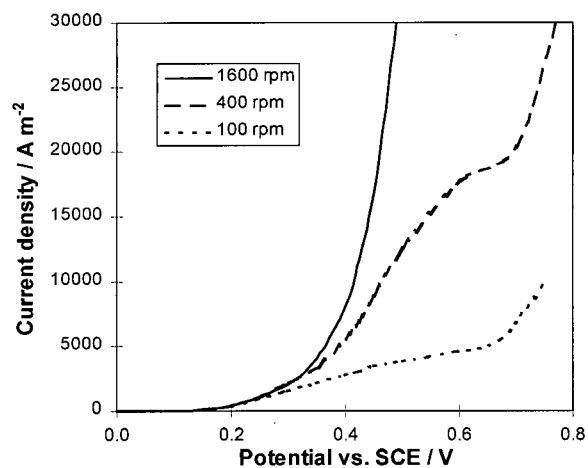
(c) 50 °C
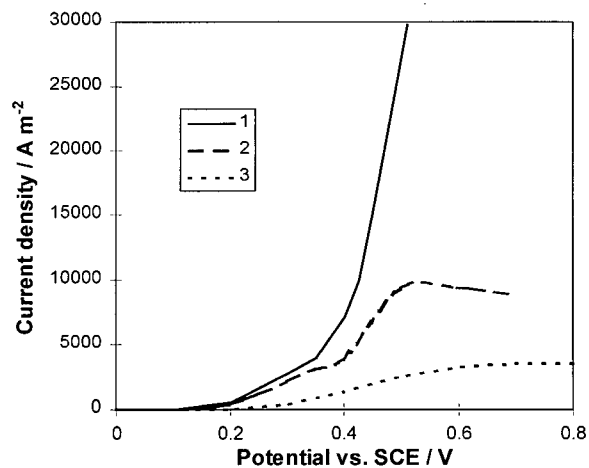
(d) 60 °C

Figure 8-14 Polarization curves at different temperatures. Electrolyte: 3.5 M CN⁻, 1 M Cu⁺, 0.25 M NaOH, 0.5 M Na₂SO₃.
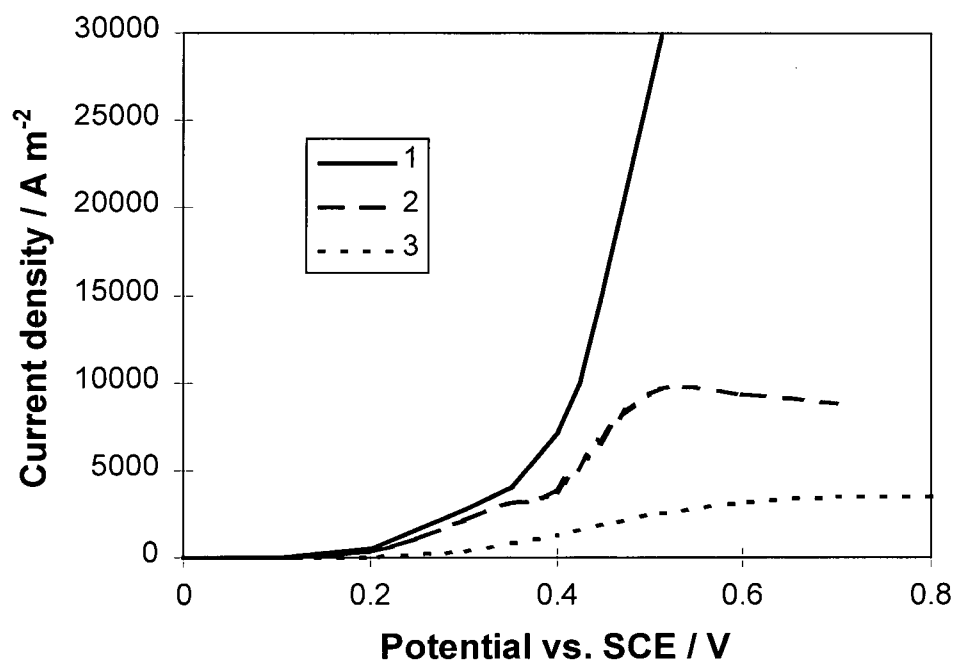
Figure 8-15 Polarization curves for (1)3.5 M CN⁻, 1 M Cu⁺, 0.25 M NaOH and 0.5 M Na$_2$SO$_3$, (2) 3 M CN⁻, 1 M Cu⁺, 0.25 M NaOH and 0.5 M Na$_2$SO$_4$ and (3) 0.5 M Na$_2$SO$_3$, 0.25 M NaOH at 400 rpm and 60 °C.

(a) 25 °C

(b) 40 °C

(c) 50 °C

(d) 60 °C
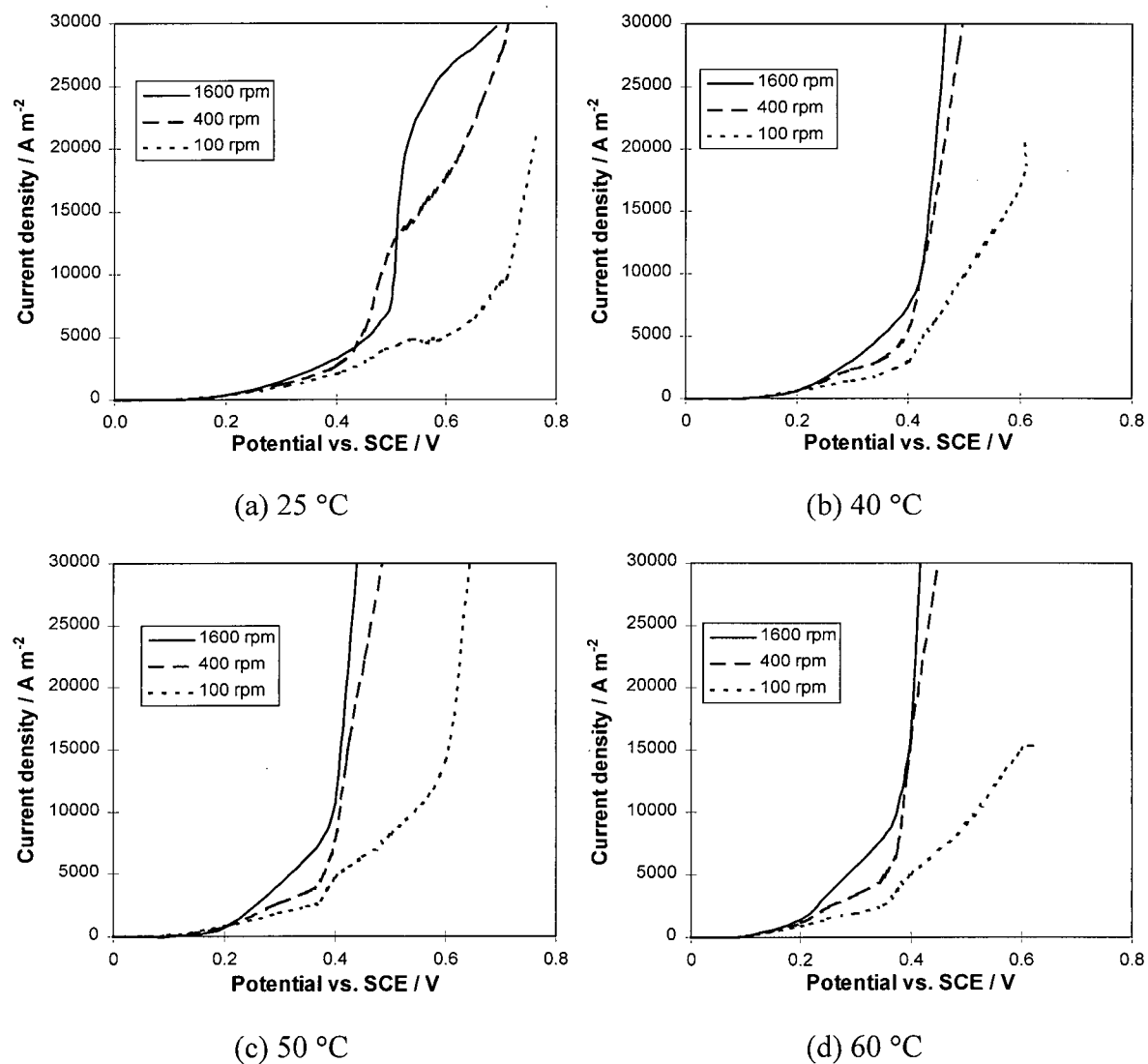
Figure 8-16 Polarization curves at different temperatures. Electrolyte: 4 M CN⁻, 1 M Cu⁺, 0.25 M NaOH, 0.5 M Na₂SO₃.
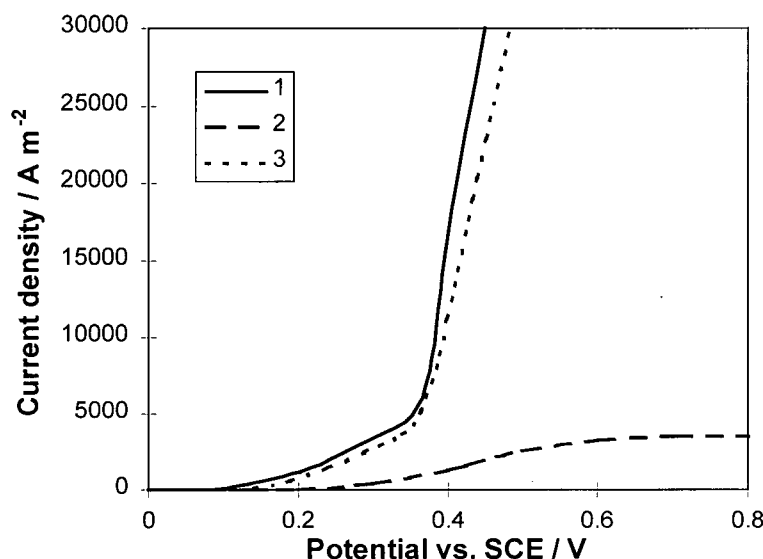
Figure 8-17 Polarization curves for (1) 4 M CN⁻ + 1 M Cu⁺ + 0.25 M NaOH + 0.5 M Na₂SO₃, (2) 0.5 M Na₂SO₃ + 0.25 M NaOH + 1 M Na₂SO₄ and (3) 4 M CN⁻ + 1 M Cu⁺ + 0.25 M NaOH + 0.5 M Na₂SO₄ at 400 rpm and 60 °C.

8.3 Coulometric Measurements

The coulometric measurements were conducted using controlled potential and controlled current methods to investigate the anodic current efficiencies of cyanide and copper oxidation in the presence of sulphite. The results obtained using the controlled potential method are listed in Table 8-1.

Tests 1-4 show the anodic current efficiencies of cyanide and copper for the solution with 0.05 M CN⁻, 0.0167 M (CN:Cu mole ratio = 3), 0.4 M Na₂SO₃, 0.25 M OH⁻ and 1 M Na₂SO₄. In the presence of 0.4 M Na₂SO₃, the current efficiency decreased from 86 % to about 10 % for cyanide (CN⁻ → CNO⁻) and from 13 % to about 3 % for copper (Cu⁺ → CuO or Cu(OH)₂). This means that sulphite can effectively limit the anodic oxidation of copper cyanide. The anodic current efficiency for cyanide at 0.5 V vs. SCE was a little bit higher than that at 0.3 V vs. SCE because at 0.5 V SCE, the current for sulphite and copper cyanide was closest to a limiting value and sulphite was less efficient in limiting the oxidation of copper cyanide. The anodic current efficiency at 60 °C is a slightly higher than that at 50 °C.

Tests 5-8 show the anodic current efficiencies of cyanide and copper for the solution with 0.05 M CN⁻, 0.0125 M (CN:Cu mole ratio = 4), 0.4 M Na₂SO₃, 0.25 M OH⁻ and 1 M Na₂SO₄. In the presence of 0.4 M Na₂SO₃, the anodic current efficiency decreased from 90 %

to about 12 % for cyanide and from 10 % to about 2 % for copper (I). Similar to Tests 1-4, the anodic current efficiencies of copper cyanide at 0.60 V vs. SCE are slightly higher than those at 0.4 V vs. SCE. The anodic current efficiency of cyanide in Tests 5-8 is higher than that in Tests 1-4, the anodic current efficiency of copper (I) in Tests 5-8 is lower than that in Tests 1-4 possibly because the speciation of copper cyanide shifted to $Cu(CN)_4^{3-}$ and more free cyanide was present in the solution.

Table 8-1 Current efficiencies from copper cyanide using controlled potential coulometric measurements (supporting electrolyte: 1 M Na_2SO_4)

Test No.	Composition	Controlled potential (V vs. SCE)	Temperature (°C)	Rotational speed (rpm)	Current efficiency for CN (%)	Current efficiency for Cu (%)
1	0.05 M CN⁻,	0.3	50	100	9	2
2	CN:Cu = 3	0.3	60	100	8	2
3	0.4 M SO_3^{2-}	0.5	50	100	12	3
4	0.25 M OH⁻	0.5	60	100	13	3
5	0.05 M CN⁻,	0.4	50	100	11	1
6	CN:Cu = 4	0.4	60	100	12	1
7	0.4 M SO_3^{2-}	0.6	50	100	13	2
8	0.25 M OH⁻	0.6	60	100	14	2

Table 8-2 lists the anodic current efficiencies of cyanide and copper (I) for the solutions with different composition using the controlled current method. Tests 1-6 list the anodic current efficiencies of cyanide and copper for the solution with 0.05 M CN⁻, 0.0167 M (CN:Cu = 3), 0.4 M Na_2SO_3, 0.25 M OH⁻ and 1 M Na_2SO_4 at different current densities and rotational speeds. The rotational speeds (100-1600 rpm) and the current densities (250- 500 A m⁻²) do not significantly affect the current efficiencies of cyanide and copper (I). Similar results for the solutions with 0.05 M CN⁻, 0.0125 M Cu^+, 0.4 M Na_2SO_3, 0.25 M NaOH and 1 M Na_2SO_4 (Tests 7-12) were obtained. The difference is that almost no copper oxide was formed on the anode due to the high mole ratio of cyanide to copper. The current efficiency of cyanide did not change very much when the cyanide concentration was increased from 0.05 M to 0.4 M (Tests 13-16) and 1 M (Tests 17-20) and the concentrations of the other species were kept constant.

From Tests 1-8 and Tests 21-26, at CN:Cu mole ratio = 3, when the concentration of hydroxide decreased from 0.25 M to 0.05 M and the concentrations of the other species were kept at constants, the anodic current efficiency of cyanide decreased while the anodic current efficiency of copper (I) decreased to almost zero. This means that sulphite was more efficient

in limiting the oxidation of copper cyanide at low hydroxide concentration. However, at CN:Cu mole ratio = 4, the decrease in the concentration of hydroxide from 0.25 to 0.05 M did not affect the anodic current efficiency. This may be related to the distribution of copper cyanide species.

Table 8-2 Current efficiencies from copper cyanide using controlled current coulometric measurements (supporting electrolyte: 1 M Na_2SO_4)

Test No.	Composition	Controlled current (A m^{-2})	Temperature (°C)	Rotational speed (rpm)	Current efficiency for CN (%)	Current efficiency for Cu (%)
1	0.05 M CN⁻,	250	50	1600	13	3
2	CN:Cu = 3	250	60	1600	10	2
3	0.4 M SO_3^{2-}	250	50	100	14	2
4	0.25 M OH⁻	250	60	100	11	3
5		500	50	100	13	3
6		500	60	100	12	3
7	0.05 M CN⁻,	250	50	1600	14	0
8	CN:Cu = 4	250	60	1600	11	0
9	0.4 M SO_3^{2-}	250	50	100	13	0
10	0.25 M OH⁻	250	60	100	11	0
11		500	50	100	15	-
12		500	60	100	12	-
13	0.4 M CN⁻,	500	50	100	14	0
14	CN:Cu = 3 0.4 M SO_3^{2-} 0.25 M OH⁻	500	60	100	9	
15	0.4 M CN⁻,	500	50	100	17	0
16	CN:Cu = 4 0.4 M SO_3^{2-} 0.25 M OH⁻	500	60	100	15	
17	1 M CN⁻, CN:Cu	500	50	100	15	2
18	= 3 0.4 M SO_3^{2-} 0.05 M OH⁻	500	60	100	10	0
19	1 M CN⁻, CN:Cu	500	50	100	18	
20	= 4 0.4 M SO_3^{2-} 0.25 M OH⁻	500	60	100	14	
21	0.05 M CN⁻,	250	50	1600	10	
22	CN:Cu = 3	250	60	1600	6	
23	0.4 M SO_3^{2-}	500	50	1600	9	
24	0.05 M OH⁻	500	60	1600	8	
25		500	50	100	8	
26		500	60	100	7	
27	0.05 M CN⁻,	250	50	1600	14	0
28	CN:Cu = 4	250	60	1600	13	0
29	0.4 M SO_3^{2-}	500	50	1600	14	0
30	0.05 M OH⁻	500	60	1600	12	0

Table 8-3 lists the anodic current efficiencies of cyanide and copper when the cyanide concentration was increased to 3 or 4 M. From Tests 1-4, in the presence of 0.5 M Na_2SO_3, at $[CN^-] = 3$ M and $[Cu^+] = 1$ M, the anodic current efficiency of cyanide decreased to around 12 % from about 82 % in the absence of sulphite and the anodic current efficiency of copper (I) decreased to about 2.5 % from 13.6 % in the absence of sulphite. Thus sulphite can limit the oxidation of copper cyanide. The decrease in the concentration of hydroxide from 0.25 to 0.10 M (Tests 5-8) or 0.05 M (Tests 9-12) resulted in a slight decrease in the anodic current efficiency. There was no precipitation of copper oxide when the other compositions were the same. So sulphite more efficiently limits the oxidation of copper cyanide at a low pH. From Tests 1-4 and Tests 13-24, the current efficiency of cyanide increased with increasing concentration of cyanide. From Tests 9-12 and 25-28, the anodic current efficiency for cyanide increased by about 7-8 % with decreasing sulphite concentration from 0.5 to 0.3 M.

Table 8-3 Current efficiencies from copper cyanide using controlled current coulometric measurements at 100 rpm (0.5 M Na_2SO_4)

Test No.	Composition	Controlled current (A m^{-2})	Temperature (°C)	Current efficiency for CN (%)	Current efficiency for Cu (%)
1	3 M CN$^-$, 1M Cu$^+$	250	50	13	2.4
2	(CN:Cu = 3)	250	60	12	2.6
3	0.5 M SO$_3^{2-}$	500	50	12	2.0
4	0.25 M OH$^-$	500	60	11	2.5
5	3 M CN$^-$, 1M Cu$^+$	250	50	13	0
6	(CN:Cu = 3)	250	60	12	0
7	0.5 M SO$_3^{2-}$	500	50	12	0
8	0.10 M OH$^-$	500	60	11	0
9	3 M CN$^-$, 1M Cu$^+$	250	50	10	0
10	(CN:Cu = 3)	250	60	9	0
11	0.5 M SO$_3^{2-}$	500	50	12	0
12	0.05 M OH$^-$	500	60	11	0
13	3.2 M CN$^-$, 1M Cu$^+$	250	50	13	0
14	(CN:Cu = 3.2)	250	60	12	0
15	0.5 M SO$_3^{2-}$	500	50	15	0
16	0.25 M OH$^-$	500	60	14	0
17	3.5 M CN$^-$, 1M Cu$^+$	250	50	19	0
18	(CN:Cu = 3.5)	250	60	18	0
19	0.5 M SO$_3^{2-}$	500	50	22	0
20	0.25 M OH$^-$	500	60	21	0
21	4 M CN$^-$, 1M Cu$^+$	250	50	40	0
22	(CN:Cu = 4)	250	60	39	0
23	0.5 M SO$_3^{2-}$	500	50	45	0
24	0.25 M OH$^-$	500	60	46	0
25	3 M CN$^-$, 1M Cu$^+$	250	50	17	0
26	(CN:Cu = 3)	250	60	16	0
27	0.3 M SO$_3^{2-}$	500	50	18	0
28	0.05 M OH$^-$	500	60	16	0

In the above tests, the anodic current efficiencies of cyanide and copper (I) were obtained from the analysis of the cyanide concentration and the amount of the copper oxide precipitated on the anode. From the anodic current efficiencies of cyanide and copper (I), we cannot predict the amount of oxidized sulphite because sulphite can be oxidized to sulphate (two electrons process) and dithionate (one electron process) and there are possible side reactions such as oxygen evolution. Therefore the amount of oxidized sulphite was determined directly.

Table 8-4 lists the anodic current efficiencies of cyanide, copper (I) and sulphite (assuming sulphite was oxidized to sulphate). From Table 8-4, the sum of the anodic current efficiencies of cyanide, copper (I) and sulphite is very close to 100 % and so sulphite was oxidized to sulphate. Table 8-5 lists the current efficiency for cyanide, copper and sulphite using controlled potential method. At a higher potential, the current was at a limiting value and the anodic current efficiency for sulphite was low.

Table 8-4 Current efficiency for copper cyanide using controlled current coulometric measurements (supporting electrolyte: 1 M Na_2SO_4 for Tests 1 and 2) at 100 rpm*

Test No.	Composition	Controlled current (A m^{-2})	Temperature (°C)	Current efficiency for SO_3^{2-} (%)	Current efficiency for CN (%)	Current efficiency for Cu^+ (%)
1	0.05 M CN⁻,	500	50	86	12	1.6
2	0.0167 M Cu⁺	500	60	89	10	1.8
	0.4 M SO_3^{2-}					
	0.25 M OH⁻					
3	3 M CN⁻, 1 M	250	50	83	14	2.2
4	Cu^+ (CN:Cu = 3)	250	60	86	13	2.4
5	0.5 M SO_3^{2-}	500	50	84	15	2.5
6	0.25 M OH⁻	500	60	86	12	2.6
7	3 M CN⁻, 1 M	250	25	88	15	0
8	Cu^+ (CN:Cu = 3)	250	40	88	14	0
9	0.5 M SO_3^{2-}	250	50	89	10	0
10	0.05 M OH⁻	250	60	87	09	0

* For Tests 3-10, the initial concentration of sulphite was 0.6 M. The amount of electricity passed decreased the concentration of sulphite to 0.4 M assuming 85 % for the anodic current efficiency of sulphite.

Table 8-5 Current efficiency for copper cyanide using controlled potential coulometric measurements (supporting electrolyte: 1 M Na_2SO_4 for Tests 1 and 2) at 100 rpm*

Test No.	Composition	Controlled potential (V vs. SCE)	Temp. (°C)	Current efficiency for CN (%)	Current efficiency for Cu^+ (%)	Current efficiency for SO_3^{2-} (%)
1	0.05 M CN⁻, 0.0167 M Cu^+	0.3	60	11	2.2	87
2	0.4 M SO_3^{2-} 0.25 M OH⁻	0.5	60	13	2.9	84
3	0.05 M CN⁻, 0.0125 M Cu^+	0.4	60	10	1.3	85
4	0.4 M SO_3^{2-} 0.25 M OH⁻	0.6	60	13	2.8	83
5	0.05 M CN⁻, 0.0167 M Cu^+	0.25	60	9	0	89
6	0.4 M SO_3^{2-} 0.05 M OH⁻	0.6	60	11	0	90
9	0.05 M CN⁻, 0.0125 M Cu^+	0.25	60	11	0	89
10	0.4 M SO_3^{2-} 0.05 M OH⁻	0.6	60	13	0	88
11	3 M CN⁻, 1 M Cu^+	0.3	60	13	2.3	87
12	0.5 M SO_3^{2-}, 0.25 M NaOH	0.6	60	52	0	47
13	3 M CN⁻, 1 M Cu^+	0.3	60	11	0	87
14	0.5 M SO_3^{2-}, 0.05 M NaOH	0.6	60	48	0	57

For Tests 11-14, the initial concentration of sulphite was 0.6 M. The amount of electricity passed decreased the concentration of sulphite to 0.4 M assuming 85 % for the anodic current efficiency of sulphite.

8.4 Possible Anodic Reactions

The anodic behaviour of mixed copper cyanide and sulphite solution is a function of hydroxide, sulphite and cyanide concentrations, the mole ratio of cyanide to copper, temperature and rotational speed. The current for mixed copper cyanide solution was not just the sum of the currents of copper cyanide and sulphite when they are present separately in the solution. Sulphite oxidation was affected significantly by the oxidation of copper cyanide. Copper cyanide oxidation was also affected by sulphite ions. Comparing Figures 8-12, 15 and 17, the higher the mole ratios of cyanide to copper , the less the effect on the oxidation of copper cyanide and sulphite. This may be related to the distribution of copper cyanide species. Probably the discharge of $Cu(CN)_4^{3-}$ is less affected by sulphite. So sulphite also has a smaller effect on the oxidation of cyanide. The oxidation of $Cu(CN)_3^{2-}$ is more affected by sulphite. So sulphite has a greater effect on the oxidation of copper cyanide. One effect of sulphite is to reduce the precipitation of copper oxide and so affect the oxidation of copper cyanide. At a concentration of hydroxide below a certain level, sulphite completely suppresses the precipitation of copper oxide. Therefore the probable anode reactions are:

$$Cu(CN)_n^{-(n-1)} \rightarrow Cu(CN)_n^{-(n-2)} + e \ (n = 2, 3, 4) \tag{8-1}$$

$$SO_3^{2-} + 2OH^- \rightarrow SO_4^{2-} + H_2O + 2e \tag{8-2}$$

$$2Cu(CN)_n^{-(n-2)} + 2CN^- \rightarrow 2Cu(CN)_n^{-(n-1)} + (CN)_2 \tag{8-3}$$

$$(CN)_2 + 2OH^- \rightarrow CN^- + CNO^- + H_2O \tag{8-4}$$

$$2Cu(CN)_n^{-(n-2)} + SO_3^{2-} + 2OH^- \rightarrow 2Cu(CN)_n^{-(n-1)} + SO_4^{2-} + H_2O \tag{8-5}$$

$$Cu(CN)_n^{-(n-2)} + 2OH^- \rightarrow Cu(CN)_n^{-(n-1)} + Cu(OH)_2 (or\ CuO + H_2O) \tag{8-6}$$
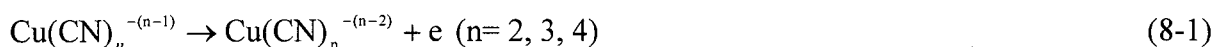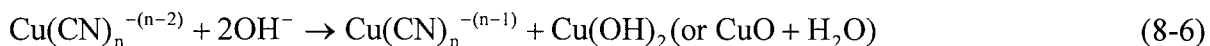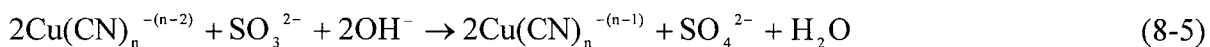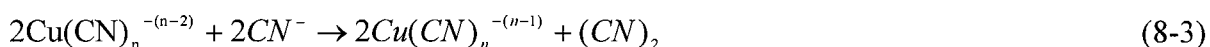
Reaction 8-5 may undergo the following steps similar to the reaction between ferricyanide and sulphite [337]:

$$Cu(CN)_n^{-(n-2)} + SO_3^{2-} \rightarrow Cu(CN)_n^{-(n-2)} SO_3^{2-} \tag{8-7}$$

$$Cu(CN)_n^{-(n-2)} SO_3^{2-} + Cu(CN)_x^{-(n-2)} \rightarrow Cu(CN)_n^{-(n-2)} SO_3^- + Cu(CN)_n^{-(n-1)} \tag{8-8}$$

$$Cu(CN)_n^{-(n-2)} SO_3^- + 2OH^- \rightarrow Cu(CN)_n^{-(n-1)} + SO_4^{2-} + H_2O \tag{8-9}$$
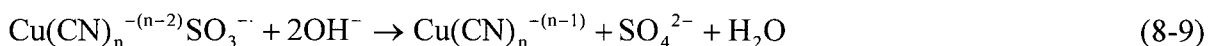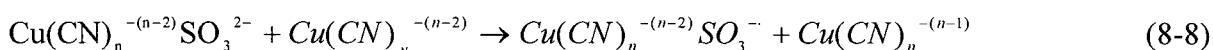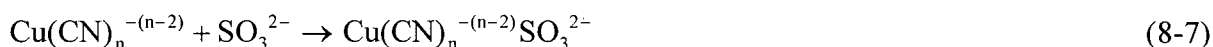
Reaction 8-1 is catalyzed by sulphite ions when n = 3. SO_3^{2-} may be bound to $Cu(CN)_3^{2-}$ and form $Cu(CN)_3^{2-}SO_3^{2-}$ which may be discharged faster than $Cu(CN)_3^{2-}$. So the oxidation of sulphite and copper cyanide is significantly catalyzed. With increasing mole ratio of cyanide to copper, the concentration of $Cu(CN)_3^{2-}$ is decreased and so it is less affected by sulphite.

8.5 Summary

The anodic behaviour of mixed sulphite and copper cyanide is not just the sum of sulphite and copper cyanide when they are present separately in the solution. Sulphite oxidation is enhanced by the presence of copper cyanide.

The effect of sulphite on limiting the oxidation of copper cyanide decreases with increasing mole ratio of cyanide to copper. This is related to the shift in the discharged species from $Cu(CN)_3^{2-}$ to $Cu(CN)_4^{3-}$ with increasing mole ratio of cyanide to copper. Sulphite ions affect the discharge of $Cu(CN)_3^{2-}$ more than that of $Cu(CN)_4^{3-}$.

Sulphite is oxidized to sulphate. At [Cu] = around 1 M, CN:Cu mole ratio = 3 -3.2, [OH⁻] = 0.05-0.25 M, [SO_3^{2-}] = 0.4-0.6 M and the temperature = 50-60 °C, the anodic current efficiency of sulphite oxidation reached 80-90%. The above conditions are suitable for

obtaining a good copper deposition current efficiency and therefore would be suitable for industrial application.

9. CONCLUSIONS

The following are the principal conclusions resulting from the study of the thermodynamics of copper cyanide, direct copper electrowinning from dilute cyanide solution, copper electrowinning from concentrated copper cyanide solution using alternative anodic reactions, the anodic oxidation of sulphite, the anodic oxidation of copper cyanide and the anodic oxidation of mixed sulphite and copper cyanide solution.

(1) The distributions and the equilibrium potentials of copper cyanide species, calculated using reliable stability constants, are shown to be functions of the mole ratio of cyanide to copper, total cyanide concentration, pH and temperature.

With increasing CN:Cu mole ratio, the distribution of copper cyanide species shifts more completely to the highly coordinated complex ($Cu(CN)_4^{3-}$) at a high cyanide concentration than that at a low cyanide concentration. With increasing CN:Cu mole ratio, the equilibrium potential for Cu(I)/ Cu decreases rapidly at a CN:Cu mole ratio < about 4 and more slowly at a CN:Cu mole ratio > about 4. Increasing pH is similar to increasing free cyanide concentration.

Increasing temperature results in decreasing the stability constants. Therefore the distribution of copper cyanide shifts to the lowly coordinated complexes.

The potential measurements have confirmed the validity of the calculated results.

In the pH - potential diagrams. CuCN, $Cu(CN)_2^-$, $Cu(CN)_3^{2-}$ and $Cu(CN)_4^{3-}$ can predominate in the different pH regions.

(2) The current efficiency of copper deposition on a graphite felt electrode decreases with increasing mole ratio of cyanide to copper. Due to the low conductivities of the solution and the graphite felt, the potential and current distribution of copper throughout the 3-dimensional electrode are not uniform. The accumulation of deposited copper on the graphite felt as the plating proceeds significantly improves the conductivity of the graphite felt and increases the specific surface area benefiting copper deposition.

Copper can be efficiently deposited on the graphite felt from solutions of low concentration (0.5 g -2 g L^{-1} Cu) at a high mole ratio of cyanide to copper (CN:Cu = 3-9).

The energy requirement for copper deposition was as low as 1-2 kwh/kg Cu (1000-2000 kwh/tonne Cu) in the current range 30-100 Am^{-2}. These values compare favorably with that obtained in conventional copper electrowinning from sulphuric acid-copper sulphate solutions.

(3) Of four sacrificial species (sulphite, methanol, thiocyanate and ammonia), only sulphite can effectively limit the oxidation of cyanide. When the composition of the electrolyte was controlled at 50-60 g L^{-1} Na_2SO_3, 70 g L^{-1} Cu, CN:Cu = 3-3.2, the anodic current efficiency of cyanide decreased from about 100 % to 10-20 % in the current range 250-500 A m^{-2} and the temperature range 50-60 °C. Under the above conditions, the copper deposition current efficiency was 90-96 % and the energy consumption was 0.76-1.0 kWh/kg Cu. The anodic current efficiency of cyanide increased from about 15 % to 56 % with increasing CN:Cu mole ratio from 3 to 4.5 at [Cu] = 70 gL^{-1}. With increasing the current density, the anodic current efficiency of cyanide decreases greatly at a current density > 500 A m^{-2} and slightly at a current density < 500 A m^{-2}. The anodic current efficiency of cyanide decreases slightly with increasing temperature. The copper deposition current efficiency decreases with increasing CN:Cu mole ratio and decreasing temperature. The presence of thiocyanate increases the copper deposition current efficiency at CN:Cu mole ratio > 4.5.

(4) At low potentials (e.g. < 0.25 V vs. SCE at 25 °C), the reaction order for the oxidation of sulphite is below 1 and decreases with increasing sulphite concentration. The Tafel slope is 0.060 -0.065 V $decade^{-1}$. At high potentials (> 0.4 V vs. SCE), the reaction order with respect to sulphite ions is 1 up to 0.4 M and the Tafel slope is 0.19 - 0.21 V $decade^{-1}$. The reaction order with respect to hydroxide ions is close to zero.

The activation energy for the kinetic current decreases from 85.2 $kJmol^{-1}$ at 0.2 V vs. SCE to 45.3 $kJmol^{-1}$ at 0.6 V vs. SCE.

The diffusion coefficients of sulphite ions were 5.6, 8.6, 9.99 and 12.4 × 10^{-10} m^2 s^{-1} respectively for 25, 40, 50 and 60 °C.

Sulphite oxidation in alkaline solution appears to undergo a radical-electron mechanism. At low potentials, the adsorbed sulphite oxidation is dominant and at high potentials, the sulphite ions are oxidized directly on the electrode surface.

(5) Copper has a significant catalytic effect on cyanide oxidation. At low potentials (roughly 0 to 0.4 V vs. SCE), cuprous cyanide is oxidized to cupric cyanide complexes which produce cyanogen, which in turn reacts with hydroxide to form cyanate. In the middle potential region (roughly 0.4 to 0.6 V vs. SCE), cuprous cyanide is oxidized to cupric oxide and cyanate. The potential for the precipitation of copper oxide increases with increasing mole ratio of cyanide to copper. In the high potential region (> about 0.60 V vs. SCE), oxygen is evolved at the electrode. However, when the concentration of cyanide was high and the concentration of hydroxide was low, no copper oxide was precipitated and but cyanogen gas was evolved.

The electrochemical kinetic behavior is dependent on CN:Cu mole ratio, pH and total cyanide concentration. At CN:Cu = 3 and $[OH^-]$ = 0.25 M, the Tafel slope is about 0.12 V decade^{-1} and the reaction order with respect to $Cu(CN)_3^{2-}$ is one. $Cu(CN)_3^{2-}$ is discharged on the electrode. The current and Tafel slope decrease with decreasing hydroxide concentration and so hydroxide is involved in the rate-determining step.

With increasing mole ratio of cyanide to copper, the anodic behaviour of copper cyanide changes. When the mole ratio of cyanide to copper is larger than a certain value which depends on the total cyanide concentration, e. g. about 4 at $[CN^-]$ = 0.05 M and 3.5 at $[CN^-]$ = 3.5 M, a Tafel slope of about 0.06 V decade^{-1} was observed over the potential range 0.1 - 0.25 V vs. SCE. A second Tafel slope of about 0.17 -0.20 V decade^{-1} was noted over the higher potential range. This change is related to the change in the distribution of copper cyanide species. The current is proportional to the concentration of tetracyanide and almost independent of the total cyanide concentration.

pH has little effect on cyanide oxidation and the Tafel slopes do not change with pH. In the potential region where copper oxide was precipitated, the current at a constant potential decreases with decreasing hydroxide concentration and the rate-controlling step involves hydroxide. The catalysis of copper oxide is limited with increasing copper cyanide concentration and temperature.

(6) The anodic behaviour of mixed sulphite and copper cyanide is not just the sum of sulphite and copper cyanide when they are present separately in the solution. Sulphite oxidation is catalyzed by the oxidation of copper cyanide. It also affects the oxidation of copper cyanide.

The effect of sulphite on the oxidation of copper cyanide decreases with increasing mole ratio of cyanide to copper. This is related to the shift in the discharged species from $Cu(CN)_3^{2-}$ to $Cu(CN)_4^{3-}$ with increasing mole ratio of cyanide to copper. Sulphite ions affect the discharge of $Cu(CN)_3^{2-}$ more than that of $Cu(CN)_4^{3-}$. At [Cu] = around 1 M, CN:Cu = 3 -3.2, [OH^-] = 0.05-0.25 M, [SO_3^{2-}] = 0.4-0.6 M and the temperature = 50-60 °C, the anodic current efficiency of sulphite reached 80-90%. In relation to the recovery of copper from cyanide gold leach solution, it has been shown that in the electrowinning step, it is possible to limit the oxidation of cyanide by using the oxidation of sulphite as an alternative anode reaction with an electrolyte having a composition similar to that indicated above. At a current density of 250 to 500 Am^{-2}, copper can be electrowon at a current efficiency of 95 % with a energy requirement of about 0.8 kWh/kg Cu.

10. RECOMMENDATIONS

Many important aspects have not been investigated due to the time constraint. Regarding the fundamental aspects and the practical application of copper electrownning, the following areas need to be studied in the future.

The morphology and distribution of the copper deposit should be studied to better understand the effect of the copper deposit on the copper deposition current efficiency. The BET method needs to be used to measure the real surface area of the graphite fibre with and without a copper deposit. The objective would be to understand how the copper deposits so as to improve the current efficiency of copper deposition. Polarization curves should be measured to better understand copper deposition on the graphite from cyanide solution. The measurement should be carried out for current passing in the same and opposite directions to the electrolyte flow. The effect of temperature, CN:Cu ratio, supporting electrolyte, deposited copper and flow rate should be studied. Hydrogen evolution on the graphite fibre with and without deposited copper could be studied using steady-state polarization measurements.

There are some reports on the effect of thiocyanate [92, 94-96, 98] and sulphite [90] in copper cyanide plating baths. However, there is a lack of fundamental work about how thiocyanate and sulphite affect the copper deposition process. The conditions used in plating may not be the same as those employed in copper electrowinning. For example, the deposition time for electrowinning is much longer than that for plating. Some phenomena occurring in electrowinning may not be observed in plating. So the effect of thiocyanate and sulphite on the electrowinning process needs to be studied carefully. Comprehensive experiments should be conducted using a small-scale pilot cell operating conditions to optimize the electrowinning condition.

Hydroxide and sulphite catalyze the discharge of $Cu(CN)_3^{2-}$ on the anode. However, it is not clear how they affect the anodic oxidation of copper cyanide. It is possible that hydroxide and sulphite are bound to $Cu(CN)_3^{2-}$. Spectroscopic studies such as Raman, UV, nuclear magnetic resonance might be useful in leading to an understanding of the above phenomena.

11. REFERENCES

1. M. C. Jha, "Refractory of Certain Gold Ores to Cyanidation: Probable Causes and Possible Solutions", Mineral Processing and Extractive Metallurgy Review", 2, 1987, pp. 331-352.

2. H. V. Michaelis, "Gold Processing Update, The Prospects for Alternative Leach Reagents, Can Precious Metals Producers Get along without Cyanide?", Engineering & Mining Journal, 1987, pp. 43 - 47.

3. J. A. King, and D. B. Dreisinger, "Autoclaving of Copper Concentrates", Proc. Copper'95, edited by W. C. Cooper, D. B. Dreisinger, J. E. Dutrizac, H. Hein and G. Ugarte, Can. Inst. Min. Met., Montreal, 1995, pp. 511-534.

4. N. W. Hanf and C. G. Schmidt, "The Roasting of Witwatersrand Pyrite Concentrates", J. S. Afr. Inst. Min. Metall., Vol. 79, 1979, pp. 365 - 371.

5. J. O. Marsden, J. G. Mansanti and J. G. Sass, "Innovative Methods for Precious Metals Recovery in North America", Mining Engineering, Vol. 45, 1993, pp. 1144-1151.

6. C. D. McDoulett and G. W. Reschike, "Metal Leaching and Recovery Process", U.S. Patent 5364444, Nov. 15,1994.

7. R. Poulin and R. W. Lawrence, "Economic and Environment Niches of Biohydrometallurgy", Minerals Engineering, Vol. 9, pp. 1996, pp. 799 -810.

8. C. L. Brierley, "Gold and Copper Ore/Concentrate Bioleaching", Conference of Impurities Control and Disposal in Hydrometallurgical Processes", Toronto, 1994, Canadian Institute of Minning, Metallurgy and Petroleum (Canada), pp. 371-379.

9. G. Deschenes, "Literature Survey in the Recovery of Gold from Thiourea Solutions and the Comparison with Cyanide", C. I. M. Bulletin, Vol. 79, 1986, pp. 76-83.

10. R. Y. Wan, "Importance of Solution Chemistry for Thiosulphate Leaching Gold", Conference - World Gold '97, Australasian Institute of Mining and Metallurgy, 1997, pp. 159-162.

11. A. Dadgar and J. Howarth, "Advances in Bromide Gold Leaching Technology", EPD Congress '92, edited by J. P. Hager, TMS, pp. 123 - 137.

12. S. Vukcevic, "The Mechanism of Gold Extraction and Copper Precipitation from Low Grade Ores in Cyanide Ammonia Systems", Minerals Engineering, Vol. 10, 1997, pp. 309-326.

13. J. S. Scott, "An Overview of Gold Mill Effluent Treatment", The Proceedings of Gold Mining Effluent Treatment Seminars", Vancouver, British Columbia, Feb. 15-16, 1989, pp.1-22.

14. V. McNamara, "The AVR Process for Cyanide Recovery, and Cyanide Control for Barren Recycle and Barren Bleed", The Proceedings of Gold Mining Effluent Treatment Seminars, Vancouver, British Columbia, Feb. 15-16, 1989, pp.199-239.

15. N. L. Piret and H. J. Schippers, "Cyanide Destruction versus Cyanide Regeneration - Evaluation of the Processes for Optimum Mill Effluent", Extraction Metallurgy'89, London, UK, 10-13 July 1989, The Institution of Mining and Metallurgy, pp.1041 - 1080.

16. M. J. Kitney, "Cyanide Regeneration from Gold Tailings - Golconda Beaconsfield's Experience", The Proceedings of Gold Mining Effluent Treatment Seminars, Vancouver, British Columbia, Feb. 15-16, 1989, pp.389-399.

17. H. Soto, F. Nava and J. Jara, "Cyanide Regeneration and Copper Recovery from Cyanide Solutions", Global Exploration of Heap Leachable Gold Deposits , edited by D. M. Hausen, TMS, 1997, pp. 151-160.

18. A. Bergmann, A. Guzman and G. M. Potter, "Regeneration of Cyanide, A Case Study: Pilot Cyanidation of a High Copper Ore from Punitiaqui, Chile", Conference on Cyanide and the Environment, Tucson, Arizona, Dec. 1984, pp.457-467.

19. E. L. Coltrinari, "Method for Recovery of Cyanide from Waste Streams", U.S. Patent No. 4,708,804, November 24, 1987.

20. S.A. Patent 866,244 (1986), "A Process for Recovering Cyanide from Effluent Solutions".

21. G. W. Lower, "Electrolytic Recovery of Copper from Copper Cyanide Leaching Solutions", U.S. Patent 3,463,710, Aug. 26, 1969.

22. Orocon Inc Technology Report, "CELEC Cyanide Regeneration System".

23. ECO Corporation report, "ECO-Metal Recovery System".

24. HAS REACTORS Limited Technology Report, "Copper Recovery/Cyanide Regeneration".

25. D. G. Dickson, "Electrochemical Reactor for Copper Removal from Barren Solution", U. S. Patent 4,911,804, Feb. 1, 1988.

26. C. A. Fleming, W. G. Grot and J. A. Thorpe, "Hydrometallurgical Extraction Process", U. S. Patent, 5,411,575, May 2, 1995.

27. G. R. Maxwell, J. A. Thorpe, K. M. Schall and K. A. Brunk, "ACCS Technology from Lab to Feasibility Study", Global Exploration of Heap Leachable Gold Deposits , edited by D. M. Hausen, TMS, 1997, pp. 141-149.

28. D. B. Dreisinger, J. Ji, B. Wassink, and J. King, "The Solvent Extraction and Electrowinning Recovery of Copper and Cyanide Using XI 7950 Extractant and Membrane Cell Electrolysis, The Proceedings of Randol Gold Forum - Perth' 95, 1995, pp. 239-244.

29. A. G. Sharpe, "The Chemistry of Cyano Complexes of the Transition Elements", Academic Press, London, 1976.

30. W. H. Vigoe, "The Chemistry of Copper Cyanides", Eng. Min. J., Vol. 77(20), 1901, pp. 795-796.

31. S. Glasstone, "Studies of Electrolytic Polarization. Part VIII, Complex Cyanides: (b) Copper", J. Chem. Soc., Vo.132, 1929, pp. 702-713.

32. M. G. Vladimirova and I. A. Kakovsky, "The Physicochemical Constants Characteristic of the Formation and Composition of the Lowest Cuprous Cyanide Complex", Journal of Applied Chemistry of the USSR, Vol. 23, 1950, pp. 615 - 632.

33. R. A. Penneman and L. H. Jones, "Infrared Absorption of Aqueous Complex Ions II Cyanide Complexes of Cu (I) in Aqueous Solutions", J. Chem. Phys., Vol. 14 (2), 1956, pp. 295-296.

34. G. W. Chantry and R. A. Plane, "CN Stretching Bands in the Raman Spectra of Some Group Ib and Group IIb Complex Cyanides", J. Chem. Phys., Vol.33(2), 1960, pp. 736-740.

35. A. Brenner, "Determination of the Composition of Complexes and Their Instability Constants by Calorimetry 1. The Cuprocyanide Complexes", J. Electrochem. Soc., Vol. 112, 1965, pp. 611- 621.

36. D. Cooper and R. A. Plane, "Raman Study of Complex Cyanides of Copper(I)", Inorganic Chem., Vol. 5 (1), 1966, pp.16-20.

37. D. Cooper and R. A. Plane, "Mixed Complexes of Copper(I) Cyanide", Inorganic Chem., Vol. 5 (12), 12, 1966, pp.2209-2212.

38. R. M. Izatt, H. D. Johnston, G. D. Watt and J. J. Christensen, "Thermodynamics of Metal Cyanide Coordination VI. Copper(I)- and Silver(I)- Cyanide Systems", Inorganic Chemistry, Vol.6 (1), 1967, pp. 132-135.

39. E. A. Simpson and G. M. Waind, "The Ultraviolet Absorption Spectra and Stability Constants of Cuprous Cyanide Complexes", J. Chem. Soc., 1958, pp. 1746-1749.

40. J. S. Coleman, R. Gorge, L. Allaman and L. H. Jones, "Stepwise Formation of Cyanide Complexes of Copper (I) in Anion Exchangers", J. Phys. Chem., Vol. 72 (7), 1968, pp.2605-2608.\

41. H. L. Noblitt, "Complex Ions of Copper and Cyanide", Mines Branch Research Report R268, Department of Energy, Mines and Resources, Ottawa, Canada, 1973.

42. H. P. Rothbaum, "The Composition of Copper Complexes in Cuprocyanide Solutions", J. Electrochem. Soc., Vol. 104 (10), 1957, pp. 862-686.

43. T. Yamamoto, H. Haraguchi and S. Fujiwara, "Copper Nuclear Magnetic Resonance Study of Cyanocuprate(I) Ions in Solution. Formation of Polynuclear Species and Mixed Complex", J. Phys. Chem., Vol. 74 (25), 1970, pp. 4369-4373.

44. P. Duby, "The Thermodynamic Properties of Aqueous Inorganic Copper Systems", The International Copper Research Association, New York, 1977, pp. 64-65.

45. G. G. Simulin, S. B. Lebed, V. D. Domashich and V. V. Kosenko, "IR Spectroscopic Investigation of a Ferrocyanide Electrolyte for Copper-Plating Steel", Elektrokhimiya, Vol. 8 (6), 1971, pp. 791-794.

46. R. D. Hancock, N. P. Finkelstein and A. Evers, "Stabilities of the Cyanide Complexes of the Monovalent Group IB Metal Ions in the Aqueous Solutions", J. Inorg. Nucl. Chem. Vol. 34, 1972, pp. 3747 - 3751.

47. R. Yu. Bek , B. D. Zhukov, "Electrodeposition of Copper from Cyanide Electrolytes Pt. II, Formation Constants for Copper Cyanide Complexes", IZV. Sib. Otd. Akad. Nauk SSSR, Ser. Khim. Nauk, (4), 1973, pp. 52-56.

48. C. Kappenstein and R. Hugel, "Cyanocuprate (I) in Neutral and Acidic Aqueous Solution", J. Inorg. Nucl. Chem., Vol. 36, 1974, pp. 1821-1825.

49. R. Izatt, J. Christensen , R. Pack and R. Bench, "Thermodynamics of Metal -Cyanide Coordination. I. Pk, ΔH^0, ΔS^0 Values as a Function of Temperature for Hydrocyanic Acid Dissocation in Aqueous Solutions", Inorg. Chem., Vol.1, 1962, pp.828-831.

50. J. S. Solis, P. M. May and G. Hefter, "Cyanide Thermodynamics Part 4, Enthalpies and Entropies of Cyanide Complexation of Cu^+, Ag^+, Zn^{2+} and Cd^{2+}", J. Chem. Soc. Faraday Trans., Vol. 92, 1996, pp. 641-644.

51. A. R. Taylor, M. H. Brown and E. G. Taylor, "Heat of Formation of Cuprous Cyanide and Its Heat Capacity from 10 to 400 K", U. S. Bureau of Mines, Report of Investigation 7499, 1972.

52. M. T. Beck, "Critical Survey of Stability Constants of Cyano Complexes", Pure & Appl. Chem., Vol. 59, 1987, pp. 1703-1720.

53. B. D. Zhokov, L. I. Borodikhina, V. M. Shchekotikhin, N. P. Poddubny and R. Yu. Bek, "Investigation of the Electrodeposition of Copper from Cyanide Electrolytes III Composition of Cuprocyanide Solutions", IZV. Sib. Otd. Akad. Nauk, (4), 1973, 1966, pp. 57-60.

54. I. Banyai, J. Blixi, J. Glaster and I. Toth, "On the Dissociation of Hydrogen Cyanide in Aqueous Solutions Containing Different Ionic Media. A Combined Potentiometric and Carbon-13 NMR Study", Acta Chem. Scand., Vol. 46, 1992, pp. 138-141.

55. J. S. Solis, P. M. May and G. Hefter, "Cyanide Thermodynamics Part 3, Enthalpies and Entropies of Ionization of Water and Hydrogen Cyanide", Aust. J. Chem., Vol. 49, 1996, pp. 651-657.

56. V. Gaspar and M. T. Beck, " The Influence of the Ionic Strength on the Dissociation Constant of Hydrogen Cyanide", Acta Chim. Acad. Sci., Vol. 110 (4), 1982, pp.425-427.

57. P. Verhoeven, G. Heffer and P. M. May, "Dissociation Constant of Hydrogen Cyanide in Saline Solutions", Mineral & Metallurgical Processing , 1990, pp. 185 - 188.

58. J. H. Baxendale and D. T. Westcott, "Kinetics and Equilibria in Copper (II) - Cyanide Solutions", J. Chem. Soc., 1959, pp. 2347-2351.

59. G. Hefter, P. M. May and P. Sipos, "A General Method for the Determination of Copper (I) Equilibria in Aqueous Solution", J. Chem. Soc. Chem. Commun., 1993, pp. 1704 - 1706.

60. D. Cooper and R. A. Plane, "Cyanide Complexes of Copper with Ammonia and Ethylenediamine", Inorg. Chem., Vol. 5, 1966, pp.1677 - 1682.

61. "Gmelin Habdbuch" Cu[B] 60 , Verlag Chemie Gmbh (1965), p. 1447.

62. T. Chitani, "Muki Kagaku", Sangyo Tosho, Tokyo, 1964, p. 479.

63. A. Glasner and K. R. S. Asher, "A Violet Water-Soluble Copper Cyanide", J. Chem. Soc., 1949, p. 3296-3299.

64. W. P. Griffith, "Cyanide Complexes of Transition Metals", Quart. Rev. Chem. Soc. (London) Vol. 16, 1962, pp. 188-207.

65. F. R. Duke and W. G. Courtney, "Complexes in Oxidation-Reduction Reactions. The Copper(II) - Cyanide Reaction", J. Phys. Chem. Vol. 56, 1952, pp. 19-21.

66. N. Tanaka, M. Kamada and T. Murayma, "Kinetics of the Reaction between Copper(II) -Ethylenediamine-tetra-acetate Complex and Cyanide", Bull. Chem. Soc. Japan, Vol. 31, 1959, pp. 895-900.

67. A. Longo and T. Buch, "Complex Cyanides of Copper(II)", Inorganic Chemistry, Vol. 6(3), 1967, pp. 556-562I.

68. O. Monsted and J. Bjerrum, "Spectrophotometric and Reaction Kinetic Studies of the Tetracyanocuprate (II) Complex in Methanol - Water Mixture at Low Temperatures", Acta Chem. Scand. Vol. 21, 1967, pp. 116-118.

69. R. Paterson and J. Bjerrum, "Stability of the Tetracyanocuprate(II) Complex from E.M.F. Measurements in a Methanol - Water Solvent at Low Temperature", Acta Chem. Scand. Vol. 19, 1965, pp. 729-734.

70. A. Katagiri, S. Yoshimura and S. Yoshizawa, "Formation Constant of the Tetracyanocuprate(II) Ion and the Mechanism of its Decomposition", Inorg. Chem., Vol. 20, 1981, pp. 4143 - 4147.

71. A. Katagiri, S. Yoshimura and S. Yoshizawa, Addition and correction for "Formation Constant of the Tetracyanocuprate(II) Ion and the Mechanism of Its Decomposition", Inorg. Chem., Vol. 25, 1986, pp. 2278.

72. G. Nord and H. Matthes, "A Stopped-flow Kinetics Study of the Copper (II) Cyanide Reaction in Water and in Aqueous Methanol", Acta Chem. Scand. A, Vol. 28, 1974, pp. 13-19.

73. S. Yoshimura, A. Katagiri, Y. Deguchi and S. Yoshizawa, "Studies of the Anodic Oxidation of the Cyanide Ion in the Presence of the Copper Ion. IV. The Kinetics and Mechanism of the Decomposition of the Intermediate Tetracyanocuprate (II) Ion", Bull. Chem. Soc. Japan, Vol. 53, 1980, pp. 2437-2442.

74. R. R. Tessier, "Cyanide Removal from Waste Waters by Catalytic Oxidation with Hydrogen Peroxide and Copper Sulphate Catalyst", Canadian Patent CA 1,257,019, July 4, 1989.

75. G. H. Robbins, "Historical Development of the INCO SO$_2$/AIR Cyanide Destruction Process", CIM Bulletin, Vol. 89, 1996, pp. 63-69.

76. Y. Chen, C. You and W. Ying, "Cyanide Destruction by Catalytic Oxidation", 46th Purdue Industrial Waste Conference Proceedings, 1992, Lewis Publishers, Inc., Chelsea, Michigan, pp.539 - 545.

77. R. Shantz and J. Reich, "A Review of Copper Cyanide Metallurgy", Hydrometallurgy, Vol. 3, 1978, pp.99-109.

78. J. E. Clennell, "The Cyanide Handbook", 2nd Edition, McGraw-Hill Book Co., New York, 1915.

79. C. P. Richmond, "Electrolytic Precipitation of Cyanide Solutions", Eng. Min. J., Vol.83(11), 1907, pp. 512-515.

80. F. Passal, "Copper Plating during the Last Fifty Years", Plating, Vol. 46(6), 1959, pp. 628-638.

81. A. G. Gray, "Modern Electroplating", John Wiley & Sons, New York, 1953, pp.194-224.

82. F. A. Lowenheim, "Modern Electroplating", 3RD Edition, John Wiley & Sons, New York, 1974, pp. 165-182.

83. J. V. Petrocelli, "A Study of the Electrolysis of Sodium Cuprocyanide Solution", Trans. Am. Electrochem. Soc., Vol. 78, 1940, pp.133-144.

84. G. H. Clevenger, "The Electrolytic Precipitation from Cyanide Solutions", Trans. Am. Electrochem. Soc., Vol. 28, 1916, pp. 263 - 306.

85. G. H. Clevenger, "Electrolytic Precipitation from Cyanide Solution", Engineering and Mining Journal, Vol. 102, No. 14, 1916, pp. 579-582.

86. O. C. Watts and A. Brann, "The Evolution of Hydrogen from Cyanide Plating Bath", Trans. Am. Electrochem. Soc., Vol. 31, 1917, pp. 303-310.

87. G. M. Smith and J. M. Breckenridge, "Cathode Potentials and Electrode Efficiencies of Copper in Copper Cyanide Solutions", Trans. Am. Electrochem. Soc., Vol. 56, 1930, pp. 397-408.

88. S. Glasstone, "The Limiting Current Density in the Electrodeposition of Noble Metals", Trans. Am. Electrochem. Soc., Vol. 59, 1931, pp. 277-285.

89. H. L. Benner and C. J. Wernlund, 'The High Efficiency Cyanide Copper Bath", Trans. Am. Electrochem. Soc., Vol. 80, 1942, pp. 355-365.

90. A. K. Graham and H. J. Read, "Rochelle Copper Plating", Trans. Am. Electrochem. Soc., Vol. 80, 1942, pp. 341-354.

91. I. C. Pan, "Concentrated Copper Cyanide Solutions", Trans. Am. Electrochem. Soc., Vol. 68, 1936, pp. 471-482.

92. J. Horner, "A Study of the Effect of Some Variables on the Speed and Distribution of Deposits from Cyanide Copper Plating Solutions", Technical Proceedings of the American Electroplaters' Society, Vol. 51, 1964, pp. 71-80.

93. E. Ivaskevic, "Electrodepsoition of Copper from Cyanide Solutions Containing Additives. II. Effect of Selenite and Selenide Additives on Electrode Process", Liet. TSR Moksu Akad. Darb., Ser. B, No. 5, 1989, pp24-30.

94. E. H. Hadley and K. A. Van Lente, "Copper(I) Thiocyanate Sodium Cyanide Electroplating Baths", Plating, Vol.60(3), 1973, pp.256-260.

95. C. J. Wernlund, "Bright Copper Plating", US Patent 2,347,448, April 25, 1944.

96. C. J. Wernlund, N. Tonawanda, and H. L. Benner and R. R. Bair, "Copper Plating", US Patent 2,287,654, June 2, 1942.

97. G. W. Jernstedt and J. D. Patrick, "Electroplating of Copper From Cyanide Electrolyte", U S Patent 2,636,850, April 28, 1953.

98. C. J. Wernlund "Addition Agent for Copper Plating", US Patent 2,774,728, Dec. 18, 1956.

99. G. N. Shivirin and E. M. Shivirina, "Electrode Processes in Copper Cyanide and Thiocyanate Solutions", Izvestiia Vysshikh Uchebnykh Zavedentii. Tsvetnaia Metallurgiia Tsvetnaia Metallurgiia, No. 4, 1977, pp.18-22.

100. G. N. Shivirin and E. M. Shivirina, "Kinetics of the Electrochemical Reduction of Copper from Copper Cyanide and Thiocyanate Solutions", Izvestiia Vysshikh Uchebnykh Zavedentii. Tsvetnaia Metallurgiia, No. 4, 1977, pp.23-27.

101. R. Jagmines and B. Girdauskas, "Electrodeposition of Cu in Cu (I) Cyanide Solutions Containing a Thicyanate Additive 1. Electrodeposition under Steady-State Conditions of Electrolysis", Chemijia, (4).1994, pp. 74-79.

102. G. R. Rogers and K. J. Taylor, "The Electrodeposition of Copper from Alkaline Cyanide Solution - I the Effect of Trace Selenide", Electrochimica Acta, Vol. 20, 1975, pp. 695-702.

103. E. Ivaskevic, I. Zitkeviciute and A. Steponavicius, "Electrodeposition of Copper from Cyanide Solution Containing Additives. 11. Effect of Selenate Additives on Electrode Processes", Liet. TSR Mokslu Akad. Darb., Ser. B, (4), 1989, pp. 15-21.

104. E. Ivaskevic, I. Zitkeviciute and A. Steponavicius, "Electrodeposition of Copper from Cyanide Solution Containing Additives. 11. Effect of Selenite and Selenide Additives on Electrode Processes", Liet. TSR Mokslu Akad. Darb., Ser. B, (5), 1989, pp. 24-30.

105. B. S. Krasikov and A. M. Gvozd, "Investigation of a Thiocyanate Electrolyte for Copper Plating", Journal of Applied Chemistry of the USSR, Vol. 30(6), 1957, pp. 1012-1016.

106. S. I. Uspenskii and M. A. Shluger, "The Influence of Ultrasonics on the Electrodeposition of Copper II Cyanide Electrolyte", Elektrokhimiya, Vol. 2, 1964, pp. 326-329.

107. U. Bertocci and D. R. Turner, "Copper", Encyclopedia of Electrochemistry of the Elements, Vol. 2, edited by A. J. Bard, Marcel Dekker Inc. New York, 1974, pp. 383-497.

108. M. L. Blanc and K. Schick, "Electrolysis with AC", Z. Phys. Chem., Vol. 46, 1903, pp. 213-243.

109. N. Pangarrov, I. Nenov and I. Khristova, "Predominant Orientation of Electrodeposited Copper and Nickel", IZV. INST. FIZIKOKIM. BURLGAR. AKAD. NAUK, Vol. 3, 1963, pp. 133-140.

110. M. Costa, "Kinetics of the Reaction of the Copper-Potassium Copper Cyanide Electrode", J. Rech. Centre Natl. Sci. Lab. Bellevue(Paris), No. 64, 1963, pp. 285-315.

111. F. D. Lowenheim, Electroplating, McGraw-Hill, New York, 1978, p. 126.

112. R. Raub and K. Muller, Fundamentals of Metal Deposition, Elsevier Publishing Co., Amsterdam, 1967, pp 64-65.

113. R. Yu. Bek , B. D. Zhukov, "Mechanism and Kinetics of Copper Electrodeposition from Cyanide Electrolytes. Pt I, Hydrogen Evolution of Copper from Alkali Metal Cyanide Solutions", IZV. Sib. Otd. Akad. Nauk SSSR, Ser. Khim. Nauk, (4), 1972, pp. 37-40.

114. R. Yu. Bek , B. D. Zhukov, "Mechanism and Kinetics of Copper Electrodeposition from Cyanide Electrolytes. Pt. 4, Concentration Polarization in Cyanide Cu-Plating Bath", IZV. Sib. Otd. Akad. Nauk SSSR, Ser. Khim. Nauk, (6) (14), 1974, pp. 35-40.

115. R. Yu. Bek , B. D. Zhukov, "Electrodeposition of Copper from Cyanide Electrolytes Pt. V, Mechanism of the Process", IZV. Sib. Otd. Akad. Nauk SSSR, Ser. Khim. Nauk, (6), 1974, pp. 40-44.

116. R. Yu. Bek and B. D. Zhukov, "Mechanism and Kinetics of Copper Electrodeposition from Cyanide Electrolytes", Elektrokhimiya, Vol. 129 (9), 1975, pp. 1291-1295.

117. A. A. Dikchyus, "Electrodeposition of Cu from Cyanide Solutions Pt1, Formation of Poor-Solubility Compounds on the Surface of a Cu Cathode", TRUDY AKADEMII NAUK LITOVSKOI SSR. SERIIA B., Vol.3 (100), 1977, pp. 23-28.

118. R. E. Sinitski, V. Srinivski and R. Haynes, "Electrode Kinetics of Copper Deposition from Copper Cyanide Solution", J. Electrochem. Soc., Vol.127 (1), 1980, pp. 47-51.

119. A. Juozenas, "Study of Surface of Copper Electrode in Cyanide Solutions", TRUDY AKADEMII NAUK LITOVSKOI SSR. SERIIA B., Vol.2 (147), 1985, pp. 16-22.

120. O. Dzilbute, "Influence of Conditions and Time of Electrolysis on Structure of Copper Deposits from Cyanide Solutions", TRUDY AKADEMII NAUK LITOVSKOI SSR. SERIIA B, Vol. 1 (152), 1986, pp. 30-42.

121. O. P. Koshcheev, V. I. Kichigin and V. V. Kamelin, "Electrodeposition of Copper on Highly Porous Cellular Materials", J. Appl. Chem. USSR, Vol. 65 (7), 1992, pp. 1251-1255.

122. D. Chu and P. S. Fedkiw, "The Electrochemistry of a Cuprous Cyanide Strike-Plating Bath", J. Electroanal. Chem., Vol. 345, 1993, pp. 107-120.

123. P. G. Hatherley, K. G. Watkins and M. McMahon, "The Properties of Copper Cyanide Electrolysis: a Comparison of Sodium and Potassium Formations", Trans. Inst. Met. Fin., Vol.70(4), 1992, pp. 177-183.

124. P. G. Hatherley and P. J. Carpenter, "Cathode Efficiency in Copper Cyanide Plating", Trans. Inst. Met. Fin., Vol.73(3), 1995, pp. 85-90.

125. R. Yu Bek, A. F. Zherebilov, "Copper Electrodepostion on Carbon Fibres", Zh. Prikl. Khim., Vol. 68(9), 1995, pp. 1470-1473.

126. D. A. Dudek and P. S. Fedkiw, "A Model of Mass-Transport Limited Copper Electrodeposition from Cyanide Electrolyte", The 83rd Ann. Tech. Conf., American Electroplaters and Surface Finshers Society, 1996, pp. 803 - 818.

127. A. Steponavicious, B. Radziuniene, E. Ivaskevic and B. Girdauskas, "On the Mechanism of the Cathodic Reaction in Cu(I) Cyanide Solution", Chemija, 1996, pp. 48-54.

128. A. Katagiri, H. Inoue and N. Ogure, "Cathodic Polarization of Copper Electrode in the CuCN-KCN solutions and the Current Distribution for Copper Deposition on Grooved Substrates", J. Appl. Electrochem., Vol. 27, 1997, pp. 529-538.

129. Y. J. Hsu and M. J. Tran, "Electrochemical Study on Copper Cementation from Cyanide Liquors Using Zinc", Electrochemimica Acta, Vol. 44 (10), 1999, pp. 1617-1625.

130. A. C. Halferdahl, "The Problem of Treating Cupriferous Precious Ores by the Cyanide Process", Eng. Min. Journal", Vol. 128(9), 1929, pp. 350-357.

131. A. T. Kuhn, "Electrolytic Decomposition of Cyanides, Phenols and Thiocyanates in Effluent Streams- A Literature Review", J. Appl. Chem. Biotechnol., Vol.21, 1972, pp. 29-34.

132. A. T. Kuhn, "The Role of Electrochemistry in Enviromental Control" in Modern Aspects of Electrochemistry, Vol. 8, edited by J. O'M. Bockris and B. E. Conway, Plenum Press, New York, 1972.

133. G. H. Clevenger and M. I. Hall, "The Electrolysis of Aqueous Solutions of the Simple Alkaline Cyanide", Trans. Am. Electrochem. Soc., Vol. 24, 1914, pp. 271-296.

134. D. Lay, "Electrical Precipitation of Cyanide Solution", Engineering and Mining Journal, Vol. 110, No.2, 1920, pp. 58-62.

135. L. B. Sperry and M. R. Caldwell, "Destruction of Cyanide Copper Solution by Hot Electrolysis", Plating, Vol. 36, 1949, pp. 343-347.

136. Von Hass Schmidta and Hass Meinert, "Electrolysen von Cyaniden in Wabrigen Losungen", Zeit. Für Anorgan. Allg. Chem, Vol. 293, 1957, pp. 214-227.

137. Yu. Yu. Lure and V. E. Genkin, "Electrochemical Purification of Waste Waters Containing Cyanide Compounds", J. Appl. Chem., USSR, Vol. 33 (2), 1960, pp. 379-384.

138. D. T. Sawyer and R. J. Day, "Electrochemical Oxidation of Cyanide Ion at Platinum Electrodes", J. Electroanal. Chem., Vol. 5, 1963, pp. 195-203.

139. M. C. Dart, J. D. Jentles and D. G. Renton, "Electrolytic Oxidation of Cyanide Wastes", J. Appl. Chem., Vol. 13, 1963, pp. 55-64.

140. J. Drogon and L. Pasek, "Continuous Electrolytic Destruction of Cyanide Waste", Plating and Surface Finishing, Vol. 18, 1965, pp 310-313.

141. J. K. Easton, "Electrolytic Decomposition of Concentrated Cyanide Plating Waste", Plating, Vol. 53, 1966, pp 1340-1342.

142. J. J. Byerley and K. Enns, "Laboratory Study of Continuous Electrooxidation of Dilute Cyanide Waste", U.S.N.I.T.S., A.D. Rep., pp 1-49, 1974.

143. T. Arikado, C. Iwakura, H. Yoneyama and H. Tamura, "Anodic Oxidation of Potassium Cyanide on the Graphite Electrode", Electrochimica Acta, Vol. 21, 1976, pp. 1021-1027.

144. S. Yoshimura, A. Katagiri and S. Yoshizawa, "Studies on the Anodic Oxidation of Cyanide Ion in the Presence of Copper Ion I. Behavior of Cyano Complexes of Copper(I) as a Catalyst in the Anodic Oxidation of Cyanide Ion", Deki Kagaku Oyobi Kogyo Butsuri Kagaku, Vol. 47(8), 1979, pp. 360-366.

145. S. Yoshimura, A. Katagiri and S. Yoshizawa, "Studies on the Anodic Oxidation of Cyanide Ion in the Presence of Copper Ion II. Behavior of Cyano Complexes of Copper(I) as a Catalyst in the Anodic Oxidation of Cyanide Ion", Deki Kagaku Oyobi Kogyo Butsuri Kagaku, Vol. 47(6), 1979, pp. 488-491.

146. Z. Alaune, "Anodic Oxidation of Oxalic Acid and Cyanide Ions during Electrodeposition of Gold from Cyanide-Oxalate Solutions", Liet. TSR Mokslu Akad. Darb. Ser. B, (6), 1980, pp. 11-18.

147. S. Yoshimura, A. Katagiri, Y. Deguchi and S. Yoshizawa, "Studies of the Anodic Oxidation of the Cyanide Ion in the Presence of the Copper Ion. III. The Kinetics and Mechanism of the Decomposition of the Intermediate Tetracyanocuprate (II) Ion", Bull. Chem. Soc. Japan, Vol. 53, 1980, pp. 2434-2436.

148. S. S. Telepnev, "Modern State of Waste Purification from Cyanide in Gold Extraction Plants", Tsvetnye Metally, (9), 1980, pp. 102-106.

149. S. Yoshimura, A. Katagiri and S. Yoshiawa, "Reaction Products of Anodic Oxidation of Cyanide Ion in the Presence of Copper Ion", Nippon Kagaku Kaishi, No. 9, 1980, pp.1327-1333.

150. A. Katagiri, S. Yoshimura, Y. Deguchi and S. Yoshizawa, "Catalytic Effect of Copper Ion on the Anodic Oxidation of Cyanide Ion", Proceedings of the Symposium on Electrocatalysis, (PV 82-2), Edited by W. E. O'Grady, P. N. Ross, Jr., and F. G. Will, The Electrochemical Society, Softbound proceedings series, Pennington, NJ (1982), pp. 336-346.

151. R. J. Daubaras, "Waste Treatment for Plating in the Soviet Union", Plating and Surface Finishing, Vol. 68, 1981, pp. 62-64.

152. S. Ehdaie, M. Fleischmann and R. E. W. Jansson, "Application of the Trickle Tower to Problems of Pollution Control III. Heavy Metal Cyanide Solutions", J. Appl. Electrochem., Vol.12, 1982, pp. 75-80.

153. S. Ehdaie, M. Fleischmann and R. E. W. Jansson, " Application of the Trickle Tower to Problems of Pollution Control. II. The Direct and Indirect Oxidation of Cyanide", J. Appl. Electrochem., Vol.12, 1982, pp. 69-73.

154. S. Ehdaie, M. Fleischmann and R. E. W. Jansson, " Application of the Trickle Tower to Problems of Pollution Control. I. The Scavenging of Metal Ions", J. Appl. Electrochem., Vol.12, 1982, pp. 59-67.

155. F. Kitamura, M. Takahashi and M. Ito, "Oxidation of the Cyanide Ion at a Platinum Electrode Studied by Polarization Modulation Infrared Reflection Absorption Spectroscopy", Chemical Physics Letters, Vol. 130, 1986, pp. 181-184.

156. F. Hine, M. Yasuda, T. Iida and Y. Ogata, "On the Oxidation of Cyanide Solutions with Lead Dioxide Coated Anode", Electrochimica Acta, Vol. 31, No.11, 1986, pp. 1389-1395.

157. J. Y. Hwang, Y. Y. Wang and C. C. Wan, "Electrolytic Oxidation of Cuprocyanide Electroplating Waste Waters under Different pH Conditions", J. Appl. Electrochem., Vol. 17, 1987, pp. 684-694.

158. F. Kitamura, M. Takahashi and M. Ito, "Anodic Oxidation of Cyanide and Cyanate Ions on a Platinum Electrode", Chemical Physics Letters, Vol. 136, No.1, 1987 pp. 62-66.

159. B. Wells and D. C. Johnson, "Electrocatalysis of Anodic Oxygen Transfer Reactions: Oxidation of Cyanide at Electrodeposited Copper Oxide Electrodes in Alkaline Media", J. Electrochem. Soc., Vol. 137, 1990, pp. 2785-2791.

160. T. C. Tan, W. K. Teo and O-T. Chin, "Electrochemical Destruction of Complex Ions", Chem. Eng. Commun., Vol. 38, 1985, pp. 125-133.

161. G. H. Kelsall, "Cyanide Oxidation at Nickel Anodes II. Voltammetry and Coulometry of Ni/CN-H$_2$O Systems at 298 K ", J. Electrochem. Soc., Vol. 138, No. 1, 1991, pp. 117-116.

162. M. L. Lin, Y. Y. Wang and C. C. Wan, "A Comparative Study of Electrochemical Reactor Configurations for the Decomposition of Copper Cyanide Effluent", J. Appl. Electrochem. Vol. 22, 1992, pp. 1197-1200.

163. C. S. Hofseth and T. W. Chapman, "Indirect Electrochemical Processes at a Rotating Disk Electrode: Catalytic Alkaline Cyanide Oxidation", J. Electrochem. Soc., Vol. 139 (9), 1992, pp. 2525-2529.

164. C. D. Zhou and D. T. Chin, "Copper Recovery and Cyanide Destruction with a Plating Barrel Cathode and a Packed-Bed Anode", Plating and Surface Finishing, Vol. 80 (6), 1993, pp. 69-78.

165. A. Socha, E. Kusmierek and E. Chrzescijanska, "Electrochemical Oxidation of Cyanides at Carbon Fibre and at Electrodeposited Copper Oxide Electrode", Polish Journal of Chemistry, Vol. 67(3), 1993, pp. 517-527.

166. C. W. Hwang, Y. Y. Wang and C. C. Wan, "Anodic Kinetics of Cyanide Ions in an Copper Cyanide Solution", J. Chin. Inst. Chem. Eng., Vol. 24, 1993, pp. 349 - 353.

167. L. Szpyrkowiz, F. ZilioGrandi, S. N. Kaul and S. RingoniStern, "Electrochemical Treatment of Copper Cyanide Wastewaters Using Stainless Steel Electrodes", Water Science and Technology, Vol. 38, 1998, pp. 261-268.

168. C. S. Hofseth and T. W. Chapman, "Electrochemical Treatment of Copper Cyanide Wastewaters Using Stainless Steel Electrodes", J. Electrochem. Soc., Vol. 146 (1), 1999, pp. 199-207.

169. M. N. Hughes, "General Chemistry", Chemistry and Biochemistry of Thiocyanic Acid and its Derivatives, edited by A. A. Newman, Academic Press, London, 1975, pp. 2-61.

170. J. E. Clennell, "Electrolytic Cyanide Regeneration", The Engineering and Mining Journal, May 27, 1911, pp. 1064-1066.

171. W. J. Crook, L. E. Booth and A. Thiel, "Electrolysis of Alkaline Solutions of Potassium Sulphate", Metallurgical and Chemical Engineering, Vol. 14, No.10, 1916, pp. 587-591.

172. E. F. Kern, "The Electrolysis of Cyanide Solutions", Trans. Am. Electrochem. Soc., Vol. 24, 1924, pp. 241-270.

173. H. Kerstein and R. Hoffmann, "The Electrolytic Production of Free Thiocyanate from Alkali Thiocyanates", Ber. Vol. 57, 1924, pp. 491-496.

174. R. Gauguin, "Potentiometric Study of the Reducing Properties of the Thiocyanate Ion", J. Chem. Phys., Vol. 42, 1945, pp. 136-148.

175. R. Gauguin, "Reducing Properties of Thiocyanate and Cyanide Ions - Oxidation-Reduction Potentials of Irreversible Systems", Ann. Chim 1949, pp. 832-835.

176. R. Gauguin, "Electrochemical Oxidation of the Thiocyanate Ion. Application to Determination and the Study of Reactions", Analytica Chimica Acta, Vol. 5, 1951, pp. 200-214.

177. A. Rius and S. T. Alonso, "Anodic Oxidation of Thiocyanate I", Anales Real Soc. Espan. Fis. Y Quim, Vol. 44B, 1948, pp. 1234-1250.

178. A. Rius and S. T. Alonso, "Anodic Oxidation of Thiocyanate II. Polarization Study in an Alkaline Medium", Anales Real Soc. Espan. Fis. Y Quim, Vol. 44B, 1948, pp. 1251-1260.

179. A. Rius and S. T. Alonso, "Anodic Oxidation of Thiocyanate II. Polarization Study in an Alkaline Medium", Anales Real Soc. Espan. Fis. Y Quim, Vol. 45B, 1949, pp. 359-366.

180. M. M. Nicholson, " Voltammetry of Thiocyanate Ion at the Stationary Platinum Electrode", Analytical Chemistry, Vol.31, No. 1, 1959, pp. 128-132.

181. A. J. Calandra, M. E. Martins and A. J. Arvia, "Kinetics of Anodic Reactions of Molten Potassium Thiocyanate on Platinum: Formation and Growth of Anodic Film", Electrochimica Acta, Vol. 16, 1971, pp. 2017-2080.

182. A. J. Arvia, A. J. Calandra and M. E. Martins, "Electrochemical Kinetics of Molten Potassium Thiocyanate on Platinum. Mechanisms of Anodic Film Formation and its Cathodic Dissolution", Electrochimica Acta, 1972, Vol.17, pp. 741-761.

183. C. Martinez, A. J. Calandra and A. J. Arvia, "The Anodic Oxidation of Thiocyanate Ion Dissolved as KSCN in Dimethylsulphoxide", Electrochimica Acta, 1972, Vol. 17, pp. 2153-2179.

184. R. Piereiro, A. J. Arvia and A. J. Calandra, " Kinetics of the $SCN^-/(SCN)_2$ Couple on Platinum in Acetonitrile", Electrochim Acta, 1972, Vol. 17, pp. 1723-1734.

185. D. A. Holtzen and A. S. Allen, "Kinetics Parameters for the Anodic Oxidation of Thiocyanate at the Glassy Carbon Electrode", Anal. Chim. Acta, Vol. 69, 1974, pp. 153-160.

186. O. V. Belyi, L. M. Belaya and N. E. Karalovskaya, "A Potential and Galvanostatic Study of the Electrooxidation of the Thiocyanate Ion on a Stationary Platinum Electrode", Elektrokhimiya, Vol. 11, No. 3, 1975, pp.356-359.

187. L. Yu. Matulyaskene, "Behaviour of Thiocyanate Ions in Cyanide Bath for Electroplating of Copper", Lietuvos Tsr Mokslu Adademitijos Darbai. Serig B, Vol. 3 (100), 1977, pp. 9-15.

188. L. M. Tyrina and A. F. Morozov, "Electrochemical Treatment of Industrial Waste Water Containing Copper Cyanide and Thiocyanate", Khimiia Tekhnologiia Vody, Vol. 4 (5), 1982, pp.462-464.

189. V. K. Varentsov and Z. T. Belyakova, "Oxidation of Cyanide and Thiocyanate Ions in Effluent on Flow Type Plate and Fiber Anodes", Tsvetnye Metally, Vol. 24, No. 3, 1983, pp. 121-122.

190. V. K. Varentsov and Z. T. Belyakova, "Influence of Process Parameters on Oxidation of Cyanide and Thiocyanate Ions on Oxide Anode", Tsvetnye Metally, Vol. 25, No. 2, 1984, pp. 105-106.

191. V. K. Varentsov and Z. T. Belyakova, "Use of Titanium-Based Oxide Anodes in the Electrolytic Purification of Cyanide-Thiocyanate Solutions", Tsvetnye Metally, Vol. 25, No. 10, 1984, pp. 21-22.

192. E. Itabashi, "Identification of Electrooxidation Products of Thiocyanate Ion in Acidic Solutions by Thin-layer Spectroelectrochemistry", J. Electroanal. Chem., Vol. 177, 1984, pp. 311-315.

193. J. J. Byerley and K. Enns, "Electrochemical Regeneration of Cyanide from Waste Thiocyanate for Cyanidation', CIM Bulletin, 1984, pp. 87-93.

194. J. J. Byerley and K. Enns, "Processes for the Recovery of Cyanide from Aqueous Thiocyanate Solutions and Detoxication of Aqueous Thiocyanate Solutions", US Patent 4,526,662, July 28, 1985.

195. J. J. Byerley and K. Enns, "Processes for the Recovery of Cyanide from Aqueous Thiocyanate Solutions and Detoxication of Aqueous Thiocyanate Solutions", US Patent 4,519,880, May 28, 1985.

196. John K. Foley and Stanley Pons, "Fourier Transform Infrared Spectroelectrochemical Studies of Anodic Processes in Thiocyanate Solutions", Langmuir 1985, Vol. 1, pp. 697-701.

197. Zuana Tocksteinova and Fantisek Opekar, "The Electrochemical Generation of Small Amounts of Hydrogen Cyanide", Talanta, Vol. 33, No.8, 1986, pp. 688-690.

198. James A. Cox and Thomas J. Gray, "Controlled Potential Electrolysis of Bulk Solutions at a Modified Electrode: Application to Oxidation of Cysteine, Cystine, Methionine and Thiocyanate", Anal Chem, Vol. 62, 1990, pp. 2742-2744.

199. Eugene Y. Cao, Ping Gao, John Y. Gui, Frank Lu, Donald A. Stern and Arthur T. Hubbard, "Adsorption and Electrochemistry of SCN^-: Comparative Studies at Ag(111), and Pt(111) Electrodes by means of AES, CV, HREELS and LEED", J Electroanal. Chem., Vol. 339, 1992, pp. 311-325.

200. A. Zulauskaite, "Electrochemical Characteristics of System Containing Thiocyanate Complexes of Copper and Tin of Various Oxidation States", Chemija , No. 2, 1991, pp. 31-41.

201. P. Krishnan and V. G. Gurjar, "Electrochemical Thiocyanation by Two Phase Electrolysis", J Appl. Electrochem., Vol. 23, 1993, pp. 268-270.

202. P. Krishnan and V. G. Gurjar, "Electrochemical Oxidation Thiocyanate in a Two-Phase Electrolyte", J. Appl. Electrochem. Vol. 25, 1995, pp. 792-796.

203. T. Loucka and P. Janos, "Adsorption and Oxidation of Thiocyanate on a Platinum Electrode", Electrochimica Acta, Vol. 41, No. 3, 1996, pp. 405- 410.

204. I. G. Casella, M. R. Guascito and G. E. DeBenedetto, "Electrooxidation of Thiocyanate on the Copper-Modified Gold Electrode and Its Amperometric Determination", Analyst, Vol. 123 (6), 1998, pp. 1359-1363.

205. N. N. Greenwood and A. Earnshaw, "Chemistry of the Elements", Chapter 15, Pergamon Press, New York (1990), pp. 851-853.

206. S. I. Zhdanov, "Sulphur", in Encyclopedia of the Electrochemistry of the Elements, A. J. Bard, ed., Vol.4, Marcel Dekker, New York, 1975, pp. 333-335.

207. F. Foerster and A. Friessner, "The Kinetics of Electrolytic Oxidation of Sulphite and Synthesis of Dithionate", Ber., Vol. 35, 1902, pp. 2525-2519.

208. V. A. Friessner, "Electrolytic Oxidation of Sulphite and Synthesis of Dithionate", Z. Electrochemie, Vol. 17, 1904, pp. 266-291.

209. O. Essin, "The Electrolytic Formation of Dithionate", Z. Elektrochem. Angew. Physik. Chem., Vol.34, 1928, pp. 78-84.

210. S. Glasstone and A. Hickling, "A New Volumetric Method for the Estimation of Dithionates", J. Chem. Soc., 1933, pp.5.

211. S. Glasstone and A. Hickling, "Studies in Electrolytic Oxidation. Part III. The Formation of Dithionate by the Electrolytic Oxidation of Potassium Sulphite", J. Chem. Soc., 1933, pp. 829-836.

212. H. Basset and A. J. Henry, "The Formation of Dithionate by the Oxidation of Sulphurous Acid and Sulphates", J. Chem. Soc., 1935, pp. 914-929.

213. T. I. Kunin, V. F. Postnikov and E. F. Derbeneva, "Electrolysis of Aqueous Solutions of Sulphurous Acid", J. Appl. Chem. (Zh. Prikl. Khim.), Vol. 11, 1938, pp. 776-785.

214. I. F. Ivanei, "Electrolysis of an Aqueous Solution of Sulfurous Acid", J. Appl. Chem. (Zh. Prikl. Khim.), Vol. 13, 1940, pp. 181-184.

215. I. F. Ivanei, "Electrolysis Oxidation of Ammonium Sulphite to Ammonium Sulphate", J. Appl. Chem. (Zh. Prikl. Khim.), Vol. 14, 1940, pp. 355-358.

216. K. I. Rozental and V. I. Veselovskii, "The Mechanism and Kinetics of Electrochemical Oxidation of Sulphite by the Method of Anodic Polarography on a Platinum Electrode", Zhur. Fiz. Khim. Vol. 27, 1953, pp. 1163-71.

217. D. A. Bogdanovskii, " The Oxidation of Sulphur Dioxide ", Zh. Fiz. Khim., Vol. 27, 1953, pp. 1195-1207.

218. G. A. Bogdanovskii and A. I. Shlygin "The Mechanism of the Electrolyte Oxidation of Sulphur Dioxide", Zh. FIZ. Khim, Vol. 32, 1958, pp. 418-421.

219. K. A. Lezhneva, T. I. Borisova and M. G. Silinko, "Anodic Oxidation of Sulphur Dioxide on Gold and Platinum-Gold Alloys", Kinetics and Catalysis, Vol. 2, 1961, pp. 775-782.

220. A. I. Shlygin and G. A. Bogdanovskii, "Mechanism of Electrooxidation of Some Compounds on Platinum", Proceedings of the 4th Soviet Conference on Electrochemistry, Moscow, 1956, Vol. 2. pp. 171-174 (translation 1961).

221. G. L. Klyanina and A. I. Shlygin, "Mechanism of the Anodic Oxidation of Sodium Sulphite", Russ. J. Phys. Chem., Vol. 35, 1962, pp. 692-694.

222. E. T. Seo and D. T. Sawyer, "Determination of Sulphur Dioxide in Solution by Anodic Voltammetry and by U V Spectrophotometry", J. Electroanal. Chem., Vol. 7, 1964, pp. 184-189.

223. E. T. Seo and D. T. Sawyer, "Electrolytic Oxidation of Dissolved Sulphur Dioxide at Platinum and Gold Electrodes", Electrochimica Acta, 1965, Vol. 10, 1965, pp. 239-252.

224. T. Loucha, "Adsorption of Oxidation of Sulphur and of Sulphur Dioxide at the Platinum Electrode", J. Electroanal. Chem. Vol.31, 1971, pp. 319-332.

225. K. Wiesener, "The Electrochemical Oxidation of Sulphur Dioxide at Porous Catalyzed Carbon Electrodes in Sulphuric Acid", Electrochimica Acta, Vol. 18, 1973, pp. 185-189.

226. I. P. Voroshilov, N. N. Nechiporenko and E. P. Voroshilova, "Electrooxidation of Sulphur Dioxide at a Porous Graphite Anode", Elektrokhimiya, Vol. 10, 1974, pp. 1316-1315.

227. Z. Samec and J. Weber, "Study of the Oxidation of SO_2 Dissolved in 0.5 M H_2SO_4 on a Gold Electrode - I Stationary Electrode", Electrochimica Acta, Vol. 20, 1975, pp. 403-412.

228. Z. Samec and J. Weber, "Study of the Oxidation of SO_2 Dissolved in 0.5 M H_2SO_4 on a Gold Electrode-II A Rotating Disc Electrode", Electrochimica Acta, Vol. 20, 1975, pp. 413-419.

229. S. A. Anurov, N. V. Keltsev, V. I. Smola and N. S. Torocheshnikov, " The Mechanism of the Adsorption of Sulphur Dioxide on Carbonaceous Adsorbents", Russ. Chem. Reviews (Usp. Khim.), Vol. 46, 1977, pp. 32-49.

230. G. H. Farbman, R. L. Ammon, C. C. Hardman and S. Spewock, "Development Progress on the Sulphur Cycle Water Decomposition Systems", Twelfth Intersoc. Energy Convers. End. Conf., Washington D. C., 1977, pp. 928-932.

231. A. J. Appleby and B. Pichon, "Electrochemical Aspects of the H_2SO_4-SO_2 Thermoelectrochemical Cycle for Hydrogen Production', in Hydrogen Energy System, Proceedings of the 2nd World Hydrogen Energy Conference, Zurich, Switzerland, 21-24 Aug., 1978, pp. 687-797.

232. A. Q. Contractor and H. Lal, "The Nature of Species Adsorbed on Platinum from SO_2 Solutions", J. Electroanal. Chem., Vol. 93, 1978, pp. 99-107.

233. A. Q. Contractor and H. Lal, "The Forms of Chemisorbed Sulphur on Platinum and Related Studies", J. Electroanal. Chem., Vol. 96, 1979, pp. 175-181.

234. A. J. Appleby and B. Pichon, "The Mechanism of the Electrochemical Oxidation of Sulphur Dioxide in Sulphuric Acid Solutions", J. Electroanal. Chem., Vol. 95, 1979, pp. 59-71.

235. C. Audry and M. Voinov, "Inhibition of the SO_2 Electrochemcial Oxidation Reactions on Platinum in Sulphuric Acid Solution", Electrochimica Acta, Vol. 25, 1980. pp. 299-301.

236. P. W. T. Lu and R. L. Ammon, "An Investigation of Electrode Materials for the Anodic Oxidation of Sulphur Dioxide in Concentrated Sulphuric Acid", J. Electrochem. Soc., Vol. 137(12), 1980, pp. 2610-2616.

237. H. Saab and R. Spotnitz, "An Investigation of Electrode Materials for the Anodic Oxidation of Sulphur Dioxide in Concentrated Sulphuric Acid", J. Electrochem. Soc., Vol. 128, 1981, pp. 1298-1299.

238. K. A. Radyushkina, M. R. Tarasevich, O. A. Levina and V. N. Andreev, "Electrolytic Oxidation of Sulphur Dioxide on Cobalt Dibenzotetraazaannulene and Polymers Based on it", Elektrokhimiya, Vol. 181982, pp. 1166-1169.

239. M. R. Tarasevich, V, N. Andreev, V. E. Kazarinov, O. A. Levina and K. A. Radyushkina, "Adsorption and Electrooxidation of Sulphur Dioxide on Platinum", Elektrokhimiya, Vol. 17 1981, pp. 1402-1407.

240. N. A. Urisson, G. V. Shteinberg, M. R. Tarasevich, V. S. Bagotskii, "Electrochemical Oxidation of Sulphur Dioxide at Activated Carbon", Elektrokhimiya, Vol. 19, No. 2, 1983, pp. 243-248.

241. K. A. Spring and J. W. Evans, "An Investigation of Sulphite Ion Oxidation as an Alternative Anodic Reaction in Fluidized Bed Electrowinning or Other High Rate Electrolysis Cells", J. Applied Electrochem., Vol. 15, 1985, pp. 609-618.

242. S.-C. Yen and T. W. Chapman, "Indirect Electrochemical Processes at a Rotating Disk Electrode, Oxidation of Sulfite Catalyzed by Iodide", J. Electrochem. Soc., Vol. 132, 1987, pp. 2149-2155.

243. M. R. Tarasevich and E. I. Khrushcheva, "Electrocatalytic Properties of Carbon Materials", in Modern Aspects of Electrochemistry, No. 19, edited by B. E. Conway, J. O'M Bockris and R. E. White, Plenum Press, 1989, pp. 295-359.

244. G. F. Pace and J. C. Stauter, "Direct Electrowinning of Copper from Synthetic Pregnant Leach Solutions Utilizing SO_2 and Graphite Anodes - Pilot-Plant Results", CIM Bulletin, 1974, pp. 85-90.

245. A. V. Cooke, J. P. Chilton and D. J. Fray, "Anode Depolarisers in the Electrowinning of Copper", Extraction'81, The Institute of Mining and Metallurgy, London, England, 1981, pp. 430-441.

246. K. K. Mishra and W. C. Cooper, "Electrochemical Aspects of the Direct Electrowinning of Copper from Sulphuric Acid Leach Solutions in the Presence of Iron Using Gas Sparging", Anodes for Electrowinning, Proceedings of the Sessions sponsored by the Electrolytic Processes Committee of The Metallurgical Society AIME, AIME Annual Meeting in Los Angeles, California, 1984, pp.13-36.

247. D. J. Robinson, "SO_2 Electrowinning in Copper Hydrometallurgy for Energy Conservation", Journal of Metals, 1984, pp. 43-47.

248. A. V. Cook, J. P. Chilton and D. J. Fray, "Ferrous/Ferric Depolarization in Copper Electrowinning: Mass Transport and Current Efficiency Considerations", Proceedings, AIME Annual Meeting, New York, NY,1985, pp. 111-141.

249. P. Iliev, I. Nikolov, T. Vitanov and E. Budevski, "Influence of Nitrogen Oxides on the Electrocatalytic Oxidation of Sulphur Dioxide", J. Appl. Electrochem., Vol. 22, 1992, pp. 425-428.

250. S. P. Sandoval and K. P. V. Lei, "Evalution of the Ferrous/Ferric-Sulphur Dioxide Anode Reaction for Integration into the Copper Leaching-Solvent Extraction-Electrowinning Circuit", Hydrometallurgy Fundametals, Technology and Innovations, edited by J. B. Hiskey and G. W. Warren, Colorado, 1993, pp. 1091-1105.

251. J. Lee, "Electrochemical Sulphur Dioxide Oxidation with Platinum-Aluminum Electrocatalysis", J. Appl. Electrochem., Vol. 25, 1995, pp. 353-357.

252. S. P. Sandoval, W. J. Dolinar, J. W. Langhans, and K. P. V. Lei, "A Substitued Anode Reaction for Electrowinning Copper', Proceedings of Copper'95, Santiago, Chile, Vol. III, Electrorefining and Hydrometallurgy of Copper, CIM, Montreal, 1995, pp. 423-436.

253. T. Hunger, F. Lapicque and A. Storck, "Electrochemical Oxidation of Sulphite Ions at Graphite Electrodes", J. Appl. Electrochem., Vol. 21, 1991, pp. 588-596.

254. T. Hunger, F. Lapicque, "Electrochemistry of the Oxidation of Sulphite and Bisulfite Ions at a Graphite Surface: An Overall Approach", Electrochimia Acta, Vol. 36, No 5/6, 1991, pp. 1073-1082.

255. C. A. S. Brevett and D. C. Johnson, "Anodic Oxidation of Sulphite, Thiosulphate, and Dithionite at Doped PbO_2-Film Electrodes", J. Electrochem. Soc., Vol. 139, 1991, pp. 1314-1319.

256. V. D. Stankovic, Z. D. Stankovic, M. Rajcic-Vujasinovic, "Electrochemcial Oxidation of Sulphite Ions", ISE 46 th Annual Meeting , 1995, Vol. 2, p.8-05.

257. J. N. Murray and P. G. Grimes, "Methanol Fuel Cell", in Fuel Cells, edited by Editors of Chemical Engineering Progress, American Institute of Chemical Engineers, 1963, pp. 57-65.

258. B. S. Baker, in "Hydrocarbon Fuel Cell Technology", Academic Press, London, 1965, pp. 79-169.

259. Y. B. Vasil'ev and V. S. Bagotskii, "Some Problems in the Electro-oxidation of Organic Materials", in Fuel Cells. Their Electrochemical Kinetics, edited by V. S. Bagotskii and Y. B. Vasil'ev, Institute of Electrochemistry, Academic of Science of the USSR, Consultants Bureau, New York, 1966, pp.77-95.

260. W. Vielstich, "Fuel Cells - Modern Processes for the Electrochemical Production of Energy", translated by D. J. G. Ives, Willey-Interscience, New York, 1970, pp. 76-118.

261. H. Binder, A. Kohling, W. H. Kuhn, W. Linder and G. Sandstede, "Hydrogen and Methanol Fuel Cells with Air Electrodes in Alkaline Electrolyte", in From Electrocatalysis to Fuel Cells, edited by G. Sandstede, University of Washington Press, Seattle, 1972, pp. 131-141.

262. V. S. Bagotzky, A. M. Skundin and E. K. Tuseeva, "Adsorption of Hydrogen and Oxygen and Oxidation of Methanol on Ruthenium Electrodes", Electrochimica Acta, Vol. 21, pp. 29-36.

263. C. Lamy, "Electrocatalytic Oxidation of Organic Compounds on Noble Metals in Aqueous Solution", Electrochimica Acta, Vol. 29, 1984, pp. 1581-1588.

264. F. Kitamura, M. Takahashi and M. Ito, "Oxidation of HCHO and CH_3OH on a Pt Electrode Studied by Polarization Modulation Infrared Spectroscopy", Chemical Physics Letters, Vol. 123, No. 4, 1986, pp. 273-276.

265. A. Kawashima, "Amorphous Alloy Catalysis for Electro-oxidation of Methanol and its Derivatives in a Sulphuric Acid Solution", Materials Science and Engineering, Vol. 99, 1988, pp. 521-5234.

266. A. J. Appleby and F. R. Foulkes, Fuel Cell Handbook, Van Nostrand Reinhold, New York, 1989, pp. 340-350.

267. P. N. Ross, "Characterization of Alloy Electrocatalysis for Direct Oxidation of Methanol: New Methods", Electrochimia Acta, Vol. 36, No. 14, 1991, pp. 2053-2062.

268. S. Swathirajan and Y. M. Mikhail, "Methanol Oxidation on Platinum-Tin Catalysis Dispersed on Poly(3-methyl) Thiophene Conducting Polymer", J. Electrochem. Soc. Vol. 139(8), 1992, pp. 2105-2110.

269. S. R. Wang and P. S. Fedkw, "Pulsed-Potential Oxidation of Methanol I. Smooth Platinum Electrode with and without Tin Surface Modification", J. Electrochem. Soc. Vol. 139(9), 1992, pp. 2519-2525.

270. S. H. Bergens, C. E. Lee, Y. Xing and P. B. Teige, "Controlled Synthesis of Platinum-Ruthenium Catalytic Surfaces of Oxidation of Methanol in Fuel Cells", Proc. Electrochem. Soc. 97-6,(Fundametals and Potential Application of Electrochemical Synthenesis), 1997, pp. 236-247.

271. R. Kartik, T. Mahadevan, J. Srikanth and R. Patabiraman, "Electro-oxidation of Methanol on Carbon Supported Pt + Pervokite Electrodes in Alkaline Solutions", Trans. SAEST, Vol. 31, 1996, pp. 102-108.

272. A. Dowgird, L. Kwiatkowski and M. Radzikowski, "Preparation and Study of Oxide Films on Titanium", Inz. Powierzchni, (1), 1996, pp. 42-52.

273. T. D. Jarvi, and E. M. Stuve, "Fundamental Aspects of Vacuum and Electrocatalytic Reactions of Methanol and Formic Acid on Platimum Surface", Electrocatalysis edited J. Lipkowski, P. N. Ross, Wiley-VCH, New York, 1998, pp. 75-133.

274. G. T. Burstein, C. J. Barnett, A. R. Kucernak and K. R. Williams, "Aspects of the Anodic Oxidation of Methanol", Catal. Today, Vol. 38, pp. 425-437.

275. J. Vereecken, C. Capel-Boute, and R. Winand, "A Study of Anodic Oxidation of Methanol in Sulphuric Acid and its Use for Reducing Energy Consumption in Zinc Electrowinning", ATB Metallurgie (Mons, Belgium), 10(4), 1970, pp. 113-114.

276. P. H. Vining, J. A. Scott, and P. F. Duby, "Aqueous Electrowinning of Metals", U.S. Patent No. 4,279,711, July 21, 1981.

277. P. H. Vining and P. F. Duby, "The Use of Methanol to Reduce Energy Consumption in Electrowinning", TMS Paper Selection No.A80-62, The Metallurgcal Society of AIME, Warrendale, PA 1980.

278. K. Mushiake, N. Masuko and M. Takahashi, "Electrocatalytic Anodes for Zinc Electrowinning by Methanol Depolarization Process in Sulphuric Acid Bath", Journal of Mining and Metallurgy Institue of Japan, Vol. 101, 1985, pp. 787-793.

279. P. Ramachandran, R. M. Meyyappan, K. V. Venkateswaran and R. Srinivasan, "Catalytic Anodes for Electrowinning - Part I: Effect of Methanol Addition", Bulletin of Electrochemistry, Vol.4(6), 1988, pp. 593-595.

280. P. F. Duby and J. A. Scott, "Fuel-Assisted Metal Electrowinning", Energy Reduction Techniques in Metal Electrochemical Processses, edited by R. G. Baustista and R. J. Wesely, Proceedings of a Symposium sponsored by the Electrolytic Process Committee of the Metallurgical Society, held at the TMS-AIME Ann. Meeting in New York, February 24-28, 1985, pp. 339-352.

281. W. J. Plieth, "Nitrogen", Encyclopedia of Electrochemistry of the Elements, Edited by A. J. Bard, Vol VIII, Marcel Dekker Inc., New York, 1978, pp. 322-459.

282. A. R. Despic, D. M. Drazic and P. M. Rakin, "Kinetics of Electrochemcal Oxidation of Ammonia in Alkaline Solutions", Electrochimica Acta, Vol. 11, 1966, pp. 997-1005.

283. H. G. Oswin and M. Salomon, "The Anodic Oxidation of Ammonia at Platinum Black Electrodes in Aqueous KOH Electrolyte", Can. J. Chem., Vol. 41, 1963, pp. 1686-1695.

284. D. Spahibier and G. Wolf, "Anodic Oxdation of Ammonia", Z. Naturforsch., A, Vol. 19, 1964, pp. 614-619.

285. D. W. McKee, A. J. Scarpelline, Jr., I. F. Danzig, and M. S. Pak, "Improved Electrocatalysts for Ammonia Fuel Cell Anodes", J. Electrochem. Soc., Vol. 116 (5), 1969, pp. 562-568.

286. E. L. Simons, E. J. Cairns and D. J. Surd, "The Performance of Direct Ammonia Fuel Cells", J. Electrochem. Soc., Vol.116 (5), 1969, pp. 556-561.

287. K. Sasaki and Y. Hisatomi, "Oxidation and Adsorption of Ammonia on a Platinized Platinum Electrode", J. Electrochem. Soc., Vol. 117, 1970, pp. 758-762.

288. T. Katan and R. J. Galiotto, "Current Efficiencies for the Anodic Oxidation of Ammonia in Potassium Hydroxide Solution", J. Electrochem. Soc., Vol. 110, 1963, pp. 1022-1023.

289. General Electric Co., "Fuel Cell for Generating Electricity", British Patent 1,226,762 (April 7, 1971).

290. J. Ge and D. C. Johnson, "Electrocatalysis of Anodic Oxygen-transfer Reactions: Oxidation of Ammonia at Anodized Ag-Pb Eutectic Alloy Electrode Electrodes", J. Electrochem. Soc., Vol. 142 (10), 1995, pp. 2543-2548.

291. M. Donten, W. Hyk, M. Ciszkowska and Z. Stojek, "Electrooxidation of Ammonia and Simple Amines at Titanium Electrodes Modified with a Mixture of Ruthenium and Titanium Dioxides", Electroanalysis, Vol. 9 (10), 1997, pp. 751-754.

292. M. Olper, "The EZINEX Process- A New and Advanced Way for Electrowinning Zinc from a Chloride Solution", World Zinc '93, Hobart, 10-13 October, 1993, pp.491-494.

293. K. E. Haque and D. J. Mackinnon, "The Halide Mediated Electro-oxidation of Ammonia, Cyanide, Cyanate and Thiocyanate in Mine/Mill Waste Waters", CIM Bulletin, Vol. 89, 1996, pp. 104-106.

294. S. Kotrily and L. Sucha, Handbook of Chemical Equilibria in Analytical Chemistry, Chapter 2, Ellis Horwood Limited, New York, 1985. G. Milazzo, S. Caroli and V. K. Sharma, "Tables of Standard Electrode Potentials", Project of the IUPAC Electrochemistry Commission, John Wiley & Sons, New York, 1978.

295. G. Milazzo, S. Caroli and V. K. Sharma, "Tables of Standard Electrode Potentials", Project of the IUPAC Electrochemistry Commission, John Wiley & Sons, New York, 1978.

296. A. J. Bard, R. Parsons and J. Jordan, "Standard Potentials in Aqueous Solution", IUPAC, 1985.

297. J. S. Newman, Electrochemical Systems, Prentice Hall, New York, second edition, 1991.

298. R. S. Wenger and D. N. Bennion, "Electrochemical Concentrating and Purifying from Dilute Copper Solutions", J. Appl. Electrochem., Vol. 6, 1976, pp. 385-396.

299. J. A. Trainham and J. Newman, "A Flow-Through Porous Electrode Model: Application to Metal Ion Removal from Dilute Streams", J. Electrochem. Soc., Vol. 124, 1977, pp. 1528-1540.

300. D. Yaniv and M. Ariel, "Electrodeposition and Stripping at Graphite Cloth Electrodes", J. Electroanal. Chem. Vol. 79, 1977, pp. 159-167.

301. B. Fleet and S. D. Gupta, "Carbon Fiber Electrode", US patent 4,046,663, Sept. 6 1977; 4,108,754 and 4,108,757, Aug. 22, 1978.

302. J. L. Weininger and B. M. Kim, "Electrowinning of Noble Metals", US. Patent 4,406,752, Sept. 27, 1983.

303. R. Yu. Bek, A. P. Zamyatin and V. K. Varentsov, "Electrochemical Concentration of Metals by Use of Porous Flow-Through Electrodes", Elektrokhimiya (English translation), Vol. 15, 1978, pp. 1978-1545.

304. R. Yu. Bek, A. P. Zamyatin, A. N. Koshev and N. P. Poddubny, "Mathematical Model of the Process of Electrodeposition of Metals in the Pores of a Flow-Type", Izvestiia Sibirskogo Otdelenniia Akademii Nauk SSSR Seriia Khimicheskih Nauk, 1980, pp. 110-115.

305. D. Yaniv and M. Ariel, "Electrodeposition and Stripping at Graphite Cloth Electrodes in A Flow-Through Cell", J. Electroanal. Chem., Vol. 129, 1981, pp. 301-313.

306. S. D. Gupta, J. K. Jacobs and S. Mohanta, "Apparatus for Waste Treatment Equipment", US. Patent 4308122, Dec. 29, 1981.

307. Y. Oren and A. Soffer, "Graphite Felt as an Efficient Porous Electrode for Impurity Removal and Recovery of Metals", Electrochimica Acta, Vol. 28, pp. 1649-1654.

308. J. L. Weininger and B. M. Kim, "Electrochemical Removal of Heavy Metals from Wastewater", Hydrometallurgy, Research, Development and Plant Practice, Proceedings of the 3rd International Symposium and Plant Practice, Atlanta, Georgia, March 6-10, 1983, edited by K. Osseo-Asare and J. D. Miller, pp. 270-279.

309. R. Kammel, H. G. Eran and H. W. Lieber, "Review and Outlook on Continuous Metal Electrowinning and Recovery Process from Aqueous Solution", Proceedings of the Symposium on Electrochemical Process and Plant Design, edited by R. C. Alkire, T. R. Beck and R. D. Varjian, The Electrochemical Society Inc., 1983, Pennington, pp. 647-657.

310. A. P. Zamyatin and R. Yu. Bek, "Effect of Hydrogen Evolution on Gold Electrodeposition Efficiency at Porous Flow-Through Electrodes", Elektrokhimiya (English translation), Vol. 20, 1982, pp. 328-332.

311. A. N. Koshev, V. K. Varentsov and V. G. Kamburg, "Mathematical Modelling of the Electrodeposition of Metals from Multi-component Systems onto Flow-Through Bulk-Porous Electrodes", Izv. Sib. Otd. Aka. Nauk SSSR, Ser. Khim. Nauk, 1984, pp. 24-27.

312. E. Theodoridou, A. D. Jannakoudakis and D. Jannakoudakis, "Electrodeposition of Metals after Cation Exchange on Modified Carbon Fibre Electrodes", Synthetic Metals, Vol. 9, 1984, pp. 19-30.

313. J. Farkas, "An Ecological and Economic Process for Transition Metal Recovery", Journal of Metals, 1985, pp. 72-75.

314. S. N. Atchison, R. P. Burford and D. B. Hibbert, "Chemical Effects on the Morphology of Supported Electrodeposited Metals", J. Electroanal. Chem., Vol. 371, 1994, pp. 137-148.

315. J. Przyluski, A. Darkowski and M. Gabryszewski, "Recovery of Copper from Rinsing Water after Electroplating", The Proceedings of the Second Conference of the Recycle of Metals, Mar. 14, 1994, Amsterdam, pp. 397-402.

316. R. Yu. Bek, and A. P. Zamyatian, "Mass Transfer Coefficient and Area Accessible to Electrolysis in Flow-through Graphite Carbon Electrodes", Elektrokhimiya, Vol. 14, 1977, pp. 1034-1039.

317. K. Kinoshita and S. C. Leach, "Mass Transfer Study of Carbon Felt, Flow-Through Electrode", J. Electrochem. Soc., Vol. 129, 1982, pp.1993-1997.

318. D. Schmal, J. V. Erkel, and P. J. Van Duin, "Mass Transfer at a Carbon Fiber Electrode", J. Appl. Electrochem., Vol. 16, 1986, pp. 422-430.

319. N. Vatista, P. F. Marconi and M. Bartolozzi, "Mass-Transfer Study of the Carbon Felt Electrodes", Electrochimia Acta, Vol. 36, 1991, pp. 339-343.

320. R. Carta, S. Palmas, A. M. Polcaro and G. Tola, "Behaviour of a Carbon Felt Flow-By Electrode, Part I, Mass-Transfer Characteristics", J. Appl. Electrochem., Vol. 21, 1991, pp. 7893-798.

321. C. Oloman, M. Matte and C. Lum, "Electronic Conductivity of Graphite Fibre Fixed-Bed Electrodes", J. Electrochem. Soc., Vol. 138, 1991, pp. 2330-2334.

322. V. G. Levich, Physicochemical Hydrodynamics, translated by Scripta Technica Inc., Prentice Hall Inc., Englewood Cliffs, N.J. 1962.

323. Yu. V. Pleskov and V. Yu. Filinovskii, The Rotating Disk Electrode, translated by H. S. Wroblowa and edited by H. S. Wroblowa and B. E. Conway, 1976.

324. F. Opekar and P. Beran, "Rotating Disk Electrodes", Journal of Electroanalytical Chemistry and Interfacial Electrochemistry, Vol. 69, 1976, pp. 1 - 108.

325. C. Oloman, Electrochemical Engineering Course Notes, University of British Columbia.

326. J. F. Zemaitis, Jr., D. M. Clark, M. Rafal and N. C. Scrivner, "Handbook of Aqueous Electrolyte Thermodynamics -Theory & Application, American Institute of Chemical Engineers, New York, 1986.

327. K. S. Pitzer and J. J. Kim, "Thermodynamics of Electrolytes. IV. Activity and Osmotic Coefficients for Mixed Electrolytes", J. Am. Chem. Soc., Vol. 96, 1974, pp. 5701-5705.

328. K. S. Pitzer, Activity Coefficients in Electrolyte Solution, 2nd edition, CRC Press, Boca Raton, Florida, 1991.

329. R. A. Robinson and R. H. Stokes, Electrolyte Solutions, 2nd edition, Academic Press Inc., New York, 1965.

330. D. R. Lide and H. V. Kehiaian, CRC Handbook of Thermophysical and Thermochemical Data, CRC Press, Boca Raton, Florida, 1994.

331. J. Kielland, "Individual Activity Coefficients of Ions in Aqueous Solutions", J. Am. Chem. Soc., Vol. 59, 1937, pp. 1675-1678.

332. P. Henderson, Z. Physik. Chem., Vol. 59, 1907, p. 118 and Vol. 63, p. 325.

333. A. J. Bard and L. R. Faulkner, Electrochemical Methods- Fundamentals and Applications, John Wiley & Sons, New York, 1980.

334. K. Kinoshita, Chemical and Surface Properties in Carbon - Electrochemical and Pysicochemical Properties, John Wiley & Sons, New York, 1988, pp. 86-173.

335. J. O'M. Bockris, Modern Aspects of Electrochemistry, No. 1, Chapter 4, edited by J. O'M. Bockris and B. E. Conway, Butterworths, London, 1954.

336. J. O'M. Bockris and A. K. N. Reddy, Modern Electrochemistry, Vol. 2, Chapter 9, Plenum Press, New York, 1970.

337. J. M. Lancaster and R. S. Murray, "The Ferricyanide-Sulphite Reaction", J. Chem. Soc. (A), 1971, pp. 2755-271.

338. N. J. Csikai and A. J. Barnard, Jr., "Determination of Total Cyanide in the Thiocyanate-Containing Wasterwater", Aanl. Chem. Vol. 55, 1983, pp. 1677-1682.

339. R. Pribil, Classification of EDTA Complexes, in Applied Complexometry, Vol. 5, Chapter 6, translated by R. Pribil and M. Stulikova, edited by R. A. Chalmers, Pergamon Press , New York, 1982, pp. 149-153.

340. D. C. Harris, Quantitative Chemical Analysis, Third Edition, W. H. Freeman and Company, New York, 1991, pp. 401 - 411.

341. R. Dolhez, "The Existence of Copper (III) Oxide II", Bull. Soc. Roy. Sci. Liege, Vol. 30, 1961, pp. 446-451.

342. A. M. Shams El Din and F. M. Abd El Wathab, "The Behaviour of the Copper Electrode in Alkaline Solutions upon Alternate Anodic and Cathodic Polarization", Electrochemica Acta, Vol. 9, 1964, pp. 113-121.

343. B. Miller, "Split-Ring Disk Study of the Anodic Processes at a Copper Electrode in Alkaline Solution", J. Electrochem. Soc., Vol. 116, 1969, pp. 1675-1980.

344. F. Beck and U. Barsch, "Formation and Cathodic Re-reduction of Cu (III) States in Y-Ba-Cu Perovikse", J. Electroanal. Chem., Vol. 282, 1990, pp. 175-187.

345. D. Meyerstein, F. M. Hawkride and T. Kuwana, "On the Spectroelectrochemical Characterization of the Electrocatalytic Oxidation of Cu(II) Ethlenediamine", J. Electroanal. Chem., Vol. 40, 1972, pp. 377-384.

Appendix 1 Initial Economic Assessment

The economic assessment of the copper electrowinning process for gold extraction is based on the process mass balance and process data (shown in calculation section). The costs of capital, maintenance and labour are estimated based on similar hydrometallurgical plant values. The compositions and some properties of treated ore are listed in Table 1. The values of the materials involved are listed in Table 2.

Table 1 Compositions and properties of ore

Au	Soluble Cu	Compound of Cu	Recovery of Au	Recovery of Cu	Cyanide consumption	Recoverable cyanide
2 g/tonne	2 kg/ tonne	½ Cu_2S ½ CuO	90 %	90 %	5.4 kg/ tonne	4.63 kg/tonne

Table 2 Values of the materials involved

Au	value of cyanide consumed	Economic potential without recovery of NaCN and Cu	Value of recovered Cu	recycled cyanide value	Economic potential with recovery of NaCN and Cu
14.4 $/tonne	7.02 $/tonne	7.45 $/tonne	2.97 $/tonne	6.02 $/tonne	16.44 $/tonne

From Table 2, if complexed copper cyanide and cyanide are not recovered, the total economic potential is only 7.45 $/tonne ore and the economics of the gold extraction process are poor due to the cost of gold recovery process. If copper and cyanide are recovered, the total economic potential is about 16.44 $/tonne ore, much higher than the former. The costs for direct electrowinning process are listed in Table 3. The total potential benefit is 15.01 $/tonne ore if copper and cyanide are recovered using direct electrowinning process.

Table 3 Cost of direct electrowinning process

Power	Reagents	Maintenance	Capital cost	Labour cost	Total cost	Net benefit
0.167 $/ kg Cu	0.126 $/ kg Cu	0.08 $/ kg Cu	0.335 $/ kg Cu	0.167 $/ kg Cu	0.80 $/ kg Cu	15.01 $/ tonne ore

The costs for solvent extraction-electrowinning are listed in Table 4. The potential economic potential benefit is about 14.12 $/tonne

Table 4 Cost of solvent extraction-electrowinning process

Cost of electrowinning	Cost of solvent extraction	Cost of AVR	Total cost	net benefit
0.59 $/ kg Cu	0.464 $/ kg Cu	0.23 $/ kg Cu	1.29 $/ kg Cu	14.12 $/ tonne ore

Conclusions

The initial economic assessment of the copper electrowinning process for the gold extraction process was conducted based on the mass balance. The economic benefit with the recovery of leached copper and the recycle of complexed cyanide is much higher than that without the recovery of copper cyanide. The developed copper electrowinning processes would greatly benefit the gold extraction process.

Calculation

The flowsheet of developed gold extraction process is shown below:
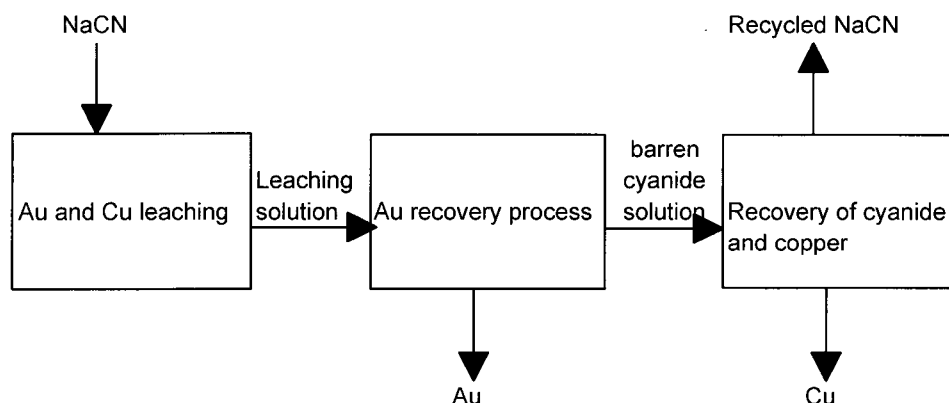
Reagents:	NaCN	Au	Cu	NaOH	Na_2SO_3	H_2SO_4	CaO
Price ($/kg)	1.3	8040	1.65	0.1	0.1	0.025	0.057
Molecular weight (g/mole):	49.01	197	63.54	39.998	126.04	98.076	56

Reagents:	XI 78	Solvessi:	Exxsol D-80:
Price ($/kg)	5 (per liter	1(/liter)	1(liter)

The prices of NaCN, NaOH, H2SO4 and CaO are from Chemical Marker Reported,

The prices of Na2SO3 is based on the consumption of sulphur and sodium hydroxide.

the prices of Au and Cu are from Financial Post, the prices of XI78,Solvessi annd Exssol D-80 from Henkel C

	Au	Cu
Contents in ore (kg/ton):	0.002	2

Half copper soluble in cyanide solution is CuO and the other is Cu_2S

Leaching reaction (Au cyanidation is neglected):

$2CuO + 7\ NaCN + H_2O\ = 2\ Na_2Cu(CN)_3 + NaCNO + 2\ NaOH$

$Cu_2\ S + 7\ NaCN + H2O + 1/2O_2 = 2\ Na_2Cu(CN)_3 + NaCNS + 2\ NaOH$
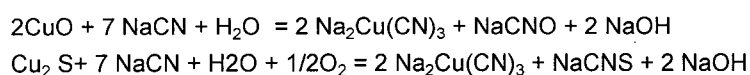
Cyanide consumption: 1 mole Cu consumes 3.5 mole NaCN

Cyanide consumption per ton ore: 5.40 kg/ tonne ore

Value for cyanide consumption: 7.02 $/tonne ore

Recovery for Au:	0.90	
Extractable Au:	0.0018	kg/tonne ore
Value of Au:	14.47	$/tonne ore

If cyanide and copper are not recovered,

Total economic potential :   7.45 $/tonne ore

If cyanide and copper are recovered,

Recovery for Cu:	90.00%	
Extracted Cu:	1.80	kg/ tonne ore

Value of extracted Cu   2.97 $/tonne ore
Recycled cyanide: 4.63 kg/ tonne ore
Value of recycled cyanide: 6.02 $/tonne ore
Value for Cu and cyanide: 8.99 $/tonne ore
Total economic potential: 16.44 $/tonne ore

Cost for copper direct electrowinng process

The flowsheet of copper direct electrowinning processs is shown below:

Composition of barren cyanide leach solution:
Cu: 1 g/l
CN:Cu: 3
NaOH: 0.4 g/l
SCN⁻;   0.5 g/l

Power for electrowinning:

Cell reaction

$(4/x)NaOH$ (anolyte) $+ 4 Na_2(Cu(CN)_3 = (1/x)O_2 + 12 NaCN + 4 Cu + (2/x)H_2O + (4/x - 4) NaOH$ (catholyte)
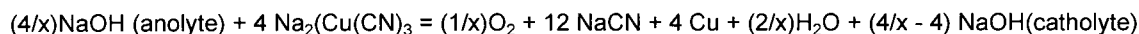
where x = current efficiency for Cu

Current density :   60 A/m^2
Current efficiency: 50.00%
Cell voltage   3 V
Power consumption: 2.53 kwh/kg Cu
Power price: 0.06 $/kwh

Power cost: 0.15 $/kg/Cu

Power for electrorefining:
Reaction of electrorefining (in sulphate solution):
Anode: $Cu = Cu^{2+} + 2e$
Cathode: $Cu^{2+} + 2e = Cu$
Current density: 250 A/m^2
Current efficiency: 100.00%
Cell voltage: 0.3 V
Power consumption: 0.253 kwh/kg Cu
Power cost: 0.015 $/kg Cu
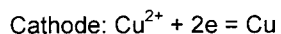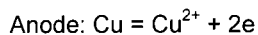
Total power cost: 0.167 $/kg Cu

Reagent: NaOH

Consumption of NaOH :	2 mole NaOH/mole Cu
	1.259 kg NaOH/kg Cu
Value of NaOH:	0.126 $ NaOH/kg Cu

Capital cost for electrowinning

Cathode cost:	300 $/m^2
Anode cost:	200 $/m^2
Membrane Cost:	800 $/m^2
Miscellaneous	100 $/m^2

| Total for electrowinning: | 1400 $/m^2 |

Capital cost for electrorefining:

Cathode cost:	300 $/m^2
Cell cost:	200 $/m^2
Miscellaneous:	100 $/m^2
Total for refining:	600 $/m^2

| Total for electrowinning & refini | 2000 $/m^2 |

Assume the life of plant:	10 years
Capital cost per year:	200 $
Working days per year:	350 days/year
Cu produced per year	597.34 kg
Capital cost for Cu:	0.335 $/kg Cu

| Maintenance Cost: | 50 $/m^2 year |
| Maintenance Cost for Cu: | 0.08 $/kg Cu |

| Labour cost: | 50 $/m^2 year |
| Labour cost for Cu: | 0.08 $/kg Cu |

| Total cost: | 0.80 $/kg Cu |

| Benefit | 15.01 $/tonne ore |

Cost for solvent extraction - electrowinning process

The flowsheet of solvent extraction - electrowinning process is shown below:
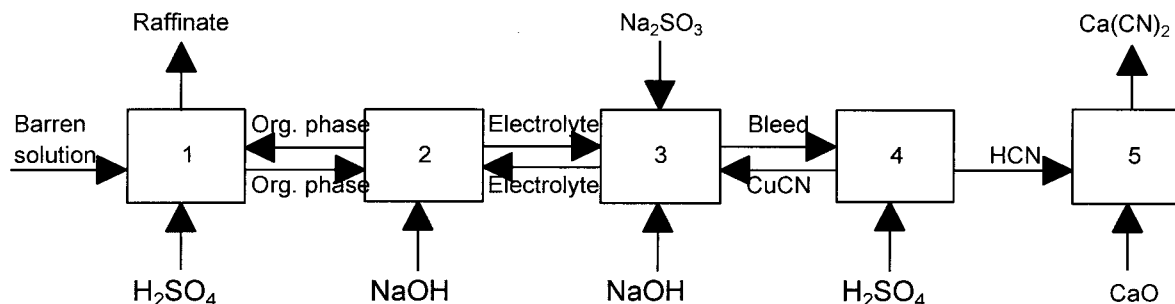
where 1 -Loading, 2 - stripping, 3 - electrowinning, 4 - acidification - volatilization, 5 - neutralization

The process consists of solvent extraction (loading -1 and stripping - 2), electrowinning (3), and acidification - volatilization - regeneration (acidification - 4, netrualization - 5)

(1) Cost for electrowinning:
Power

Current density:	100	A/m^2
Current efficiency for Cu:	95.00%	
Current efficiency for sulphite:	90.00%	
Cell voltage:	1.7	volts
Power consumption:	0.755	kwh/kg Cu
Power price:	0.060	$/kwh
Power cost:	0.045	$/kg Cu

Reagents: sulphite, NaOH
Reaction for electrowinning:

$(y/x)Na_2SO_3 + 2Na_2Cu(CN)_3 + 2NaOH + 2(1/x-1)H_2O = (y/x)Na_2SO_4 + 2Cu + (6-(1-y)/x)NaCN + (1/x-1)H_2$
$+((1-y)/x)NaCNO$
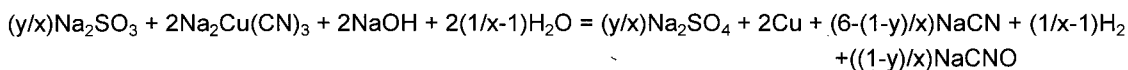
where x - copper current efficiency, y - sulphite anodic current efficiency

Composition of electrolyte:

Cu:	70	g/l
NaOH:	4	g/l
CN:Cu mole ratio:	3	
Na$_2$SO$_3$:	30	g/l
SCN$^-$:	40	g/l
CN:Cu mole ratio for precipitate:	0.5	(after acidification-volatization-regeneration)

Consumption of NaOH:	1	mole NaOH/mole Cu (for anodic reaction)
	0.63	kg NaOH/kg Cu
Consumption of Na$_2$SO$_3$:	0.95	mole Na$_2$SO$_3$/mole C (for anoidic reaction)
	1.88	Kg Na$_2$SO$_3$/kg Cu
Bleed:	16.55	liters/kg Cu
Consumption of NaOH:	0.07	kg NaOH/kg Cu (for bleed)

Consumption of Na$_2$SO$_3$:   0.50 kg Na$_2$SO$_4$/kg Cu   (for bleed)

Value of NaOH: 0.07 $/kg Cu   (for electrowinning)

Value of Na$_2$SO$_3$:   0.24 $/kg Cu   (for electrowinning)

Consumption of NaCN: 0.11 mole NaCN/mole Cu

      0.081 kg NaCN/kg Cu

Value of NaCN: 0.11 $/kg Cu

Reagent cost for electrowinning: 0.41 $/kg Cu

Capital cost:

Anode cost: 200 $/m^2

Cathode cost: 400 $/m^2

Cell cost: 200 $/m^2

Miscellaneous cost: 200 $/m^2

Total capital cost: 1000 $/m^2

Assume the life of plant   10 years

Capital cost per year: 100 $/year

Working days per year: 350 days/year

Cu production rate: 1891.58 kg Cu/year

cost for Cu: 0.053 $/kg Cu

Maintenance cost: 100 $/year

Maintenance cost for Cu   0.05 $/Cu

Labour cost: 50 $/m^2 year

Labour cost for Cu: 0.026 $/kg Cu

Total cost for electrowinning: 0.59 $/kg Cu

(2) Solvent-extraction:

Reagents:

Loading reaction:

Na$_2$Cu(CN)$_3$ +2R$_4$NOAr (org.) + 1.5H$_2$SO$_4$ = (R$_4$N)$_2$Cu(CN)$_3$(org.) + 2HOAr(org.) + 1.5Na$_2$SO$_4$ + 2H$_2$O
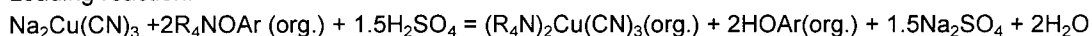
where, R$_4$N - solvent extractant,

Stripping reaction:

(R$_4$N)$_2$Cu(CN)$_3$(org.) + 2HOAr + 2NaOH = Na$_2$Cu(CN)$_3$ +2R$_4$NOAr(org.) + 2H$_2$O
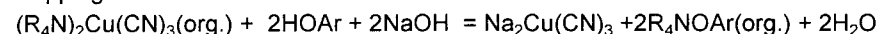
Consumption of H$_2$SO$_4$:   1 mole H$_2$SO$_4$/ mole C   (for solvent extraction)

      1.54 kg H$_2$SO$_4$/kg Cu

Value of H$_2$SO$_4$:   0.04 $ H$_2$SO$_4$/kg Cu

Consumption of NaOH: 2 mole NaOH/mole Cu (for stripping)

      1.26 kg NaOH/kg Cu

Value of NaOH: 0.13 $ NaOH/kg Cu

Composition of barren solution: 1 g/l Cu

Extraction efficiency for Cu: 99.00%

Volume of barren solution: 1010.10 liters/kg Cu

Loss of of organic phase: 0.0001 liter/liter barren solution

Loss of of organic phase for Cu: 0.10 liter/kg Cu

Composition of organic phase:

XI 78:   12%

Exxsol D-80:   70%
Solvessi: 18%

Consumption of XI 78:   0.012 liter/kg Cu
Value of XI 78   0.061 $/kg Cu
Consumption of Exxsol D-80:   0.071 liter/kg Cu
Value of Exxsol D-80:   0.071 $/kg Cu
Consumption of Solvesso: 0.018 liter/kg Cu
Value of Solvesso: 0.018 $/kg Cu
Cost of organic phase: 0.149 $/kg Cu

Total cost of reagent for SX: 0.314 $/kgCu

Capital cost: 0.050 $/kg Cu
Maintenance cost: 0.050 $/kg Cu
Labour cost: 0.050 $/kg Cu

Total cost for solvent extraction: 0.464 $/kg Cu

(3) Cost for acidfication volatilization regeneration (AVR):
Reagents: sulphuric acid, lime
Acidification reaction:
$2NaCN + H_2SO_4 = 2HCN + Na_2SO_4$
Consumption of H_2SO_4:   1.5 mole H_2SO_4/mole Cu
                                     2.32 kg H_2SO_4/kg Cu
Value of H_2SO_4:   0.06 $/kg Cu
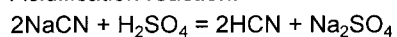
Neutralization reaction:
$2HCN + CaO = Ca(CN)_2 + H_2O$
Consumption of CaO: 1.5 mole CaO/mole Cu
                                     1.32 kg CaO/kg Cu
Value of CaO: 0.075 $/kg Cu
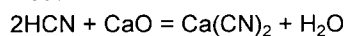
Capital cost :   0.05 $/kg Cu
Maintenance cost: 0.05 $/kg Cu
Labour cost: 0.05 $/kg Cu

Total cost for AVR: 0.23 $/kg Cu

Total cost for SX-EW: 1.29 $/kg Cu

Benefit: 14.12 $/tonne ore

Appendix 2 Total Cyanide Analysis

Introduction

This method for total cyanide analysis consists of (1) the separation of cyanide from solutions as HCN by distillation at pH 4 in the presence of EDTA, (2) absorption of HCN gas in caustic solution and (3) titration with silver nitrate. EDTA strongly complexes transition metal cations and helps facilitate dissociation of cyanide from the metals. The method is largely based upon a published procedure [338].

A commonly applied distillation method involves the use of a sulfuric acid-$MgCl_2$ solution. Thiocyanate in such a system decomposes to form COS and other species. This in turn hydrolyzes to form sulfide, which in the basic absorber solution is oxidized to form elemental sulfur. Ultimately, these sulfur species react with cyanide to reform thiocyanate, which results in a negative interference, or the sulfide may react with silver during the titration to give a black precipitate, obscuring the endpoint. The use of a pH 4 distillation solution minimizes thiocyanate hydrolysis. Thiocyanate can also react with oxidants such as nitrate to form cyanide and sulfate, a positive interference. This can be overcome with sulfamic acid (NH_2SO_3H) which acts as a reducing agent. Free sulfide interferes by distilling as H_2S. This causes essentially the same problem as thiocyanate hydrolysis to COS mentioned earlier. In addition, sulfide in the sample may be oxidized to elemental sulfur which then consumes cyanide as above. Copper above a threshold concentration causes losses of cyanide also. This can be overcome by using small amounts of sample. Sulfite in the presence of copper significantly lowers the amount of cyanide recovered in the distillation. Barium chloride can be used to precipitate sulfite as $BaSO_3$. $BaSO_3$ is removed from the sample before distillation by centrifugation or filtration, since $BaSO_3$ is soluble in acid solution. Thiosulfate if present in sufficient amount can interfere by hydrolyzing during distillation to form sulfur dioxide and possibly other reduced sulfur species.

Some metal cyanide complexes, most notably those of Co and Au do not liberate cyanide during the distillation involving EDTA. It may be that some of the cyanide bound to

mercury is not liberated either. If samples are high in mercury, a test with a mercury cyanide solution should be done to see what kind of recoveries are achieved.

Sample Preservation and Handling

Ideally the sample should be analyzed right after it is collected. This is not always practical. In order to preserve the sample it should be treated with NaOH such that the pH is >12. The sample should then be stored in a refrigerator in the dark. Under these conditions it can keep for several weeks. To prevent sulfide interference the sample must be treated with a metal salt such as $Pb(O_2CCH_3)_2$ or $PbCO_3$ or $CdCO_3$ etc. to precipitate a metal sulfide. The sample must then be filtered right away to remove the solid since freshly formed metal sulfides are prone to air oxidation, again forming elemental sulfur. The treatment to remove sulfide should be done prior to adjusting the basicity of the sample.

Apparatus and Reagents

A diagram of the distillation apparatus is shown in Figure 1. Ground glass joints are preferred for all connections, but rubber stoppers, wrapped with teflon tape, are also suitable. All connections involving ground glass joints only should be lightly greased with silicone grease. Connections involving rubber stoppers should not be greased.
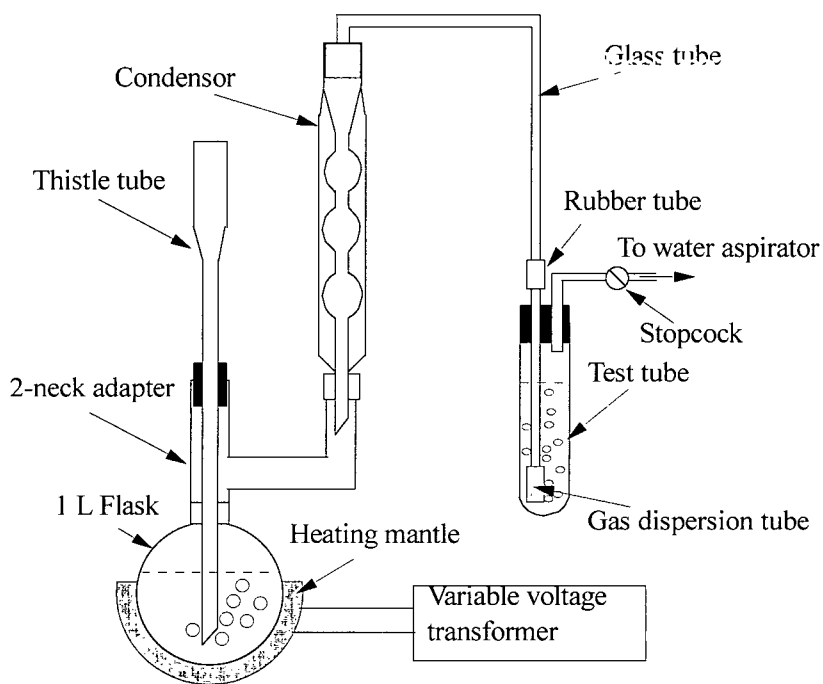
Figure 1 Schematic diagram of distillation

The following is a list of equipment for the distillation:

-variable voltage transformer

-heating mantle (e.g. 380 watts)

-1-L round bottom flask with ground glass standard taper 24/39 joint or equivalent

-magnetic stirring plate

-teflon coated magnetic stir bar

-glass beads (3-5 mm)

-two-neck adapter, with standard taper 24/39 joints

-thistle tube, seated snugly in #5 rubber stopper, teflon taped

-water cooled condensor (preferably Allihn type, but a straight tube condensor will do), fitted inside #5

 stopper, teflon taped

-glass tube, ~6mm i.d., seated in rubber stopper (as per diagram)

-coarse porosity gas dispersion tube fitted into a two-hole #8 rubber stopper

-butyl or neoprene rubber tubing to connect glass tube and dispersion tube

-38 X 200 mm test tube

-water aspirator (a manifold having at least six lines can be attached to a single aspirator)

-tubing and stopcock or needle valve connected to aspirator and the #8 stopper (see diagram)

-centrifuge (eg 3000 rpm) with capacity for 50-mL sample tubes

-centrifuge tubes, plastic, 50 mL

The titration requires the ability to dispense small volumes, readable to within 0.001 mL, or less preferably 0.01 mL. This is accomplished with an autotitrator. The following equipment for the titration is used for titration:

-Radiometer ABU 80 Autoburrette, equipped with a 10-mL buret, or equivalent equipment

-250-mL Erlenmeyer flask

-magnetic stirring plate

-teflon coated magnetic stir bar

The following analytical reagent grade and deionized water are used through the analysis:

-deionized water

-0.25 M NaOH (10 g/L)

-1 M NaOH (40 g/L)

-0.2 M $BaCl_2$ solution (49 g/L)

-sulfamic acid (NH_2SO_3H)

-$Na_2EDTA\cdot2H_2O$

-methyl red indicator (1 g/L in ethanol, 95%)

-acetate buffer (54 g $NaO_2CCH_3\cdot3H2O$ + 100 mL glacial acetic acid, to 1 L, pH adjusted to 4.00 with
 NaOH)

-0.018 M $AgNO_3$ solution (3.06 g/L); prepare weekly and store in a glass vessel in the dark.

-*p*-dimethylaminobenzal rhodanine indicator (200 mg/L in acetone)

-standard NaCl solution (0.04 M = 2.3377 g/L prepared every two weeks from NaCl, powdered and dried 24 hours at 120°C)

-chromate indicator (50 g/L K_2CrO_4)

Procedure

Preserve the sample upon collection as outlined in the appended material. The presence of sulfide can be ascertained by dipping a piece of lead acetate test paper moistened with pH 4 buffer into a portion of the sample. If the paper turns brown or black, PbS has formed and sulfide is present. If sulfide is determined to be present, the sample should be treated to remove it right away. Once this has been accomplished, adjust the alkalinity of the sample, if necessary, so that the pH is above 12. Store samples in tightly sealed plastic bottles in a refrigerator and in the dark.

Set up the distillation apparatus as shown in Figure 1, but do not attach the round bottom flask yet. Add 50 mL of 0.25 M NaOH to the absorber test tube. Attach this to the glass tube by means of a 2-3 cm length of rubber tubing. Make sure all connections are secure. Add a teflon stir bar (2 cm) and ~5 glass beads (3-5 mm) to the flask. Add enough deionized water to the flask such that the volume of water plus sample in the flask will be ~500 mL Add enough 1 M NaOH to ensure than the pH is above 12. Mix well.

Make an appropriate dilution of the sample as required such that a convenient volume will contain at least 0.5 mg of cyanide (but preferably 1 mg or more) as CN, and not more than 5 mg of copper. Copper acts to lower the amount of cyanide recovered, perhaps by oxidation. The sample should be added to a solution of NaOH such that the pH of the final solution will be >12. If the sample also contains sulfite, $BaCl_2$ must be added during the dilution step. The amount of Ba^{2+} added should exceed the sulfite concentration by a factor of at least five. If there is much sulfate present, the Ba^{2+} should exceed the sulfite plus sulfate by >5 times. If need be, a more concentrated solution of $BaCl_2$ may be used. Add the $BaCl_2$ solution after the sample has been added to the NaOH solution. Mix well and make up to volume. The volume occupied by the solid precipitate will be negligible if the sulfite plus sulfate content is not greater than the cyanide content. Centrifuge the sample to settle out the precipitate. The time required depends on the speed of the centrifuge. The supernatant liquid should be clear. If need be the sample may be filtered instead. A 0.2 um pore size membrane filter (nylon or teflon) should suffice. Pipette a portion of the centrifuged or filtered sample into the round bottom flask.

Attach the flask containing the sample to the rest of the apparatus. Start the air purge by adjusting the valve or stopcock attached to the absorber. The rate of bubbling should be about 3-4 bubbles per second. A froth should form on the absorber solution that is about 0.5 cm thick. Gently stir the solution. Add 2 g of sulfamic acid through the top of the thistle tube. Wash it in with water. Stir until dissolved. Add 5 g of $Na_2EDTA\cdot2H_2O$ and stir until dissolved. A fine white precipitate might gradually form, probably the protonated EDTA. Add 6 drops of methyl red indicator. Wash this in. If the solution turns red, it is acid with respect to methyl red. In this case add 1 M NaOH until the colour becomes just pale orange. If the solution turns faint yellow upon adding the indicator, it is relatively basic. If this occurs add 0.5 M H_2SO_4 until the colour is again faint orange. Finally add 55 mL of the acetate buffer and wash this in.

Stop the stirring and put the heating mantle in place. Heat the solution to boiling. It is better to heat the solution at high heat (e.g. full power with the 380 watt heating mantles) for an initial period of time and then to back off the power a few minutes prior to boiling commencing. At the onset of boiling the flask fills with vapours and this can cause liquid to rise in the thistle tube. This should be avoided. Adjust the air suction rate if necessary. Once boiling has stabilized readjust the suction rate if need be to keep a froth on the absorber solution that is about 0.5 cm thick. Adjust the heat such that the reflux rate is about 2-3 drops per second from the condensor and the vapours do not rise more than ~3/4 of the way up the condensor. Reflux the solution for 2 hours. Check occasionally to be sure the system is stable. After two hours remove the heating mantle and continue the air purge for at least 15 minutes.

Remove the thistle tube. Turn off the aspirator suction and break the connection between the absorber and the aspirator tubing. Detach the absorber from the glass tubing. Quantitatively transfer the contents of the absorber into a 250-mL Erlenmeyer flask. The gas dispersion tube should be rinsed thoroughly with deionized water, e.g. with the use of a large pipet bulb to flush it. Rinse the glass connecting tube with a little water also and pour this into the Erlenmeyer flask. Make up the volume of the solution to about 150 mL. Add 15 drops of rhodanine indicator solution. Titrate the solution with standardized 0.018 M $AgNO_3$

solution until the yellow colour turns into a light orange-pink. The endpoint is sharp and clear, even though the colours are light. It is recommended that the analyst practice the procedure on an NaCN/NaOH solution which is analyzed by titration with and without distillation. The results should agree within about 99% after some familiarization.

A blank correction is required. Pour about 50 mL of 0.25 M NaOH into a 250-mL Erlenmeyer flask. Add enough water to make the volume ~150 mL. Add 15 drops of rhodanine indicator solution and titrate with 0.018 M NaOH as above. With a little practice blank values of <0.1 mL can be achieved routinely. The titration reaction and calculation are:

$$Ag^+ + 2CN^- = Ag(CN)_2^-$$
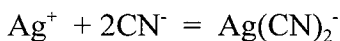
$$[CN^-] = \{[AgNO_3] \times (Vt\text{-}Vb) \times 2 \times DF\}/Vs$$

[CN⁻] = cyanide content (mol/L; multiply by 26.018 for CN in g/L)

[AgNO₃] = silver titrant concentration (mol/L)

Vt = titration volume (mL)

Vb = blank correction volume (mL)

Vs = sample volume (mL)

DF = dilution factor

The silver nitrate solution may be standardized by any convenient method. Check this daily. One way is titration with standardized NaCl. Sodium chloride can be dried in an oven at 120 °C for 24 hours and stored in a desiccator. Pipette 4.00 mL of 0.04 M NaCl into a beaker. Add 12 mL of water. Add 0.50 mL of the chromate indicator. Titrate the solution with the 0.018 M AgNO₃ until the lemon yellow colour turns into a more ochre yellow. The change is subtle, but distinct. At the endpoint Ag_2CrO_4 forms, which is a dark red solid. Potentiometric endpoint detection may also be employed. Again a blank correction is required. An adequate blank titration may be made by adding 25 mL of water to a beaker and 0.25 g of $CaCO_3$. The latter provides a white background similar to that formed by AgCl during the standardization. Add 0.50 mL of chromate indicator. Titrate as above. Blank

values of ~0.1 mL may be anticipated. The stoichiometry for the standardization is one to one:

$Ag^+ + Cl^- = AgCl$
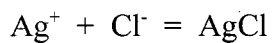
$[Ag^+] = \{[Cl^-] \text{ X } 4\}/\{Vt\text{-}Vb\}$

4 = volume of chloride standard (mL)

[Ag+] = silver concentration (mol/L)

[Cl-] = standard chloride concentration (mol/L)

Vt = titration volume (mL)

Vb = blank correction volume (mL)

Once the cyanide titration is completed, the apparatus should be thoroughly rinsed with deionized water. It is then ready for the next analysis.

Appendix 3 Copper Titration using EDTA

1. Method

Excess EDTA is added to a copper solution (all Cu in +2 state; no strong complexing agents present). The residual EDTA is titrated with standardized Zn^{2+} using xylenol orange as the indicator. The pH must be controlled at 5 - 5.5 or else the indicator will not respond properly [339].

2. Reagents

0.015 M EDTA solution (Na_2EDTA $2H_2O$ (over 99.7 %) is dried at 80 °C for several hours to remove residual traces of water)

0.2 % xylenol orange solution as indicator

1 M sodium cyanide solution

1 g/L zinc nitrate standard solution

solid hexamine

3. Procedure

Standardization of EDTA

Pipette 5 mL of EDTA solution to a 250-mL beaker with a stir bar and make up 70 mL solution, add solid hexamine (0.1g) to the beaker, measure the pH with a calibrated pH probe (pH 7 and 4 buffers), adjust the pH of the solution to 3 to 4 with 1 M NaOH , add about 0.1 g solid hexamine (avoid adding much hexamine because it competes with EDTA for metal ions at too high concentration), adjust the pH to 5.5 with 0.1 - 1 M HCl or 1 M NaOH as required, add 3 drops of xylenol orange solution (the solution become yellow) and finally is titrated with zinc nitrate standard solution from a yellow or yellowish colour to pink. Throughout the titration maintain the pH at 5.0 - 5.5.

Copper titration

An excess of EDTA solution is added to an acid sample solution containing 2 - 10 mg copper to 250-mL beaker and make up 70 mL solution, insert the pH probe. Adjust the pH 3 - 4. Add 0.1 g solid hexamine . pH is adjusted to 5.5 with sodium hydroxide. Add xylenol orange indicator, back titrated with zinc nitrate solution from yellow to pink.

Blank Correction

Add 70 mL of water to a 250-mL beaker containing a stir bar. Add 0.1 g hexamine. Insert the pH probe. Adjust the pH to 5.5. Add 2 drops of the xylenol indicator. Titrate to a pinkish-purple colour with Zn^{2+}. A value of about 0.006 mL was obtained. To get a better idea of the blank in the presence of copper, titrate the blank solution with a combination of $Zn^{2+} + Cu^{2+}$ each at 0.0075 M. The concentration need not be known with high precision since the blank error is small.

Appendix 4 Determination of Sulphite Ions by the Iodimetric Method

1. Method

The iodimetric determination is based on the following equations [340]:

$$SO_3^{2-} + I_2 + H_2O = SO_4^{2-} + 2H^+ + 2I^-$$

$$HSO_3^- + I_2 + H_2O = SO_4^{2-} + 3H^+ + 2I^-$$
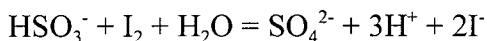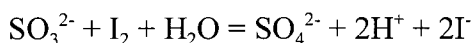
Molecular iodine is only slightly soluble in water (0.0013 M at 20 $^{\circ}$C), but its solubility is greatly enhanced by complexation with iodide.

$$I_2(aq) + I^- = I_3^- \qquad K = 0.007$$

Pure potassium iodate and KI are used to give a standard solution of I_3^-. Addition of excess strong acid (pH about 1) gives a quantitative reverse disproportionation reaction in which I_3^- is formed:

$$IO_3^- + 8I^- + 6H^+ = 3I_3^- + 3H_2O$$

A freshly acidified solution of iodate plus iodide can be used to standardize thiosulphate and titrate sulphite. The reagent must be used immediately, or else air oxidation of I^- takes place. The excess of the above solution is added to titrate sodium sulphite. The excess of iodine is then titrated with standard sodium thiosulphate. The reaction is:

$$2S_2O_3^{2-} + I_2 = S_4O_6^{2-} + 2I^-$$
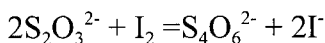
Starch is used as an indicator for iodine. In a solution with no other colored species, it is possible to see the color of 0.00005 M I_3^-. With a starch indicator, the limit of detection is extended by about a factor of ten.

2. Reagents

(1) 25 g $Na_2S_2O_3 \cdot 5H_2O$ + 10 M mg HgI_2 in one liter of freshly boiled, deionized water (pH is adjusted to about 9 with 0.1 - 0.2 g of solid Na_2CO_3). This makes a 0.1M thiosulphate solution. Store in an amber glass bottle.

(2) 5.35g of KIO_3 (99.9%, dried at 120 $^{\circ}$C for 1 hour) in one liter of water.

(3) Solid potassium iodide.

(4) Starch indicator solution. (Mix 2 g of soluble starch and 2 mg of HgI_2 with 20 mL of water. Pour this into 200 ml of boiling water and continue to boil until clear. Prepare this fresh every other day.)

(5) 4 M hydrochloric acid solution.

(6) 1 M $BaCl_2$ solution

3. Procedure

1. Standardization of 0.1M thiousulphate.

(1) Pipette 20 ml of 0.025 M KIO_3 into 250-ml Erlenmeyer flask and add 1.6 g KI and 10 ml of 4M HCl.

(2) Immediately titrate with the thiosulphate solution until the colour is straw yellow.

(3) Add enough water to make the volume up to 200 mL and add 2 mL of starch solution.

(4) Continue the titration until the last trace of blue colour disappears.

2. Titration of Sulphite

(1) Pipette 10 ml of 0.025 M KIO_3 into 250-ml flask and add 1.6 g KI until the complete dissolution of KI. Add 5 ml 4M HCl and mix briefly.

(2) Add the sulphite solution sample (react with about 75 % of iodine) slowly with good stirring, titrate the excess iodine with standard sodium thiosulphate using starch indicator.

3. Determination of Sulphite in Copper Cyanide Solution

(1) Take the solution containing about 0.001 mole of sulphite to a 50 mL test tube, add 20 mL of 1 M NaOH and 20 mL of 1M $BaCl_2$.

(2) Put the test tube into a centrifuge to separate $BaSO_3$ from the solution, transfer the solution to a volumetric flask for cyanide analysis, add some water into a test tube and pull out the solution into the volume flask and repeat the above washing procedure 4 -5 times. Water should be gently added to avoid stirring $BaSO_3$. If the white precipitate is mixed with the solution, the solution should be centrifugalized again. The alternative is to use a membrane filter to separate the solid from the solution.

(3) Wash the solid into a 250-mL Erlenmeyer flask to make up about 100 mL of solution and use a magnetic stir bar to disperse the solid particles completely.

(4) Add 25 mL of 0.025 M KIO_3 and 1.6 g of KI into the flask

(5) Add 50 mL of 4 M HCl and wait for over 1 minute to make the complete oxidation of sulphite to sulphate ($BaSO_3$ is oxidized to $BaSO_4$) by I_2. ($BaSO_3 + 2H^+ = Ba^{2+} + SO_2 + H_2O$, $SO_2 + I_2 + H_2O = SO_4^{2-} + 2I^- + 2H^+$ and $Ba^{2+} + SO_4^{2-} = BaSO_4$)

(6) titrate the excess iodine with standard sodium thiosulphate using starch indicator. The analyzed result is 96 - 98 % of the actual value from the analysis tests.

Appendix 5 Calculation of Activity Coefficient Using Pitzer Method

The excess Gibbs free energy is due to the ionic interaction and can be expressed by the following equation [326, 328]:

$$\frac{G^{ex}}{RT} = n_w f(I) + \frac{1}{n_w} \sum_i \sum_j \lambda_{i,j}(I) n_i n_j + \frac{1}{n_w^2} \sum_i \sum_j \sum_k \mu_{i,j,k} n_i n_j n_k \tag{1}$$

where:

n_w - kilograms of solvent

n - moles of solutes i, j, k

$$I = 0.5 \sum_i m_i z_i^2$$

z_i - ionic charge

$m_i = n_i \, \Omega \, / \, n_w$ ionic molality

Ω - the number of moles of solvent in a kilogram (55.51 for water)

f(I) - function describing the long-range electrostatic effects as a function of temperature in the Debye-Hückel manner.

λ_{ij} - term for describing the short-range interionic effects as a function of ionic strength to display the type of behaviour caused by the hard core effect. It is assumed to be symmetrical.

μ_{ijk} - term for triple ion interactions which ignores any ionic strength dependence. It is assumed to be symmetrical.

The chemical potentials of species i (μ_i) is expressed as:

$$\mu_i = \mu_i^0 + RT \ln a_i = \mu_i^0 + RT \ln(m_i \gamma_i) \tag{2}$$

where μ_I^0 is the chemical potential in the solute (molality) standard state, a_i the activity, m_i the molality and γ_I the activity coefficient. For the solvent as water, the chemical potential is:

$$\mu_w = \mu_w^0 + RT \ln a_w \tag{3}$$

where μ_w^0 is the standard potential of pure water. The activity of water a_w is commonly expressed by the osmotic coefficient ϕ:

$$\phi = -(\Omega / \sum m_i) \ln a_w \tag{4}$$

where $\sum m_i$ covers all solute species. The total Gibbs free energy of mixing from the standard is

$$\Delta_{mix} G = n_w (\mu_w - \mu_w^0) + \sum n_i (\mu_i - \mu_i^0) = RT(n_w \ln a_w + \sum n_i \ln a_i) \tag{5}$$

From Equations 2, 4 and 5 and $m_i = n_i \Omega / n_w$, the following equation is obtained:

$$\Delta_{mix} G = RT \sum n_i [-\phi + \ln(m_i \gamma_i)]$$ (6)

The Gibbs free energy from mixing can be divided into two parts: one part independent of γ_i or ϕ which gives the primary dependence of the Gibbs free energy on solution composition, and a second part for the corrective terms in $(1-\phi)$ and γ_i. The later can be called an excess Gibbs free energy which can expressed as:

$$G^{ex} = \Delta_{mix} G + RT \sum n_i (1 - \ln m_i) = RT \sum n_i (1 - \phi + \ln \gamma_i)$$ (7)

The activity coefficient (γ_i)is derived from the Gibb's excess free energy equation according Equations 1 and 7:

$$\ln \gamma_i = \frac{1}{RT} \frac{\partial G^{ex}}{\partial n_i} = \frac{z_i^2}{2} f^{'} + 2\sum_j m_j \lambda_{i,j} + \sum_i \sum_k m_{jk} (\frac{z_i^2}{2} \lambda_{jk}^{'} + 3\mu_{ijk})$$ (8)

where:

$f^{'}$ - df/dI

$\lambda_{ij}^{'}$ - dλ_{ij}/dI

After rearranging, the activity coefficients for anion A can be expressed as:

$$\ln \gamma_A = z_A^2 f^{\gamma} + \sum_c m_c [2B_{cA} + (2\sum_a m_a z_a)C_{cA}] + \sum_a m_a (2\theta_{Aa} + \sum_c m_c \psi_{Aac})$$
$$+ \sum_c \sum_a m_c m_a (z_A^2 B_{ca}^{'} + |z_A| C_{ca}) + 0.5 \sum_c \sum_{c'} m_c m_{c'} \cdot \psi_{cc'A}$$ (9)

where:

$$f^{\gamma} = -A_\Phi [[\frac{\sqrt{I}}{1 + b\sqrt{I}} + \frac{2}{b} \ln(1 + b\sqrt{I})]$$

$A_\Phi = (1/3)(2\pi N_0 d_w / 1000)^{1/2} (e^2 / \epsilon kT)^{3/2}$ - the Debye-Hückel constant for the osmotic coefficient, 0.3915, 0.4023, 0.4103,0.4190 respectively for 25, 40, 50 and 60 ^{0}C.

b = 1.2

a - subscript denoting anions

c - subscript denoting cations

$$B_{ij} = \beta_0 + \frac{2\beta_1}{\alpha_1^2 I}[1 - (1 + \alpha_1 \sqrt{I})\exp(-\alpha_1 \sqrt{I})] + \frac{2\beta_2}{\alpha_2^2 I}[1 - (1 - \alpha_2 \sqrt{I})\exp(-\alpha_2 \sqrt{I})]$$

$$B_{ij}^{'} = \frac{2\beta_1}{\alpha_1^2 I^2}[-1 + (1 + \alpha_1 \sqrt{I} + 0.5\alpha_1^2)\exp(-\alpha_1 \sqrt{I})] + \frac{2\beta_2}{\alpha_2^2 I^2}[-1 + (1 + \alpha_2 \sqrt{I} + 0.5\alpha_2^2)\exp(-\alpha_2 \sqrt{I})]$$

in the case of Equation 9, i denotes A

$\alpha_1 = 2.0$ for 1-1, 2-1, 1-2,3-1, 4-1 electrolyte

$\alpha_2 = 0.0$ for 1-1, 2-1, 1-2,3-1, 4-1 electrolyte

β_0 - Pitzer's parameter

β_1 - Pitzer's parameter

β_2 - Pitzer's parameter for 2-2 electrolyte

$C = C^\phi / [2(Z_+ Z_-)^{1/2}]$

C^ϕ - Pitzer's parameter

θ - Pitzer's interaction parameter for like charged ions

ψ - Pitzer's ternary parameter

ϕ can be calculated by the following equation and so the activity of water can be calculated:

$$\phi = -1 + (\sum_i m_i)^{-1} [2 I f^\phi + 2 \sum_c \sum_a m_c m_a (B_{ca}^\phi + \frac{(\sum mz)}{\sqrt{z_c z_a}} C_{ca}^\phi) +$$
$$\sum_c \sum_{c'} m_c m_{c'} (\theta_{cc'} + I\theta'_{cc'} + '\sum_a m_a \psi_{cc'a}) + \sum_a \sum_{a'} m_a m_{a'} (\theta_{aa'} + I\theta'_{aa'} + \sum_c m_c \psi_{caa'})]$$

(5)

where:

θ' is Pitzer's parameter for un-symmetrical mixing which can be neglected for solutions of electrolytes which are similar or not too different

$$B_{ca}^\phi = \beta_0 + \beta_1 \exp(-\alpha_1 \sqrt{I}) + \beta_2 \exp(-\alpha_2 \sqrt{I})$$

$$(\sum mz) = \sum_a m_a |z_a| + \sum_c m_c z_c$$

Table 1 Pitzer's parameters for Na_2SO_4 and $NaOH$ [326, 328]

β_0 (Na^+,SO_4^{2-})	$\partial\beta_0/\partial T$ (Na^+, SO_4^{2-})	β_1 (Na^+, SO_4^{2-})	$\partial\beta_1\partial/\partial T$ (Na^+, SO_4^{2-})
0.01958	0.00236	1.113	0.00563
β_0 (Na^+, OH^-)	$\partial\beta_0/\partial T$ (Na^+, OH^-)	β_1 (Na^+, OH^-)	$\partial\beta_1\partial/\partial T$ (Na^+, OH^-)
0.0864	0.0007	0.253	0.000134
C^ϕ (Na^+,SO_4^{2-})	$\partial C^\phi/\partial T$ (Na^+,SO_4^{2-})	C^ϕ (Na^+, OH^-)	$\partial C^\phi/\partial T$ (Na^+, OH^-)
0.00497	-0.000486	0.0044	-0.000189
C (Na^+,SO_4^{2-})	C (Na^+, OH^-)	θ (OH^-, SO_4^-)	ψ (OH^-, SO_4^{2-},Na^+)
0.00176	-0.0022	-0.013	-0.009

Appendix 6 Measurement of the Kinematic Viscosity

The kinematic viscosity is measured using Cannon-Fenske routine viscometer (Size 25). The viscometer constant (C_0) at 24 ^{0}C is 0.001802 mm^2 s^{-2} and its temperature coefficient (B) is 46×10^{-6} ^{0}C. Therefore the viscometer constant at temperature T is $C_0(1-B(T-T_0))$. The kinematic viscosity is the efflux time multiplied by the viscometer constant.

The experiment set-up is shown in the following figure:
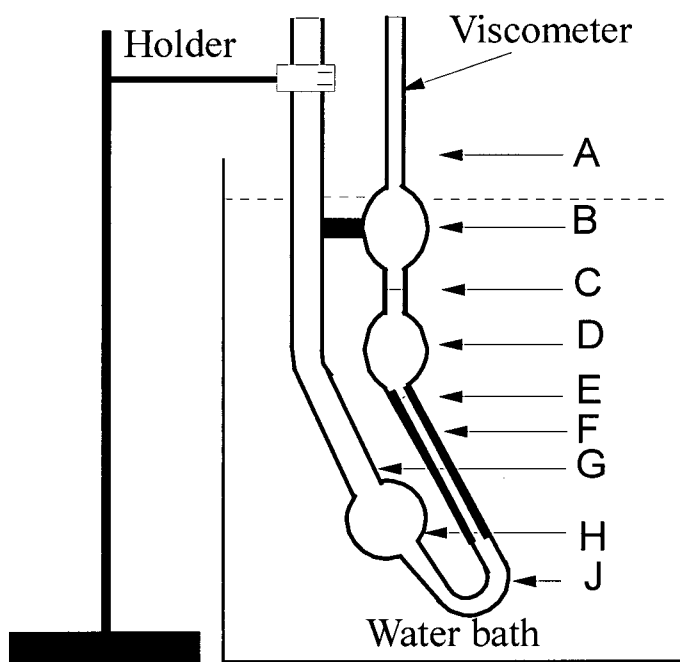
Schematic diagram for the viscosity measurement

Measuring procedure:

1. Clean the viscometer using acetone and by passing pure N$_2$ gas through the instrument to remove the final traces of solvents. Periodically, traces of organic deposits are removed with chromic acid.

2. If there is a possibility of lint, dust, or other solid material in the liquid sample, filter the sample through a sintered glass filter or fine mesh screen.

3. To charge the sample into the viscometer, invert the instrument and apply suction to tube G, immersing tube A in the liquid sample, and draw liquid to mark E. Wipe clean arm A, and turn the instrument to its normal vertical position.

4. Place the viscometer into the holder, and insert into the constant temperature bath.

5. Allow about 15 minutes for the sample to come to the bath temperature.

6. Apply suction to tube A (or pressure to tube F) and draw the liquid slightly above mark C.

7. To measure the efflux time, allow the liquid sample to flow freely down past mark C, measuring the time for the meniscus to pass from mark C to mark E.

8. A check run may be made by repeating steps 6 and 7.

9. Calculate the viscosity of the sample by multiplying the efflux time by the viscometer constant.

Appendix 7 Calculation of Liquid Junction Potential

The liquid junction potential arises from two different ionic solutions (concentration difference, or different electrolytes) in contact due to the different mobilities of ions across the junction. The reference electrode is often isolated from the working electrode compartment by a salt bridge or a Luggin capillary. Hence a liquid junction potential exists and affects the potential measurement of the working electrode. The direct potentiometric measurement of a junction potential is not possible because of the impossibility of directly measuring a single electrode potential. However, it is possible to estimate junction potentials indirectly or to make calculations based on assumptions about the geometry and distribution of the ions in the region of the junction. The basic equation relating the junction potential (E_j) between Phases β and α to the transport number, charge and activity of the ions forming the junction is:

$$E_j = E^\beta - E^\alpha = \frac{-RT}{F} \int_\alpha^\beta \sum \frac{t_i}{z_i} d \ln a_i \tag{1}$$

where t_i is the transport number (related to the mobility of the ion) of the ith ion, z_i the algebraic value of the charge on the ion, a_i the activity of the ion, and n the number of the ions. It is too difficult to solve the above equation because we have to know how the concentration, the activity coefficient and the transport number of each species vary in the junction region. If the activity coefficients are taken to be unity and the concentration of each ion is assumed to vary linearly from C_α to C_β, the liquid junction potential can be expressed as [332]:

$$E_j = \frac{-RT}{F} \frac{\sum_i \frac{|z_i| u_i}{z_i} [C_i^\beta - C_i^\alpha]}{\sum_i |z_i| u_i [C_i^\beta - C_i^\alpha]} \ln \frac{\sum_i |z_i| u_i C_i^\beta}{\sum_i |z_i| u_i C_i^\alpha}$$

$$= \frac{-RT}{F} \frac{\sum_i \frac{|z_i| \lambda_i}{z_i} [C_i^\beta - C_i^\alpha]}{\sum_i |z_i| \lambda_i [C_i^\beta - C_i^\alpha]} \ln \frac{\sum_i |z_i| \lambda_i C_i^\beta}{\sum_i |z_i| \lambda_i C_i^\alpha} \tag{2}$$

where λ_i is the equivalent conductivity of the species i ($|z_i| u_i F$), C_i^α and C_I^β the concentrations in Phases α and β. For accuracy, it is better to use the mobility or equivalent conductivity in the two phases. However, these data are lacking. As an approximation, the equivalent

conductivities can be used to estimate the liquid junction potential. The equivalent conductivities for SO_4^{2-}, SO_3^{2-}, Cl^-, OH^-, Na^+ and K^+ at infinite dilution are 80, 80, 76.34, 197.6, 50.1 and 73.6 $\times 10^{-4}$ m^2 mho equiv.$^{-1}$ [330] Table 1 lists the liquid junction potentials at different potentials. The concentration of saturated KCl solution is 4.16 M at 25 °C [325].

Table 1 Liquid junction potentials for different compositions between the solutions in the cell and saturated potassium chloride solution ($E_j = E_{cell} - E_{SCE}$)

Na_2SO_4 / M	$Na_2 SO_3^-$ / M	NaOH / M	E_j / mV
1	0.05	0.25	0.2
1	0.1	0.25	0.2
1	0.2	0.25	~0
1	0.4	0.25	-0.2
1	0.5	0.25	-0.3
1	0.1	0.025	-1.8
1	0.1	0.025	-1.9

Appendix 8 Figures

(a) 25 °C

(b) 40 °C

(c) 50 °C
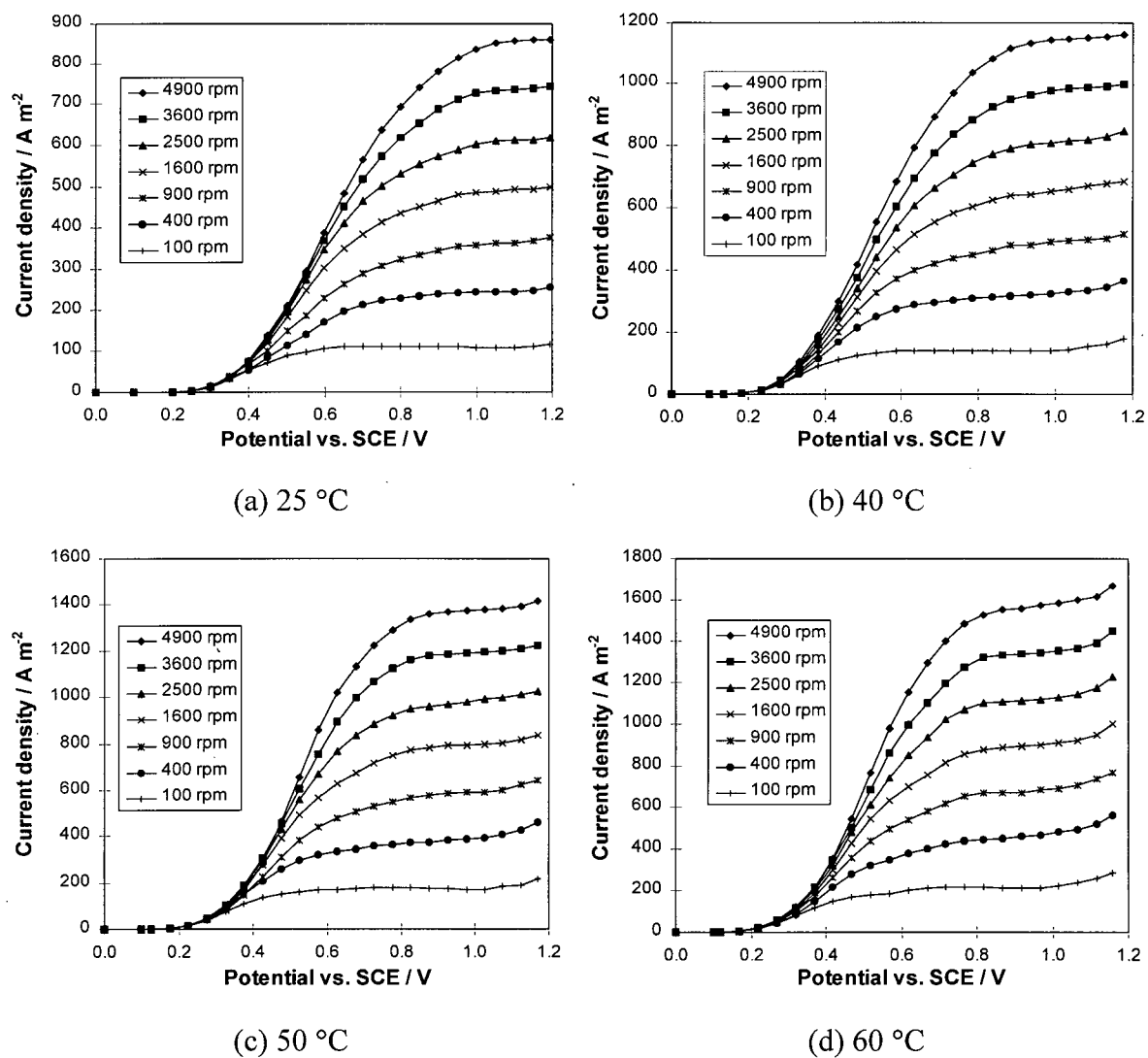
(d) 60 °C

Figure A-1 Polarization curves of sulphite oxidation using rotating disk at 25, 40, 50 and 60 °C. Electrolyte: 0.05 M Na_2SO_3, 0.25 M NaOH and 1 M Na_2SO_4.
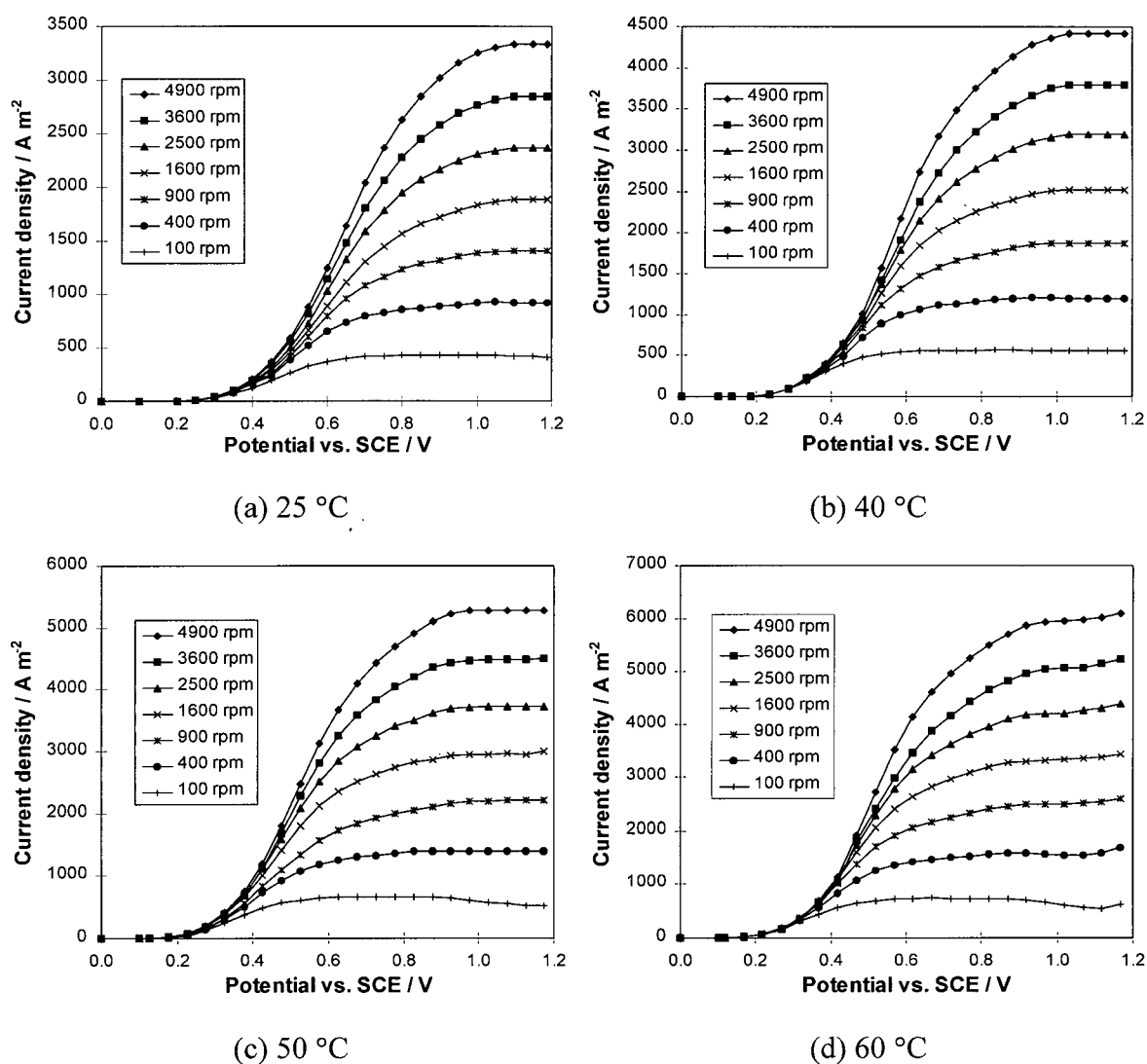
Figure A-2 Polarization curves of sulphite oxidation using rotating disk at 25, 40, 50 and 60 °C. Electrolyte: 0.2 M Na_2SO_3, 0.25 M NaOH and 1 M Na_2SO_4.
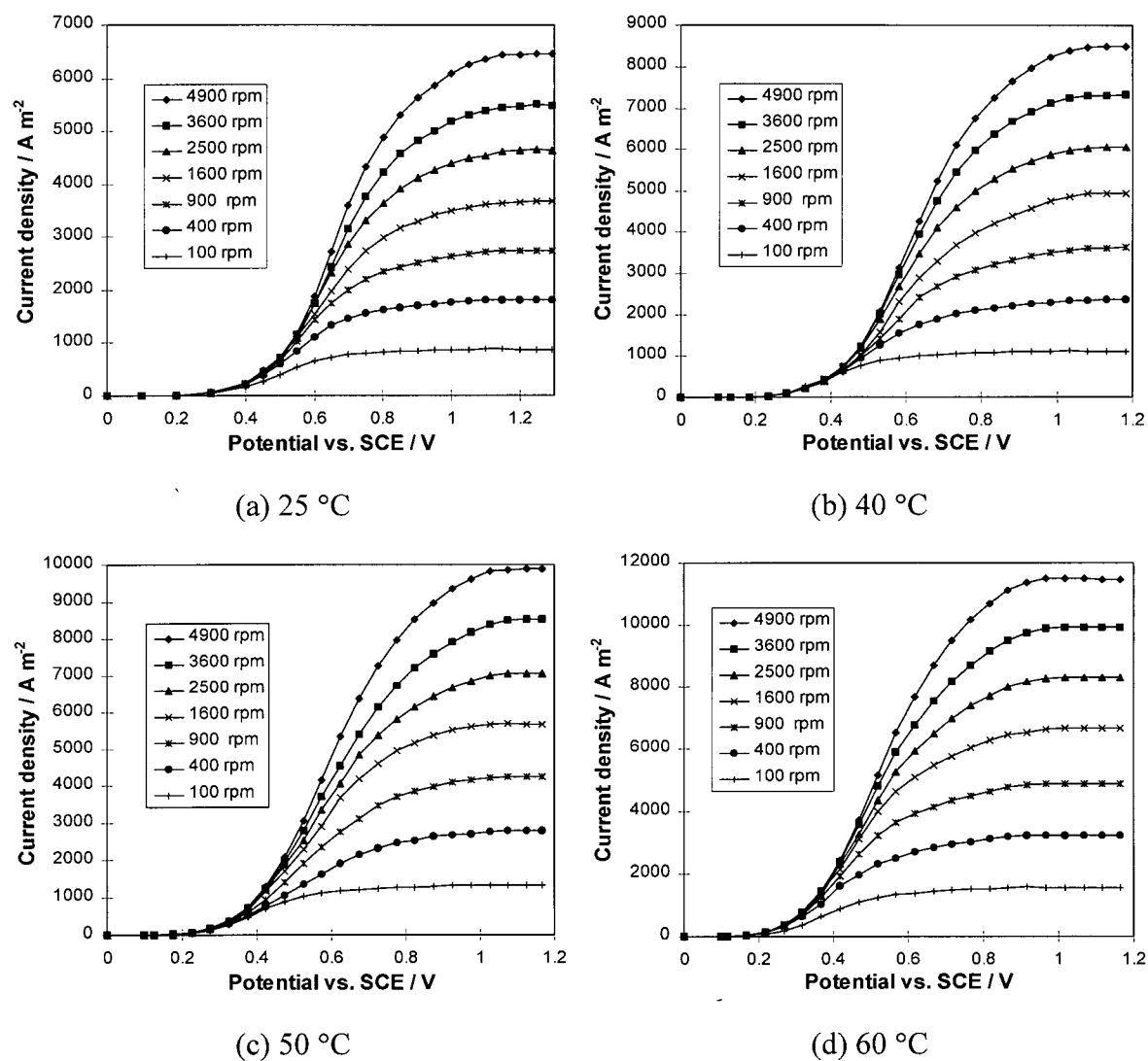
Figure A-3 Polarization curves of sulphite oxidation using rotating disk at 25, 40, 50 and 60 °C. Electrolyte: 0.4 M Na_2SO_3, 0.25 M NaOH and 1 M Na_2SO_4.

(a) 25 °C

(b) 40 °C

(c) 50 °C
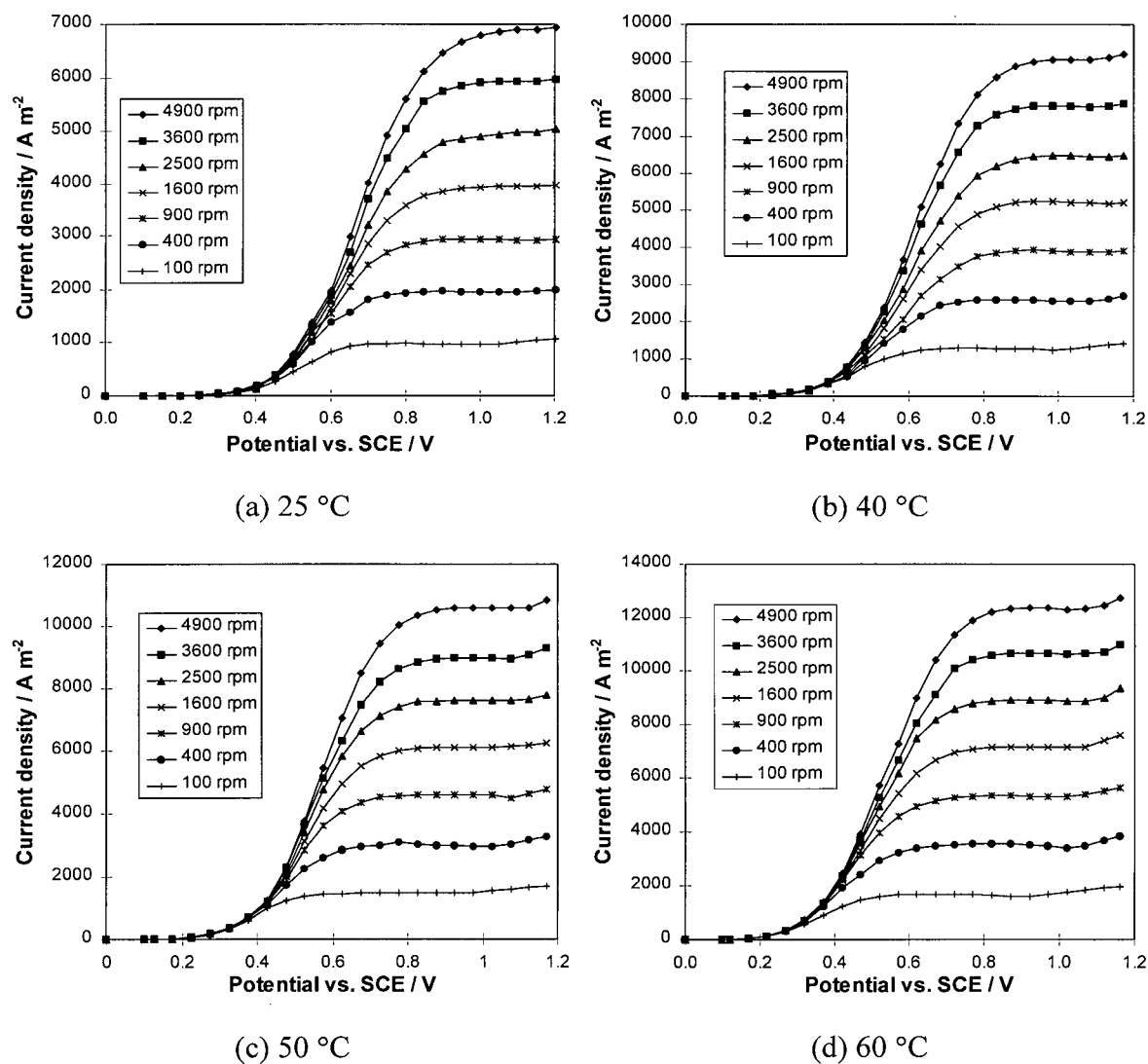
(d) 60 °C

Figure A-4 Polarization curves of sulphite oxidation using rotating disk at 25, 40, 50 and 60 °C. Electrolyte: 0.5 M Na_2SO_3, 0.25 M NaOH and 1 M Na_2SO_4.
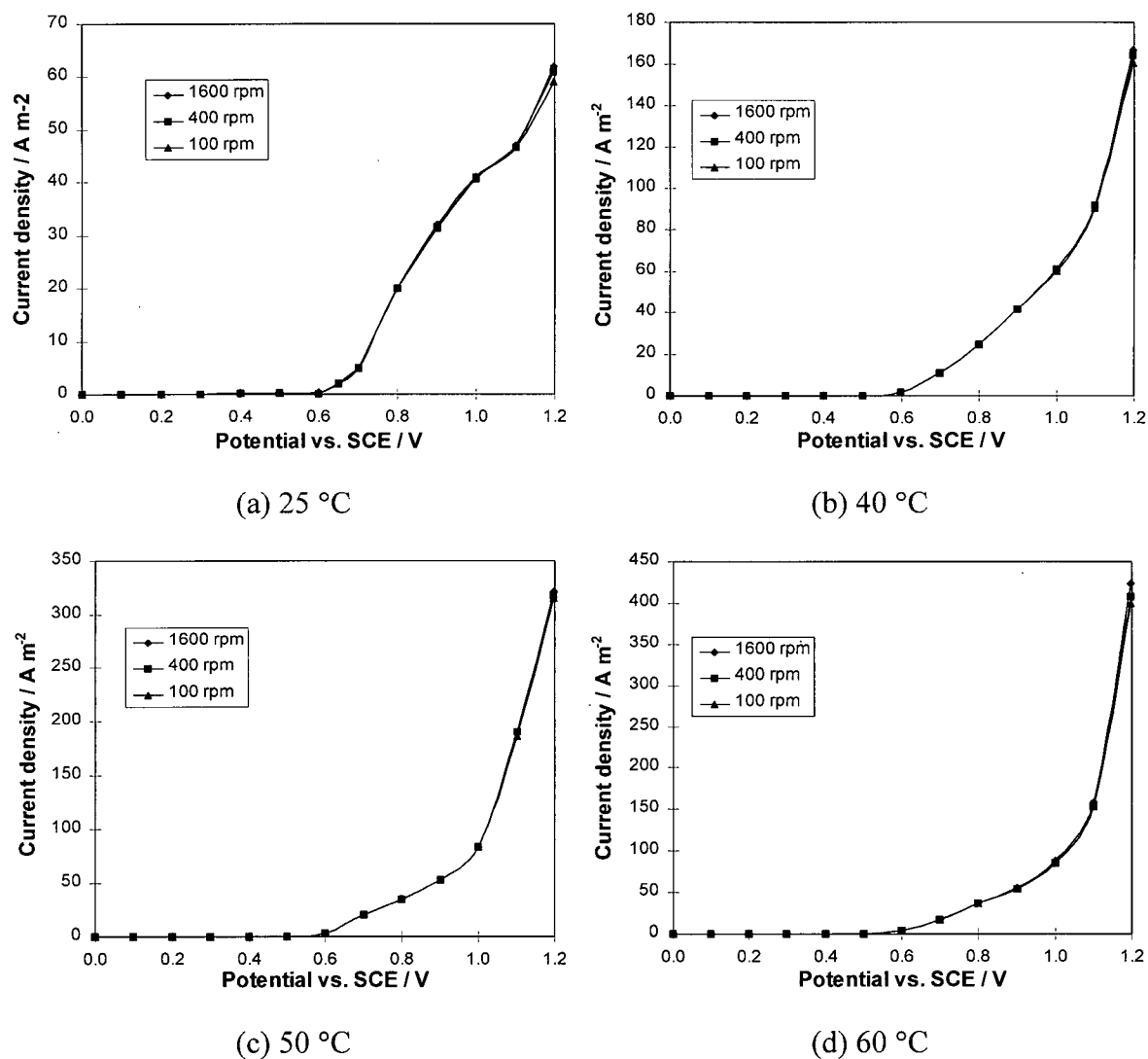
Figure A-5 Background current density vs. potential on graphite rotating disk at 25, 40, 50 and 60 °C. Electrolyte: 0.25 M NaOH and 1 M Na_2SO_4.
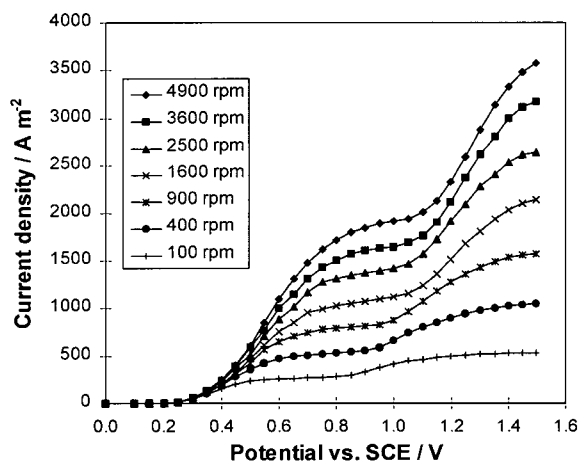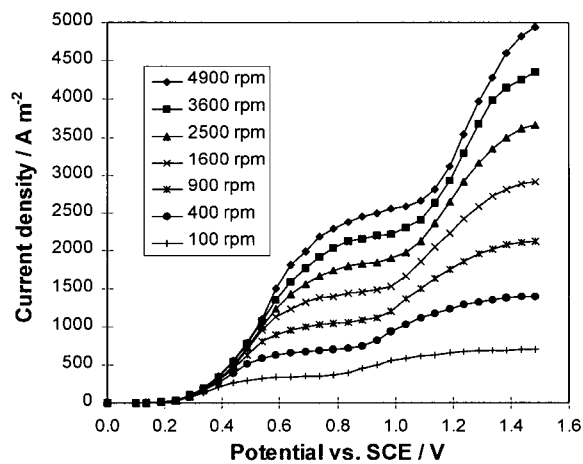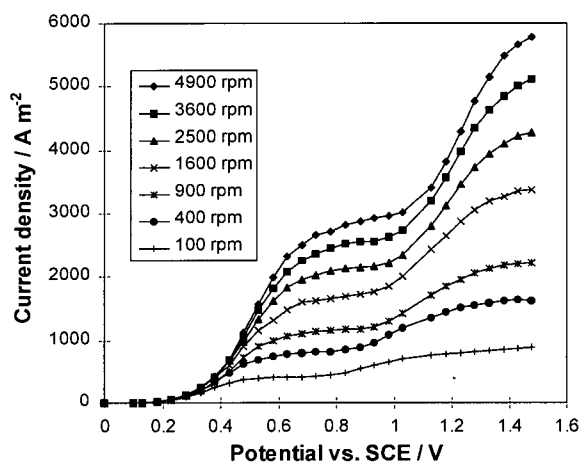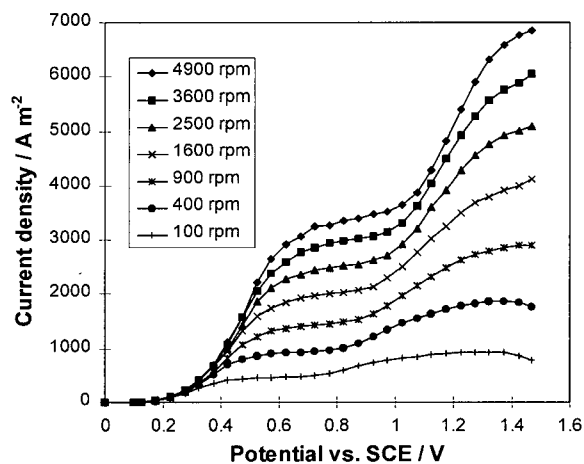
Figure A-6 Polarization curves of sulphite oxidation using rotating disk at 25, 40, 50 and 60 °C. Electrolyte: 0.2 M Na_2SO_3, 0.05 M NaOH and 1 M Na_2SO_4.
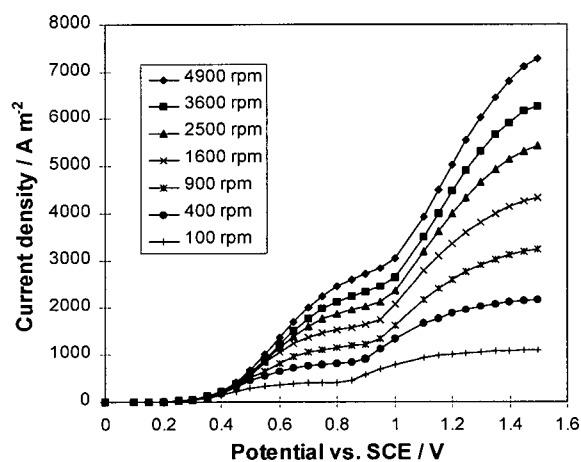
(a) 25 °C
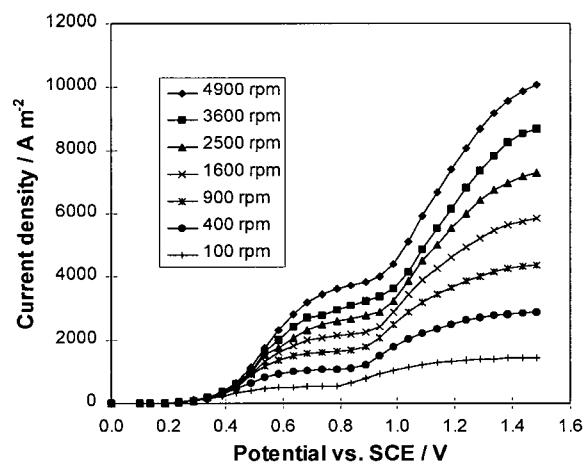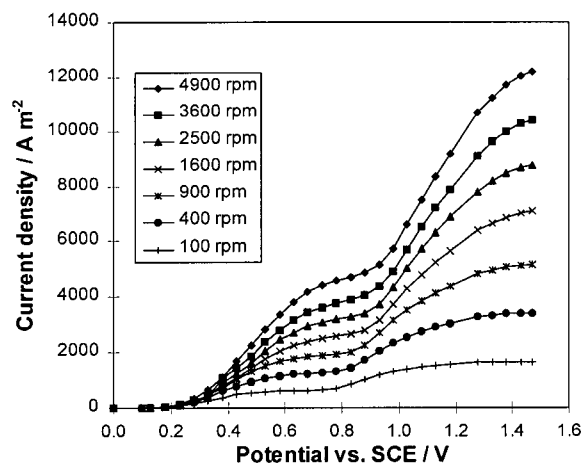
(b) 40 °C

(c) 50 °C
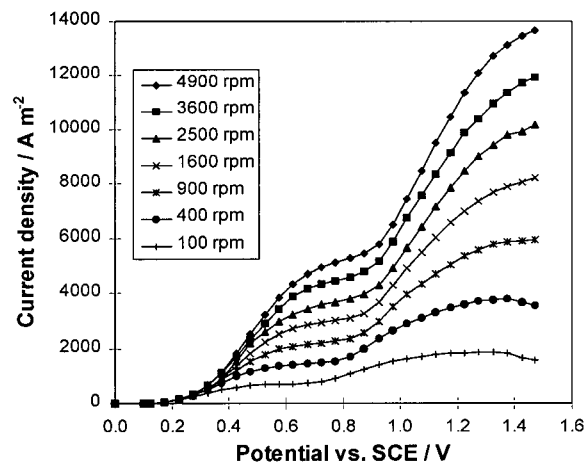
(d) 60 °C

Figure A-7 Polarization curves of sulphite oxidation using rotating disk at 25, 40, 50 and 60 °C. Electrolyte: 0.4 M Na_2SO_3, 0.05 M NaOH and 1 M Na_2SO_4.
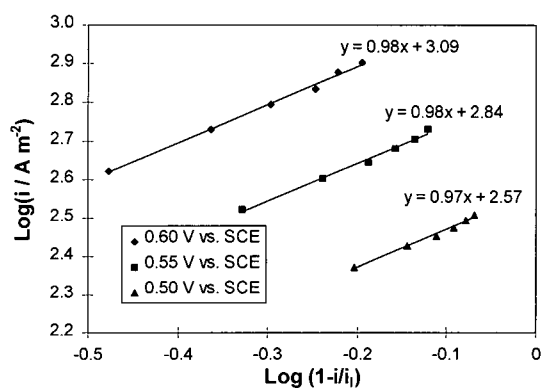
(1a) 40 °C
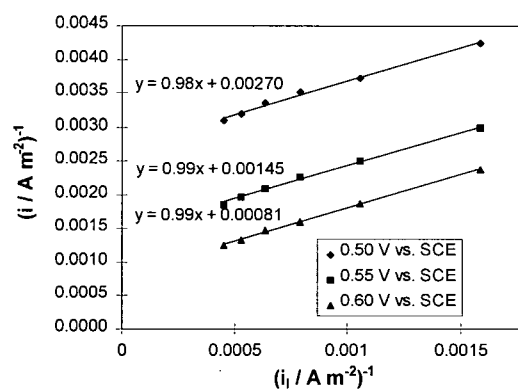
(1 b) 40 °C
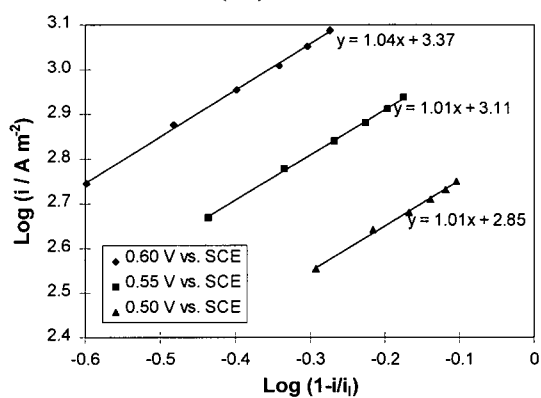
(2a) 50 °C
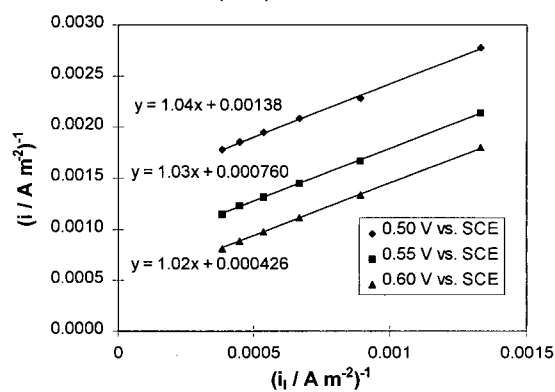
(2 b) 50 °C
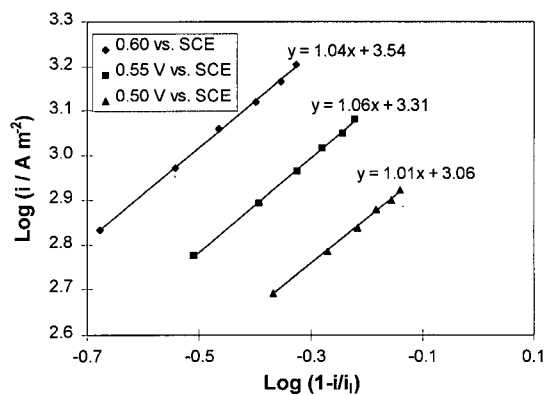
(3a) 60 °C
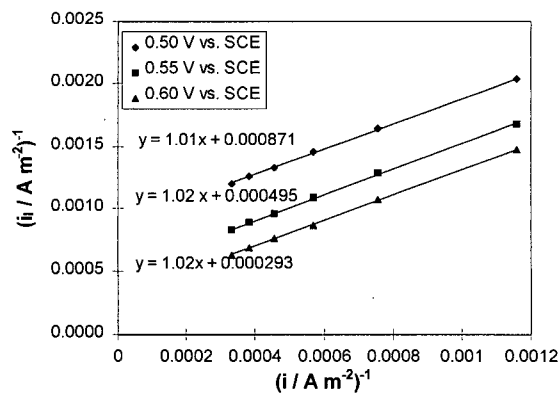
(3 b) 60 °C

Figure A-8 Log (i) vs. Log $(1-1/i_l)$ (a) and $1/i$ vs. $1/i_l$ (b) at 40 (1), 50 (2) and 60 (3) °C and the corresponding fitted function (y vs. x) are in the diagram. Electroyte: 0.1 M Na_2SO_3, 0.25 M NaOH and 1 M Na_2SO_4.
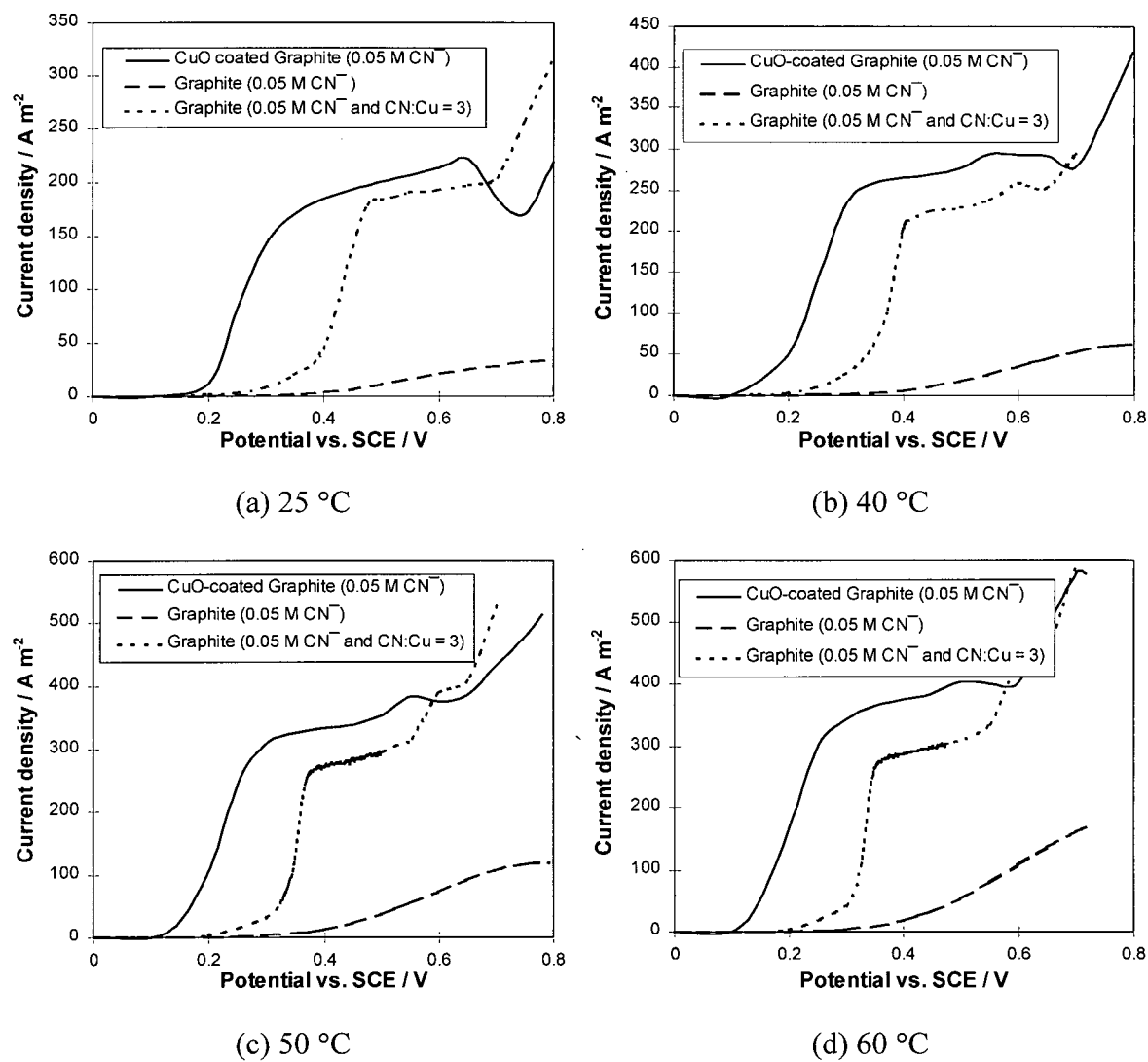
Figure A-9 Comparison of the effects of CuO-coated graphite and copper ions in the solution at 100 rpm and different temperatures. Electrolyte:0.25 M NaOH and 1 M Na_2SO_4.
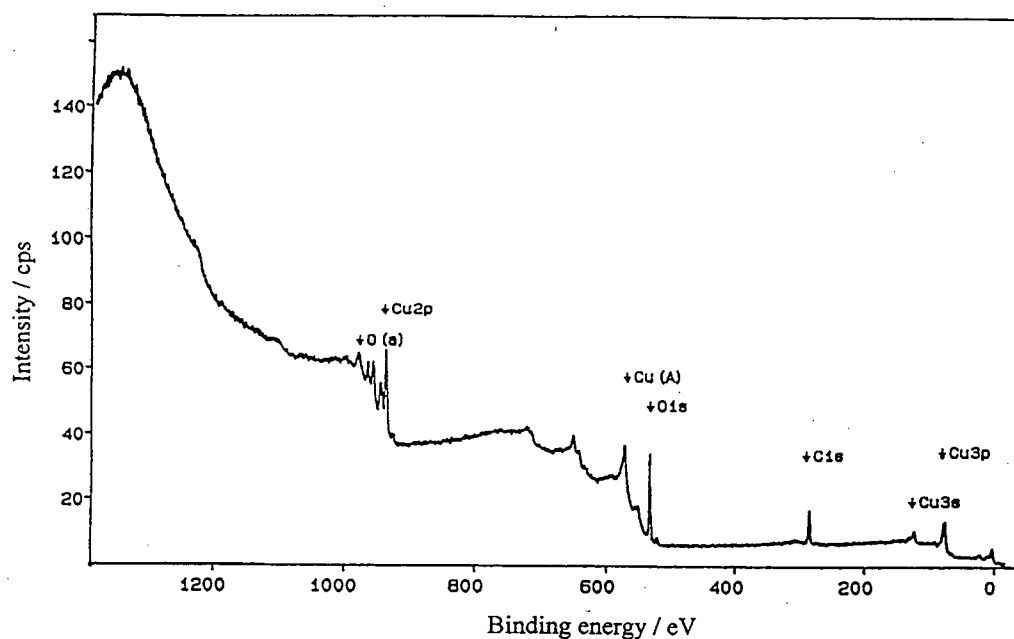
Figure A-10   XPS spectrum of the precipitate prepared at 25 °C and 0.5 V vs. SCE. Electrolyte: 0.05 M NaCN, CN:Cu mole ratio = 3, 0.25 M NaOH and 1 M Na_2SO_4.
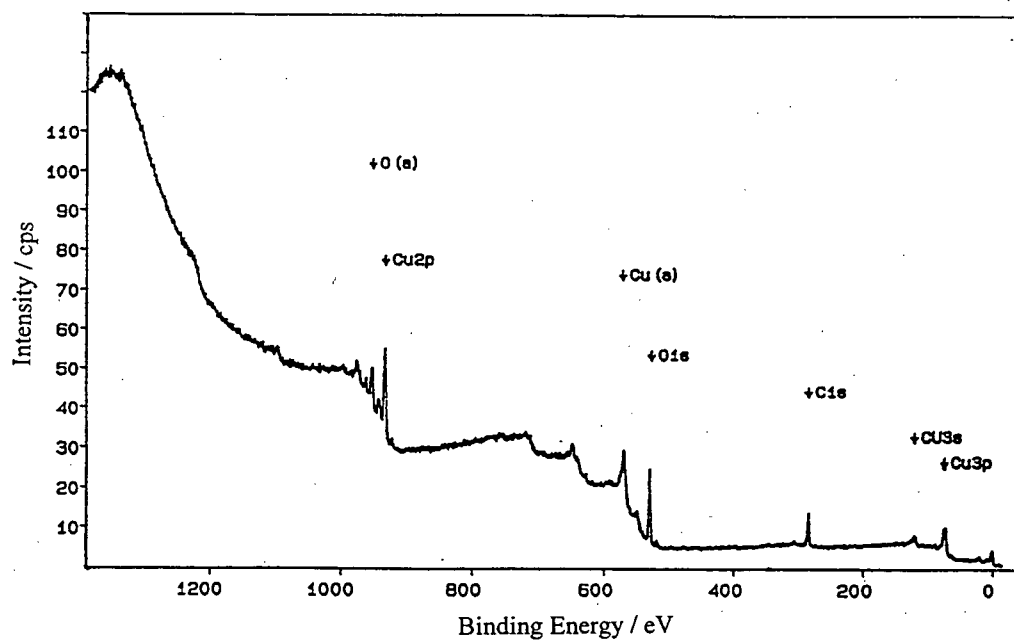
Figure A-11   XPS spectrum of the precipitate prepared at 60 °C and 0.5 V vs. SCE. Electrolyte: 0.05 M NaCN, CN:Cu mole ratio = 3, 0.25 M NaOH and 1 M Na_2SO_4.
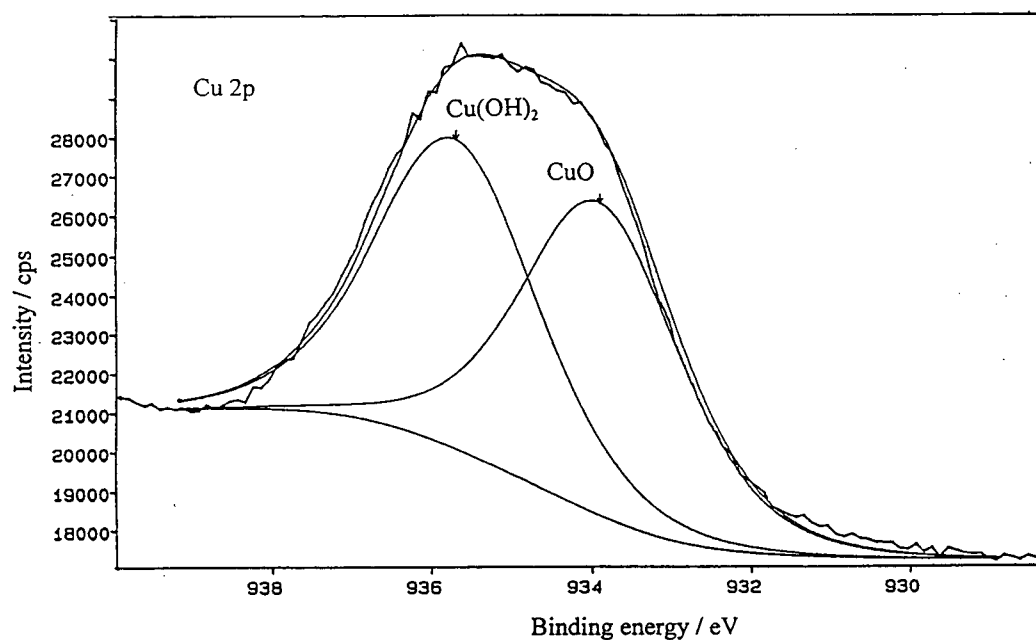
Figure A-12 XPS spectrum of the precipitate prepared at 25 °C and 0.5 V vs. SCE. Electrolyte: 0.05 M NaCN, CN:Cu mole ratio = 3, 0.25 M NaOH and 1 M Na$_2$SO$_4$.
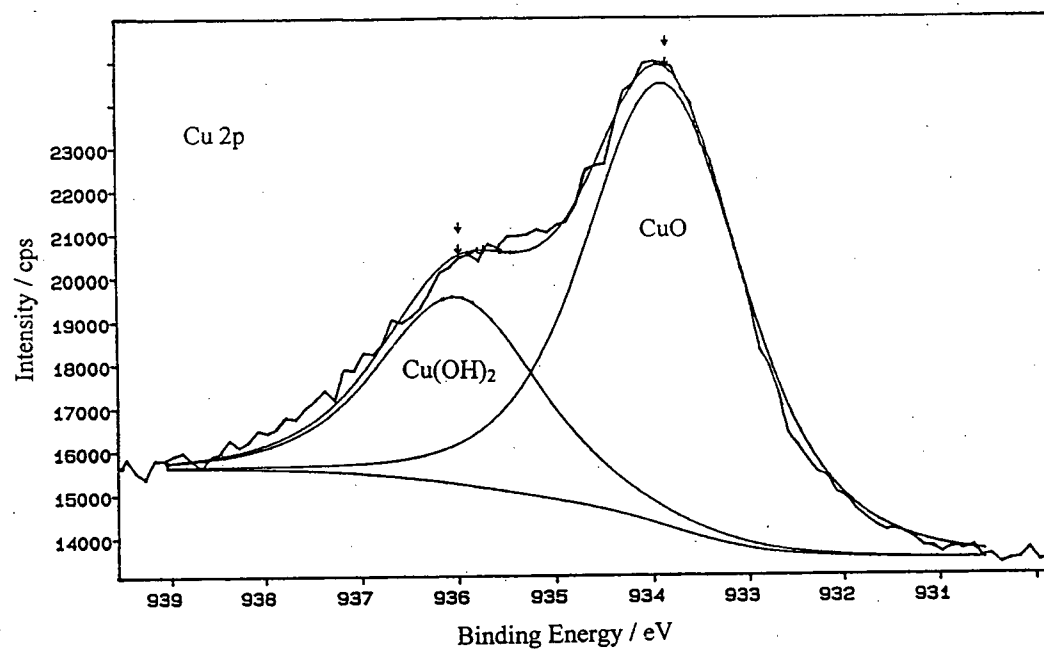
Figure A-13 XPS spectrum of the precipitate prepared at 60 °C and 0.5 V vs. SCE. Electrolyte: 0.05 M NaCN, CN:Cu mole ratio = 3, 0.25 M NaOH and 1 M Na$_2$SO$_4$.
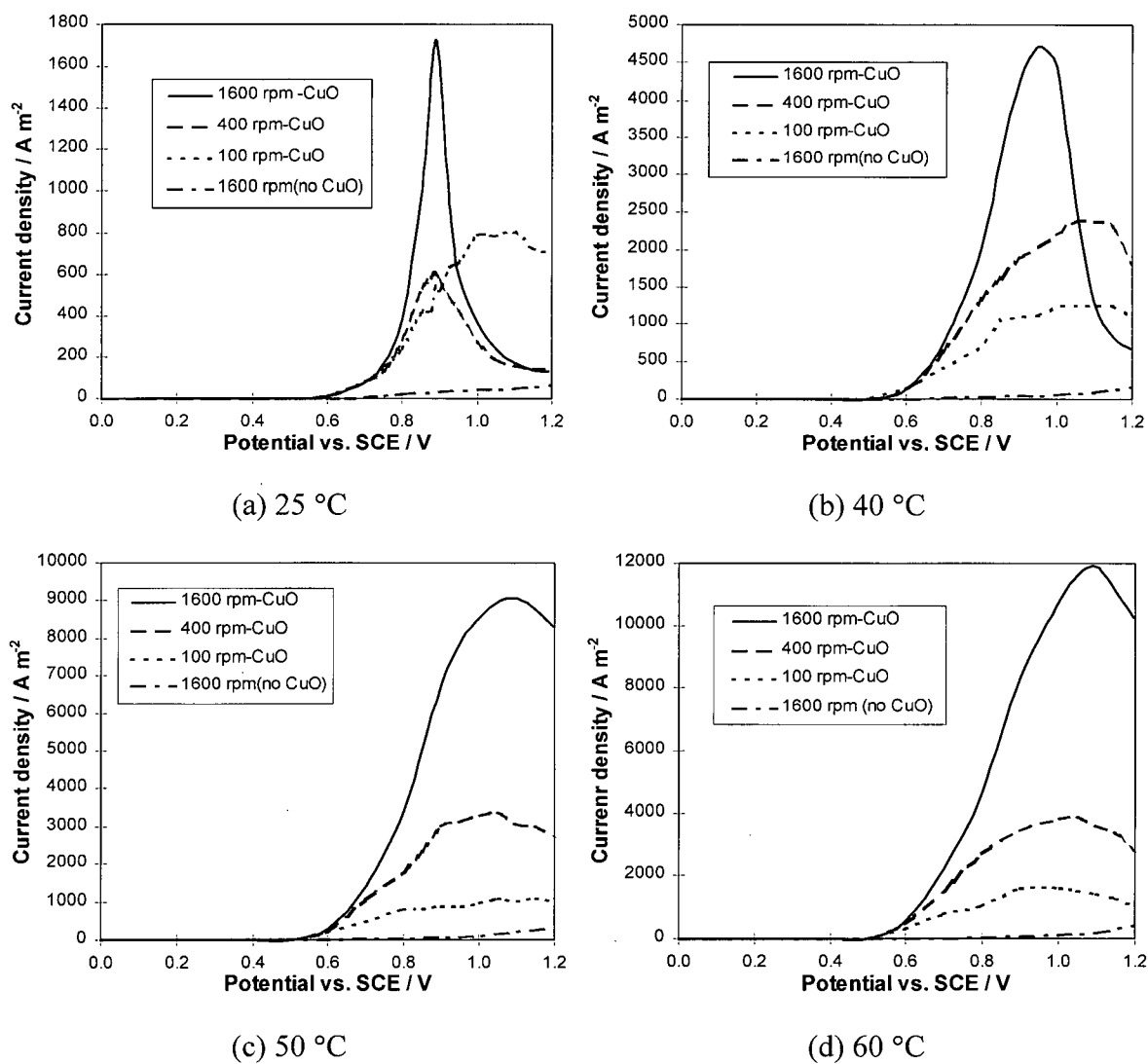
Figure A-14   Polarization curves on the graphite coated with CuO and no CuO in the absence of cyanide and copper at different temperatures. Electrolyte: 0.25 M NaOH and 1 M Na_2SO_4.
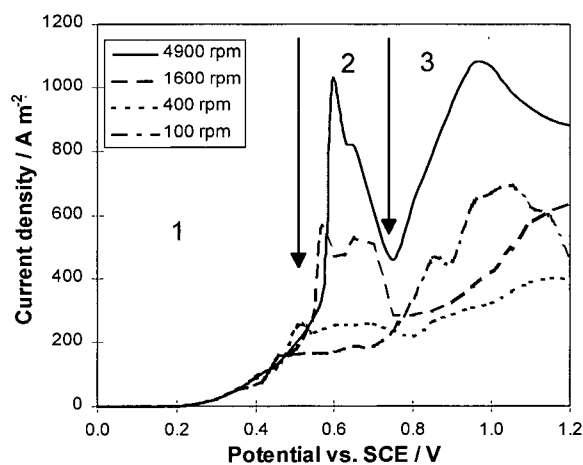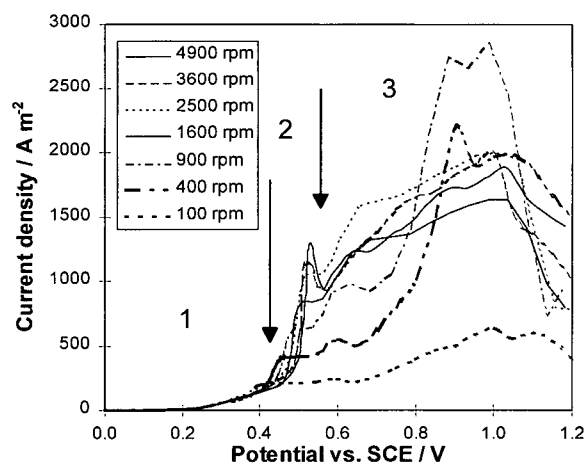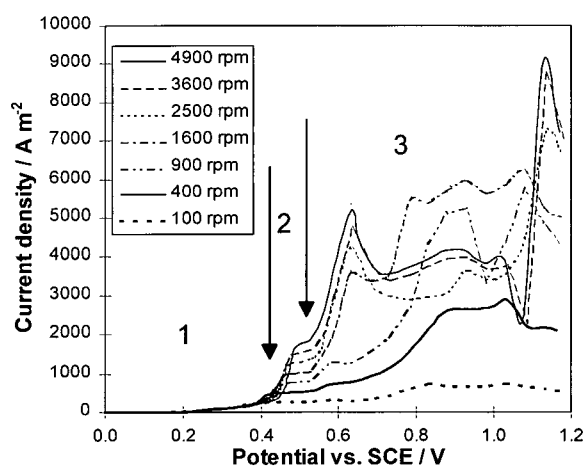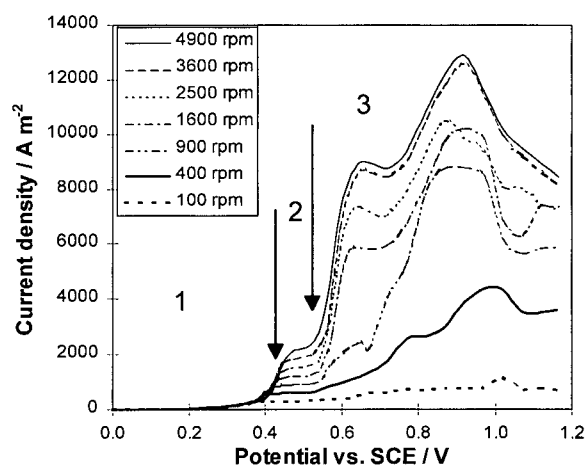
Figure A-15 Polarization curves at different rotational speeds and temperatures. Electrolyte: 0.05 M CN⁻, CN:Cu mole ratio = 3.5, 0.25 M NaOH and 1 M Na₂SO₄. Keys: 1 - no precipitation of copper oxide, 2 - precipitation of copper oxide and 3 - evolution of oxygen.
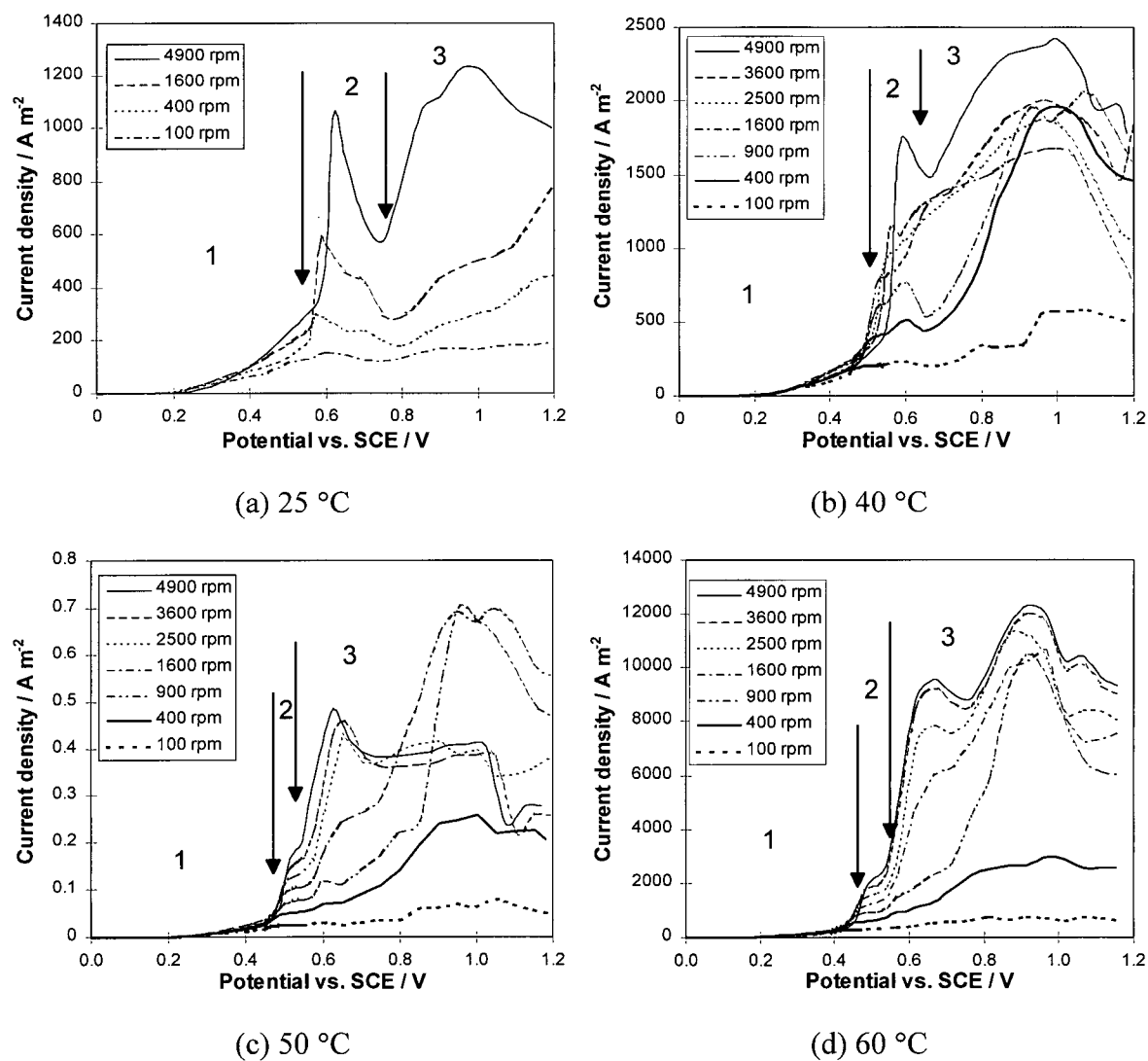
Figure A-16 Polarization curves at different rotational speeds and temperatures. Electrolyte: 0.05 M CN⁻, CN:Cu mole ratio = 3.5, 0.25 M NaOH and 1 M Na₂SO₄. Keys: 1 - no precipitation of copper oxide, 2 - precipitation of copper oxide and 3 - evolution of oxygen.
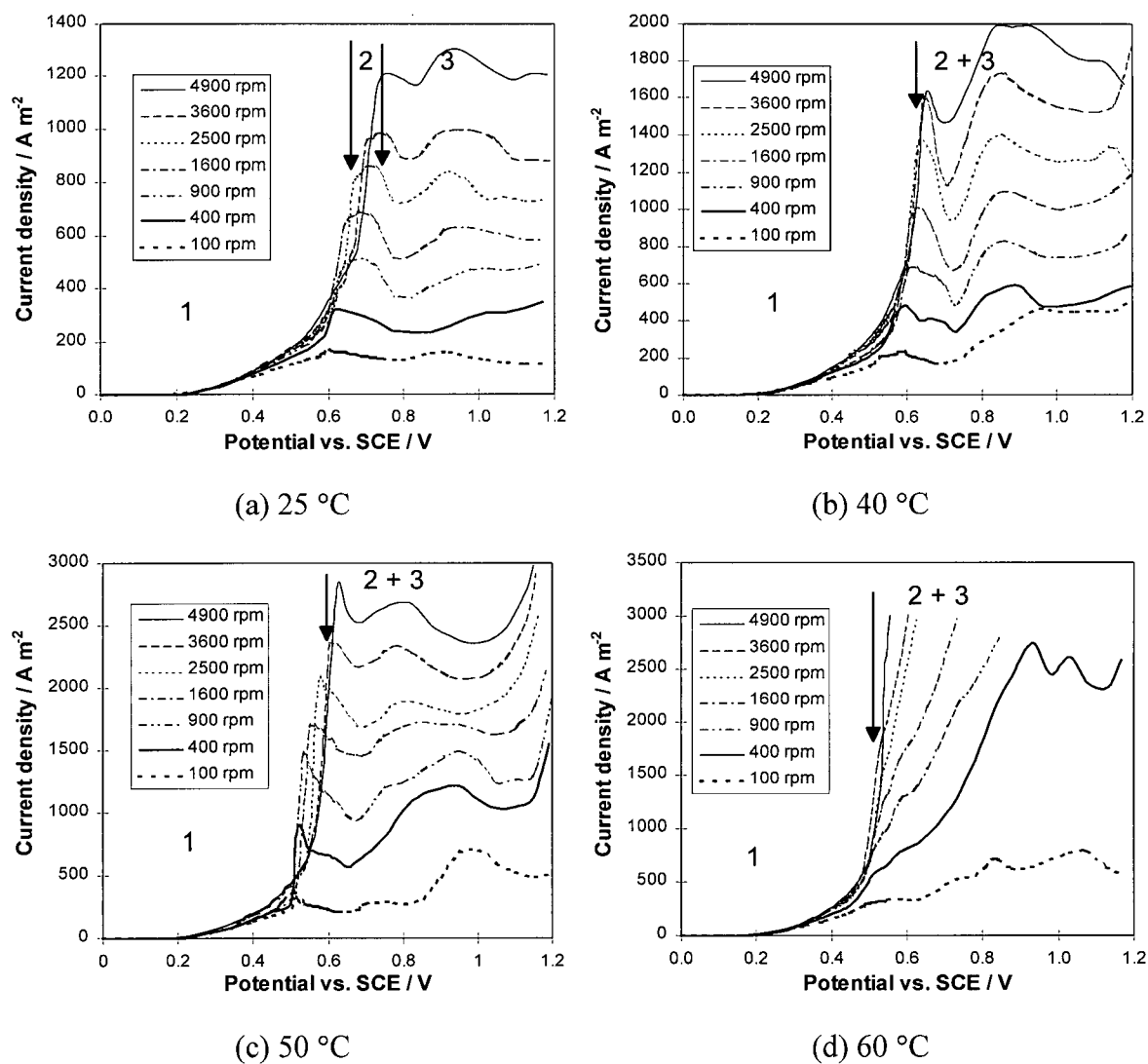
Figure A-17 Polarization curves at different rotational speeds and temperatures. Electrolyte: 0.05 M CN⁻, CN:Cu mole ratio = 6, 0.25 M NaOH and 1 M Na₂SO₄. Keys: 1 - no precipitation of copper oxide, 2 - precipitation of copper oxide, 3 - evolution of oxygen and 2+3 - copper oxide and oxygen appeared almost at the same potential.
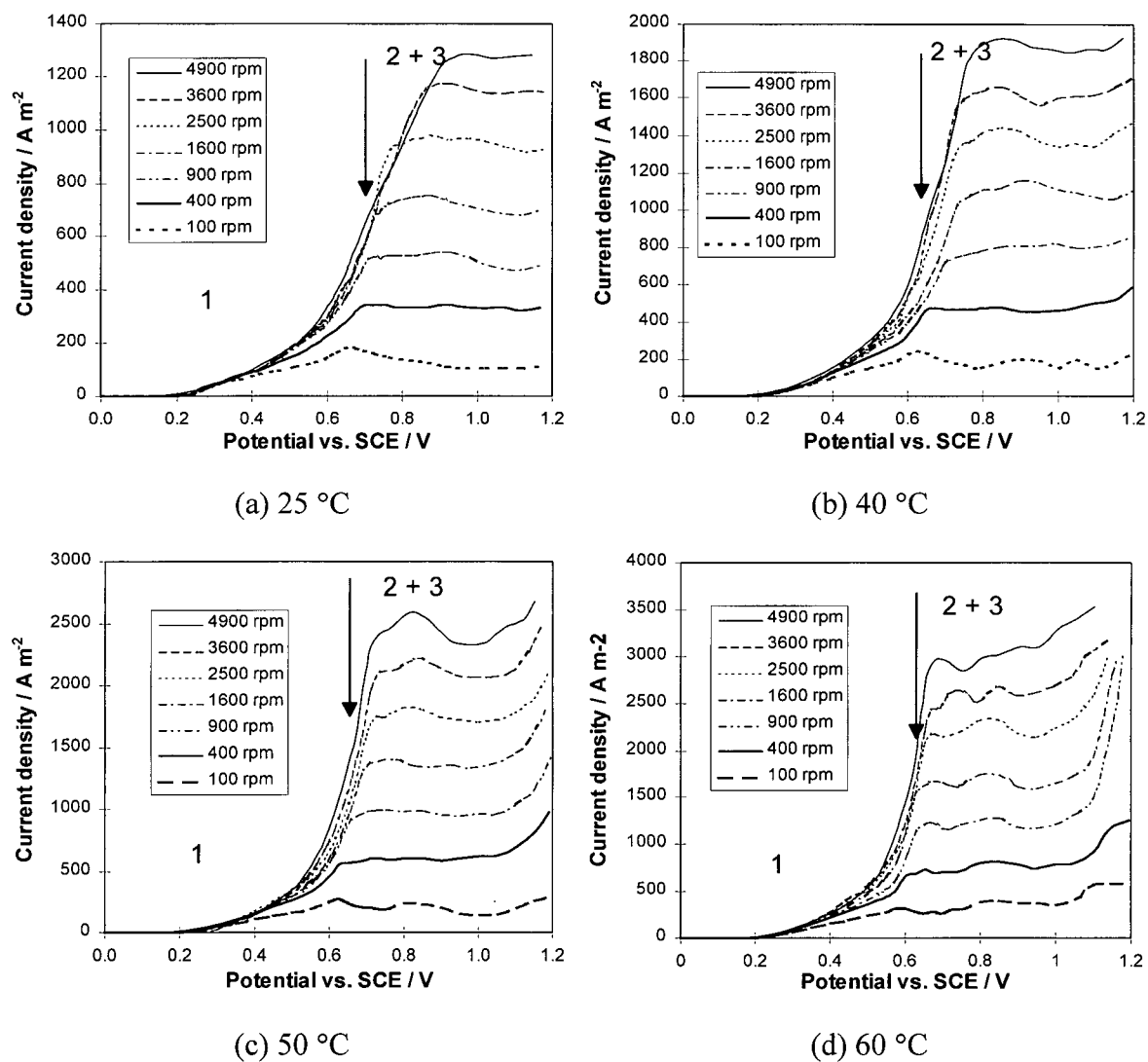
Figure A-18 Polarization curves at different rotational speeds and temperatures. Electrolyte: 0.05 M CN⁻, CN:Cu mole ratio = 12, 0.25 M NaOH and 1 M Na_2SO_4. Keys: 1 - no precipitation of copper oxide, 2 - precipitation of copper oxide, 3 - evolution of oxygen and 2+3 - copper oxide and oxygen appeared almost at the same potential.
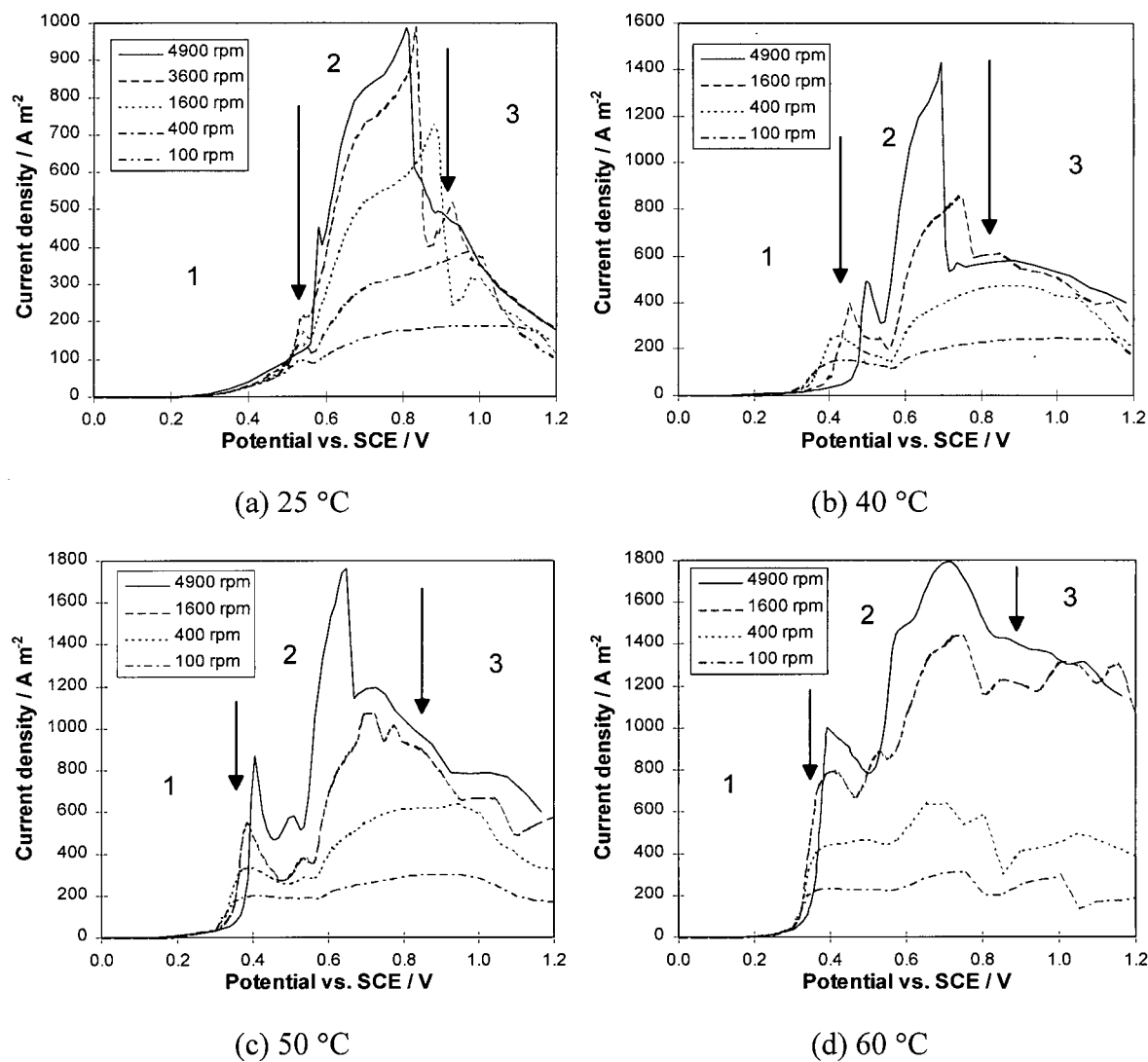
Figure A-19   Polarization curves at different rotational speeds and temperatures. Electrolyte: 0.05 M CN⁻, CN:Cu mole ratio = 3, 0.05 M NaOH and 1 M Na_2SO_4. Keys: 1 - no precipitation of copper oxide, 2 - precipitation of copper oxide and 3 - evolution of oxygen.

(a) 25 °C

(b) 40 °C

(c) 50 °C

(d) 60 °C
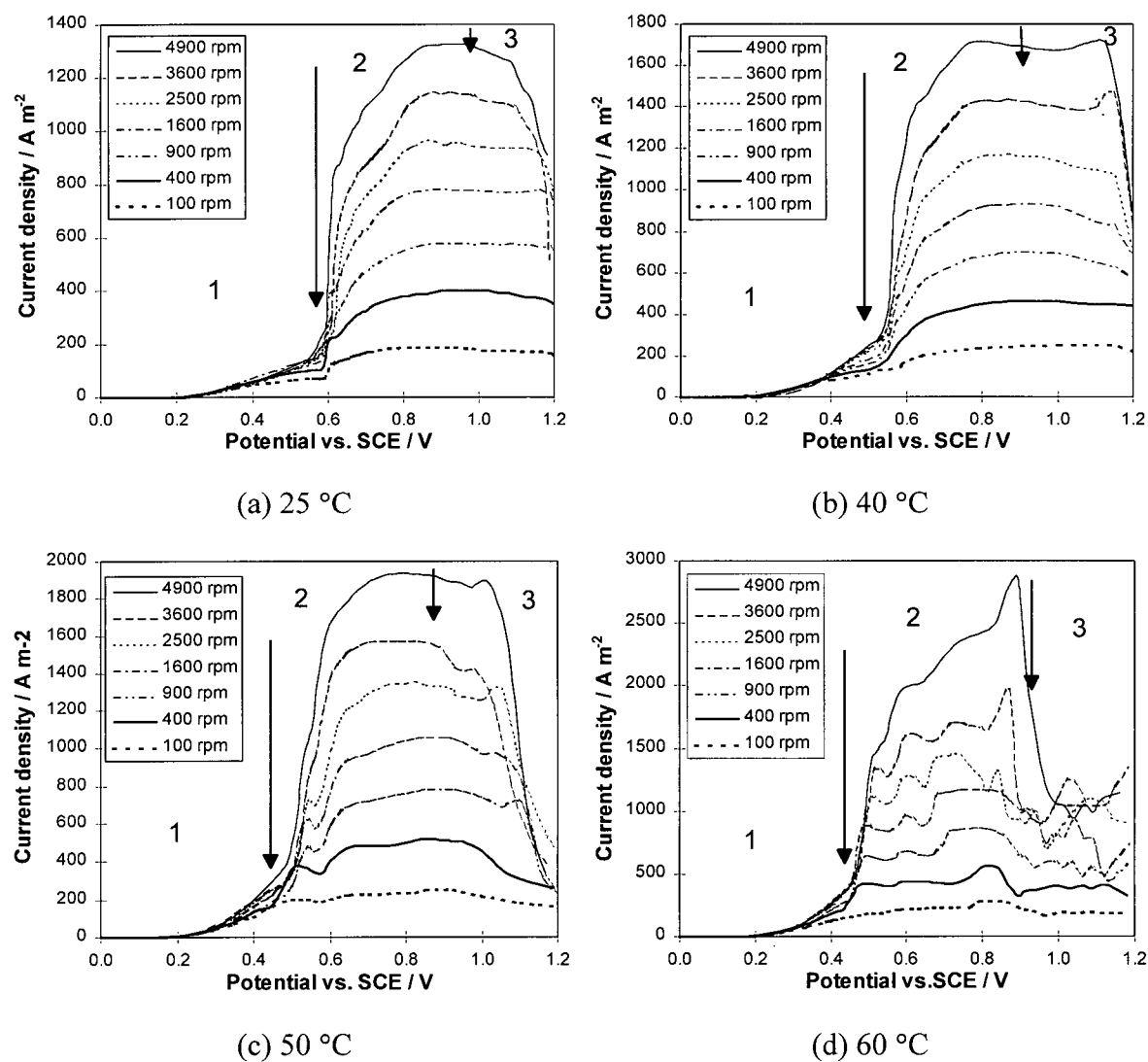
Figure A-20   Polarization curves at different rotational speeds and temperatures. Electrolyte: 0.05 M CN⁻, CN:Cu mole ratio = 4, 0.05 M NaOH and 1 M Na_2SO_4. Keys: 1 - no precipitation of copper oxide, 2 - precipitation of copper oxide and 3 - evolution of oxygen.
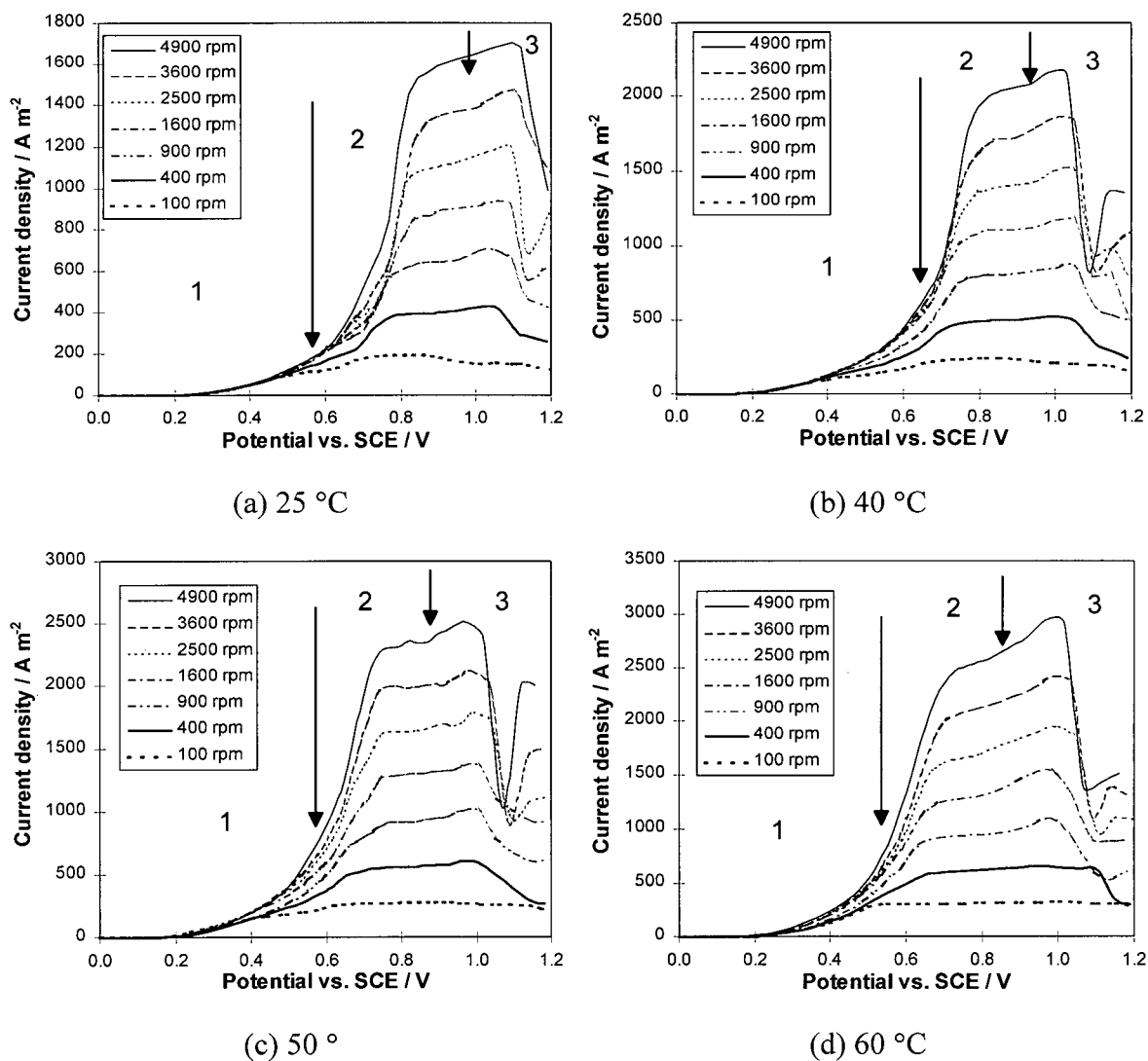
Figure A-21 Polarization curves at different rotational speeds and temperatures. Electrolyte: 0.05 M CN⁻, CN:Cu mole ratio = 12, 0.05 M NaOH and 1 M Na₂SO₄. Keys: 1 - no precipitation of copper oxide, 2 - precipitation of copper oxide and 3 - evolution of oxygen.
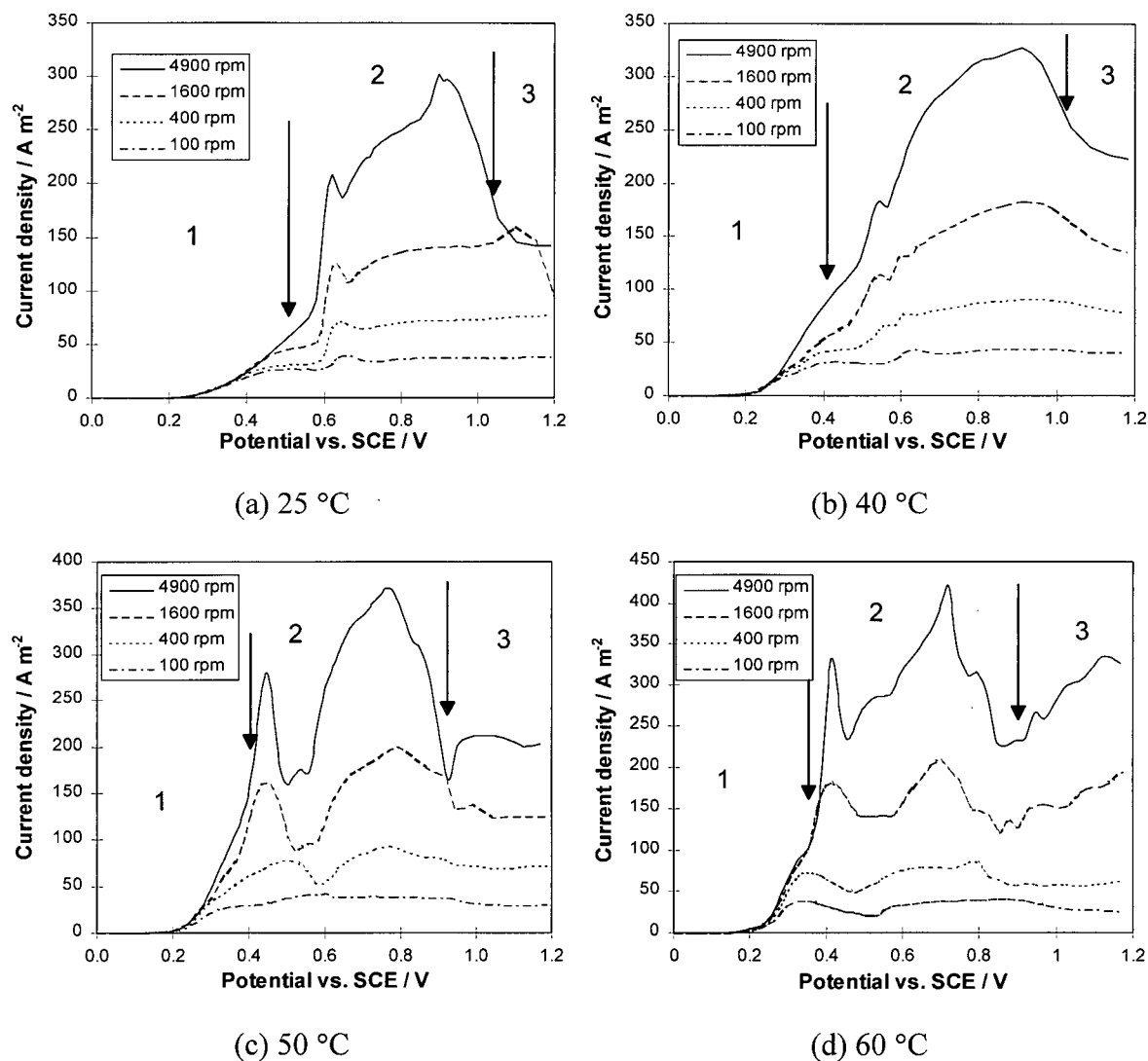
Figure A-22   Polarization curves at different rotational speeds and temperatures. Electrolyte: 0.05 M CN^-, $CN:Cu$ mole ratio = 3, 0.01 M $NaOH$ and 1 M Na_2SO_4. Keys: 1 - no precipitation of copper oxide, 2 - precipitation of copper oxide and 3 - evolution of oxygen.

(a) 25 °C

(b) 40 °C

(c) 50 °C

(d) 60 °C
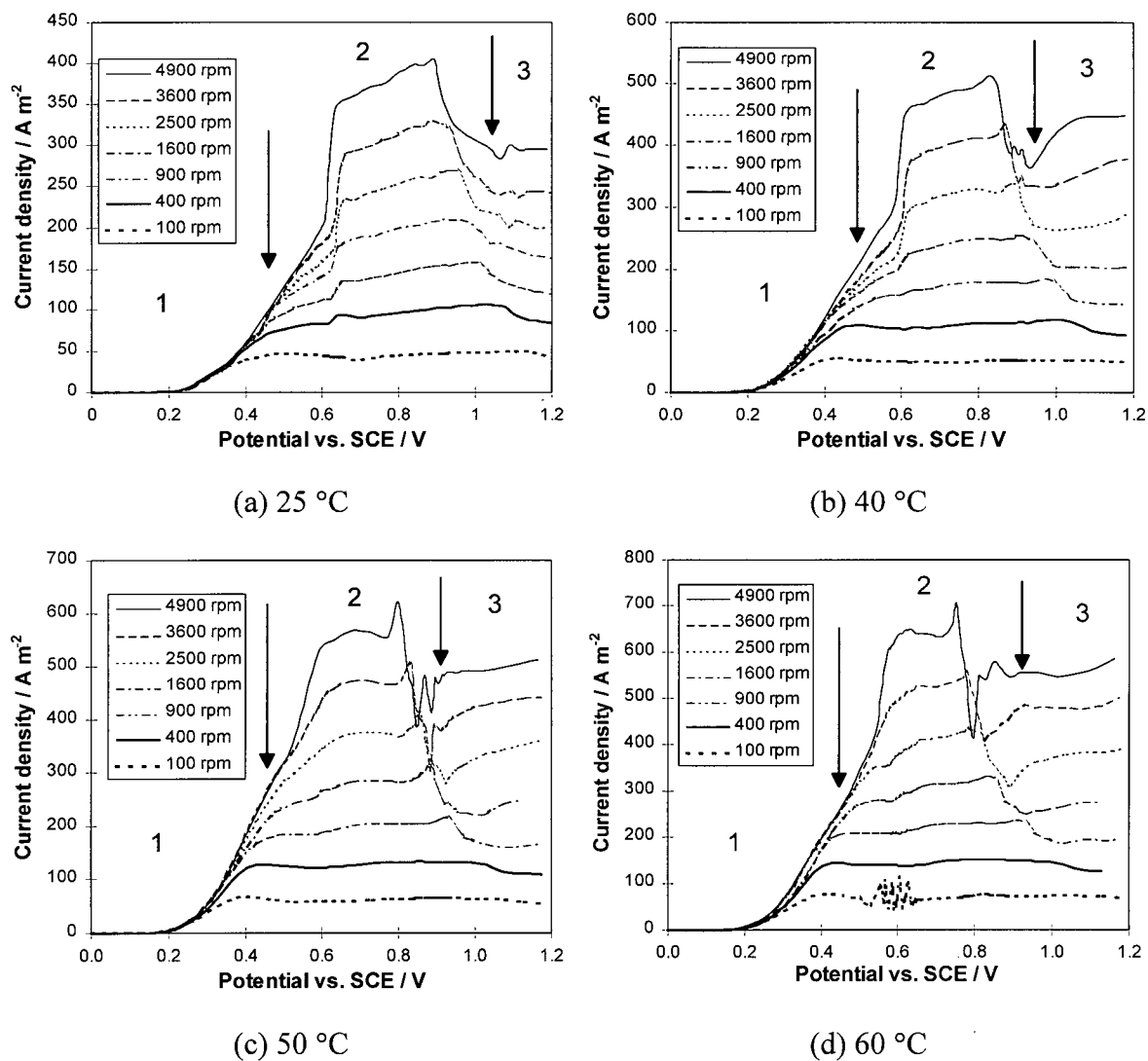
Figure A-23   Polarization curves at different rotational speeds and temperatures. Electrolyte: 0.05 M CN⁻, CN:Cu mole ratio = 4, 0.01 M NaOH and 1 M Na$_2$SO$_4$. Keys: 1 - no precipitation of copper oxide, 2 - precipitation of copper oxide and 3 - evolution of oxygen.

(a) 25 °C

(b) 40 °C

(c) 50 °C

(d) 60 °C
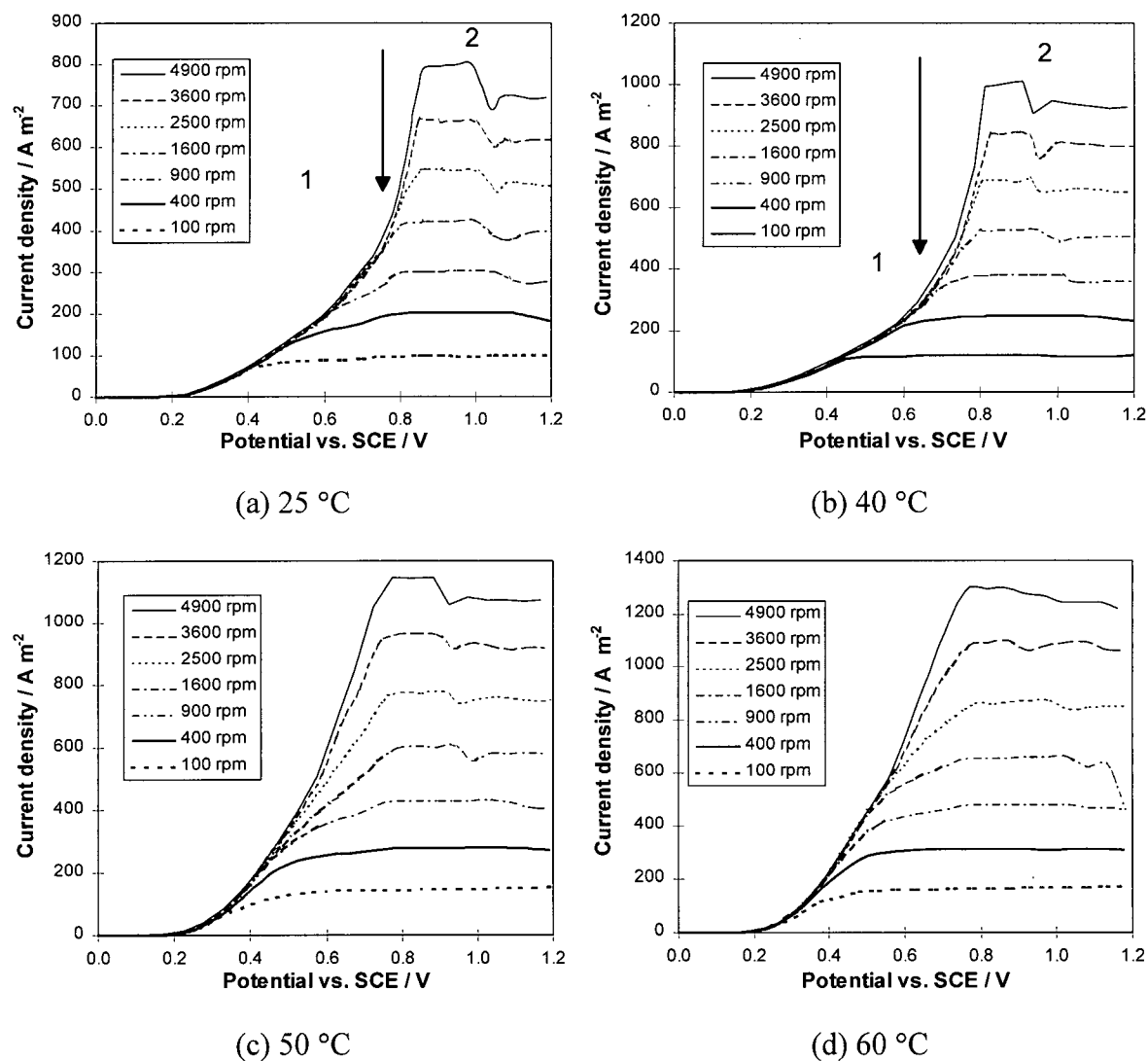
Figure A-24 Polarization curves at different rotational speeds and temperatures. Electrolyte: 0.05 M CN⁻, CN:Cu mole ratio = 12, 0.01 M NaOH and 1 M Na₂SO₄. Keys: 1 - no precipitation of copper oxide, 2 - precipitation of copper oxide and 3 - evolution of oxygen.
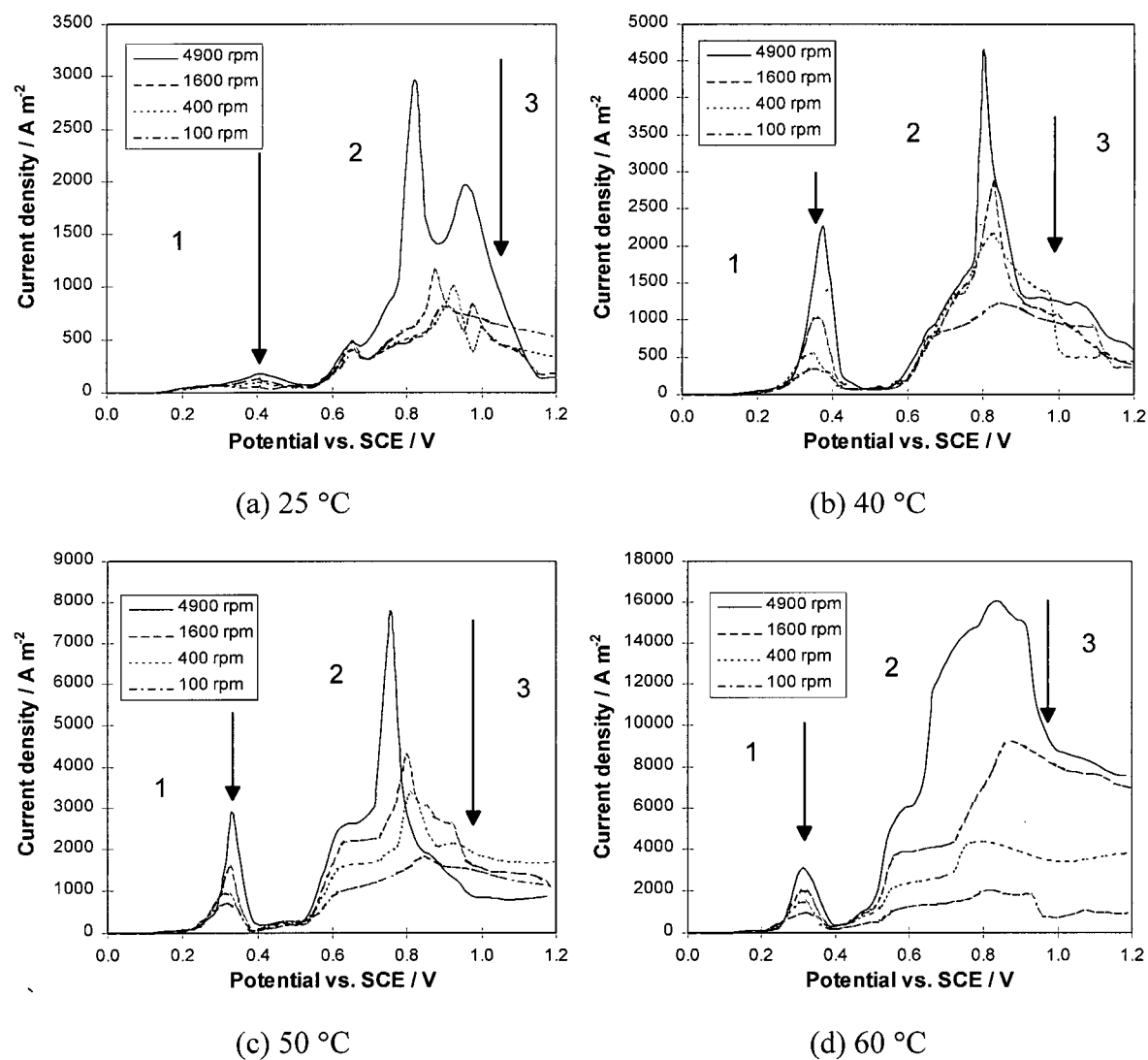
Figure A-25 Polarization curves at different rotational speeds and temperatures. Electrolyte: 0.5 M CN⁻, CN:Cu mole ratio = 3, 0.25 M NaOH and 1 M Na_2SO_4. Keys: 1 - no precipitation of copper oxide, 2 - precipitation of copper oxide and 3 - evolution of oxygen.
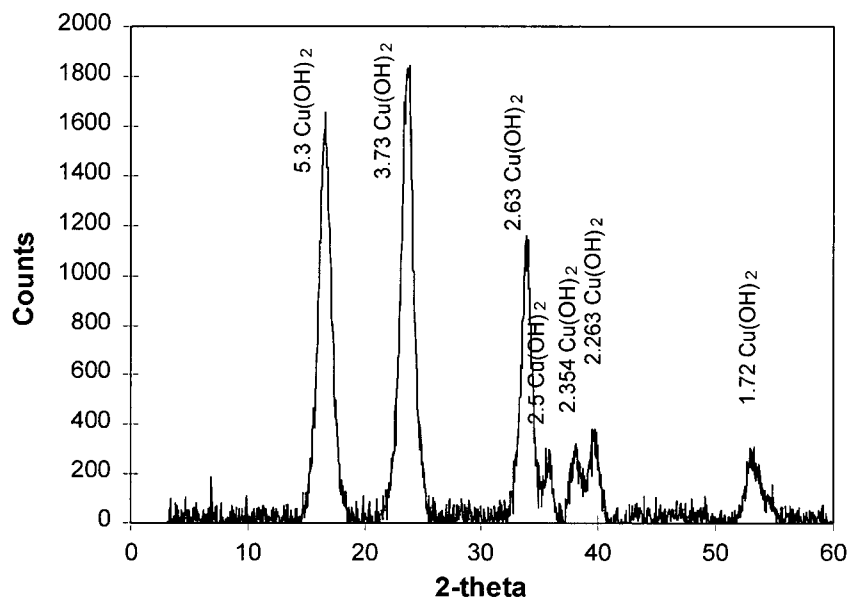
Figure A-26 X-ray diffraction pattern of the anodic precipitate prepared under the conditions: 3 M CN⁻, 1 M Cu (I), 0.25 M NaOH, 0.5 M Na₂SO₄, 25 °C, 0.5 V vs. SCE, and 100 rpm.
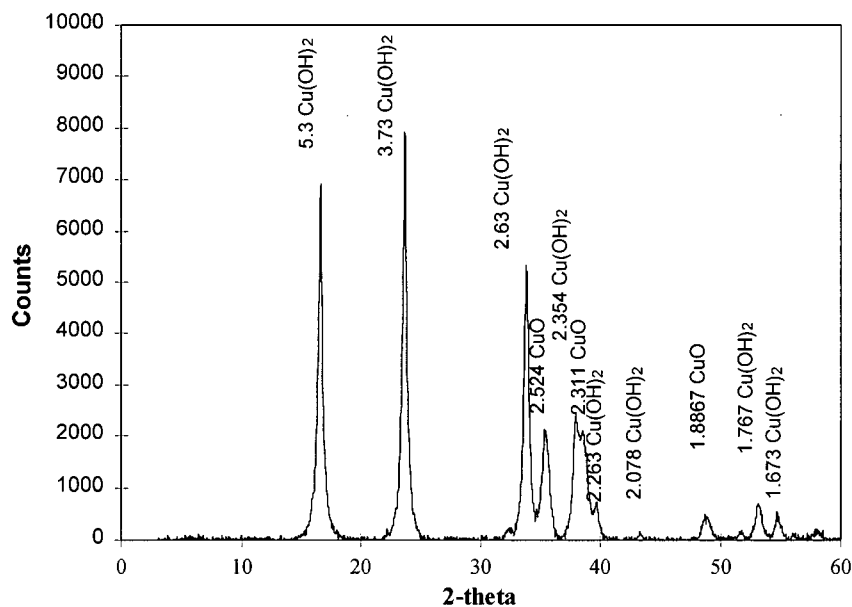
Figure A-27 X-ray diffraction pattern of the anodic precipitate prepared under the conditions: 3 M CN⁻, 1 M Cu (I), 0.25 M NaOH, 0.5 M Na₂SO₄, 60 °C, 0.5 V vs. SCE, and 100 rpm.
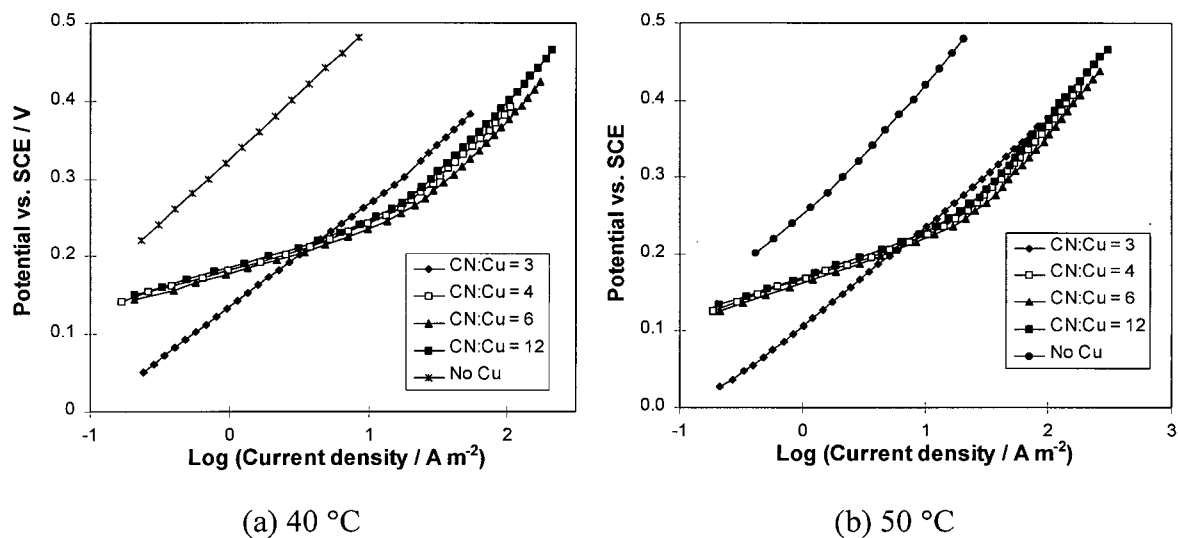
Figure A-28 Effect of the mole ratio of cyanide to copper on cyanide oxidation - potential vs. log (current density) on a graphite rotating disk at 4900 rpm (40 and 50 °C). Electrolytes : 0.05 M CN⁻, CN:Cu mole ratio = 3, 4, 6, 12 and no copper, 0.25 M NaOH and 1 M Na_2SO_4.
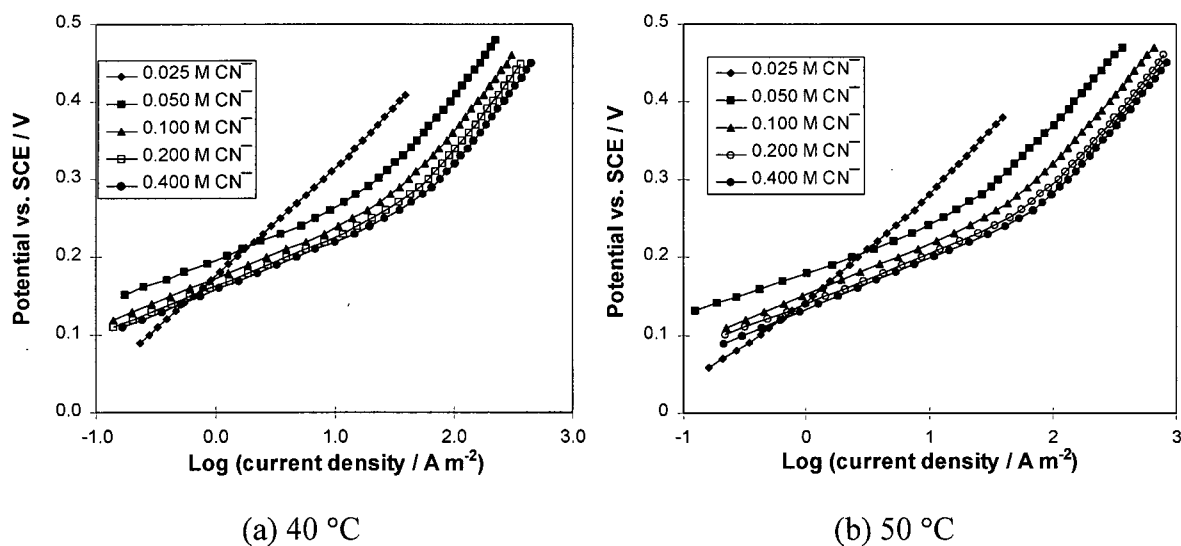
Figure A-29 Effect of the mole ratio of cyanide to copper on cyanide oxidation - potential vs. log (current density) on a graphite rotating disk at 4900 rpm (40 and 50 °C). Electrolytes : $[Cu^+]$ = 0.00833 M, $[CN^-]$ = 0.025, 0.05, 0.1, 0.2 and 0.4 M, 0.25 M NaOH and 1 M Na_2SO_4.

(a) 40 °C   (b) 50 °C
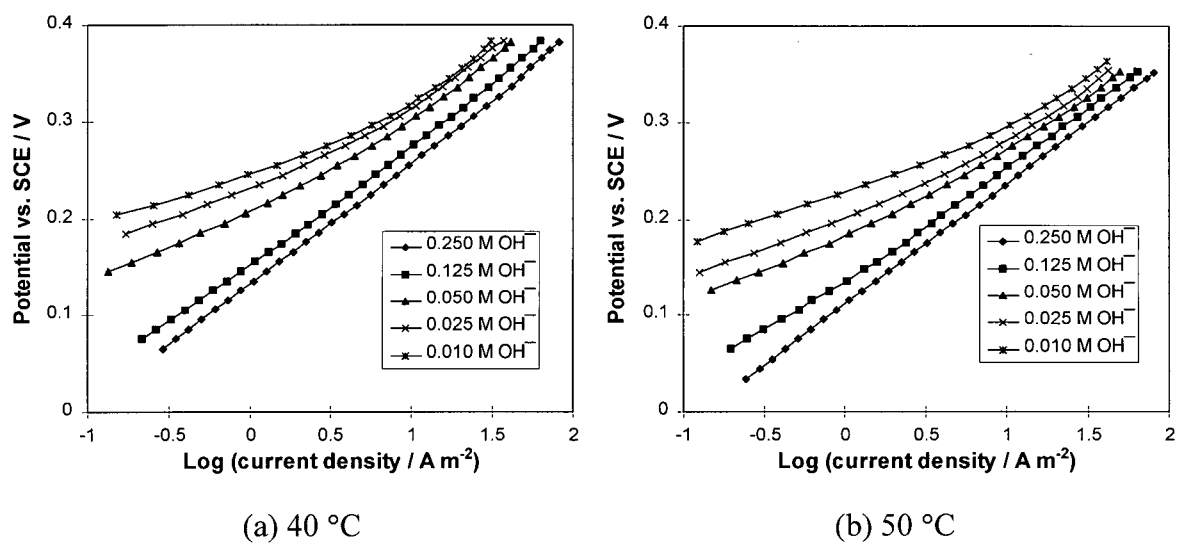
Figure A-30 Effect of pH on cyanide oxidation - potential vs. log (current density) on a graphite rotating disk at 4900 rpm (40 and 50°C). Electrolytes : 0.05 M CN⁻, a CN:Cu mole ratio of 3, [OH⁻] = 0.25, 0.125, 0.05, 0.025 and 0.01M and 1 M Na₂SO₄.
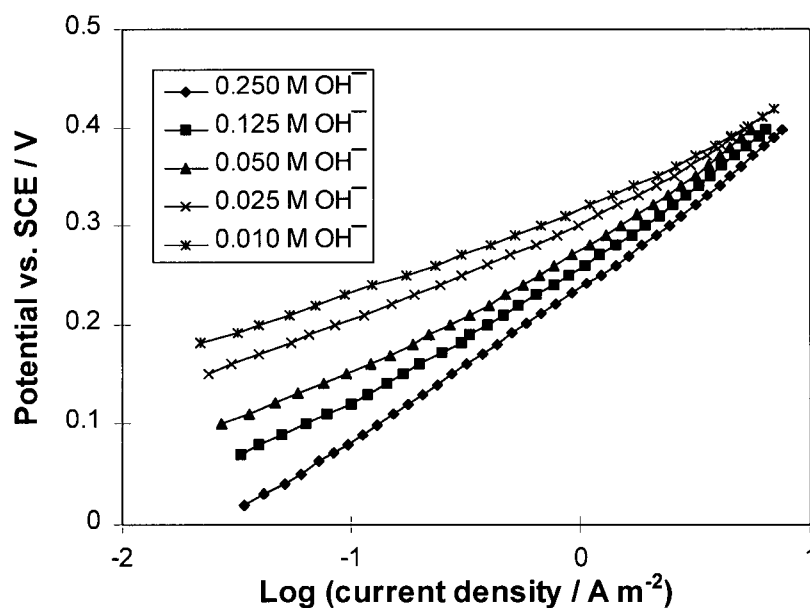
Figure A-31 Effect of pH on cyanide oxidation - potential vs. log (current density) on a Pt graphite rotating disk at 4900 rpm and 25 °C. Electrolytes : 0.05 M CN⁻, a CN:Cu mole ratio of 3, [OH⁻] = 0.25, 0.125, 0.05, 0.025 and 0.01M and 1 M Na₂SO₄.

(a) 40 °C   (b) 50 °C
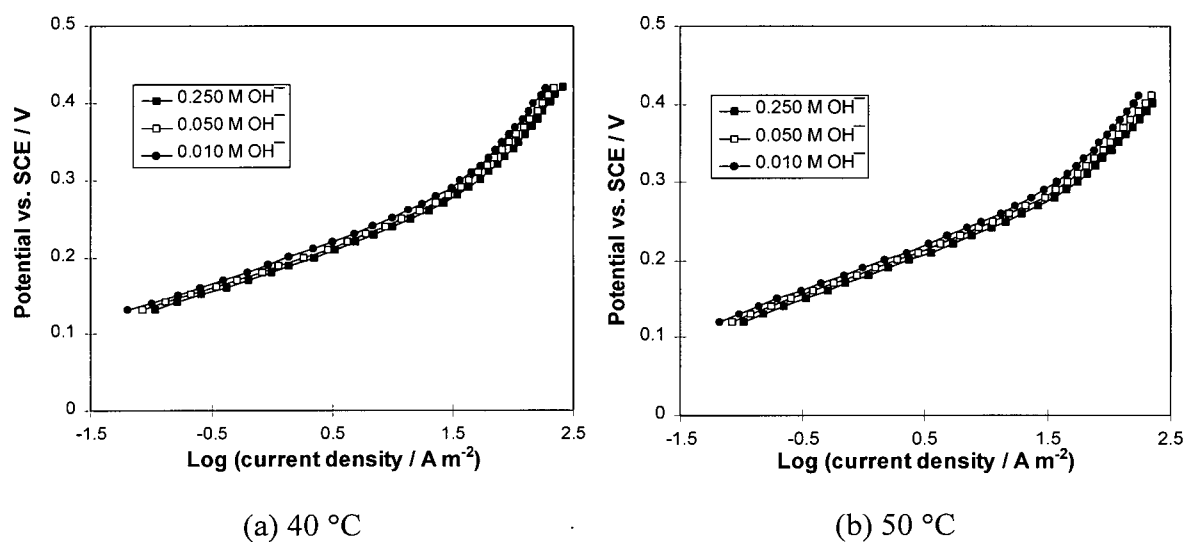
Figure A-32 Effect of pH on cyanide oxidation - potential vs. log (current density) on a graphite rotating disk 4900 rpm (40 and 50 °C). Electrolytes : 0.05 M⁻ CN⁻, a CN:Cu mole ratio of 4, [OH⁻] = 0.25, 0.05, and 0.01M and 1 M Na$_2$SO$_4$.

(a) 40 °C   (b) 50 °C
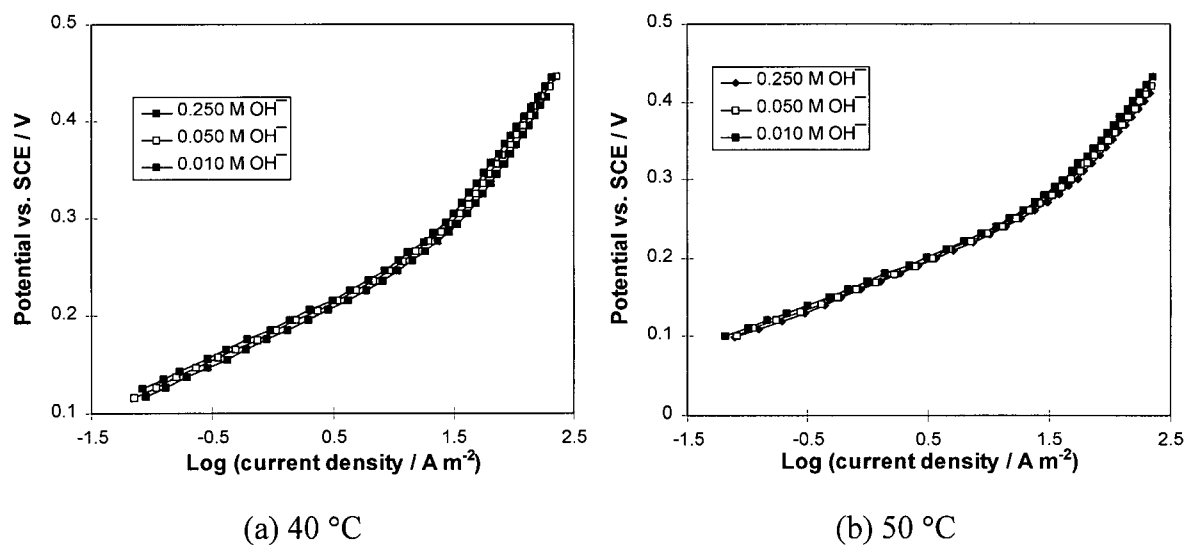
Figure A-33 Effect of pH on cyanide oxidation - potential vs. log (current density) on a graphite rotating disk at 4900 rpm (40 and 50 °C). Electrolytes : 0.05 M⁻ CN⁻, a CN:Cu mole ratio of 12, [OH⁻] = 0.25, 0.05 and 0.01M and 1 M Na$_2$SO$_4$.
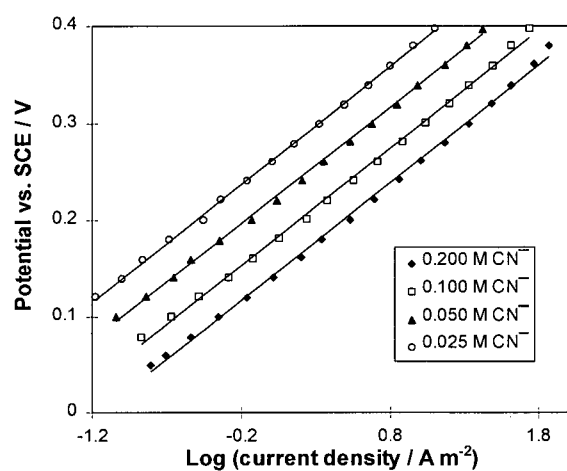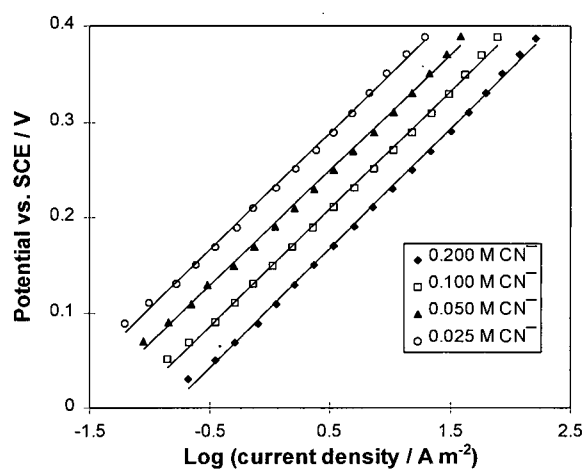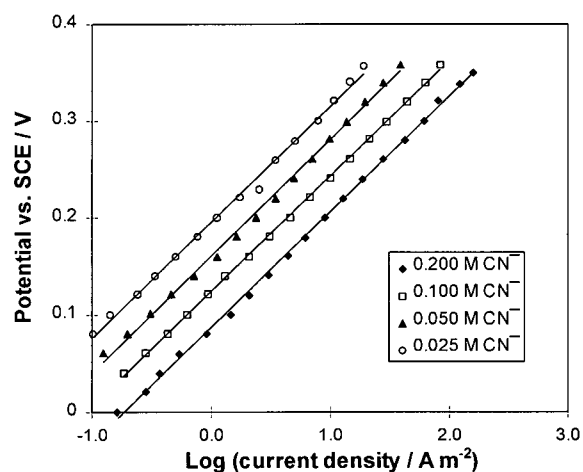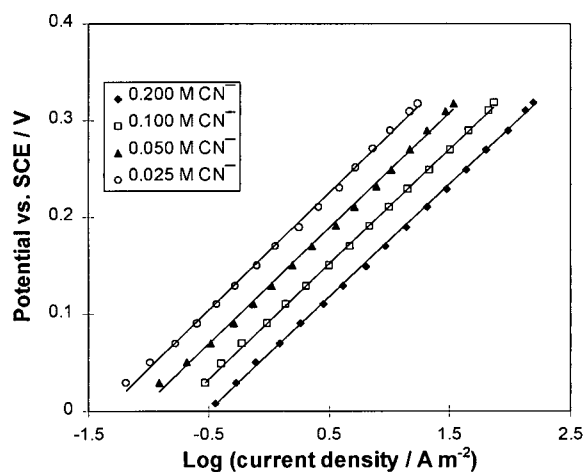
Figure A-34 Plots of potential vs. log (current density) on a graphite rotating disk at 4900 rpm and different temperatures. Electrolytes : [CN⁻] = 0.025, 0.05, 0.1 and 0.20 M, a CN:Cu mole ratio = 3, [OH⁻] = 0.25 M and 1 M Na_2SO_4.
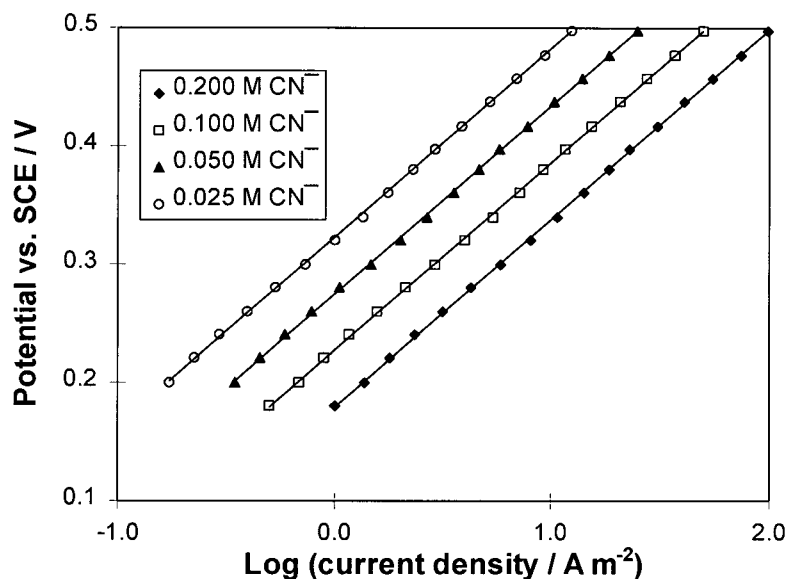
Figure A-35   Plots of the potential vs. log (current density) on a pyrolytic graphite rotating disk at 4900 rpm and 25 °C. Electrolytes: $[CN^-]$ = 0.025, 0.05, 0.1 and 0.20 M, a CN:Cu mole ratio = 3, $[OH^-]$ = 0.25 M and 1 M Na_2SO_4.
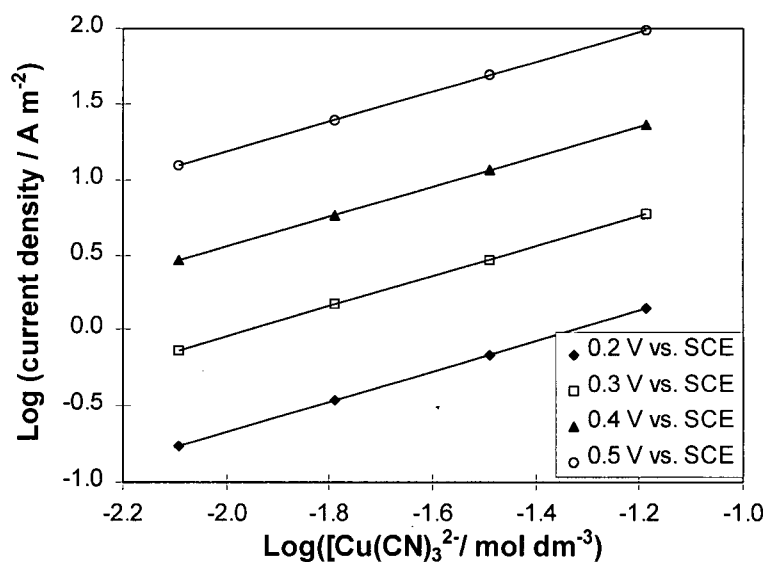
Figure A-36   Plots of log (current density) vs. log ($[Cu(CN)_3^{2-}]$) on a pyrolytic graphite rotating disk at 4900 rpm and 25 °C. Electrolytes: $[CN^-]$ = 0.025, 0.05, 0.1 and 0.20 M, a CN:Cu mole ratio = 3, $[OH^-]$ = 0.25 M and 1 M Na_2SO_4.
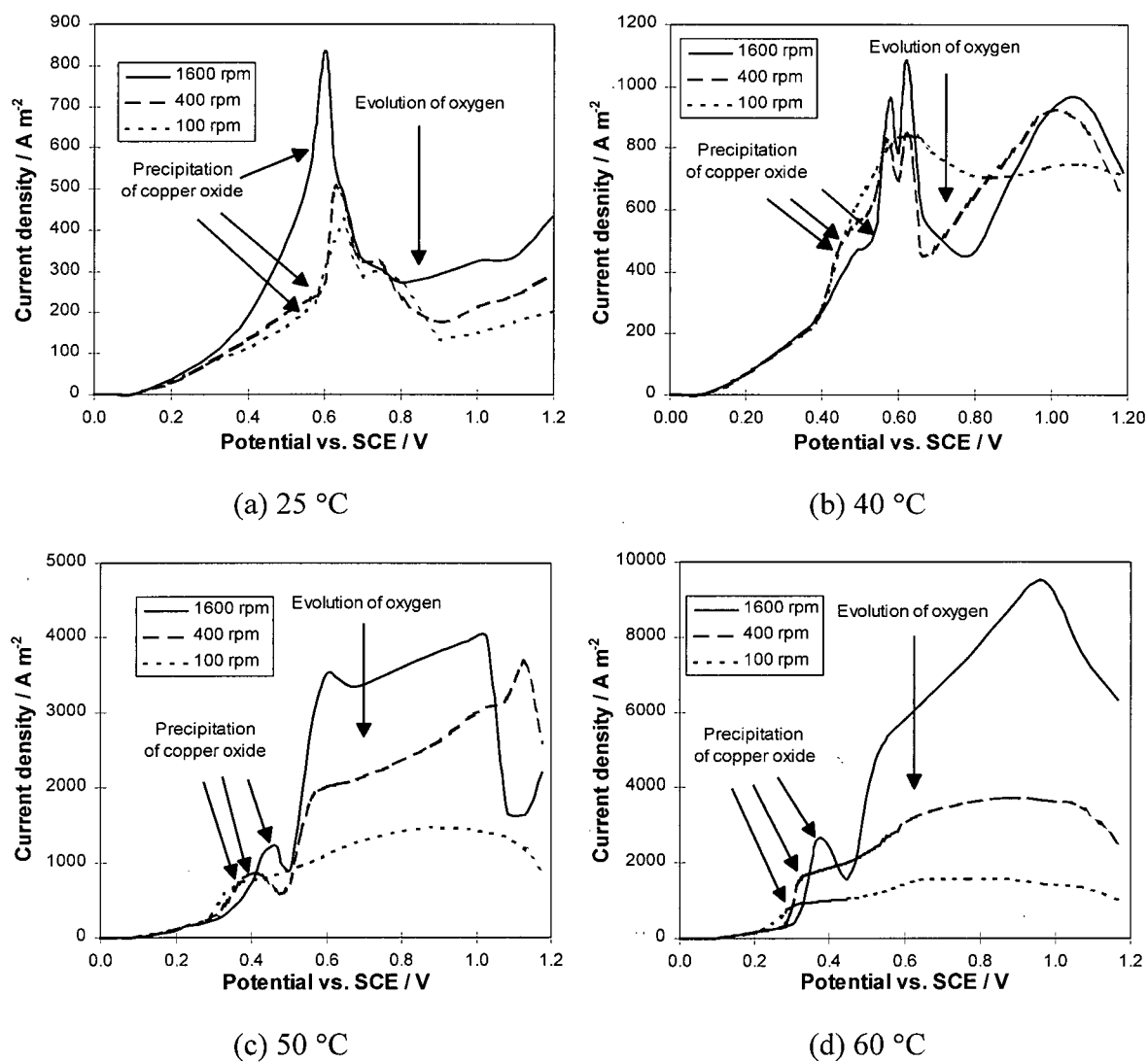
Figure A-37 Polarization curves at different temperatures. Electrolyte: 0.05 M CN⁻, 0.0167 M Cu⁺ (CN:Cu mole ratio = 3), 0.25 M NaOH, 0.2 M Na₂SO₃ and 1 M Na₂SO₄.
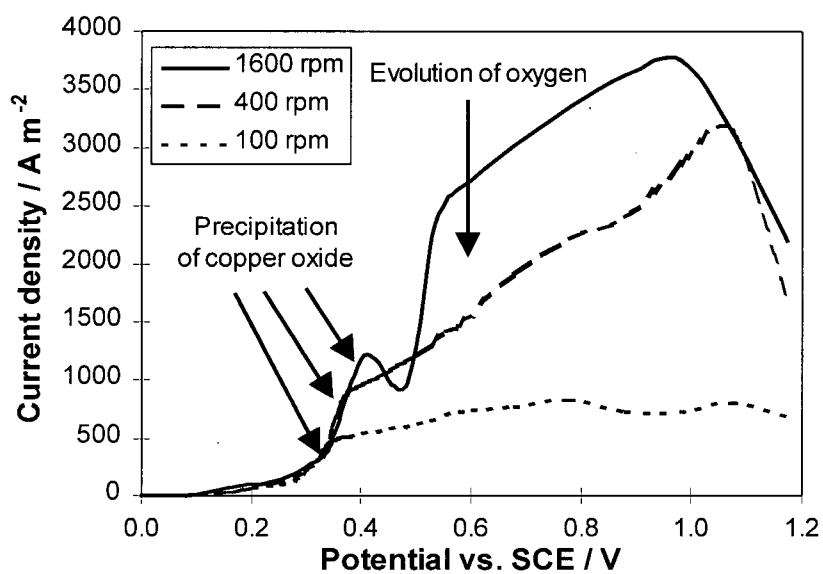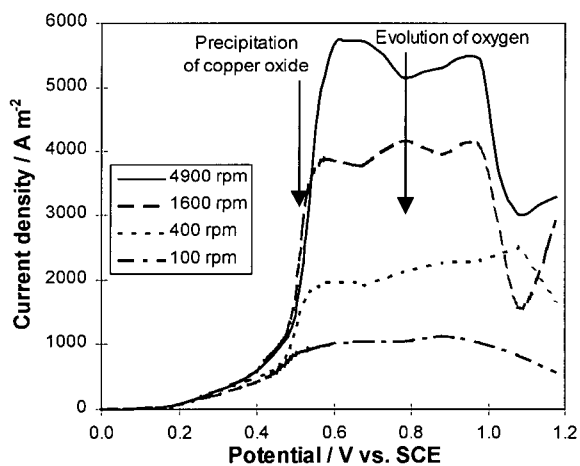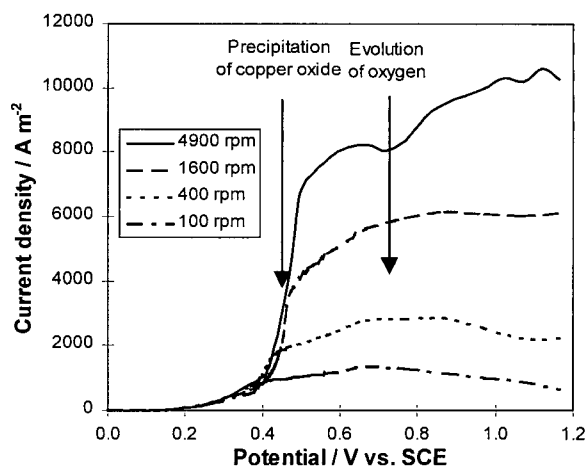
(a) 50 °C
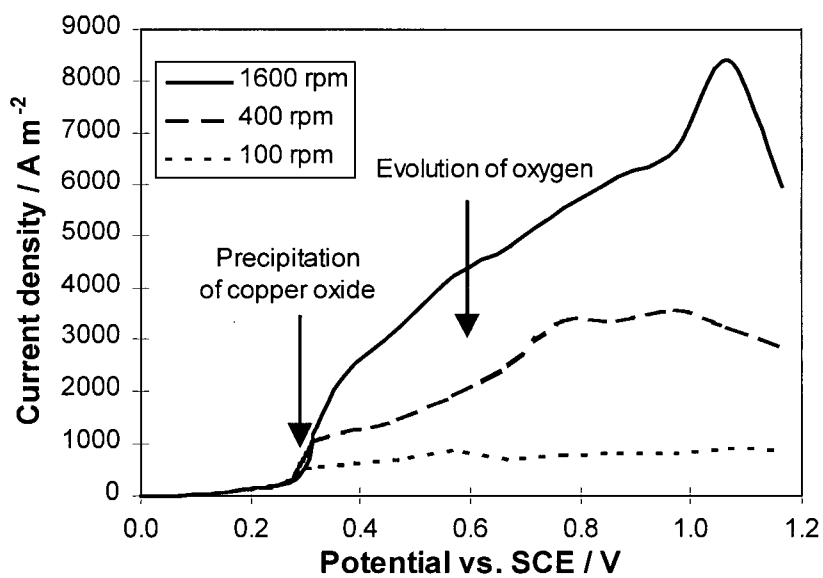
(b) 60 °C

Figure A-38 Polarization curves at different temperatures. Electrolyte: 0.05 M CN⁻,
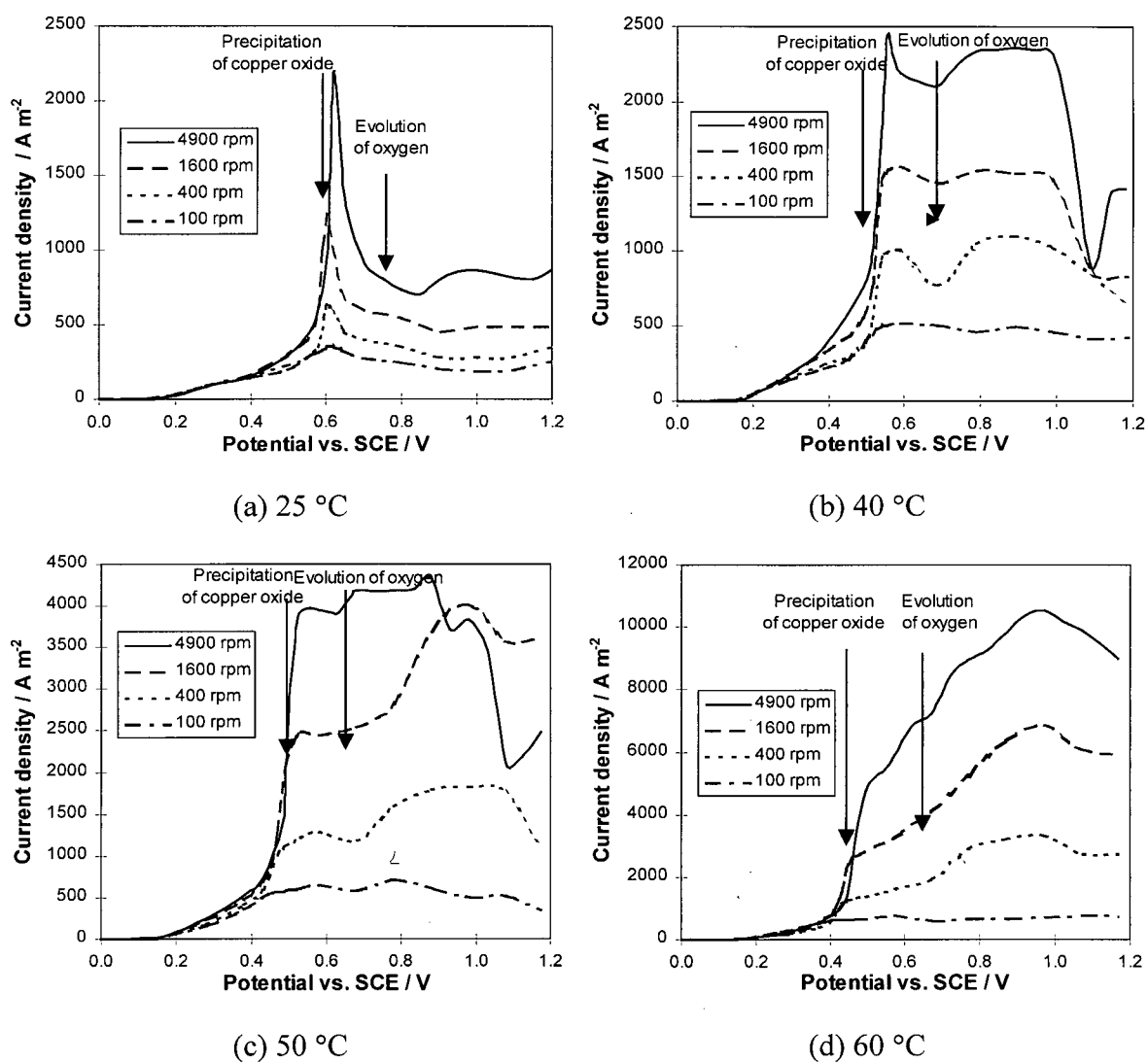0.0167 M Cu⁺ (CN:Cu mole ratio = 3), 0.25 M NaOH, 0.1 M Na_2SO_3 and 1 M Na_2SO_4.
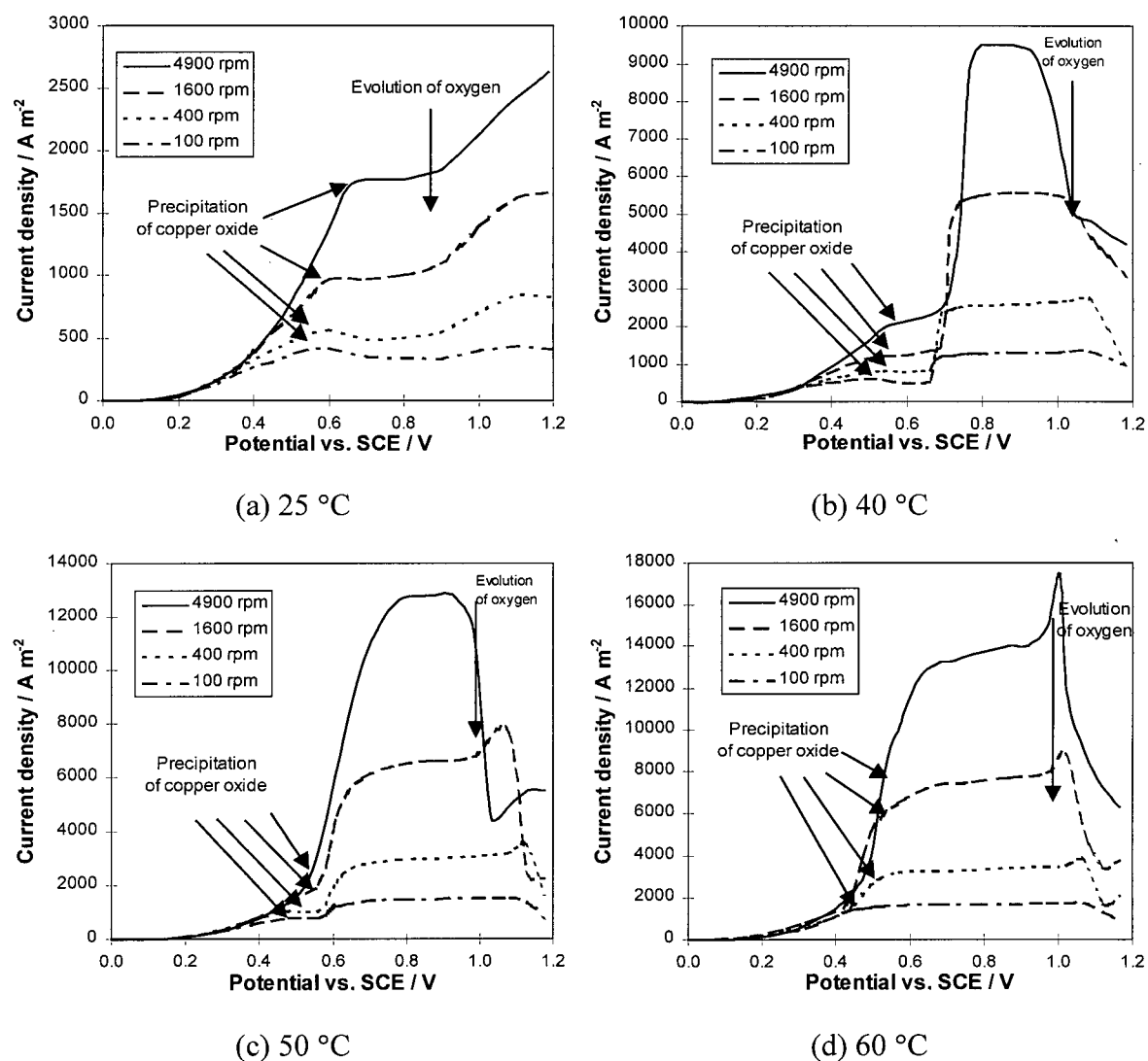
Figure A-39 Polarization curves at different temperatures. Electrolyte: 0.05 M CN⁻,
0.0125 M Cu⁺ (CN:Cu mole ratio = 4), 0.25 M NaOH, 0.4 M Na₂SO₃ and 1 M Na₂SO₄.
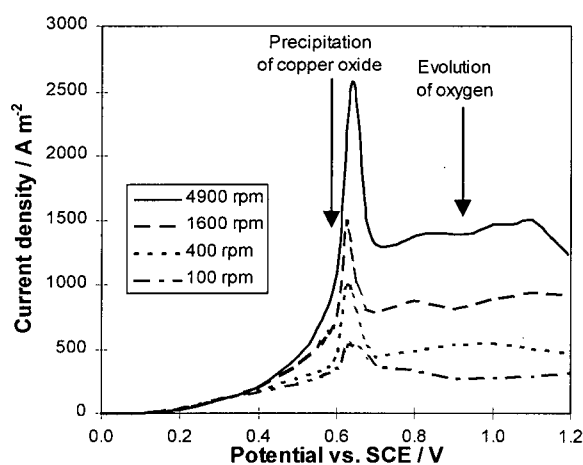
(a) 25 °C (a)
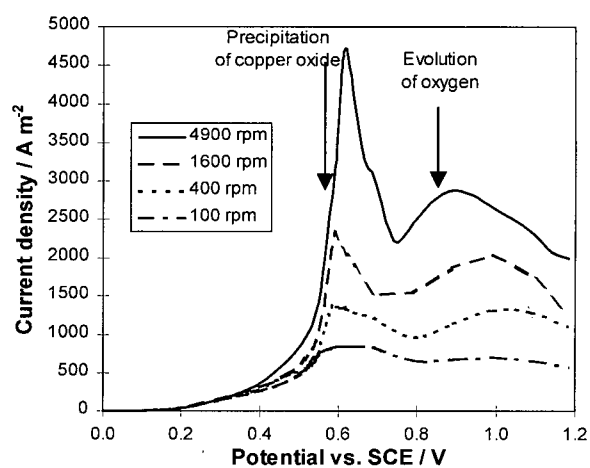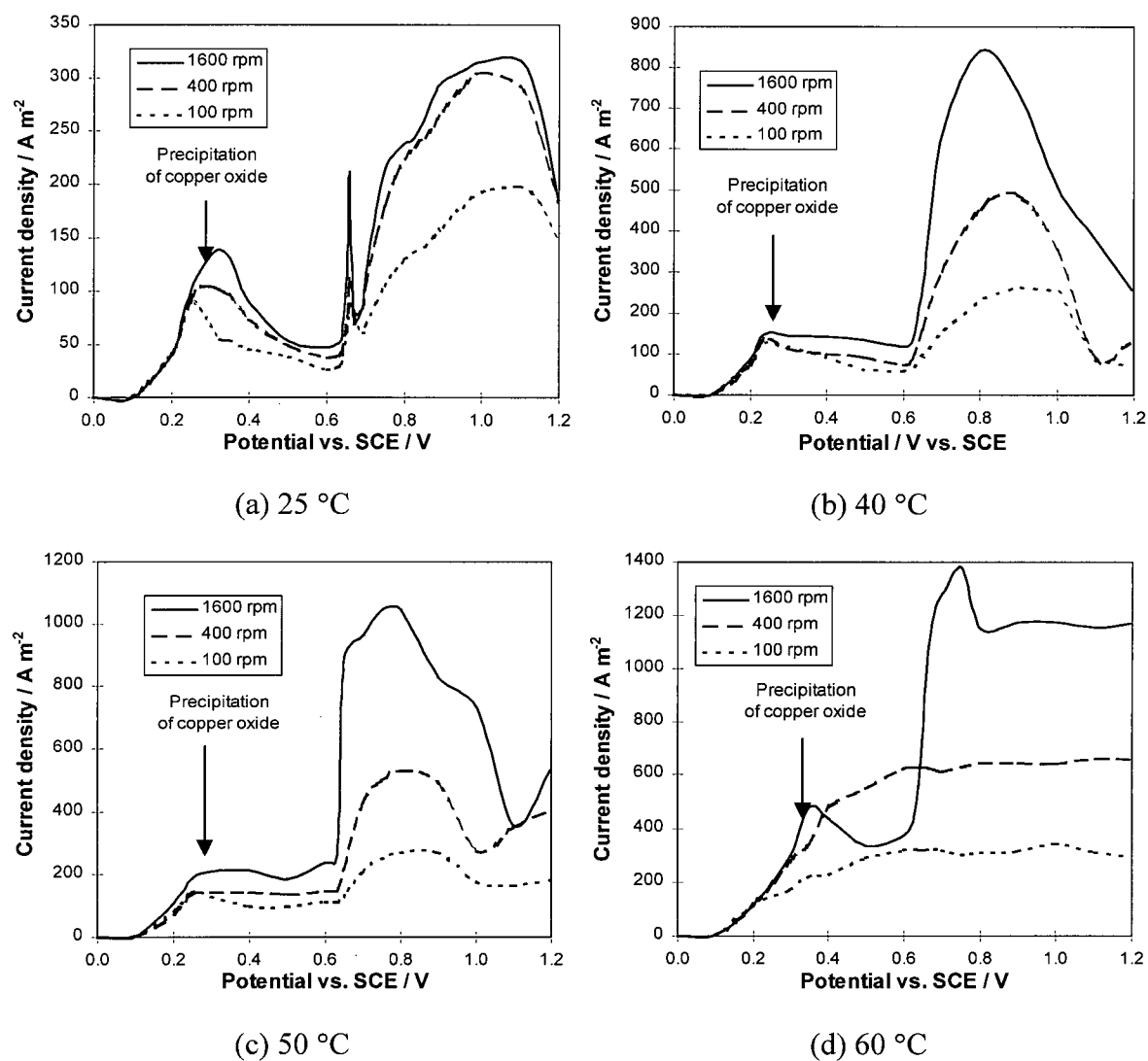
(b) 40 °C

(c) 50 °C

(d) 60 °C
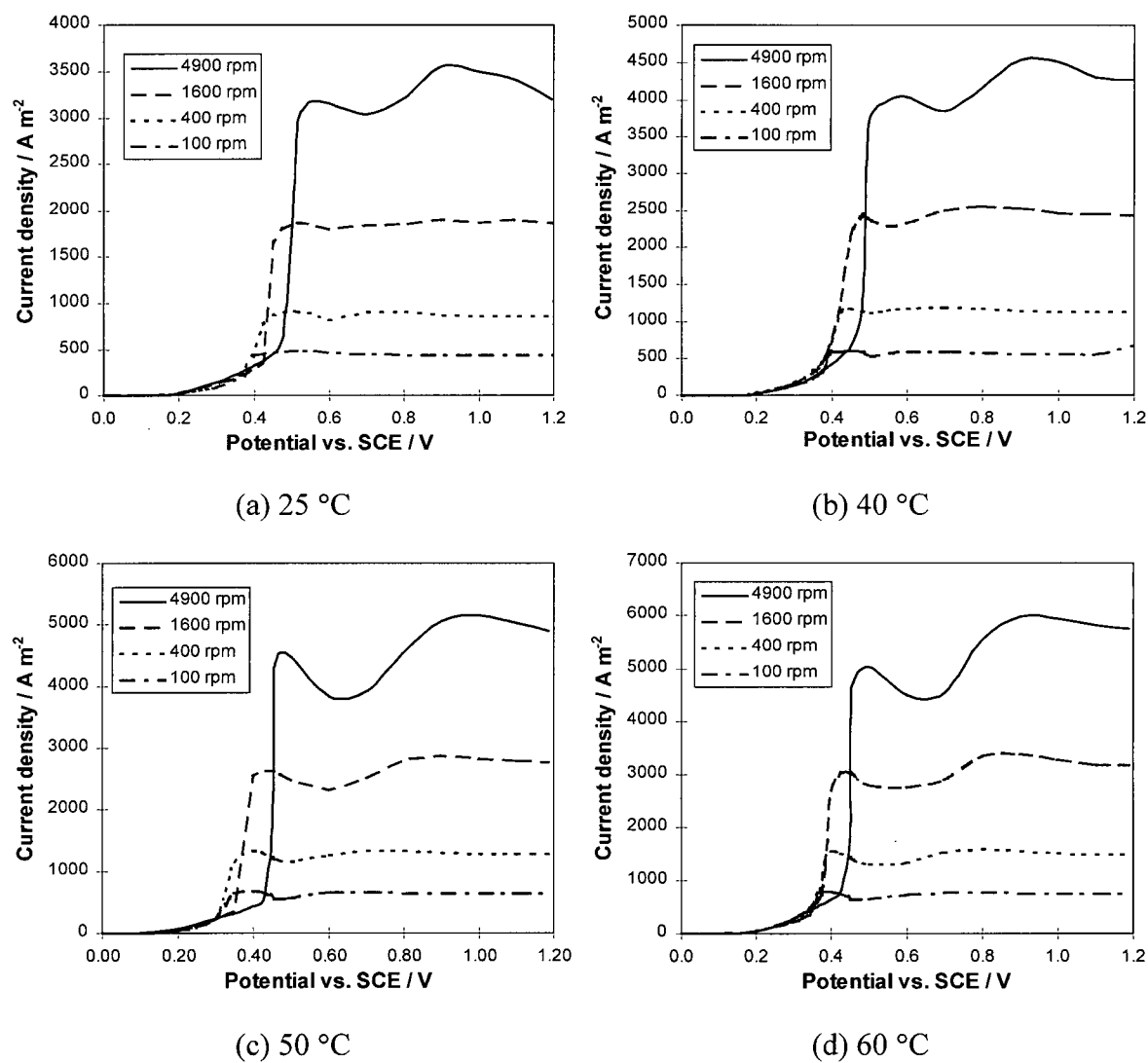
Figure A-40 Polarization curves at different temperatures. Electrolyte: 0.05 M CN^-, 0.0125 M Cu^+ (CN:Cu mole ratio = 4), 0.25 M NaOH, 0.2 M Na_2SO_3 and 1 M Na_2SO_4.

Figure A-41 Polarization curves at different temperatures. Electrolyte: 0.05 M CN⁻, 0.0125 M Cu⁺ (CN:Cu mole ratio = 4), 0.25 M NaOH, 0.1 M Na_2SO_3 and 1 M Na_2SO_4

(a) 25 °C

(b) 40 °C

(c) 50 °C

(d) 60 °C
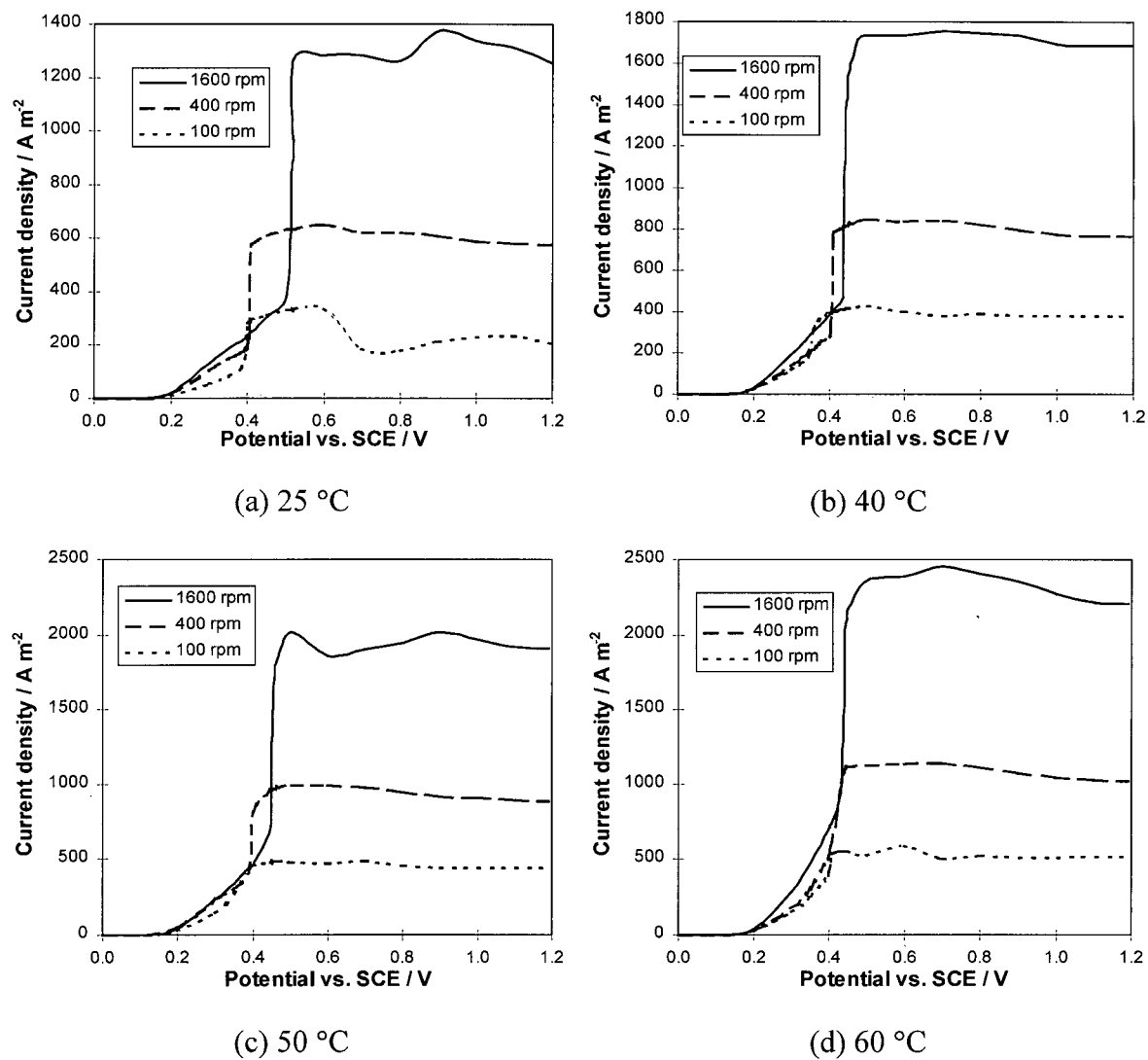
Figure A-42 Polarization curves at different temperatures. Electrolyte: 0.05 M CN$^-$, 0.0167 M Cu$^+$ (CN:Cu mole ratio = 3), 0.05 M NaOH, 0.2 M Na$_2$SO$_3$ and 1 M Na$_2$SO$_4$.

(a) 25 °C

(b) 40 °C

(c) 50 °C

(d) 60 °C

Figure A-43 Polarization curves at different temperatures. Electrolyte: 0.05 M CN^-, 0.0125 M Cu^+ (CN:Cu mole ratio = 4), 0.05 M NaOH, 0.4 M Na_2SO_3 and 1 M Na_2SO_4.

Figure A-44 Polarization curves at different temperatures. Electrolyte: 0.05 M CN⁻, 0.0125 M Cu⁺ (CN:Cu mole ratio = 4), 0.05 M NaOH, 0.2 M Na₂SO₃ and 1 M Na₂SO₄.

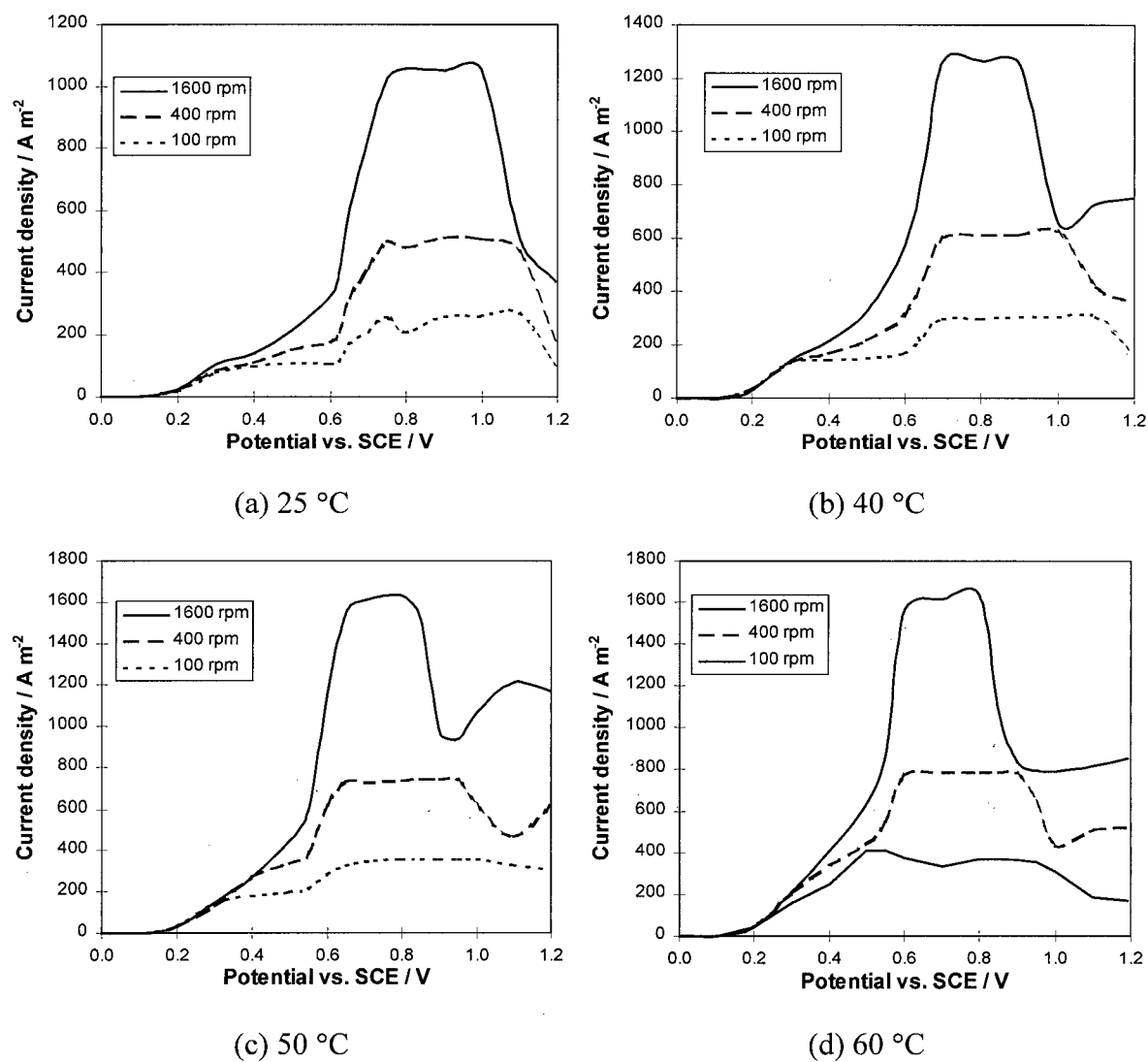Figure A-45 Polarization curves at different temperatures. Electrolyte: 0.05 M CN⁻,
0.0125 M Cu⁺ (CN:Cu mole ratio = 4), 0.05 M NaOH, 0.1 M Na₂SO₃ and 1 M Na₂SO₄.